Radiocarbon constraints reveal time scales of soil carbon persistence

Von der Naturwissenschaftlichen Fakultät der

Gottfried Wilhelm Leibniz Universität Hannover

zur Erlangung des Grades

Doktor der Naturwissenschaften (Dr. rer. nat)

genehmigte Dissertation

von

Jeffrey Prescott Beem-Miller, Master of Science, Cornell University

2023

Abstract

Soils are currently a sink for atmospheric C, but may become a source in the coming decades. Predicting future gains or losses in soil C will require quantifying the time scales on which C cycles through soils, as well as deepening our understanding of the mechanisms controlling these cycling rates. Global patterns of soil C stocks and the radiocarbon (^{14}C) signature of bulk soil C ($\Delta^{14}C_{bulk}$) establish temperature as a master control on soil C ages and accumulation rates. Yet emerging understanding underscores the importance of mineral control for both soil C cycling rates and the temperature sensitivity of decomposition. The central aim of this dissertation is to quantify the time scales of soil C cycling on which mineralogical controls are relevant and the influence of the soil mineral assemblage on the responses of soil C ages and transit times to climate.

Radiocarbon is a sensitive tracer for quantifying time scales of soil C cycling. The mean age of soil C can be constrained with observations of $\Delta^{14}C_{bulk}$, but the ^{14}C signature of heterotrophically respired CO_2 ($\Delta^{14}C_{respired}$) adds a powerful constraint on the age of C returning to the atmosphere i.e., soil C transit time. Incubating archived soils would enable the construction of time series of $\Delta^{14}C_{respired}$, substantially reducing uncertainty from observations at single point in time. The objective of the first study in this dissertation (Ch. 2) is to assess the feasibility of measuring $\Delta^{14}C_{respired}$ in archived soils by quantifying potential biases caused by air-drying, rewetting, and storage of soils prior to incubation. Results indicate storage has a negligible impact, but air-drying and rewetting leads to a small increase in the relative contribution of older C to respiration. However, the absolute bias in $\Delta^{14}C_{respired}$ from air-drying and rewetting was minimal (±12‰ to ±40‰), suggesting that constructing time series of $\Delta^{14}C_{respired}$ from incubations of archived soils is promising as long as soils undergo the same air-drying and rewetting procedure.

In Ch. 3 of this dissertation, I compare the distribution and change over time in $\Delta^{14}C_{bulk}$ and $\Delta^{14}C_{respired}$ among soils developed on different parent materials (andesite, basalt, granite) but with similar mean annual soil temperature (MAST) and climate regime (warm ~ 12.0 °C, cool ~ 8.6 °C, cold ~ 6.6 °C) using archived soils. The results provide new evidence that mineral assemblages: 1) mediate climatic control of soil C turnover, and 2) are relevant for C cycling on annual to decadal time scales as well as centennial and longer. Furthermore, the effect of MAST on the change observed in $\Delta^{14}C_{respired}$ over time was only significant in the soils with the lowest content of poorly crystalline metal (oxy) hydroxide (PCM) content, implying that soil organic matter interactions with these minerals may attenuate temperature sensitivity of soil C ages and transit times.

Determining ages and transit times of soil C requires the use of a model. In Ch. 4 of this dissertation (Ch. 4) I demonstrate how time series of $\Delta^{14}C_{respired}$ and $^{14}C_{bulk}$ can be used to constrain soil C models using the data from Ch. 3. Different two-pool model structures yielded similar estimates for soil C ages, transit times, and inputs, indicating that $^{14}C_{respired}$ and $^{14}C_{bulk}$ are robust constraints for such a system. Trends in mean ages and transit times with respect to climatic and mineralogical factors were similar to those in $\Delta^{14}C_{bulk}$ and $\Delta^{14}C_{respired}$, respectively. However, the models also yield probability distributions of age and transit time. The distributions reveal that in some soils, such as those with abundant PCMs, small amounts of highly $\Delta^{14}C$-depleted C can bias estimates of the mean, potentially leading to overestimates of ages or transit times. Modeled estimates of the pre-aging of soil C inputs show an increase with depth, adding to the growing recognition that observed increases in ^{14}C age with depth may not be due solely to slower turnover, but also vertical transport.

The central theme of this dissertation is that mineral-associated soil organic matter is not a homogenous pool, and in soils consisting of a wide range of soil mineral assemblages, consists of C cycling on time scales ranging from annual to millennial. Furthermore, ages and transit times of C in the PCM-rich soils of this study were less sensitive to temperature than in PCM-poor soils, highlighting the importance of accounting for mineral assemblages in predicting the effect of rising temperatures on soil C stocks.

"[Science] has two rules. First: there are no sacred truths; all assumptions must be critically examined; arguments from authority are worthless. Second: whatever is inconsistent with the facts must be discarded or revised." – Carl Sagan

"If it should turn out that we have mishandled our own lives as several civilizations before us have done, it seems a pity that we should involve the violet and the tree frog in our departure." – Loren Eisley

"The chief value of a PhD is that no one ever assumes you're stupid, they just keep thinking they don't understand you" – Plaque in my grandfather's study

Keywords

Soil carbon cycling

Radiocarbon

Soil incubation

Table of contents

Table of Contents

Table of Contents

List of Tables

List of Figures

Abbreviations

2p	two pool model
2pp	two pool parallel model
2ps	two pool series model
3pp	three pool parallel model
3ps	three pool series model
^{14}C	radiocarbon
α	proportion of output flux transferred from one model pool to another
γ	proportion of inputs partitioned to a model pool
$\Delta^{14}C_{bulk}$	$\Delta^{14}C$ of bulk soil organic matter
$\Delta^{14}C_{respired}$	$\Delta^{14}C$ of heterotrophically respired CO_2
$\Delta\Delta^{14}C$	difference in sample $\Delta^{14}C$ from $\Delta^{14}C$ of atmospheric CO_2
AIC	Aikaike's Information Criterion
AIC_c	Aikaike's Information Criterion corrected for small sample sizes
AMS	Accelerator mass spectrometry
CBCM	California Basin Characterization Model
CRM	crystalline metal oxides
DOC	dissolved organic carbon
GPS	global positioning system
k	decomposition rate
LKJ	Lewandowski-Kurowicka-Joe
LMM	linear mixed modeling
MAOM	mineral-associated soil organic matter
MAP	mean annual precipitation
MAST	mean annual soil temperature
MCMC	Markov Chain Monte Carlo
MPI-BGC	Max Planck Institute for Biogeochemistry
NEON	National Ecological Observatory Network
NEP	net ecosystem productivity
oPOM	occluded particulate organic matter
OX	sum of oxalate extractable Al and half of oxalate extractable Fe
PCM	poorly crystalline mineral
PET	potential evapotranspiration
POM	particulate organic matter
PRISM	Parameter-elevation Regressions on Independent Slopes Model
$Q10_c$	climatological Q10
RMSE	root mean square error
SOAP	Soap Root Saddle NEON site
SOC	soil organic carbon
TEAK	Lower Teakettle NEON site
UCI	University of California, Irvine
WHC	water holding capacity

1. General Introduction

1.1. Anthropogenic climate change and the global C cycle

Life as we know it exists on Earth due to the greenhouse effect, a property of the atmosphere that allows incoming solar radiation to be transmitted, but enables reabsorption of much of the longwave radiation emitted from the planet's surface. The atmosphere of the Earth is composed of 79% inert nitrogen gas, 20.9% oxygen, and small amounts of trace gases. These trace gases include the so-called greenhouse gas species, which are characterized by their ability to absorb longwave electromagnetic radiation. The most important of these trace species, with respect to the aggregate amount of heat absorbed, is carbon dioxide (CO_2). The amount of CO_2 in the atmosphere (at the time of this writing) is 422 ppm, which represents an increase in concentration of more than 50% since the start of the modern industrial era (1750), and is also the highest level reached in the past three million years (Canadell et al., 2021).

Total fossil fuel derived CO_2 emissions over the period 1750 to 2007 are estimated to be 350 Pg C, with half of the total CO_2 emitted since the year 1980 (Andres et al., 2012). Current anthropogenic C emissions are 10.8 Pg C y^{-1}, but the net rate of atmospheric CO_2 increase is about half of that amount (5.2 Pg C y^{-1}) due to the absorption of excess CO_2 by both the ocean and land sinks (2.9±0.4 Pg C y^{-1} and 3.1±0.6 Pg C y^{-1}, respectively) (Friedlingstein et al., 2022). The long-term concentration of CO_2 in the atmosphere has been maintained at nearly constant levels (280 ppm) throughout the Holocene, reflecting the balance of processes operating on time scales ranging from annual to millennial, including: physical exchanges between the ocean and atmosphere, volcanic outgassing and rock weathering, freshwater outgassing, and the give and take of photosynthesis and heterotrophic respiration (Canadell et al., 2021). We humans have substantially disrupted this balance through our ever-growing consumption of fossil fuels, a process through which we are releasing C that has been absent from the atmosphere for hundreds of millions of years — C that took tens of thousands of years to accumulate — in a matter of decades.

1.1.1 Soil C dynamics key for predicting future climate change

The fate of the land sink is a major source of uncertainty in predicting future fluxes of C in global climate models, reflecting the need for further constraints on the sensitivity of terrestrial C cycling to evolving environmental conditions (Friedlingstein et al., 2014; Huntzinger et al., 2017; Todd-Brown et al., 2018). Increases in atmospheric CO_2 concentration may lead to sequestration of additional

atmospheric CO_2 by way of increases in plant productivity. However, if environmental changes lead to losses of current soil C stocks, soils would shift from being a sink for atmospheric CO_2 to a source.

The balance of C fluxes between the soil and atmosphere is embedded in soil C transit times, i.e., the length of time that C inputs remain in the soil before returning to the atmosphere. Soil C transit times typically reflect processes of soil C persistence that operate on annual to decadal time scales, in contrast to soil C ages, which give insight into soil C persistence mechanisms operating on decadal to centennial or longer time scales (Sierra et al., 2018). In this dissertation I will demonstrate how observations of bulk soil and respired radiocarbon over time can be used to constrain estimates of ages and transit times of soil C across a range of mineralogical and climatic conditions, yielding novel insights into the sensitivity of C gains or losses.

The importance of soils in the global C cycle stems from the large amount of C stored in soils relative to other pools. Although the oceans are the largest global C reservoir (~39,500 Pg), soils are the largest terrestrial reservoir (1,700 Pg C), followed by permafrost (1,400 Pg), and vegetation (450 Pg) (Friedlingstein et al., 2022). The total amount of C in the atmosphere is just over half of the amount stored in soils (875 Pg), making the atmosphere sensitive to relatively small changes in the soil C reservoir (Paustian et al., 2019). The net flux of C from the atmosphere to the land is currently 3.1 Pg C y^{-1}, but rising CO_2 concentrations and changes in climate are predicted to alter the strength of this sink (Todd-Brown et al., 2014). However, global climate models diverge with regards to both the magnitude and direction of the predicted change (Friedlingstein et al., 2014).

Global climate models infer increases in soil C inputs over the past decades in response to increases in net ecosystem productivity (NEP) (Sitch et al., 2015); and such increases are expected to continue in the future under continued climate change (Fernández-Martínez et al., 2019). Increases in NEP are a vegetative response to the lengthening of the growing season in high latitude regions as well as the CO_2 fertilization effect, through which photosynthesis increases under elevated CO_2 and higher temperatures (Mooney et al., 1991; Schimel et al., 2015). The relative strength of these effects in the future may be offset by reductions in NEP from nutrient limitation or unfavorable climate changes, but most global C models predict overall increases in NEP the coming decades, with a commensurate increase expected for soil C inputs (Ainsworth and Rogers, 2007; Todd-Brown et al., 2014; Kolby Smith et al., 2016; Fernández-Martínez et al., 2019). Increased soil C inputs may lead to increased C storage, but both current model simulations and empirical datasets reveal a concurrent increase in heterotrophic respiration, suggesting that these additional inputs may not persist long enough in

soils to have a substantial effect on soil C stocks, or may have a priming effect on existing soil C stocks (Sitch et al., 2015; Bernal et al., 2016; Bond-Lamberty et al., 2018; Hicks Pries et al., 2017).

Decomposition rates are predicted to accelerate in the coming decades as a result of the response of the soil microbial community to rising temperatures (Crowther et al., 2016). However, empirical studies considering the effect of warming on soil C stocks lack consensus, showing gains, losses, or no discernible effect at all (Conant et al., 2011; Haddix et al., 2011; Hamdi et al., 2013; Giardina et al., 2014; Hicks Pries et al., 2017; Soong et al., 2021). One explanation for this variability is the high degree of heterogeneity in soil organic matter, which can be found in free particulate forms, occluded in aggregates, or associated with soil minerals in myriad arrangements (Lehmann and Kleber, 2015). Organic matter in these different forms is thought to differ with respect to microbial decomposability, based on turnover times assigned on the basis of differences in radiocarbon among empirically defined soil C fractions (Heckman et al., 2018). A substantial amount of the variation in the distribution of organic matter among these fractions can be explained by soil forming factors: most prominently climate, parent material, and vegetative cover (Heckman et al., 2022). Yet the sensitivity of different soil fractions to changes in environmental conditions such as temperature remains poorly quantified (Conant et al., 2011; Frey et al., 2013), as does the degree to which these fractions correspond to meaningful soil C pools in situ (Abramoff et al., 2018).

Most C that enters the soil is quickly lost, with only a small proportion remaining in the soil on decadal or longer time scales (Sierra et al., 2018). This is relevant for the uncertainty in global C fluxes in global climate models, as increases to soil C inputs would lead to minimal increases in soil C storage if they are quickly lost through respiration, but to substantial gains if inputs remain for decades or longer. This response can be inferred from transit time, with faster transit time indicating smaller gains in C per unit of input, and slower transit times indicating higher gains. Similarly, faster decomposition rates would be expected to decrease the amount of time C inputs remain in the soil, but may also lead to accelerated losses of currently sequestered C. Determining the temperature sensitivity of decomposition in soil C pools turning over at different rates remains a key challenge for understanding the impact of predicted temperature increases on the soil C reservoir (Conant et al., 2011). I provide insight into this issue in this dissertation by comparing soil C ages and transit times in soils along a gradient of MAST and across a range of parent materials. These ages and transit times must be estimated with a model, which I constrain using a time series of $\Delta^{14}C_{bulk}$ and $\Delta^{14}C_{respired}$.

1.2.   Radiocarbon as a tracer for soil C dynamics

Radiocarbon is an essential tool for quantifying the age of C in soils and the rate at which C cycles between soils and the atmosphere. The use of radiocarbon for dating organic materials began in the mid-20th century following the publication of a short letter published by Willard Libby, in which he estimated the production rate of ^{14}C via cosmic ray spallation, and suggested that enough ^{14}C should be in "radioactive equilibrium" with the biosphere to make the isotope a useful tracer for organic materials (Libby, 1946). Libby would go on to receive the Nobel Prize in chemistry for this work in 1960.

The key to the success of the radiocarbon dating technique is partly due to the regular rate of production in the stratosphere, and partly due to the time scale on which the ^{14}C atom undergoes radioactive decay. Radiocarbon has a half-life of 5730 years, which makes it useful for dating materials <70,000 y (Trumbore et al., 2016). Plants and animals carry the ^{14}C signature of the atmosphere during their lifetime as a consequence of either fixing CO_2 directly from the atmosphere or ingesting plant-derived C through the consumption of other organisms. The decay rate of ^{14}C is slow enough that there is no appreciable change in ^{14}C in the tissues of all but the longest-lived species during their lifetime. However, once the open exchange of ^{14}C with the environment stops, e.g., at the moment of death, the regular decay of ^{14}C can be used to estimate the age of the sample.

A challenge in radiocarbon measurement is the relative scarcity of the ^{14}C isotope. The common ^{12}C isotope, with six protons and six neutrons, makes up the majority of C atoms on Earth (98.89%), followed by trace amounts of the stable isotope [13]C (1.11%), which has one extra neutron. Prior to human disruption of the balance between ^{14}C production and decay, the natural abundance of the ^{14}C isotope (six protons, eight neutrons) was approximately one in every trillion atoms of C. Due to this scarcity, measurements of ^{14}C rarely refer to the absolute abundance of ^{14}C, but rather to the deviation of the [14]C:[12]C ratio from a standard. This is akin to the approach used for reporting measurements of ^{13}C, where δ^{13}C is the deviation in the ratio of [13]C:[12]C of the sample relative to the universal standard, Vienna Pee Dee Belemnite. The use of standards also helps to account for biases in measurement due to the technique used, e.g., decay counting or accelerator mass spectrometry (AMS) in the case of ^{14}C, as well as differences in sample preparation between laboratories.

Differences in mass among the different isotopes of C have important implications for the way they behave in chemical reactions. Certain reactions and certain catalysts, such as biological enzymes,

discriminate against the heavier isotopes of C. These patterns of equilibrium or kinetic fractionation need to be accounted for when reporting radiocarbon. Since this fractionation is mass-dependent, discrimination against the ^{14}C isotope is roughly twice that for the ^{13}C isotope, as the mass difference between ^{14}C and ^{12}C is twice that of the difference between ^{13}C and ^{12}C. Accordingly, radiocarbon measurements are corrected for this discrimination and expressed as if the ^{13}C:^{12}C ratio of the sample had a constant value of -25‰ (denominator, Eq. 1-1).

Radiocarbon measurements must be further corrected for the process of ongoing radioactive decay in the absolute ^{14}C standard: a piece of wood from 1890, which was chosen to be representative of the pre-industrial atmosphere (Trumbore et al., 2016). Routine ^{14}C measurements rely on a reference laboratory standard, OX-1, which is derived from a crop of sugar beets grown in 1955. The activity of OX-1 is corrected for radioactive decay in the universal standard over the period 1895 to 1950 (a factor of 0.95), and for its actual δ^{13}C value of -19‰. While many different units for reporting ^{14}C exist, the primary unit for reporting ^{14}C data used in this dissertation is Δ^{14}C, which is corrected for both mass-dependent fractionation and for radioactive decay in the OX-1 sample between the year of measurement (y) and 1950 (Eq. 1-1) (Stuiver and Polach, 1977).

$$^{14}C = \left[\frac{\left[\frac{^{14}C}{^{13}C}\right]_{sample,-25}}{0.95\left[\frac{^{14}C}{^{13}C}\right]_{OX-1,-19} e^{\left(\frac{y-1950}{8267}\right)}} \right] \qquad (\,1\text{-}1\,)$$

where 8267 is the true mean life of ^{14}C.

Conventional ^{14}C ages are calculated on the basis of the amount of ^{14}C remaining in a sample (Eq. 1-2), but are never an accurate estimate of true age. One reason is that the rate of stratospheric ^{14}C production varies over time, another is that the formula uses a less accurate value for the mean life of ^{14}C for consistency with earlier measurements (Stuiver and Polach, 1977). Variations in the natural production rate of ^{14}C occur due to shifts in the solar cycle, the dipole moment of the earth, and changes in the Earth's carbon cycle related to climate. These variations can be accounted for by measuring the ^{14}C content of known-age samples and using the observed differences to calibrate conventional ^{14}C ages to calendar years. Human activities over the past few centuries have also contributed substantially to the variation of atmospheric ^{14}C, in addition to natural variations in cosmogenic production. Most prominently, these changes have been due to nuclear weapon testing and the burning of fossil fuels.

$$^{14}C\ age\ =\ -8033\ln{(F)} \tag{1-2}$$

where -8033 is the Libby mean life of ^{14}C, ln(F) is the natural logarithm of fraction modern (F), and fraction modern is equivalent to the non-decay corrected value of Δ^{14}C / 1000 + 1.

Above ground nuclear weapons testing in the mid-20th century dramatically increased atmospheric ^{14}C, doubling the concentration over the decade 1955 to 1965 (**Figure 1-1**). Following the international ban on such tests in 1965, atmospheric ^{14}C levels rapidly declined as the ocean and the land absorbed the excess "bomb-C". This rapid decrease in the atmospheric ^{14}C signal had an unexpected benefit: enabling the use of the bomb-C pulse as a tracer for shorter cycling C pools with nearly annual resolution, particularly for the decades with the most rapid rate of decline (ca. 1965 to 1990) (Broecker and Olson, 1960; Trumbore, 2000). Atmospheric ^{14}C levels have largely returned to pre-bomb levels as of 2020 (Levin et al., 2022; Hua et al., 2021; Carbone et al., 2023), but due to pre-aging of soil C inputs and the presence of soil C pools cycling on decadal and longer timescales, the bomb-C pulse will remain a useful tool for determining soil C dynamics in the decades to come.

The atmospheric ^{14}C record reveals a slowly decreasing trend over the early part of the 20th century, which can also be attributed to human activity. Termed the Suess effect, the decrease in atmospheric ^{14}C is the result of the emission of radiocarbon-free CO_2 to the atmosphere from the burning of fossil fuels (Keeling, 1979). The continued burning of fossil fuels means that Suess effect is likely to become stronger in the coming decades, creating the potential for using the annual changes in atmospheric ^{14}C driven by this process as a new tool for tracing short term C cycling in the future (Graven et al., 2020).

1.2.1 Radiocarbon in soils and the power of soil archives

The use of the radiocarbon dating technique in the field of soil science began in the late 1950s (Broecker and Olson, 1960; Paul et al., 1964). A challenge with radiocarbon dating of soil organic matter is that unlike organic tissues, in which the exchange of C with the atmosphere ceases after death, soils are an open system in which C is continuously exchanged with the atmosphere (Campbell et al., 1967). In such a system the concept of a conventional radiocarbon age (Eq. 1-2) is no longer valid, and a model is necessary to estimate the age of C in soils (Trumbore, 2000). Early efforts to apply radiocarbon dating to soil C acknowledged this issue and also noted that fractionating soils according to physical or chemical properties resulted in notable differences in radiocarbon among

fractions (Broecker and Olson, 1960; Campbell et al., 1967; Scharpenseel, 1971; Goh and Molloy, 1978; Scharpenseel and Becker-Heidmann, 1992).

The number of radiocarbon measurements of bulk soils, soil fractions, and soil C fluxes has increased substantially in the first decades of the 21st century, in part due to rapid improvements in measurement technology (Lawrence et al., 2020). Early studies of radiocarbon in soils relied on decay counting, a time-consuming method that requires a large amount of sample to measure the rate of radiocarbon decay. In contrast, the method commonly used today is AMS. In AMS, ratios of $^{14}C:^{13}C:^{12}C$ are measured directly, obviating the need to wait for ^{14}C to decay. The AMS method is faster and has a lower sample requirement than decay counting, but has been cost prohibitive historically due to the relatively scarcity of capable laboratories and the need to run a high energy accelerator. Newer AMS models with lower power requirements — and a fraction of the footprint and operating costs of the older instruments — have proliferated in laboratories around the world over the past decade, with the benefit of lowering cost and access barriers for making soil radiocarbon measurements.

Unfortunately for the field of soil organic matter research, the optimal time for measuring soil radiocarbon was in the decades immediately following the bomb-C peak when the bomb-C signal was strongest. Dilution of the bomb-C signal from the contributions of more slowly cycling pools of soil C can lead to multiple solutions when applying a model to estimate ages or transit times, and this problem is exacerbated by increasing dilution. Applying time series of radiocarbon measurements is an effective approach for constraining soil C models that mitigates the problem of multiple solutions (Trumbore et al., 1996; Baisden and Canessa, 2013). Optimally, such a time series would also contain samples from the early part of the bomb-C period in order to leverage the power of the stronger bomb-C signal. Together, the utility of the time series approach and dilution of the bomb-C signal over time highlights the value of an underappreciated resource: soil archives.

Throughout this dissertation I demonstrate the power of measuring $\Delta^{14}C$ in archived soils as a tool for quantifying changes in $\Delta^{14}C$ over time, effectively reducing uncertainty in estimates of soil ages and transit times. In the first study introduced in the dissertation (Ch. 2), I outline the application of a novel approach for obtaining a time series of $\Delta^{14}C_{respired}$ by incubating archived soils, including quantification of potential biases from the processes of air-drying, rewetting, and storage. I extend these findings in the second study (Ch. 3) to quantify the change over time in $\Delta^{14}C_{bulk}$ and $\Delta^{14}C_{respired}$ for soils developed on different parent materials and under different climate regimes. In the third study (Ch. 4), I illustrate the power of $\Delta^{14}C_{bulk}$ and $\Delta^{14}C_{respired}$ time series (constructed from archived

soils) for constraining soil C models, and how such models can be used to deepen our understanding of how soil C ages and transit times vary in response to climatic and mineralogical controls.

1.2.2 Biological fractionation of soil organic matter through incubation

Separating soil organic matter into fractions that correspond to differences in assumed turnover rates is a common technique applied to the problem of soil C heterogeneity. Reported soil C ages range from < 1 to 10^6 y, and can cover multiple orders of magnitude within a single soil sample (Koarashi et al., 2012; Heckman et al., 2022). However, soil C ages can also vary within a soil fraction. Common empirical approaches that rely on chemical or physical means to fractionate soil organic matter pools have been shown to yield mixtures of different C ages when further fractionated (Sollins et al., 2009; Plante, 2013; Heckman et al., 2018), in some cases indicating that the fraction is a mixture of different pools of soil C, rather than a single homogenous pool. For this reason, a biological approach to fractionation is advantageous when the goal is to isolate a pool of faster cycling C, i.e., more readily decomposed by the microbial community, from more slowly cycling C pools that are better protected from decomposition.

Laboratory soil incubations are a simple biological fractionation method in which soil samples are placed in a sealed non-reactive container and allowed to respire, after which the respiration products can be collected and analyzed. This method is low cost, and easy to implement and scale. There are many variations on laboratory soil incubation methods, but when the goal of incubation is to assess the $\Delta^{14}C$ signal of aerobic heterotrophic respiration, the typical approach is to remove living roots, create optimal conditions for respiration with respect to temperature and moisture conditions, and to keep the duration of the incubation short.

The duration of an incubation procedure designed for measuring $\Delta^{14}C_{respired}$ must be long enough to accumulate adequate CO_2 to measure the ^{14}C signal, but typically does not extend overly long. The CO_2 respired in the initial phases of a laboratory incubation is thought to correspond more closely to the substrates consumed by the microbial community in situ, thus shorter duration incubations minimize potential effects of substrate limitation. Shorter duration incubations also have the benefit of limiting build-up of CO_2, which has an inhibitory effect on respiration at high concentrations (Šantrůčková and Šimek, 1994). A related concern is the temperature at which incubations are performed. Temperature does not affect $\Delta^{14}C_{respired}$ directly, but can have indirect effects by way of changing respiration rates. Decomposition rates increase with increasing temperature, leading to

changes in substrate use when the most preferable substrate is depleted and potentially altering $\Delta^{14}C_{respired}$ (Vaughn and Torn, 2019).

A fundamental criticism of the laboratory incubation method is the inevitable disruption of the soil that occurs prior to initiating the incubation. Disruption starts with sample collection and continues with processing of soil samples in the laboratory. For example, sieving soils disrupts macroaggregates, rearranging the spatial distribution of decomposer community and substrates and leading to potential changes in substrate use. Whether or not dead roots are removed (or if they have been partially removed) also has a strong effect on $\Delta^{14}C_{respired}$, as root C is typically younger than that of the surrounding soil organic matter. Finally, the process of rewetting soils can also lead to changes in substrate availability via potential desorption of mineral bound organic matter, osmotic lysis of microbial cells, or through simple redistribution of microbes and dissolved organic C.

Rewetting soils typically releases a burst of CO_2, a phenomenon that has been the subject of many studies over the past several decades. This rewetting pulse is often termed the "Birch effect" after the author who published seminal work on the topic in the 1950s (Birch, 1958). Many hypotheses have been put forward to explain this pulse of CO_2, including abiotic mechanisms as well as competing biological mechanisms (Williams and Xia, 2009; Warren, 2016; Brookes et al., 2017). Different mechanisms are likely to operate under different conditions, but the debate continues as to which mechanisms are the most important and under which conditions (Borken and Matzner, 2009; Schimel et al., 2011). The effect of rewetting on (non-labeled) $\Delta^{14}C_{respired}$ has received little attention, but could yield valuable insights into the potential source of the rewetting pulse.

In the first study of this dissertation (Ch. 2), I quantify the effects of air-drying, rewetting, and soil C storage on $\Delta^{14}C_{respired}$ observed in laboratory soil incubations. The results reveal different effects for soils collected from grassland versus forest ecosystems. I provide guidelines for minimizing these biases when measuring $\Delta^{14}C_{respired}$ in incubations of archived soils, and demonstrate the application of this technique for constructing time series of $\Delta^{14}C_{respired}$ in the second study of the dissertation (Ch. 3).

1.3.   Parent material and climatic control of soil C dynamics

Soil development is controlled by five primary factors: climate, organisms, relief, parent material, and time (Jenny, 1941). These soil forming factors shape and determine the rate at which primary minerals are altered to secondary mineral phases, changes in the morphology and horizonation as

the soil profile develops, and the quantity and persistence of soil organic matter (Heckman et al., 2022). Climate, and in particular temperature, along with parent material and organisms (specifically vegetation), are consistently selected as the most important variables for predicting soil C abundance and persistence globally (Batjes, 1996; Jobbágy and Jackson, 2000; Mathieu et al., 2015; Koven et al., 2017; Abramoff et al., 2019; Shi et al., 2020). These factors are not independent, however, particularly with regards to the development of specific mineral assemblages and their effect on soil organic matter dynamics (McBratney et al., 2003; Rasmussen et al., 2007; Doetterl et al., 2018).

The mixed conifer biome on the western slope of the Sierra Nevada mountains (USA) provides an ideal natural laboratory for controlling these factors. Differences in parent material along the north-south axis of the cordillera, along with regular changes in temperature with increasing elevation moving west to east, enables mineralogical effects on soil C dynamics to be separated from effects of temperature while also controlling for the effect of vegetation (Rasmussen, 2004). Rasmussen (2004) established nine sites in 2001 along this combined parent material and climate gradient, publishing several follow-up studies on soil C dynamics and weathering processes (Rasmussen et al., 2007, 2010b, 2006, 2010a, 2018b). This dissertation builds on these earlier efforts by synthesizing the existing data alongside new measurements made on archived soils from the initial sampling campaigns, and adds data from new samples collected in 2019.

The mineral assemblage of a soil is a function of parent material as well as ongoing weathering processes (Chadwick and Chorover, 2001; Chorover et al., 2004; Dixon et al., 2016). Recent work points to the primacy of the specific minerals present in the soil, rather than the total amount of clay or surface area, in controlling soil C accumulation and persistence in soils (Torn et al., 1997; Kaiser and Guggenberger, 2003; Rasmussen et al., 2018a; Possinger et al., 2020). Specifically, the presence of reactive secondary minerals with high specific surface area and poorly crystalline structure (e.g., PCMs) have been shown to be correlated with both the age and abundance of soil C across a range of parent materials and climates (Dahlgren et al., 1997; Masiello et al., 2004; Rasmussen et al., 2018b; Kramer and Chadwick, 2018; Von Fromm et al., 2021). However, PCMs tend to be most abundant in soils developed on parent materials rich in volcanic glass and feldspars, such as Andisols (Rasmussen et al., 2007; Heckman et al., 2009; Rasmussen et al., 2010b; Slessarev et al., 2022). Furthermore, the abundance of PCMs in a given soil changes in conjunction with weathering, since these secondary minerals are metastable and crystallize to form less reactive mineral species with time (Torn et al., 1997; Masiello et al., 2004).

Persistence of soil C found in association with soil minerals varies according to the strength and type of bonds present. Current understanding of the formation of mineral-organic matter associations supports a zonal model that considers the functional groups of organic molecules as well as the availability of binding sites on mineral surfaces (Kleber et al., 2007; Sollins et al., 2006; Possinger et al., 2020). This model includes the formation of microaggregates with both mineral and organic components, as well as networks of micropore structures, which have been observed to self-assemble predictably according to specific mineral assemblages (Lehmann et al., 2007; Steffens et al., 2017). The relevance of organo-mineral interactions extends beyond the bonds formed directly between mineral surfaces and organic molecules to the formation of organo-mineral complexes, held together with additional organo-organic bonds (Kleber et al., 2015; Possinger et al., 2020). Together, these findings provide further evidence that empirical fractionation methods such as size or density may not be able to distinguish between readily desorbed or exchanged material and tightly bonded material, and this has important implications for the interpretation of $\Delta^{14}C$ values from such coarsely defined organo-mineral fractions. In Ch. 5 of this dissertation, I compare the variance in $\Delta^{14}C$ measured on density fractions, bulk soil organic matter, and respired CO_2 to evaluate the benefits of these different fractionation approaches for quantifying climate and mineralogical effects on the time scales of soil C cycling, and for constraining soil C models.

Separating the effects of climate and vegetation on soil C dynamics can be challenging, given that temperature and moisture limitations control the distribution of different biomes globally, and can also affect local plant community distributions, i.e., via microclimate effects (Whittaker, 1967; Whittaker et al., 1970; Bailey, 2004). For this reason, the effect of vegetation is often controlled within studies of climatic effects on soil C dynamics. The lifecycle of the dominant vegetation also affects the amount of time C spends in the ecosystem from the time of fixation to the time of respiration, with perennial plants capable of storing C for many years before mobilizing it in new growth. This pre-aging effect (or lag time) has important implications for interpreting radiocarbon values, for example, leading to older apparent radiocarbon ages of fine roots recovered from forest soils compared to grassland soils (Solly et al., 2018). In Ch. 2 of this dissertation, I address this issue directly by assessing the differences in $\Delta^{14}C_{respired}$ observed between grassland and forest soils, and how this may affect interpretation of $\Delta^{14}C_{respired}$ in incubations of archived soils. Furthermore, in Ch. 4 I demonstrate how lag time can be estimated as a parameter in a compartmental model of soil C dynamics, as well as potential mechanisms influencing the differences in lag times observed between soils under different climate regimes and increasing soil depth.

A key question for predicting the impact of predicted temperature increases on soil C stocks due to climate change is the temperature sensitivity of soil organic matter decomposition. The overall effect of temperature on soil C dynamics is obvious from global distributions of soil C stocks and bulk soil radiocarbon values: soil C stocks are higher and $\Delta^{14}C$ values are more depleted, i.e., soil C is older, when comparing colder regions to warmer regions (Carvalhais et al., 2014; Hengl et al., 2017; Koven et al., 2017; Shi et al., 2020). However, the mean age of soil C globally is 4,830±1,730 y (integrated to 1 m depth), indicating that the global patterns of soil C stocks and $\Delta^{14}C$ reflect long term equilibrium processes and therefore may not be representative of the response of soil C stocks to a changing climate.

Temperature sensitivity of soil organic matter decomposition is commonly measured using the Q10 metric, which gives the change in respiration rates relative to a 10 °C change in temperature (Eq. 1-3) (Davidson and Janssens, 2006). The Q10 metric is derived from the Arrhenius equation (Eq. 1-4), and therefore assumes an exponential response of reaction rates to temperature (Sierra, 2012). However, observational data do not always fit this theoretical relationship. There is substantial variation in the literature for Q10 values obtained for the decomposition of soil organic matter at different sites, and particularly among empirically defined "labile" and "resistant" soil organic matter pools (Haddix et al., 2011; Karhu et al., 2019; Lugato et al., 2021).

$$Q_{10} = \frac{K_{T+10}}{K_T} \qquad (1\text{-}3)$$

where K_T is the reaction/respiration rate observed at reference temperature T, and K_{T+10} is the rate observed for the same reaction at $T + 10$ °K.

$$k = A\, e^{\left(\frac{-E}{RT}\right)} \qquad (1\text{-}4)$$

where k is the reaction/respiration rate observed at reference temperature T, A is a pre-exponential factor, E is activation energy, and R is the universal gas constant.

Extending the Q10 concept to turnover times, another temperature sensitivity metric that avoids the mathematical constraints imposed by the Arrhenius equation is the "climatological Q10" (Q10$_c$), defined as the first derivative of the change in turnover time observed with respect to changes in mean annual temperature (Koven et al., 2017). Applying Q10$_c$ approach to a global dataset, with steady-state turnover time estimated as the ratio of soil C stocks to net primary production, Koven et

al. (2017) find that the temperature sensitivity of soil organic matter decomposition in warm climates is low ($Q10_c \sim 1$), but increases exponentially at mean annual temperatures < 4 °C. The authors attribute this overall trend in $Q10_c$ to environmental limitations on decomposition, e.g., slowing of microbial activity when soils are frozen. However, the authors also note that other factors, such as interactions between soil organic matter and mineral assemblages, need to be considered in order to account for the substantial amount of variation in soil C turnover times that remain unexplained by mean annual temperature (Koven et al., 2017).

In this dissertation I explicitly test the hypothesis that soil organic matter decomposition will differ among soils with different mineral assemblages but similar MAST by comparing $\Delta^{14}C_{bulk}$ and $\Delta^{14}C_{respired}$ (Ch. 3), as well as ages and transit times of soil C (Ch. 4), for the soils from the combined parent material by climate gradient study initiated by Rasmussen (2004). Rasmussen et al. (2006) measured differences in respiration rates and the size of the mineralizable soil C pool under simulated temperature increase at the same study sites considered in this dissertation, suggesting temperature sensitivity of soil organic matter decomposition may be controlled in part by mineral assemblages. I build on this work in by quantifying how much of the variance in the rate of change in soil C ages and transit times along the MAST gradient can be explained by parent material or PCM abundance (Ch. 4), and present the results of a model experiment using a space-for-time substitution to predict the effect of rising temperatures on soil C stock changes at the study sites (Ch. 5).

There are several potential ecological or soil-specific explanations for why temperature alone is inadequate for predicting soil organic matter decomposition rates. First, soils contain a large variety of different organic compounds, each with a different absolute reaction rate, as well as a specific "intrinsic temperature sensitivity of decomposition", which derives from the chemical complexity of the molecule in question and ambient temperature (Davidson and Janssens, 2006). Second, in the spatially heterogeneous soil environment, substrate limitation or enzyme availability may constrain reaction rates independently of temperature (Sollins et al., 1996). Finally, feedback from the soil environment by way of changes in soil water content, energy status of the microbial community, or physical disturbances all have the potential to affect substrate availability, enzyme production, and the probability of interaction between decomposer organisms and soil organic matter—an ecological complexity that goes well beyond simple temperature control (Schimel and Weintraub, 2003; Davidson and Janssens, 2006; Lehmann et al., 2007; Schimel and Schaeffer, 2012).

Recognizing the challenges of determining temperature sensitivity of soil organic matter a priori, newer generation soil C models typically assume different temperature sensitivities for different decomposition processes, e.g., depolymerization, microbial uptake of dissolved organic matter, and mineral adsorption and desorption, and tune the parameters for these relationships using observed data (Tang and Riley, 2014; Abramoff et al., 2019; Ahrens et al., 2020). The results from such model studies indicate that a better understanding of how mineral assemblages affect the temperature sensitivity of soil organic matter decomposition is a key factor in improving predictions of how soil C stocks will change in response to increases in temperature. In this dissertation I elucidate how mineral assemblages are related to soil C ages and transit times, with implications for improving soil C modeling as a function of parent material and weathering processes at sites beyond those explicitly considered here.

1.4.   Ages and transit times of soil C

The commonly used term "turnover time" is ambiguous when applied to bulk soil C, as it diverges from the age of soil C when bulk soil cannot be considered a single homogenous pool, or when the system is not at steady state. Given that the well-mixed assumption of a homogenous, steady-state system is not often met in soils, two more relevant terms for describing soil C dynamics are *age* and *transit time* (Manzoni et al., 2009; Sierra et al., 2017). The mean age of soil C refers to the average amount of time C remains in the soil, while the mean transit time refers to the average age of C in the release flux, e.g., respired CO_2 (Sierra et al., 2017). An important feature of heterogeneous (multi-pool) systems is that the system age differs from that obtained from a one-pool model, since it is determined by both the decomposition rates of each pool and transfers of C between pools.

A pool of soil C is considered to be homogenous by definition, meaning that all of the atoms of C in the pool have an equal probability of being decomposed under favorable conditions. The mean age and mean transit time for a pool of soil C are one and the same. The term turnover time is also equivalent to the inverse of the decomposition rate when applied to soil C pools; however, this may not be the same as the mean pool age due to pre-aging of inputs. Due to the element of stochastic chance in the process of decomposition, there exists a range of ages of soil C even within a homogenous pool. Scaling back up to the whole soil, it becomes apparent that the system age of bulk soil C is more accurately represented as a distribution of soil C ages resulting from the superposition of the age distributions of each constituent pool. Comparing bulk soil C age distributions from several commonly used global soil C models (including CENTURY, RothC, CLM, and CESM), a common feature

is that mean ages are typically substantially older than median ages (Sierra et al., 2018; He et al., 2016; Shi et al., 2020). This approach of characterizing soil C age as a distribution has important ramifications for interpreting radiocarbon measurements from bulk soil C and empirical fractions, particularly in light of the non-Gaussian distributions typically observed for soil C ages.

Bulk soil $\Delta^{14}C$ measurements are a useful proxy for the mean age of soil C, as they represent a mass-weighted average of the $\Delta^{14}C$ signal from each pool of soil C (regardless of how the pools are defined). Yet for the age distributions estimated for the soil C models mentioned above (Sierra et al., 2018), the median age is a better estimate of the central tendency of the distribution, not the mean. This reveals that both mean ages and $\Delta^{14}C_{bulk}$ are susceptible to leverage from extreme values, e.g., small pools of C cycling on centennial to millennial time scales. I will demonstrate this fact in the synthesis chapter of this dissertation by comparing $\Delta^{14}C$ distributions from modeled pools of soil C to those from empirically defined fractions, revealing the biases inherent in these different approaches.

The $\Delta^{14}C$ value of heterotrophically respired CO_2 from bulk soil is a useful proxy for mean transit time as it is a flux weighted average of the $\Delta^{14}C$ signal of C respired from each pool. Transit times are also characterized by a distribution, but one that is likely to take a different shape from the age distribution due to differing contributions to respiration from pools with different mean ages. By definition, in a steady state system, mean transit time is equivalent to the ratio between soil C stocks and fluxes. However, due to definitions of system boundaries, e.g., soil depth, and the time of year samples were collected, values of transit time estimated from radiocarbon-constrained models may not match those estimated from other methods. I will address this issue further in the context of the findings of this dissertation in Ch. 5.

1.5. Applying compartmental models to obtain age and transit time distributions

Age and transit time distributions can be computed for a compartmental model expressed by a system of linear differential equations. The general equation for such a model is

$$\frac{dC}{dt} = \mathbf{u} + \mathbf{B} \cdot \mathbf{C}\,(t) \qquad\qquad (\,1\text{-}5\,)$$

where dC/dt is the change in C over time, $\mathbf{u}$ is an *n* dimensional vector of inputs, $\mathbf{B}$ is an *n* x *n* matrix giving the decomposition rates of each pool on the diagonal and transfers between pools on the off-

diagonal, and $\mathbf{C}(t)$ is the n dimensional vector of C stocks. At steady-state this model has an analytical solution (Eq. 1-6) that returns the mean age (x^*) of the particles leaving the system.

$$x^* = -\mathbf{B}^{-1} \cdot \mathbf{u} \qquad (1\text{-}6)$$

The key principle for deriving the distributions of soil C ages and transit times from such a model is that the probability of a given atom of C being released from the system is the result of a stochastic process that is independent of the deterministic processes that control the decomposition rates and transfers defining soil C dynamics, i.e., the term $\mathbf{B}$ in Eqs. 1-5 and 1-6 (Sierra et al., 2018). Stated another way, we assume that the age of a given atom of C does not determine the probability that it will be decomposed, but rather that age is a consequence of the processes controlling which pool the atom is in, transfers between pools, and specific environmental conditions. Empirical studies provide support for this assumption, with soil samples from different depths decomposing at similar rates despite older C ages inferred at the deeper depths (Soong et al., 2021), and different size fractions of soil organic matter decomposing at similar rates despite differences in inferred C ages (Karhu et al., 2019).

The probability distribution of ages can be determined from a stochastic model which we define with a continuous-time absorbing Markov chain parameterized from the system of linear differential equations:

$$f(a) = -1^T \cdot \mathbf{B} \cdot e^{a \cdot \mathbf{B}} \cdot \frac{x^*}{\sum x^*} \qquad (1\text{-}7)$$

where a is the random variable age, $\mathbf{B}$ is an n x n matrix giving the probability that an atom of C will be transferred to other pools, -1^T is the transpose of an n dimensional vector of ones, $e^{a\mathbf{B}}$ is the matrix exponential of a, and $\sum x^*$ is the sum of C stocks for all model pools at steady-state.

The probability distribution for transit time can be computed similarly by the expression

$$f(\tau) = -1^T \cdot \mathbf{B} \cdot e^{\tau \cdot \mathbf{B}} \cdot \frac{\mathbf{u}}{\sum \mathbf{u}} \qquad (1\text{-}8)$$

where τ is the random variable transit time. The derivation of these expressions (Eqs. 1-7 and 1-8) are provided by Metzler and Sierra (2018).

These distributions provide further insight into the fate of C entering the soil that cannot be determined from $\Delta^{14}C_{bulk}$ and $\Delta^{14}C_{respired}$ alone. For example, in order to answer pertinent questions for the potential benefits of soil C sequestration such as "How long do annual C inputs remain in the soil, on average?", or "How long would 50% of one year of inputs remain in the soil? ", the relevant metrics would be the mean and median transit time, respectively (Crow and Sierra, 2022). These distributions can also be used to answer additional questions such as how much climate warming is avoided by the storage of C in soils over a given time frame by incorporating the radiative effect of a unit of CO_2 and integrating the area under the release curve of CO_2 (Sierra et al., 2021). Finally, the distribution of soil C ages in bulk soil or in particular pools of soil C can also provide valuable insight into the persistence mechanisms underlying these distributions. I illustrate these calculations of the climate benefit of C sequestration with the Sierra Nevada soils in the synthesis chapter of this dissertation (Ch. 5), and discuss implications of the estimated age distributions for soil C persistence mechanisms in Chs. 3, 4, and 5.

1.6.   Motivation and objectives

The motivation for this dissertation was to quantify how climate and mineralogical factors influence time scales of soil C cycling. Soil C plays an outsized role in the global C cycle due to the size of the reservoir. However, uncertainty regarding the response of soil C dynamics to changes in climate remains a major impediment for improving future climate predictions. Temperature has long been recognized as a key factor controlling soil C abundance and persistence, but is inadequate for explaining the variation observed in soil C dynamics—either on global scales or at the plot level. Mineral organic association is known to be a critical mechanism for long term persistence of soil C, but recent studies suggest that mineral-associated soil organic matter pools contain annual to decadally cycling components as well. Furthermore, mounting empirical evidence indicates that soil mineral assemblages influence the temperature sensitivity of soil organic matter decomposition.

The overall goal of quantifying the relative influence of climatic and mineralogical factors on time scales of soil C cycling was addressed in three studies, each of which consisted of the following specific objectives:

(Study 1) Impacts of Drying and Rewetting on the Radiocarbon Signature of Respired CO2 and Implications for Incubating Archived Soils. This study sought to quantify the effect of air-

drying/rewetting and storage duration on the $\Delta^{14}C_{respired}$, including an applied case study comparing soils from forest and grassland sites.

- **(Obj-¹⁴CIncubations)** Determine the feasibility of measuring $\Delta^{14}C_{respired}$ in laboratory incubations of archived soils.
- **(Obj-¹⁴CIncubations)** Quantify potential biases of air-drying/rewetting and storage duration on $\Delta^{14}C_{respired}$.
- **(Obj-¹⁴CIncubations)** Assess the influence of land cover (grassland vs. forest) on the $\Delta^{14}C_{respired}$ measured in incubations of archived soils.

(Study 2) Soil minerals mediate climatic control of soil C cycling on annual to centennial timescales. This study assesses the relationship of climatic and mineralogical factors to the distribution of $\Delta^{14}C_{bulk}$ and $\Delta^{14}C_{respired}$ at nine sites spanning a combined gradient of parent material and climate, as well as quantifying the change in $\Delta^{14}C_{bulk}$ and $\Delta^{14}C_{respired}$ between 2001 and 2019 as a function of climate, parent material, and depth.

- **(Obj-¹⁴CTimeseries)** Compare changes in $\Delta^{14}C_{bulk}$ and $\Delta^{14}C_{respired}$ over time as a function of parent material, climate, and depth.
- **(Obj-¹⁴CTimeseries)** Demonstrate the relative influence of specific climatic and mineralogical factors on $^{14}C_{bulk}$, $\Delta^{14}C_{respired}$, and the difference between $\Delta^{14}C_{respired}$ and $\Delta^{14}C_{bulk}$.

(Study 3) Mineralogical and climatic controls on age and transit time distributions of soil C. This study leverages the time series of $\Delta^{14}C_{bulk}$ and $\Delta^{14}C_{respired}$ measurements presented in Study 2 to constrain compartmental models of soil C dynamics, and outlines the implications for parameter identification and model selection using this approach. The relative influence of climatic and mineralogical factors on system age and transit time distributions obtained from these models are quantified, the mineralogical influence on temperature sensitivity of soil organic matter decomposition is discussed, and potential strategies for improving constraints on model pool dynamics are explored.

- **(Obj-Age&TransitTime)** Select optimal parameter sets and model structures for modeling soil C dynamics with a time series of $\Delta^{14}C_{bulk}$ and $\Delta^{14}C_{respired}$.

- **(Obj-Age&TransitTime)** Calculate the soil C inputs and lag times (pre-aging due to vertical transfers and storage in vegetation) required to satisfy soil C dynamics in radiocarbon-constrained compartmental models.
- **(Obj-Age&TransitTime)** Resolve the influences of temperature, depth, parent material, and reactive mineral content on soil C age and transit time distributions.
- **(Obj-Age&TransitTime)** Elucidate the effect of mineralogical factors on the sensitivity of soil C age and transit time distributions to mean annual temperature, including implications for potential changes in soil C stocks in response to increases in temperature.

1.7. Figures

Figure 1-1. Change in atmospheric $\Delta^{14}C$ content over time by latitudinal zone (data from Hua et al., 2021).

1.8.   References

Abramoff, R., Xu, X., Hartman, M., O'Brien, S., Feng, W., Davidson, E., Finzi, A., Moorhead, D., Schimel, J., Torn, M., and Mayes, M. A.: The Millennial model: in search of measurable pools and transformations for modeling soil carbon in the new century, Biogeochemistry, 137, 51–71, https://doi.org/10.1007/s10533-017-0409-7, 2018.

Abramoff, R. Z., Torn, M. S., Georgiou, K., Tang, J., and Riley, W. J.: Soil Organic Matter Temperature Sensitivity Cannot be Directly Inferred From Spatial Gradients, Global Biogeochemical Cycles, 33, 761–776, https://doi.org/10.1029/2018GB006001, 2019.

Ahrens, B., Guggenberger, G., Rethemeyer, J., John, S., Marschner, B., Heinze, S., Angst, G., Mueller, C. W., Kögel-Knabner, I., Leuschner, C., Hertel, D., Bachmann, J., Reichstein, M., and Schrumpf, M.: Combination of energy limitation and sorption capacity explains 14C depth gradients, Soil Biology and Biochemistry, 148, https://doi.org/10.1016/j.soilbio.2020.107912, 2020.

Ainsworth, E. A. and Rogers, A.: The response of photosynthesis and stomatal conductance to rising [CO2]: mechanisms and environmental interactions, Plant, cell & environment, 30, 258–270, 2007.

Andres, R. J., Boden, T. A., Bréon, F.-M., Ciais, P., Davis, S., Erickson, D., Gregg, J. S., Jacobson, A., Marland, G., Miller, J., Oda, T., Olivier, J. G. J., Raupach, M. R., Rayner, P., and Treanton, K.: A synthesis of carbon dioxide emissions from fossil-fuel combustion, Biogeosciences, 9, 1845–1871, https://doi.org/10.5194/bg-9-1845-2012, 2012.

Bailey, R. G.: Identifying ecoregion boundaries, Environmental management, 34, S14, 2004.

Baisden, W. T. and Canessa, S.: Using 50 years of soil radiocarbon data to identify optimal approaches for estimating soil carbon residence times, Nuclear Instruments and Methods in Physics Research, Section B: Beam Interactions with Materials and Atoms, 294, 588–592, https://doi.org/10.1016/j.nimb.2012.06.021, 2013.

Batjes, N. H.: Total carbon and nitrogen in the soils of the world, European journal of soil science, 47, 151–163, 1996.

Bernal, B., McKinley, D. C., Hungate, B. A., White, P. M., Mozdzer, T. J., and Megonigal, J. P.: Limits to soil carbon stability; Deep, ancient soil carbon decomposition stimulated by new labile organic inputs, Soil Biology and Biochemistry, 98, 85–94, https://doi.org/10.1016/j.soilbio.2016.04.007, 2016.

Birch, H. F.: The effect of soil drying on humus decomposition and nitrogen availability, Plant and Soil, 10, 9–31, https://doi.org/10.1007/BF01343734, 1958.

Bond-Lamberty, B., Bailey, V. L., Chen, M., Gough, C. M., and Vargas, R.: Globally rising soil heterotrophic respiration over recent decades, Nature, 560, 80–83, https://doi.org/10.1038/s41586-018-0358-x, 2018.

Borken, W. and Matzner, E.: Reappraisal of drying and wetting effects on C and N mineralization and fluxes in soils, Global Change Biology, 15, 808–824, https://doi.org/10.1111/j.1365-2486.2008.01681.x, 2009.

Broecker, W. S. and Olson, E. A.: Radiocarbon from Nuclear Tests, II: Future concentrations predicted for this isotope in the earth's carbon cycle suggest its use in tracer studies., Science, 132, 712–721, 1960.

Brookes, P. C., Chen, Y. F., Chen, L., Qiu, G., Luo, Y., and Xu, J.: Is the rate of mineralization of soil organic carbon under microbiological control?, Soil Biology and Biochemistry, 112, 127–139, https://doi.org/10.1016/j.soilbio.2017.05.003, 2017.

CAMPBELL, C., PAUL, E., RENNIE, D., and MCCALLUM, K.: FACTOR AFFECTING THE ACCURACY OF THE CARBONDATING METHOD IN SOIL HUMUS STUDIES, Soil Science, 104, 81–85, 1967.

Canadell, J. G., Monteiro, P. M. S., Costa, M. H., Cotrim da Cunha, L., Cox, P. M., Eliseev, A. V., Henson, S., Ishii, M., Jaccard, S., Koven, C., Lohila, A., Patra, P. K., Piao, S., Rogelj, J., Syampungani, S., Zaehle, S., and Zickfeld, K.: Global carbon and other biogeochemical cycles and feedbacks, edited by: Masson-Delmotte, V., Zhai, P., Pirani, A., Connors, S. L., Péan, C., Berger, S., Caud, N., Chen, Y., Goldfarb, L., Gomis, M. I., Huang, M., Leitzell, K., Lonnoy, E., Matthews, J. B. R., Maycock, T. K., Waterfield, T., Yelekçi, O., Yu, R., and Zhou, B., Climate change 2021: The physical science basis. Contribution of working group I to the sixth assessment report of the intergovernmental panel on climate change, 673–816, https://doi.org/10.1017/9781009157896.007, 2021.

Carbone, M. S., Ayers, T. J., Ebert, C. H., Munson, S. M., Schuur, E. A., and Richardson, A. D.: Atmospheric radiocarbon for the period 1910–2021 recorded by annual plants, Radiocarbon, 65, 357–374, 2023.

Carvalhais, N., Forkel, M., Khomik, M., Bellarby, J., Jung, M., Migliavacca, M., Mu, M., Saatchi, S., Santoro, M., Thurner, M., Weber, U., Ahrens, B., Beer, C., Cescatti, A., Randerson, J. T., and Reichstein, M.: Global covariation of carbon turnover times with climate in terrestrial ecosystems, Nature, 514, 213–217, https://doi.org/10.1038/nature13731, 2014.

Chadwick, O. A. and Chorover, J.: The chemistry of pedogenic thresholds, Geoderma, 100, 321–353, https://doi.org/10.1016/S0016-7061(01)00027-1, 2001.

Chorover, J., Amistadi, M. K., and Chadwick, O. A.: Surface charge evolution of mineral-organic complexes during pedogenesis in Hawaiian basalt, Geochimica et Cosmochimica Acta, 68, 4859–4876, https://doi.org/10.1016/j.gca.2004.06.005, 2004.

Conant, R. T., Ryan, M. G., Ågren, G. I., Birge, H. E., Davidson, E. A., Eliasson, P. E., Evans, S. E., Frey, S. D., Giardina, C. P., Hopkins, F. M., Hyvönen, R., Kirschbaum, M. U. F., Lavallee, J. M., Leifeld, J., Parton, W. J., Megan Steinweg, J., Wallenstein, M. D., Martin Wetterstedt, J. Å., and Bradford, M. A.: Temperature and soil organic matter decomposition rates - synthesis of current knowledge and a way forward, Global Change Biology, 17, 3392–3404, https://doi.org/10.1111/j.1365-2486.2011.02496.x, 2011.

Crow, S. E. and Sierra, C. A.: The climate benefit of sequestration in soils for warming mitigation, Biogeochemistry, https://doi.org/10.1007/s10533-022-00981-1, 2022.

Crowther, T. W., Todd-Brown, K. E. O., Rowe, C. W., Wieder, W. R., Carey, J. C., Machmuller, M. B., Snoek, B. L., Fang, S., Zhou, G., Allison, S. D., Blair, J. M., Bridgham, S. D., Burton, A. J., Carrillo, Y., Reich, P. B., Clark, J. S., Classen, A. T., Dijkstra, F. A., Elberling, B., Emmett, B. A., Estiarte, M., Frey, S. D., Guo, J., Harte, J., Jiang, L., Johnson, B. R., Kröel-Dulay, G., Larsen, K. S., Laudon, H., Lavallee, J. M., Luo, Y., Lupascu, M., Ma, L. N., Marhan, S., Michelsen, A., Mohan, J., Niu, S., Pendall, E., Peñuelas, J., Pfeifer-Meister, L., Poll, C., Reinsch, S., Reynolds, L. L., Schmidt, I. K., Sistla, S., Sokol, N. W., Templer, P. H., Treseder, K. K., Welker, J. M., and Bradford, M. A.: Quantifying global soil carbon losses in response to warming, Nature, 540, 104–108, https://doi.org/10.1038/nature20150, 2016.

Dahlgren, R. A., Boettinger, J. L., Huntington, G. L., and Amundson, R. G.: Soil development along an elevational transect in the western Sierra Nevada, California, Geoderma, 78, 207–236, https://doi.org/10.1016/S0016-7061(97)00034-7, 1997.

Davidson, E. A. and Janssens, I. A.: Temperature sensitivity of soil carbon decomposition and feedbacks to climate change, Nature, 440, 165–173, https://doi.org/10.1038/nature04514, 2006.

Dixon, J. L., Chadwick, O. A., and Vitousek, P. M.: Climate-driven thresholds for chemical weathering in postglacial soils of New Zealand, Journal of Geophysical Research: Earth Surface, 121, 1619–1634, https://doi.org/10.1002/2016JF003864, 2016.

Doetterl, S., Berhe, A. A., Arnold, C., Bodé, S., Fiener, P., Finke, P., Fuchslueger, L., Griepentrog, M., Harden, J. W., Nadeu, E., Schnecker, J., Six, J., Trumbore, S., Oost, K. V., Vogel, C., and Boeckx, P.: dynamics mediated by soil mineral weathering, Nature Geoscience, 11, https://doi.org/10.1038/s41561-018-0168-7, 2018.

Fernández-Martínez, M., Sardans, J., Chevallier, F., Ciais, P., Obersteiner, M., Vicca, S., Canadell, J., Bastos, A., Friedlingstein, P., Sitch, S., and others: Global trends in carbon sinks and their relationships with CO2 and temperature, Nature climate change, 9, 73–79, 2019.

Frey, S. D., Lee, J., Melillo, J. M., and Six, J.: The temperature response of soil microbial efficiency and its feedback to climate, Nature Climate Change, 3, 395–398, https://doi.org/10.1038/nclimate1796, 2013.

Friedlingstein, P., Meinshausen, M., Arora, V. K., Jones, C. D., Anav, A., Liddicoat, S. K., and Knutti, R.: Uncertainties in CMIP5 climate projections due to carbon cycle feedbacks, Journal of Climate, 27, 511–526, https://doi.org/10.1175/JCLI-D-12-00579.1, 2014.

Friedlingstein, P., O'Sullivan, M., Jones, M. W., Andrew, R. M., Gregor, L., Hauck, J., Le Quéré, C., Luijkx, I. T., Olsen, A., Peters, G. P., Peters, W., Pongratz, J., Schwingshackl, C., Sitch, S., Canadell, J. G., Ciais, P., Jackson, R. B., Alin, S. R., Alkama, R., Arneth, A., Arora, V. K., Bates, N. R., Becker, M., Bellouin, N., Bittig, H. C., Bopp, L., Chevallier, F., Chini, L. P., Cronin, M., Evans, W., Falk, S., Feely, R. A., Gasser, T., Gehlen, M., Gkritzalis, T., Gloege, L., Grassi, G., Gruber, N., Gürses, Ö., Harris, I., Hefner, M., Houghton, R. A., Hurtt, G. C., Iida, Y., Ilyina, T., Jain, A. K., Jersild, A., Kadono, K., Kato, E., Kennedy, D., Klein Goldewijk, K., Knauer, J., Korsbakken, J. I., Landschützer, P., Lefèvre, N., Lindsay, K., Liu, J., Liu, Z., Marland, G., Mayot, N., McGrath, M. J., Metzl, N., Monacci, N. M., Munro, D. R., Nakaoka, S.-I., Niwa, Y., O'Brien, K., Ono, T., Palmer, P. I., Pan, N., Pierrot, D., Pocock, K., Poulter, B., Resplandy, L., Robertson, E., Rödenbeck, C., Rodriguez, C., Rosan, T. M., Schwinger, J., Séférian, R., Shutler, J. D., Skjelvan, I., Steinhoff, T., Sun, Q., Sutton, A. J., Sweeney, C., Takao, S., Tanhua, T., Tans, P. P., Tian, X., Tian, H., Tilbrook, B., Tsujino, H., Tubiello, F., van der Werf, G. R., Walker, A. P., Wanninkhof, R., Whitehead, C.,

Willstrand Wranne, A., et al.: Global Carbon Budget 2022, Earth Syst. Sci. Data, 14, 4811–4900, https://doi.org/10.5194/essd-14-4811-2022, 2022.

Giardina, C. P., Litton, C. M., Crow, S. E., and Asner, G. P.: Warming-related increases in soil CO2 efflux are explained by increased below-ground carbon flux, Nature Climate Change, 4, 822–827, https://doi.org/10.1038/nclimate2322, 2014.

Goh, K. M. and Molloy, B. P. J.: RADIOCARBON DATING OF PALEOSOLS USING SOIL ORGANIC MATTER COMPONENTS, Journal of Soil Science, 29, 567–573, https://doi.org/10.1111/j.1365-2389.1978.tb00805.x, 1978.

Graven, H., Keeling, R. F., and Rogelj, J.: Changes to carbon isotopes in atmospheric CO2 over the industrial era and into the future, Global biogeochemical cycles, 34, e2019GB006170, 2020.

Haddix, M. L., Plante, A. F., Conant, R. T., Six, J., Steinweg, J. M., Magrini-Bair, K., Drijber, R. A., Morris, S. J., and Paul, E. A.: The Role of Soil Characteristics on Temperature Sensitivity of Soil Organic Matter, Soil Science Society of America Journal, 75, 56, https://doi.org/10.2136/sssaj2010.0118, 2011.

Hamdi, S., Moyano, F., Sall, S., Bernoux, M., and Chevallier, T.: Synthesis analysis of the temperature sensitivity of soil respiration from laboratory studies in relation to incubation methods and soil conditions, Soil Biology and Biochemistry, 58, 115–126, https://doi.org/10.1016/j.soilbio.2012.11.012, 2013.

He, Y., Trumbore, S. E., Torn, M. S., Harden, J. W., Vaughn, L. J. S., Allison, S. D., and Randerson, J. T.: Radiocarbon constraints imply reduced carbon uptake by soils during the 21st century, Science, 353, 1419–1424, https://doi.org/10.1126/science.aad4273, 2016.

Heckman, K., Welty-Bernard, A., Rasmussen, C., and Schwartz, E.: Geologic controls of soil carbon cycling and microbial dynamics in temperate conifer forests, Chemical Geology, 267, 12–23, https://doi.org/10.1016/j.chemgeo.2009.01.004, 2009.

Heckman, K., Lawrence, C. R., and Harden, J. W.: A sequential selective dissolution method to quantify storage and stability of organic carbon associated with Al and Fe hydroxide phases, Geoderma, 312, 24–35, https://doi.org/10.1016/j.geoderma.2017.09.043, 2018.

Heckman, K., Hicks Pries, C. E., Lawrence, C. R., Rasmussen, C., Crow, S. E., Hoyt, A. M., von Fromm, S. F., Shi, Z., Stoner, S., McGrath, C., Beem-Miller, J., Berhe, A. A., Blankinship, J. C., Keiluweit, M., Marín-Spiotta, E., Monroe, J. G., Plante, A. F., Schimel, J., Sierra, C. A., Thompson, A., and Wagai, R.: Beyond bulk: Density fractions explain heterogeneity in global soil carbon abundance and persistence, Global Change Biology, 28, 1178–1196, https://doi.org/10.1111/gcb.16023, 2022.

Hengl, T., De Jesus, J. M., Heuvelink, G. B. M., Gonzalez, M. R., Kilibarda, M., Blagotić, A., Shangguan, W., Wright, M. N., Geng, X., Bauer-Marschallinger, B., Guevara, M. A., Vargas, R., MacMillan, R. A., Batjes, N. H., Leenaars, J. G. B., Ribeiro, E., Wheeler, I., Mantel, S., and Kempen, B.: SoilGrids250m: Global gridded soil information based on machine learning, 1–40 pp., https://doi.org/10.1371/journal.pone.0169748, 2017.

Hicks Pries, C. E., Castanha, C., Porras, R., and Torn, M.: The whole-soil carbon flux in response to warming, Science, 355, 1420–1423, 2017.

Hua, Q., Turnbull, J. C., Santos, G. M., Rakowski, A. Z., Ancapichún, S., De Pol-Holz, R., Hammer, S., Lehman, S. J., Levin, I., Miller, J. B., Palmer, J. G., and Turney, C. S. M.: Atmospheric radiocarbon for the period 1950-2019, Radiocarbon, 64, https://doi.org/10.1017/RDC.2021.95, 2021.

Huntzinger, D. N., Michalak, A. M., Schwalm, C., Ciais, P., King, A. W., Fang, Y., Schaefer, K., Wei, Y., Cook, R. B., Fisher, J. B., Hayes, D., Huang, M., Ito, A., Jain, A. K., Lei, H., Lu, C., Maignan, F., Mao, J., Parazoo, N., Peng, S., Poulter, B., Ricciuto, D., Shi, X., Tian, H., Wang, W., Zeng, N., and Zhao, F.: Uncertainty in the response of terrestrial carbon sink to environmental drivers undermines carbon-climate feedback predictions, Scientific Reports, 7, 1–8, https://doi.org/10.1038/s41598-017-03818-2, 2017.

Jenny, H.: Factors of soil formation: a system of quantitative pedology, 1941.

Jobbágy, E. G. and Jackson, R. B.: The vertical distribution of soil organic carbon and its relation to climate and vegetation, Ecological Applications, 10, 423–436, https://doi.org/10.1890/1051-0761(2000)010[0423:TVDOSO]2.0.CO;2, 2000.

Kaiser, K. and Guggenberger, G.: Mineral surfaces and soil organic matter, European Journal of Soil Science, 54, 219–236, https://doi.org/10.1046/j.1365-2389.2003.00544.x, 2003.

Karhu, K., Hilasvuori, E., Järvenpää, M., Arppe, L., Christensen, B. T., Fritze, H., Kulmala, L., Oinonen, M., Pitkänen, J.-M., Vanhala, P., Heinonsalo, J., and Liski, J.: Similar temperature sensitivity of soil mineral-associated organic carbon regardless of age, Soil Biology and Biochemistry, 136, 107527, https://doi.org/10.1016/j.soilbio.2019.107527, 2019.

Keeling, C. D.: The suess effect: 13Carbon-14Carbon interrelations, Environment International, 2, 229–300, 1979.

Kleber, M., Sollins, P., and Sutton, R.: A conceptual model of organo-mineral interactions in soils: Self-assembly of organic molecular fragments into zonal structures on mineral surfaces, Biogeochemistry, 85, 9–24, https://doi.org/10.1007/s10533-007-9103-5, 2007.

Kleber, M., Eusterhues, K., Keiluweit, M., Mikutta, C., Mikutta, R., and Nico, P. S.: Mineral-Organic Associations: Formation, Properties, and Relevance in Soil Environments, Elsevier Ltd, 1–140 pp., https://doi.org/10.1016/bs.agron.2014.10.005, 2015.

Koarashi, J., Hockaday, W. C., Masiello, C. a., and Trumbore, S. E.: Dynamics of decadally cycling carbon in subsurface soils, Journal of Geophysical Research G: Biogeosciences, 117, G03033, https://doi.org/10.1029/2012JG002034, 2012.

Kolby Smith, W., Reed, S. C., Cleveland, C. C., Ballantyne, A. P., Anderegg, W. R., Wieder, W. R., Liu, Y. Y., and Running, S. W.: Large divergence of satellite and Earth system model estimates of global terrestrial CO2 fertilization, Nature climate change, 6, 306–310, 2016.

Koven, C. D., Hugelius, G., Lawrence, D. M., and Wieder, W. R.: Higher climatological temperature sensitivity of soil carbon in cold than warm climates, Nature Climate Change, 7, 817–822, https://doi.org/10.1038/nclimate3421, 2017.

Kramer, M. G. and Chadwick, O. A.: Climate-driven thresholds in reactive mineral retention of soil carbon at the global scale, Nature Climate Change, 8, 1104–1108, https://doi.org/10.1038/s41558-018-0341-4, 2018.

Lawrence, C., Beem-Miller, J., Hoyt, A., Monroe, G., Sierra, C. A., Stoner, S., Heckman, K., Blankinship, J., Crow, S., McNicol, G., Trumbore, S., Levine, P., Vindušková, O., Todd-Brown, K., Rasmussen, C., Hicks Pries, C., Schädel, C., McFarlane, K., Doetterl, S., Hatté, C., He, Y., Treat, C., Harden, J., Torn, M., Estop-Aragonés, C., Asefaw Berhe, A., Keiluweit, M., Marin-Spiotta, E., Plante, A., Thomson, A., Schimel, J., Vaughn, L., and Wagai, R.: An open source database for the synthesis of soil radiocarbon data: International Soil Radiocarbon Database (ISRaD) version 1.0, Earth System Science Data, 12, 61–76, https://doi.org/10.5194/essd-2019-55-RC6, 2020.

Lehmann, J. and Kleber, M.: The contentious nature of soil organic matter, Nature, 528, 60–68, https://doi.org/10.1038/nature16069, 2015.

Lehmann, J., Kinyangi, J., and Solomon, D.: Organic matter stabilization in soil microaggregates: Implications from spatial heterogeneity of organic carbon contents and carbon forms, Biogeochemistry, 85, 45–57, https://doi.org/10.1007/s10533-007-9105-3, 2007.

Levin, I., Hammer, S., Kromer, B., Preunkert, S., Weller, R., and Worthy, D. E.: RADIOCARBON IN GLOBAL TROPOSPHERIC CARBON DIOXIDE, Radiocarbon, 64, 781–791, https://doi.org/10.1017/RDC.2021.102, 2022.

Libby, W. F.: Atmospheric helium three and radiocarbon from cosmic radiation, Physical Review, 69, 671, 1946.

Lugato, E., Lavallee, J. M., Haddix, M. L., Panagos, P., and Cotrufo, M. F.: Different climate sensitivity of particulate and mineral-associated soil organic matter, Nature Geoscience, 14, 295–300, 2021.

Manzoni, S., Katul, G. G., and Porporato, A.: Analysis of soil carbon transit times and age distributions using network theories, Journal of Geophysical Research: Biogeosciences, 114, 1–14, https://doi.org/10.1029/2009JG001070, 2009.

Masiello, C. A., Chadwick, O. A., Southon, J., Torn, M. S., and Harden, J. W.: Weathering controls on mechanisms of carbon storage in grassland soils C, Global Biogeochemical Cycles, 2004.

Mathieu, J. A., Hatté, C., Balesdent, J., and Parent, É.: Deep soil carbon dynamics are driven more by soil type than by climate: a worldwide meta-analysis of radiocarbon profiles, Global Change Biology, n/a-n/a, https://doi.org/10.1111/gcb.13012, 2015.

McBratney, A. B., Mendonça Santos, M. L., and Minasny, B.: On digital soil mapping, Geoderma, 117, 3–52, https://doi.org/10.1016/S0016-7061(03)00223-4, 2003.

Metzler, H., Müller, M., and Sierra, C. A.: Transit-time and age distributions for nonlinear time-dependent compartmental systems, Proceedings of the National Academy of Sciences, 201705296, https://doi.org/10.1073/pnas.1705296115, 2018.

Mooney, H., Drake, B. G., Luxmoore, R., Oechel, W., and Pitelka, L.: Predicting ecosystem responses to elevated CO 2 concentrations, BioScience, 41, 96–104, 1991.

Paul, E. A., Campbell, C. A., Rennie, D. A., and Callumi, K. J. M.: Investigations of the dynamics of soil humus utilizing carbon dating techniques, Transactions - International Congress of Soil Science, 8, 201–207, 1964.

Paustian, K., Larson, E., Kent, J., Marx, E., and Swan, A.: Soil C sequestration as a biological negative emission strategy, Frontiers in Climate, 8, 2019.

Plante, A. F.: Distribution of Radiocarbon Ages in Soil Organic Matter by Thermal Fractionation, Radiocarbon, 55, 1077–1083, https://doi.org/10.2458/azu_js_rc.55.16310, 2013.

Possinger, A. R., Zachman, M. J., Enders, A., Levin, B. D. A., Muller, D. A., Kourkoutis, L. F., and Lehmann, J.: Organo–organic and organo–mineral interfaces in soil at the nanometer scale, Nature Communications, 11, 1–11, https://doi.org/10.1038/s41467-020-19792-9, 2020.

Rasmussen, C.: Pedogenesis, Soil Mineralogy, and Soil Carbon Dynamics in Sierra Nevada Conifer Systems of California, 246, 2004.

Rasmussen, C., Southard, R. J., and Horwath, W. R.: Mineral control of organic carbon mineralization in a range of temperate conifer forest soils, Global Change Biology, 12, 834–847, https://doi.org/10.1111/j.1365-2486.2006.01132.x, 2006.

Rasmussen, C., Southard, R. J., and Horwath, W. R.: Soil Mineralogy Affects Conifer Forest Soil Carbon Source Utilization and Microbial Priming, Soil Science Society of America Journal, 71, 1141, https://doi.org/10.2136/sssaj2006.0375, 2007.

Rasmussen, C., Dahlgren, R. A., and Southard, R. J.: Basalt weathering and pedogenesis across an environmental gradient in the southern Cascade Range, California, USA, Geoderma, 154, 473–485, https://doi.org/10.1016/j.geoderma.2009.05.019, 2010a.

Rasmussen, C., Matsuyama, N., Dahlgren, R. A., Southard, R. J., and Brauer, N.: Soil Genesis and Mineral Transformation Across an Environmental Gradient on Andesitic Lahar, Soil Science Society of America Journal, 71, 225, https://doi.org/10.2136/sssaj2006.0100, 2010b.

Rasmussen, C., Heckman, K., Wieder, W. R., Keiluweit, M., Lawrence, C. R., Berhe, A. A., Blankinship, J. C., Crow, S. E., Druhan, J. L., Hicks Pries, C. E., Marin-Spiotta, E., Plante, A. F., Schädel, C., Schimel, J. P., Sierra, C. A., Thompson, A., and Wagai, R.: Beyond clay: towards an improved set of variables for predicting soil organic matter content, Biogeochemistry, 137, 297–306, https://doi.org/10.1007/s10533-018-0424-3, 2018a.

Rasmussen, C., Throckmorton, H., Liles, G., Heckman, K., Meding, S., and Horwath, W. R.: Controls on Soil Organic Carbon Partitioning and Stabilization in the California Sierra Nevada, Soil Systems, 2018b.

Šantrůčková, H. and Šimek, M.: Soil microorganisms at different CO 2 and O 2 tensions, Folia microbiologica, 39, 225–230, 1994.

Scharpenseel, H.: Radiocarbon dating of soils–problems, troubles, hopes, Paleopedology: Origin, Nature and Dating of Paleosols. papers, 1971.

Scharpenseel, H. W. and Becker-Heidmann, P.: Twenty-Five Years of Radiocarbon Dating Soils: Paradigm of Erring and Learning, Radiocarbon, 34, 541–549, https://doi.org/10.1017/S0033822200063803, 1992.

Schimel, D., Stephens, B. B., and Joshua B. Fisher: Effect of increasing CO_2 on the terrestrial carbon cycle, Proceedings of the National Academy of Sciences, 112, 436–441, https://doi.org/10.1073/pnas.1407302112, 2015.

Schimel, J. P. and Schaeffer, S. M.: Microbial control over carbon cycling in soil, Frontiers in Microbiology, 3, 1–11, https://doi.org/10.3389/fmicb.2012.00348, 2012.

Schimel, J. P. and Weintraub, M. N.: The implications of exoenzyme activity on microbial carbon and nitrogen limitation in soil: A theoretical model, Soil Biology and Biochemistry, 35, 549–563, https://doi.org/10.1016/S0038-0717(03)00015-4, 2003.

Schimel, J. P., Wetterstedt, J. M., Holden, P. A., and Trumbore, S. E.: Drying/rewetting cycles mobilize old C from deep soils from a California annual grassland, Soil Biology and Biochemistry, 43, 1101–1103, 2011.

Shi, Z., Allison, S. D., He, Y., Levine, P. A., Hoyt, A. M., Beem-Miller, J., Zhu, Q., Wieder, W. R., Trumbore, S., and Randerson, J. T.: The age distribution of global soil carbon inferred from radiocarbon measurements, Nature Geoscience, 13, 555–559, https://doi.org/10.1038/s41561-020-0596-z, 2020.

Sierra, C. A.: Temperature sensitivity of organic matter decomposition in the Arrhenius equation: Some theoretical considerations, Biogeochemistry, 108, 1–15, https://doi.org/10.1007/s10533-011-9596-9, 2012.

Sierra, C. A., Müller, M., Metzler, H., Manzoni, S., and Trumbore, S. E.: The muddle of ages, turnover, transit, and residence times in the carbon cycle, Global Change Biology, 23, 1763–1773, https://doi.org/10.1111/gcb.13556, 2017.

Sierra, C. A., Hoyt, A. M., He, Y., and Trumbore, S. E.: Soil Organic Matter Persistence as a Stochastic Process: Age and Transit Time Distributions of Carbon in Soils, Global Biogeochemical Cycles, 32, 1574–1588, https://doi.org/10.1029/2018GB005950, 2018.

Sierra, C. A., E. Crow, S., Heimann, M., Metzler, H., and Schulze, E. D.: The climate benefit of carbon sequestration, Biogeosciences, 18, 1029–1048, https://doi.org/10.5194/bg-18-1029-2021, 2021.

Sitch, S., Friedlingstein, P., Gruber, N., Jones, S. D., Murray-Tortarolo, G., Ahlström, A., Doney, S. C., Graven, H., Heinze, C., Huntingford, C., Levis, S., Levy, P. E., Lomas, M., Poulter, B., Viovy, N., Zaehle, S., Zeng, N., Arneth, A., Bonan, G., Bopp, L., Canadell, J. G., Chevallier, F., Ciais, P., Ellis, R., Gloor, M., Peylin, P., Piao, S. L., Le Quéré, C., Smith, B., Zhu, Z., and Myneni, R.: Recent trends and drivers of regional sources and sinks of carbon dioxide, Biogeosciences, 12, 653–679, https://doi.org/10.5194/bg-12-653-2015, 2015.

Slessarev, E. W., Chadwick, O. A., Sokol, N. W., Nuccio, E. E., and Pett-Ridge, J.: Rock weathering controls the potential for soil carbon storage at a continental scale, Biogeochemistry, 157, 1–13, https://doi.org/10.1007/s10533-021-00859-8, 2022.

Sollins, P., Homann, P., and Caldwell, B. A.: Stabilization and destabilization of soil organic matter: mechanisms and controls, Geoderma, 74, 65–105, https://doi.org/10.1016/S0016-7061(96)00036-5, 1996.

Sollins, P., Swanston, C., Kleber, M., Filley, T., Kramer, M., Crow, S., Caldwell, B. A., Lajtha, K., and Bowden, R.: Organic C and N stabilization in a forest soil: Evidence from sequential density fractionation, Soil Biology and Biochemistry, 38, 3313–3324, https://doi.org/10.1016/j.soilbio.2006.04.014, 2006.

Sollins, P., Kramer, M. G., Swanston, C., Lajtha, K., Filley, T., Aufdenkampe, A. K., Wagai, R., and Bowden, R. D.: Sequential density fractionation across soils of contrasting mineralogy: Evidence for both microbial- and mineral-controlled soil organic matter stabilization, Biogeochemistry, 96, 209–231, https://doi.org/10.1007/s10533-009-9359-z, 2009.

Solly, E. F., Brunner, I., Helmisaari, H.-S., Herzog, C., Leppälammi-Kujansuu, J., Schöning, I., Schrumpf, M., Schweingruber, F. H., Trumbore, S. E., and Hagedorn, F.: Unravelling the age of fine roots of temperate and boreal forests, Nature Communications, 9, 3006, 2018.

Soong, J. L., Castanha, C., Hicks Pries, C. E., Ofiti, N., Porras, R. C., Riley, W. J., Schmidt, M. W. I., and Torn, M. S.: Five years of whole-soil warming led to loss of subsoil carbon stocks and increased CO2 efflux, Science Advances, 7, 1–9, https://doi.org/10.1126/sciadv.abd1343, 2021.

Steffens, M., Rogge, D. M., Mueller, C. W., Höschen, C., Lugmeier, J., Kölbl, A., and Kögel-Knabner, I.: Identification of distinct functional microstructural domains controlling C storage in soil, Environmental science & technology, 51, 12182–12189, 2017.

Stuiver, M. and Polach, H. A.: Reporting of 14C Data, Radiocarbon, 19, 355–363, https://doi.org/10.1017/S0033822200003672, 1977.

Tang, J. and Riley, W. J.: Weaker soil carbon–climate feedbacks resulting from microbial and abiotic interactions, Nature Clim Change, 5, 56–60, https://doi.org/10.1038/nclimate2438, 2014.

Todd-Brown, K., Zheng, B., and Crowther, T. W.: Field-warmed soil carbon changes imply high 21st-century modeling uncertainty, Biogeosciences, 15, 3659–3671, https://doi.org/10.5194/bg-15-3659-2018, 2018.

Todd-Brown, K. E. O., Randerson, J. T., Hopkins, F., Arora, V., Hajima, T., Jones, C., Shevliakova, E., Tjiputra, J., Volodin, E., Wu, T., Zhang, Q., and Allison, S. D.: Changes in soil organic carbon storage predicted by Earth system models during the 21st century, Biogeosciences, 11, 2341–2356, https://doi.org/10.5194/bg-11-2341-2014, 2014.

Torn, M. S., Trumbore, S. E., Chadwick, O. A., Vitousek, P. M., and Hendricks, D. M.: Mineral control of soil organic carbon storage and turnover, Nature, 389, 170–173, 1997.

Trumbore, S.: Age of soil organic matter and soil respiration: Radiocarbon constraints on belowground C dynamics, Ecological Applications, 10, 399–411, https://doi.org/10.1890/1051-0761(2000)010[0399:AOSOMA]2.0.CO;2, 2000.

Trumbore, S. E., Chadwick, O. A., and Amundson, R.: Rapid Exchange between Soil Carbon and Atmospheric Carbon Dioxide Driven by Temperature Change, Science, 272, 393–396, 1996.

Trumbore, S. E., Sierra, C. A., and Hicks Pries, C. E.: Radiocarbon nomenclature, theory, models, and interpretation: Measuring age, determining cycling rates, and tracing source pools, Radiocarbon and climate change: Mechanisms, applications and laboratory techniques, 45–82, 2016.

Vaughn, L. J. S. and Torn, M. S.: C evidence that millennial and fast-cycling soil carbon are equally sensitive to warming, Nature Climate Change, 9, https://doi.org/10.1038/s41558-019-0468-y, 2019.

Von Fromm, S. F., Hoyt, A. M., Lange, M., Acquah, G. E., Aynekulu, E., Berhe, A. A., Haefele, S. M., McGrath, S. P., Shepherd, K. D., Sila, A. M., and others: Continental-scale controls on soil organic carbon across sub-Saharan Africa, Soil, 7, 305–332, 2021.

Warren, C. R.: Do microbial osmolytes or extracellular depolymerisation products accumulate as soil dries?, Soil Biology and Biochemistry, 98, 54–63, https://doi.org/10.1016/j.soilbio.2016.03.021, 2016.

Whittaker, R. H.: Gradient analysis of vegetation, Biological reviews, 42, 207–264, 1967.

Whittaker, R. H., et al.: Communities and ecosystems., Communities and ecosystems., 1970.

Williams, M. A. and Xia, K.: Characterization of the water soluble soil organic pool following the rewetting of dry soil in a drought-prone tallgrass prairie, Soil Biology and Biochemistry, 41, 21–28, https://doi.org/10.1016/j.soilbio.2008.08.013, 2009.

2. Study 1

"Impacts of Drying and Rewetting on the Radiocarbon Signature of Respired CO2 and Implications for Incubating Archived Soils"

Contribution: I conceived the idea for the study, conducted the study, visualized the results, and wrote the manuscript with inputs from Susan Trumbore, Marion Schrumpf, Alison Hoyt, and Georg Guggenberger.

Keywords: soil carbon radiocarbon incubation soil carbon modeling climate change soil archives

Impacts of drying and rewetting on the radiocarbon signature of respired CO₂ and implications for incubating archived soils

Jeffrey Beem-Miller*[1], Marion Schrumpf[1], Alison M. Hoyt[2], Georg Guggenberger[3]

[1] Max-Planck-Institute for Biogeochemistry, Hans-Knöll-Str. 10, 07745 Jena, Germany

[2] Stanford University, Woods Institute for Environment

[3] Leibniz University Hannover, Herrenhäuser Straße 2, 30419, Hannover, Germany

* Correspondence: J. Beem-Miller; e-mail: jbeem@bgc-jena.mpg.de

2.1.   Abstract

The radiocarbon signature of respired CO_2 ($\Delta^{14}C_{respired}$) measured in laboratory soil incubations integrates contributions from soil carbon pools with a wide range of ages, making it a powerful model constraint. Incubating archived soils enriched by "bomb-C" from mid-20th century nuclear weapons testing would be even more powerful as it would enable us to trace this pulse over time. However, air-drying and subsequent rewetting of archived soils, as well as storage duration, may alter the relative contribution to respiration from soil carbon pools with different cycling rates. We designed three experiments to assess air-drying and rewetting effects on $\Delta^{14}C_{respired}$ with constant storage duration (Experiment 1), without storage (Experiment 2), and with variable storage duration (Experiment 3). We found that air-drying and rewetting led to small but significant ($\alpha < 0.05$) shifts in $\Delta^{14}C_{respired}$ relative to undried controls in all experiments, with grassland soils responding more strongly than forest soils. Storage duration (4–14 y) did not have a substantial effect. Mean differences (95% CIs) for experiments 1, 2, and 3 were: 23.3‰ (±6.6), 19.6‰ (±10.3), and 29.3‰ (±29.1) for grassland soils, versus −11.6‰ (±4.1), 12.7‰ (±8.5), and −24.2‰ (±13.2) for forest soils. Our results indicate that air-drying and rewetting soils mobilizes a slightly older pool of carbon that would otherwise be inaccessible to microbes, an effect that persists throughout the incubation. However, as the bias in $\Delta^{14}C_{respired}$ from air-drying and rewetting is small, measuring $\Delta^{14}C_{respired}$ in incubations of archived soils appears to be a promising technique for constraining soil carbon models.

2.2.   Plain Language Summary

Soils play a key role in the global carbon cycle by sequestering carbon from the atmosphere for decades to millennia. However, it is unclear if they will continue to do so as the climate changes. Microbial decomposition of soil organic matter returns carbon back to the atmosphere, and radiocarbon dating of this returning CO_2 ($\Delta^{14}C_{respired}$) can be used to quantify how long carbon is stored in ecosystems. Incubating archived soils could provide unique insight into soil carbon sequestration potential by quantifying the change in $\Delta^{14}C_{respired}$ over time. However, air-drying, duration of archiving, and subsequent rewetting of soils may bias estimates of sequestration potential by altering the balance of younger versus older carbon leaving the soil. We compared $\Delta^{14}C_{respired}$ from soils incubated with and without air-drying and archiving, and found that the air-dried soils appeared to release slightly older carbon than soils that had never been air-dried. The amount of time the soils were archived did not have an effect. Since the bias from air-drying and

rewetting was small, incubating archived soils appears to be a promising technique for improving our ability to model soil carbon cycling under global climate change.

2.3.   Key Points

- $\Delta^{14}C_{respired}$ measured in incubations of archived soils provides additional constraints for soil carbon models
- Air-drying and rewetting soils shifted $\Delta^{14}C_{respired}$ by 10‰–20‰ independent of the duration of storage
- Differences in direction and magnitude of $\Delta^{14}C_{respired}$ shifts between forests and grasslands depended on sampling year and system C dynamics

2.4.   Introduction

Soil carbon is a heterogeneous mixture of organic matter, some components of which persist in the soil for months or years, while others persist for centuries or millennia. The persistence of soil carbon can be understood through the concept of different "pools" of carbon, each defined by the mechanism by which carbon is stabilized in the soil and characterized by a distinct probability distribution of C ages (Sierra et al., 2018). Measuring the radiocarbon signature of heterotrophic respiration $\Delta^{14}C_{respired}$) in laboratory incubations is a powerful constraint for modeling soil carbon dynamics because it provides an integrated measure of the carbon-weighted contribution to the soil efflux from carbon pools with distinct C sources and cycling rates (Trumbore, 2000). Using archived soils to construct a time series of $\Delta^{14}C_{respired}$ has the potential to amplify the power of this model constraint, but it is unclear how air-drying, storage, and subsequent rewetting of archived soils may affect $\Delta^{14}C_{respired}$ observed in laboratory incubations.

The distribution of soil carbon among faster and more slowly cycling pools has important implications for predicting the response of the soil carbon reservoir to changes in inputs or decomposition rates resulting from climate change (Trumbore, 2000). Soils with large pools of slowly cycling carbon would be expected to sequester more carbon with increased inputs than soils dominated by fast cycling pools, while shifts in temperature or moisture regimes may affect decomposition rates differently depending on the stabilization mechanism. $\Delta^{14}C_{respired}$ reflects respiration fluxes dominated by the decomposition of fast cycling carbon in contrast to bulk soil $\Delta^{14}C$, which is dominated by large stocks of relatively slowly cycling carbon (Sierra et al., 2018). Together, these measurements can improve predictions of the response of soil C to global change.

Soil archives offer a window into the past, and incubating archived soils provides an opportunity to observe how $\Delta^{14}C_{respired}$ changes over time. The pulse of radiocarbon introduced into the biosphere from nuclear weapons testing ("bomb-C"), which peaked in the mid-20th century, serves as an ideal tracer (Trumbore, 2009). New C inputs to the soil over the decades following the bomb-C peak carry distinct annual radiocarbon signatures due to the decrease in the concentration of atmospheric ^{14}C over this period. Following the bomb-C tracer in $\Delta^{14}C_{respired}$ respired from soils collected and archived over the latter half of the 20th century and first decades of the 21st could therefore provide unique insight into decadal scale soil C dynamics.

A critical challenge for the interpretation of $\Delta^{14}C_{respired}$ data is that, due to the curvature of the bomb-C peak, there were two points in time at which the $\Delta^{14}C$ signature of atmospheric CO_2 was identical. This means observations of $\Delta^{14}C$ from just a single point in time can be fit to models with different intrinsic decomposition rates. Trumbore (2000) gives the example of a two independent, homogenous pools of soil carbon, one with an intrinsic decomposition rate (k) of 6.6 years and the second with k = 50 years, both of which would have had a $\Delta^{14}C$ of 166‰ in 1996. Observations of $\Delta^{14}C_{respired}$ measured in incubations of archived soils could help resolve this ambiguity by enabling the construction of a time series of $\Delta^{14}C_{respired}$. The trajectory of $\Delta^{14}C$ in a soil carbon pool turning over every 6.6 years is quite different from one with an intrinsic decomposition rate of 50 years making a $\Delta^{14}C_{respired}$ time series a strong additional constraint for model parameterization (Baisden et al., 2013).

Prior to long term storage soils are commonly air-dried. However, this process is known to affect biological, physical, and chemical properties of the soil (Bartlett and James, 1980; Jones et al., 2019). For example, incubation of soils following air-drying and rewetting typically leads to a rapid increase in CO_2 production, ranging from hours to several days (the Birch effect), before returning to equilibrium respiration rates (Birch, 1958). Hypothesized sources for the CO_2 released following soil rewetting include (and typically represent a combination of): lysis of microbial cells subjected to osmotic shock (Warren, 2016; Williams and Xia, 2009), disruption of soil aggregates, osmolytes released from microbes emerging from aridity-induced dormancy (Fierer and Schimel, 2003), and desorption of mineral-associated organic matter (Kaiser et al., 2015; Slessarev et al., 2020). While the impact of air-drying and rewetting on soil respiration rates has been extensively studied (Borken and Matzner, 2009; Schimel, 2018), the potential effects of air-drying, long-term storage, and rewetting on $\Delta^{14}C$-CO_2 has yet to be documented.

If air-drying and rewetting affects the relative contribution to respiration of soil organic matter pools with different intrinsic cycling rates, this should be detectable in $\Delta^{14}C_{respired}$. For example, disruption of soil aggregates following drying and rewetting would likely lead to greater accessibility of soil organic matter formerly protected from decomposition via physical occlusion. Drying followed by rewetting could also lead to desorption of organic matter sorbed to minerals, increasing the accessibility of this formerly protected substrate. If drying and rewetting mobilizes carbon from these relatively slowly cycling soil organic matter pools, the effect should be detectable as a shift in $\Delta^{14}C_{respired}$. However, if the rewetting pulse derives mainly from lysed microbial cells or the release of microbial osmolytes, little change in $\Delta^{14}C_{respired}$ would be expected.

Obtaining $\Delta^{14}C_{respired}$ measurements from incubations of archived soils would be a valuable tool for further constraining and improving soil carbon models, but first the possible effects of air-drying and rewetting, as well as the effect of storage duration, must be assessed.

We designed three experiments to answer the following questions:

1. Is $\Delta^{14}C_{respired}$ measured in incubations of soils prior to air-drying altered by the process of air-drying, storage, and subsequent rewetting?
2. What is the effect of air-drying and rewetting alone, that is without storage, on $\Delta^{14}C_{respired}$?
3. Does the duration of storage affect $\Delta^{14}C_{respired}$?

We present the results of these three experiments, along with an applied example of interpreting a time series of $\Delta^{14}C_{respired}$ constructed by incubating archived soils. Our results provide support for the utility of incubating archived soils to understand rates of soil C cycling and provide constraints for C cycle models. They also provide insight into long-standing questions about the substrates fueling rewetting pulse respiration, as well as differences in soil C dynamics between forest and grassland ecosystems. We conclude with suggestions for how best to employ the radiocarbon incubation technique with archived soils beyond our sample set.

2.5.   Materials and Methods

We devised three experiments to quantify potential shifts in $\Delta^{14}C_{respired}$ measured in laboratory soil incubations following air-drying, storage, and rewetting. All three experiments consider the effect of

air-drying followed by subsequent rewetting, but with varying storage duration, from less than 1 month (no storage) to 14 years. Experiment 1 focuses on the effects of air-drying and 7 years of storage prior to rewetting (air-dry/rewet + storage), Experiment 2 on the effect of air-drying and rewetting alone, that is without storage (air-dry/rewet), and Experiment 3 on the effect of varied storage duration (storage duration). All soils were split following sample collection, with one split air-dried, and the other refrigerated under field-moisture conditions until incubation. For each experiment we considered the undried split to be the control sample and the air-dried split to be the treatment sample.

2.5.1 Experiment 1: Air-Dry/Rewet With Long-Term Storage

2.5.1.1.　　　Experiment 1 Sample Selection and Field Sampling

Soils analyzed for Experiment 1 were collected in 2011 from plots established as part of the Biodiversity Exploratories project (Fischer et al., 2010). The samples used in this study comprise a subset of samples originally collected for a study by Solly et al. (2014). Two ecosystem types (forest and grassland) were sampled from two regions of central Germany, Schorfheide-Chorin (Central Germany 1) and Hainich-Dün (Central Germany 2). The two regions have similar climates, but are characterized by different soil textures (**Table 2-1**). We selected carbonate-free soils from three grassland plots (50 m by 50 m) and three forest plots (100 m by 100 m) in each of the two geographic regions (n total = 12 sites), using the criterion that the $\Delta^{14}C_{respired}$ observed in the 2011 incubations fell within the interquartile range observed for the ecosystem type and region. Further details on the soil collection and sampling strategy can be found in Solly et al. (2014).

2.5.1.2.　　　Experiment 1 Sample Preparation

Following sample collection, soils for Experiment 1 were sieved to <2 mm at field-moisture, and water holding capacity (WHC) was determined on a 10 g subsample. Briefly, we removed the tips from 50 ml centrifuge tubes and covered them with a fine mesh (<50 μm). We filled the tubes with soil and placed them upright with the mesh-side down in a glass dish filled with deionized water. Tubes were left overnight. The following day we moved them to a second glass dish filled with sand. We allowed the soils to drain for 30 min before weighing again to determine the amount of water absorbed. The remaining soil was then split, with one aliquot air-dried at 40°C (air-dry/rewet + storage treatment samples, *n* = 12), while the other aliquot was left at field moisture (control-1 samples, *n* = 12). Control-1 samples were stored in re-sealable plastic bags at 4°C until incubation.

After air-drying, air-dry/rewet + storage samples were placed in re-sealable plastic bags, and stored in large plastic boxes in a cool (ca. 15°C) dark room for seven years.

2.5.1.3.   Experiment 1 Incubations

Control-1 incubations were performed in 2011 on single samples due to time and space limitations within the original experiment. Soils were weighed out into 250 ml beakers and placed into 1,000 ml mason jars with airtight lids fitted with two sampling ports. The mass of soil used for control-1 incubations ranged from 45 to 75 g (air-dry equivalent), based on estimated respiration rates from previous work at the sites. Soil masses were adjusted to ensure that enough CO_2 would be respired to measure $\Delta^{14}C_{respired}$ (>0.5 mg) while at the same time preventing excessive CO_2 build-up, as this has been shown to negatively impact heterotrophic respiration (Šantrůčková and Šimek, 1994; MacFadyen, 1973).

Soil moisture content of control-1 samples was adjusted to 60% of WHC prior to sealing the jars. We moistened the soil from the top using a perforated luerlock cap attached to a 10 ml syringe that emitted water in small droplets for minimal disturbance. All control-1 samples were incubated for 4 days following moisture adjustment (the first enclosure period), after which the jars were flushed with CO_2-free air and allowed to accumulate CO_2 for a second enclosure period of 14 days.

We performed the air-dry/rewet + storage treatment incubations on the air-dried subsamples in 2018. We incubated the air-dry/rewet + storage samples in duplicate in order to quantify potential laboratory errors. Owing to a limited quantity of archived soil, we reduced the mass of soil incubated to 20 g. Using the same procedure as with control-1 samples, soil moisture content was adjusted to 60% WHC prior to flushing and sealing the jars. We maintained the same 4-day first enclosure period to capture the CO_2 released during the rewetting pulse. We determined the duration of the second enclosure period for the air-dry/rewet + storage treatment incubations according to the amount of CO_2 respired. We allowed the air-dry/rewet + storage treatment incubations to proceed until the same amount of CO_2 had been respired per g soil C as in the second enclosure period of corresponding control-1 sample incubations. Consequently, the incubation duration of the second enclosure period for the air-dry/rewet + storage treatment incubations varied (**Table 2-2**).

Headspace CO_2 concentrations for control-1 incubations were measured once at the end of the first enclosure period, but were measured daily during the first enclosure period for air-dry/rewet + storage incubations. We measured headspace CO_2 concentrations one to three times per week during

the second enclosure period for both control-1 and air-dry/rewet + storage treatment incubations, with more frequent measurements made for samples with faster respiration rates. Headspace gas samples were collected and analyzed for $\Delta^{14}C$ and $\delta^{13}C$ content at the end of both the first enclosure period and the second enclosure period for the air-dry/rewet + storage treatment incubations. However, these measurements were only made following the second enclosure period for control-1 samples. All samples were incubated at 20°C.

2.5.2 Experiment 2: Air-Dry/Rewet Without Long-Term Storage
2.5.2.1.   Experiment 2 Sample Selection and Field Sampling

We returned to the Central Germany 1 region (Hainich-Dün) in July 2019 to collect samples for Experiment 2 from the same plots originally sampled for Experiment 1 in 2011. We observed similar $\Delta^{14}C_{respired}$ across both Central Germany regions in Experiment 1, so we restricted the resampling to just Hainich-Dün to save on cost and time. At each plot ($n = 6$) we collected three cores from the same depth interval as 2011 (0–10 cm), which were then homogenized to yield one composite sample. Following the protocol from the 2011 sampling, any aboveground vegetation was clipped, and organic horizons were scraped away prior to coring at the forest plots.

2.5.2.2.   Experiment 2 Sample Preparation

Following sample collection, soils for Experiment 2 were sieved to <2 mm at field moisture, and WHC was determined on a 10 g subsample. The remaining soil was then split, with one aliquot air-dried at 40°C (air-dry/rewet treatment samples, $n = 6$), while the other aliquot was left at field moisture (control-2 samples, $n = 6$). Control-2 samples were stored in re-sealable plastic bags at 4°C until incubation. After air-drying, air-dry/rewet treatment samples were placed in re-sealable plastic bags, and stored in large plastic boxes in a cool (ca. 15°C) dark room for two months prior to incubation.

2.5.2.3.   Experiment 2 Incubations

Incubation conditions for control-2 and air-dry/rewet treatment samples were identical. Incubations were performed in duplicate. We weighed out 20 g (air-dry equivalent) of soil into 250 ml beakers and placed them into the same incubation vessels as we used for Experiment 1. Prior to sealing the jars, we adjusted the soil moisture content to 60% WHC in the same manner as Experiment 1 samples (section 2.5.1.3): either from field moisture (control-2 samples) or from the air-dried state (air-dry/rewet samples). Following moisture adjustment, jars were flushed with CO_2-free air, sealed, and

left to incubate for the 4-day first enclosure period. After the first enclosure period the jars were flushed, and CO_2 was allowed to accumulate for a second enclosure period (**Table 2-2**).

Headspace CO_2 concentrations of both contol-2 and air-dry/rewet incubations were measured following the same protocol as the air-dry/rewet + storage incubations in Experiment 1: daily during the rewetting pulse period, and one to three times per week during the second enclosure period, depending on respiration rates. Headspace gas samples were collected and analyzed for $\Delta^{14}C$ and $\delta^{13}C$ content at the end of both the rewetting pulse period and the second enclosure period. Control-2 samples were allowed to respire until >0.5 mg of CO_2-C was present in the jar headspace, which is the quantity needed to measure $\Delta^{14}C$. Incubations for the air-dry/rewet treatment samples were allowed to proceed until the same amount of CO_2 was respired per g of soil C as in the corresponding control-2 sample. All samples were incubated at 20°C.

2.5.3 Experiment 3: Storage Duration

Control-3 incubations were conducted by different investigators in different labs as part of six unrelated experiments. Due to the variation in experimental design among the control-3 incubations, we were forced to modify the incubation conditions for Experiment 3 samples slightly from the protocols followed in Experiments 1 and 2.

2.5.3.1.   Experiment 3 Sample Selection

The main criteria for sample selection for Experiment 3 were: (a) samples were split prior to original incubation, with one portion air-dried and archived in amounts adequate for a repeated incubation; (b) $\Delta^{14}C_{respired}$ was measured from soils incubated close to the time of collection following a relatively short (one to three weeks) incubation period. We sought to cover a range of storage duration times (between 4 and 14 years, constrained by the availability of samples), and a range of soil types and climatic conditions (**Supplemental Table 2-5**).

2.5.3.2.   Experiment 3 Sample Preparation

Sieving protocols varied among control-3 samples, with some samples sieved to 2-mm while others remained unsieved (**Supplemental Table 2-5**). All soils obtained for the storage duration incubations were air-dried splits made prior to control-3 incubations.

Experiment 3 Incubations

Soil mass and replication of corresponding storage duration treatment incubations varied (**Table 2-2**) according to the amount of soil material available. We kept the soil moisture the same between paired control-3 and storage duration treatment incubations. Incubation temperatures varied for control-3 incubations, but we conducted all storage duration treatment incubations at 20°C for simplicity. Although temperature has known effects on respiration rates, it has been shown that it does not affect $\Delta^{14}C_{respired}$ (Vaughn and Torn, 2019).

We did not have information on either the duration of the rewetting period or the corresponding amount of CO_2 respired during this period for all of the control-3 samples. Rather than impose a first enclosure period with an arbitrary duration, we decided to incubate the storage duration treatment samples for a single enclosure period beginning immediately after rewetting. We felt this was justified as we did not observe significant differences between first and second enclosure period $\Delta^{14}C_{respired}$ in the first two experiments (Results 2.6.2). We allowed respiration in the storage duration treatment samples to proceed until the same amount of CO_2 had been respired per g of soil C as in the second enclosure period of the corresponding control-3 sample incubations.

We measured headspace CO_2 concentrations every three days for the first two weeks of the storage duration treatment incubations, and weekly as needed thereafter; control-3 CO_2 measurement frequency varied. Aliquots of jar atmosphere were collected once the samples reached target CO_2 concentrations (7–48 mg CO_2 g C^{-1}), and then analyzed for $\Delta^{14}C$. We conducted the majority ($n = 16$) of the Experiment 3 storage duration treatment incubations in 2018 at the Max Planck Institute for Biogeochemistry (MPI-BGC) but the remainder ($n = 12$) of the treatment sample incubations were performed in 2009 at the University of California Irvine (UCI) (**Supplemental Table 2-5**).

2.5.4 Soil Analyses

Total carbon and nitrogen contents of the Central Germany samples were determined by dry combustion in a CN analyzer (Vario Max, Elementar Analysensysteme GmbH) following fine grinding with a ball-mill (Retsch MM400). Soil texture of the Central Germany samples was determined using the pipette method, following removal of organic matter (Schlichting et al., 1995). Soil property data for the samples from all other regions were obtained from the original studies (Cisneros-Dozal et al., 2006; Gaudinski et al., 2000; Hopkins et al., 2012; Solly et al., 2014; Koarashi et al., 2012) (**Table 2-2. Experimental design**).

2.5.5 Isotopic Analyses

For all three experiments, we separated CO_2 from the gas samples collected from incubation jar headspace using a vacuum line, with splits of the purified CO_2 analyzed for both $\delta^{13}C$ and $\Delta^{14}C$. Radiocarbon analyses were conducted at the MPI-BGC accelerator mass spectrometer facility (Steinhof, 2013) or the UCI W.M. Keck Facility for Accelerator Mass Spectrometry (Xu et al., 2007) (Table S5). Radiocarbon values are reported in units of $\Delta^{14}C$, defined as the deviation in parts per thousand of the ratio of ^{14}C–^{12}C from that of the oxalic acid standard measured in 1950. In order to account for potential mass-dependent fractionation effects, the $^{14}C/^{12}C$ ratio of all samples is corrected to a common $\delta^{13}C$ value of −25 ‰ (Stuiver and Polach, 1977). Although the effect was small, $\Delta^{14}C$ data from air-dry/rewet + storage samples (Experiments 1 and 3) were also corrected for depletion of ^{14}C in the samples due to radioactive decay occurring during storage.

Measurements of $\delta^{13}C$ (Experiments 1 and 2 only) were made at MPI-BGC (Delta⁺XL, Thermo Finnigan). Data are reported using $\delta^{13}C$ notation, which refers to the deviation in parts per thousand of the ratio of $^{13}C/^{12}C$ in the Vienna Pee Dee Belemnite standard.

2.5.6 Statistical Analysis

We compared the mean differences between treatment and control sample $\Delta^{14}C_{respired}$ and $\delta^{13}C$-CO_2 within ecosystem types for each experiment in order to assess the significance of the treatment effects. We quantified the analytical error associated with the radiocarbon incubation method by calculating the mean of the variance measured among replicates for all samples that were replicated. For samples that were not replicated we used the mean of the replicate variance measured across all samples. First we calculated mean differences between control and treatment samples, and the variance of this mean difference, and then we determined the mean and variance of the pooled sample. We calculated pooled statistics separately for forest and grassland soils in Experiments 1 and 2. Statistics were aggregated across ecosystem type for Experiment 3 as the direction of trend was the same for both forest and grassland soils (in this experiment), and we only had a limited number of grassland soils (n = 3).

The pooled mean is simply the average of the individual sample means weighted by the number of replicates. We determined the pooled variance (Eq. 2-1) using the method of O'Neil (2014), which takes into account both sampled and unsampled variance for a finite population. We used this

variance to determine 95% confidence intervals around the pooled mean difference, which we deemed significant if the confidence interval did not overlap zero.

$$S_N^2 = \frac{\sum (n_i - 1)\, s_i^2 + \sum[n_i \cdot (\bar{x}_i - \bar{X})]}{N - 1} \qquad (2\text{-}1)$$

We conducted a parallel analysis using a linear mixed model approach, which we found supported our main findings with the paired difference approach. We decided to present only the results from the paired difference analysis in the interest of simplicity. However, details of the linear mixed model analysis and the results are provided in the supporting information (section 2.9). We also conducted an exploratory analysis on the effect of the amount of C respired and the change in soil moisture content on the difference between control and treatment sample $\Delta^{14}C_{respired}$.

All statistical analyses were performed in R (R Core Team, 2020).

2.5.7 Conceptual Model

We developed a conceptual model for the forested sites from a single region, Hainich-Dün (Central Germany 2), to illustrate potential sources for the carbon respired following the air-drying and rewetting treatments imposed in this study. We did not use the $\Delta^{14}C_{respired}$ data observed in our study to constrain the model, but rather used a model developed for forested sites in the same region to validate our findings (Schrumpf and Kaiser, 2015). We implemented a two-pool parallel model, with inputs partitioned between slow and fast cycling soil C pools and no transfers between pools, using the Soil R package (Sierra et al., 2014). In an earlier study, Schrumpf and Kaiser (2015) estimated first order C cycling rates and pool sizes for empirically defined soil C pools using a density fractionation procedure. We approximated the inverse of the first order cycling rates (turnover times) for the fast and slow pools of our model using Schrumpf and Kaiser (2015)'s empirical estimates for the free light fraction and the heavy fraction from the 0–5 cm depth increment: 4 and 115 years for the fast and slow pools, respectively. Schrumpf and Kaiser (2015) found that 10% of the carbon in the 0–5 cm depth layer was in the free light fraction. We used this proportion to partition soil C between the fast and slow pools, under the assumption that the free light fraction corresponds to the fast pool. Following the earlier study, we assumed a lag time of 8 years for inputs.

2.6. Results

2.6.1 Respiration Rates

We observed consistent differences between control and treatment sample respiration rates in Experiments 1 and 2, with control sample respiration rates lower than treatment sample respiration rates in both experiments (**Figure 1-1**). However, the magnitude and timing of maximum respiration rates diverged among experiments and between grassland and forest soils (**Figure 1-1**). Maximum respiration rates were more than twice as high in grassland soils than in forest soils for air-dry/rewet + storage treatment samples in Experiment 1 (**Figure 1-1a**), but were similar across ecosystem types for the air-dry/rewet treatment samples in Experiment 2 (**Figure 1-1b**). See **Supplemental Figure 2-1** for Experiment 3 sample respiration rates. However, CO_2 flux rates cannot be meaningfully interpreted for these samples given the differences in incubation temperature, the degree to which rewetting pulse CO_2 was included in the control-3 incubations, and the wide variation in CO_2 measurement frequency among samples.

2.6.2 First and Second Enclosure Period $\Delta^{14}C_{respired}$ and $\delta^{13}C$-CO_2

We did not see significant differences when we compared $\Delta^{14}C_{respired}$ from the first enclosure period to that of the second enclosure period (**Figure 2-1**). This was true for all comparisons made within experiment, treatment, and ecosystem groups, with one exception: grassland control-2 samples had slightly higher $\Delta^{14}C_{respired}$ in the second enclosure period compared to the first (mean difference = 10.4‰, 95% CI = [6.0‰, 14.8‰]). When we combined data across experiments, ecosystem types, and treatments, the mean difference in $\Delta^{14}C_{respired}$ between enclosure periods was only 2.0‰ (95% CI = [−1.0‰, 5.0‰]), which is similar to the reported precision for ^{14}C measurements (1.7‰–2.7‰). (We excluded the forest control-2 sample that was clearly an outlier (**Figure 2-1**) from this combined analysis).

We note that, due to lower respiration rates during the first enclosure period, only three of the six forest soils in the air-dry/rewet + storage treatment group from Experiment 1 (**Figure 2-1**) generated enough CO_2 to measure radiocarbon content. In addition, it was not possible to compare $\Delta^{14}C_{respired}$ across enclosure periods for the control-1 samples as $\Delta^{14}C_{respired}$ of the first enclosure period was not measured in 2011.

In contrast to $\Delta^{14}C_{respired}$, we did observe significant differences between the $\delta^{13}C\text{-}CO_2$ of the first enclosure period and that of the second enclosure period for the forest soils in the air-dry/rewet + storage treatment group in Experiment 1 (mean difference = −1.16‰, 95% CI = [−1.69‰, −0.63‰]) and the control-2 grassland soils (Experiment 2) (mean difference = 0.85‰, 95% CI = [0.64‰, 1.07‰]) (**Supplemental Figure 2-1**). Note that as with $\Delta^{14}C$, $\delta^{13}C\text{-}CO_2$ was not measured for the first enclosure period of control-1 incubations.

2.6.3 Overall Treatment Effects on $\Delta^{14}C_{respired}$ and $\delta^{13}C\text{-}CO_2$

We observed consistent differences between control and treatment sample $\Delta^{14}C_{respired}$ in the second enclosure period in all three experiments (**Table 2-3**). Treatment sample incubations typically resulted in differences between 20‰ and 40‰ relative to control sample incubations, although the majority of the differences were within ±20‰ (dashed lines, **Figure 2-3**). The samples from Oak Ridge are an exception in that mean difference in $\Delta^{14}C_{respired}$ between storage treatment samples and corresponding control-3 samples was −44.0‰ (**Table 2-3**).

Forest and grassland soil $\Delta^{14}C_{respired}$ shifted in opposite directions following treatment in Experiment 1: the air-dry/rewet + storage treatment led to depletion in forest soils, but enrichment in grassland soils (**Table 2-3**). In contrast, both forest and grassland soils in Experiment 2 responded to the air-dry/rewet treatment with enrichment in $\Delta^{14}C_{respired}$. Experiment 3 treatment sample $\Delta^{14}C_{respired}$ tended to be depleted relative to the controls (points below the 1:1 line in **Figure 2-3**) for the majority of forest and grassland soils.

We did not find evidence of a substantial effect of the amount of C respired on $\Delta^{14}C_{respired}$, nor consistent effects due to the change in soil moisture (**Supplemental Figure 2-7**, **Supplemental Figure 2-8**).

Treatment samples in Experiment 1 and Experiment 2 showed significant differences ($\alpha = 0.05$) in $\delta^{13}C\text{-}CO_2$ relative to the controls for both forest and grassland soils (**Supplemental Figure 2-6**). Overall differences in $\delta^{13}C\text{-}CO_2$ were slightly larger for forest soils than in grassland soils (**Table 2-3**). Note that comparisons of $\delta^{13}C\text{-}CO_2$ were not made in Experiment 3 owing to a lack of data for the control-3 samples.

2.6.4 Storage Duration Effect on $\Delta^{14}C_{respired}$

We used data from both Experiment 1 and Experiment 3 to assess the effect of storage duration. The longest duration of storage was 14 years, while the shortest was 5 years. Over this range of time, we did not observe a trend in the difference between control and treatment $\Delta^{14}C_{respired}$ with increasing duration of storage (**Figure 2-4**).

2.6.5 Time Series Analysis of $\Delta^{14}C_{respired}$ (Experiments 1 and 2)

For the sites sampled in both 2011 (Experiment 1) and 2019 (Experiment 2), the absolute value of the mean difference in $\Delta^{14}C_{respired}$ between control and treatment samples was greater in grassland samples than in forest samples at both time points (**Table 2-3**). In addition to the absolute values of $\Delta^{14}C_{respired}$, the difference between $\Delta^{14}C_{respired}$ and the atmosphere in the year of sampling ($\Delta\Delta^{14}C$) is a useful indicator of soil C transit times, i.e., the duration of time from when CO_2 was fixed from the atmosphere to when it leaves the soil via respiration. We observed that sample $\Delta^{14}C_{respired}$ was enriched relative to the atmosphere across ecosystem types for all both control and treatment samples at all timepoints, that is $\Delta\Delta^{14}C$ values were all positive (**Figure 2-5**, **Table 2-3**). We measured lower $\Delta\Delta^{14}C$ values for grassland samples than forest samples in both 2011 and 2019, meaning grassland sample $\Delta^{14}C_{respired}$ was closer to the atmosphere than forest sample $\Delta^{14}C_{respired}$ (**Table 2-3**). Within ecosystem types, control sample $\Delta\Delta^{14}C$ values were lower than treatment samples for both 2011 and 2019 grassland soils, as well as the 2019 forest soils. However, we observed the opposite trend for the 2011 forest soils: for these soils the treatment sample $\Delta^{14}C_{respired}$ was closer to the atmosphere than control sample $\Delta^{14}C_{respired}$.

2.7. Discussion

2.7.1 How Closely do Incubations of Archived, Air-Dried and Rewetted Soils Match Results From Fresh Soil Incubations?

The results from all three experiments in this study show that measuring $\Delta^{14}C_{respired}$ in incubations of air-dried and archived soils is a promising technique for constructing time series of respired $\Delta^{14}C_{respired}$ and constraining soil carbon models. We observed that air-drying and rewetting shifted observed $\Delta^{14}C_{respired}$ relative to control incubations of soils that had never been air-dried, but these differences were relatively small: on the order of 10‰–25‰ (excluding the samples from the Oak Ridge labeling experiment, **Table 2-3**). However, differences between control and treatment

$\Delta^{14}C_{respired}$ were significant for all three experiments (**Table 2-3**), suggesting that the process of drying and rewetting leads to utilization of substrates with distinct $\Delta^{14}C$ signatures.

2.7.2 Effects of Air-Drying and Rewetting on the Age of Respired CO₂

We suggest that air-drying and rewetting mobilizes carbon from more slowly cycling pools than would be available to the microbial community in soils that did not undergo air-drying and rewetting. Given the trajectories of $\Delta^{14}C$ in slow and fast cycling soil carbon pools over time, we can expect different responses to air-drying and rewetting in $\Delta^{14}C_{respired}$ in soils sampled at different times. The time series data from the Hainich-Dün sites sampled in both 2011 and 2019 provide a case-study for this behavior. At these sites we observed enrichment in $\Delta^{14}C_{respired}$ following air-drying and rewetting for the forest soils collected in 2019 (Experiment 2) and the grassland soils collected in both 2011 (Experiment 1) and 2019 (Experiment 2), but depletion in the forest soils collected in 2011 (Experiment 1). We present an empirical model of soil C dynamics developed at the Hainich-Dün forest site in a previous study (Schrumpf and Kaiser, 2015) in order to illustrate the importance of the year of sampling and system-specific carbon dynamics in interpreting $\Delta^{14}C_{respired}$ following air-drying and rewetting (**Figure 2-6**).

Comparing model projections of the trajectories for fast, slow and respired $\Delta^{14}C$ with the $\Delta^{14}C_{respired}$ measured in this study (**Figure 2-6**) indicates that our data are consistent with the mobilization of carbon from the slow C pool following drying and rewetting. Following treatment, $\Delta^{14}C_{respired}$ (black points) shifts toward the slow pool $\Delta^{14}C$ curve (dashed blue line), indicating an increased contribution to respiration from this pool. Due to the crossing of the slow and fast (magenta) pool curves in 2015, increased contribution of the slow pool to respiration following air-drying and rewetting leads to relative depletion of $\Delta^{14}C_{respired}$ in 2011, but relative enrichment of $\Delta^{14}C_{respired}$ in 2019. Thus, the bias in $\Delta^{14}C_{respired}$ introduced by air-drying and rewetting could be either higher or lower relative to a sample incubated without air-drying depending on the year of sampling.

2.7.3 Explaining Differences in Forest Versus Grassland Soil $\Delta^{14}C_{respired}$ in Experiments 1 and 2

A key difference in carbon cycling between forest and grassland ecosystems is the potential for carbon storage in woody tissues after it is fixed from the atmosphere (Gaudinski et al., 2000). Carbon entering the soil in forest ecosystems may be "pre-aged" compared to inputs in grassland ecosystems.

Earlier work in some of the same Central Germany forest and grassland ecosystems analyzed in this study (the Hainich-Dün and Schorfheide-Chorin regions) provides support for the pre-ageing of carbon in forest ecosystems: Solly et al. (2014) found the mean age of the carbon in fine roots in the forest ecosystems to be approximately 10 years, in comparison to 1–2 years for fine roots in the grassland ecosystems. This pre-aging, or lag effect, for fine root inputs may explain the greater $\Delta\Delta^{14}C$ values seen for the respiration from forest ecosystems as compared to the grassland ecosystems in this study (**Table 2-3**).

In contrast to forests, the grassland soils responded to the air-drying and rewetting treatment with relative enrichment in $\Delta^{14}C_{respired}$ in both 2011 (Experiment 1) and in 2019 (Experiment 2) (**Figure 2-5**). However, we believe that the grassland soil response is due to the same mechanism as in the forest soils: a greater contribution of more slowly cycling carbon to respiration following air-drying and rewetting. The smaller positive $\Delta\Delta^{14}C$ values we observed in grassland soils, in addition to the known shorter 'lag' effect, suggest that overall C cycling rates are faster in grasslands than in forests, which would lead to an earlier crossing of the ^{14}C curves for the fast and slow cycling soil carbon pools (see **Figure 2-6**). Our results indicate that for the Central Germany sites we sampled in this study, this crossing occurred prior to 2011 for the grassland soils, but between 2011 and 2019 for the forest soils. If this is correct, even though the net change in $\Delta^{14}C_{respired}$ due to air-drying and rewetting differed between forests and grasslands in Experiment 1, both outcomes are still be consistent with the explanation that air-drying and rewetting mobilizes additional carbon from a more slowly cycling pool.

2.7.4 Is Rewetting Pulse CO$_2$ Derived From Different C Sources?

There are competing hypotheses for the source of CO_2 released immediately following rewetting, which seek to explain the immediate increase in respiration as well as the subsequent return to basal respiration rates (Fierer and Schimel, 2003; Kaiser et al., 2015; Slessarev et al., 2020; Warren, 2016; Williams and Xia, 2009). Due to the often dramatic differences in respiration rates between the rewetting period and subsequent respiration (e.g., **Figure 1-1**), previous authors posit differences in the substrates fueling rewetting versus subsequent respiration. However, we did not find a significant difference in $\Delta^{14}C_{respired}$ between these two respiration periods. This finding was true for all of the samples in which we measured $\Delta^{14}C_{respired}$ in both the rewetting pulse period and a second enclosure period (**Figure 2-3**). These results suggest that the change in substrate availability initiated by air-drying and rewetting may not be limited to the rewetting pulse.

There is a large body of literature that provides evidence for different chemistry of the substrates fueling the rewetting pulse compared to that of the substrates fueling basal respiration (Williams and Xia, 2009; Wu and Brookes, 2005; Xiang et al., 2008; Franzluebbers et al., 2000). However, as other recent work has shown, persistence of soil organic matter is not solely due to chemistry (Dungait et al., 2012; Lützow et al., 2006; Marschner et al., 2008; Schmidt et al., 2011). The similarity in $\Delta^{14}C$ across substrates utilized in the rewetting pulse and the second enclosure period, despite likely diverging in chemistry (cf. change in $\delta^{13}C\text{-}CO_2$, **Table 2-3** and **Supplemental Figure 2-6**), is therefore in line with the modern paradigm (Lehmann and Kleber, 2015; Lehmann et al., 2020). Alternatively, microbial recycling over the relatively short duration of the incubations in this study (mean = 9 d) could also explain the lack of change in $\Delta^{14}C_{respired}$ between enclosure periods. For context, we note that the mean amount of CO_2 respired in the incubations in this study was 0.8% of the initial total soil organic carbon. This microbial recycling hypothesis is also supported by the shifts in $\delta^{13}C$ observed between the rewetting pulse and the second enclosure period, which we did find to be significant.

While it is beyond the scope of this study, the age of C released has potential to help refine hypotheses about underlying mechanisms. For example, the decomposition of older, physically protected organic matter via disruption of aggregates (Kaiser et al., 2015) could be consistent with our observations, which could be tested by comparing measurements of C isotopes in physically separated aggregates to those in respired CO_2. Similarly, future experiments could be designed to investigate more specific hypotheses regarding extracellular versus microbially derived sources for fueling the rewetting pulse. For example, comparing C isotopes in microbial phospholipid fatty acids (PLFA) versus those in water extractable organic C to what is respired before and after air-drying and rewetting would be one approach for assessing the relative importance of microbial recycling versus mineral-associated C (Slessarev et al., 2020).

2.7.5 Implication of $\delta^{13}C\text{-}CO_2$ Shifts Following Drying and Rewetting

The consistent enrichment in $\delta^{13}C\text{-}CO_2$ seen following both the air-dry/rewet + storage treatment and the air-dry/rewet treatment (**Table 2-3**, **Supplemental Figure 2-5**) could have multiple possible causes. Microbial recycling has been shown to lead to $\delta^{13}C$ enrichment (Wynn et al., 2005), and to be enhanced following air-drying and rewetting (Brödlin et al., 2019; Slessarev et al., 2020). If the carbon substrate responsible for the rewetting pulse is derived from mobilization of older, microbially processed, and/or mineral-associated C, increases in $\Delta^{14}C_{respired}$ and $\delta^{13}C\text{-}CO_2$ such as those observed in both the air-dry/rewet and the air-dry/rewet + storage samples could be expected

(Wynn et al., 2005). As noted previously, the $\Delta^{14}C$ unit accounts for mass-dependent fractionation effects, thus this phenomenon does not affect the radiocarbon results as reported.

We observed greater enrichment of $\delta^{13}C\text{-}CO_2$ in forest soils than in grassland soils, which could indicate greater microbial recycling in forest soils or potentially more mobilization of mineral-associated organic matter in forest soils than in grassland soils following treatment. Mineral-associated organic matter has been shown to be more enriched in $\delta^{13}C$ as well as older on average than bulk soil organic matter (Schrumpf et al., 2013). This combination of observations indicates that more mineral-associated organic carbon may have been released upon rewetting in the forest soils than in the grassland soils. However, the similarity in the direction of the $\delta^{13}C\text{-}CO_2$ response across forest and grassland soils (**Supplemental Figure 2-5**) suggests that a similar mechanism is at work in both ecosystems.

2.7.6 Assessing Potential Storage Effects on $\Delta^{14}C_{respired}$

Data from Experiment 1 and Experiment 3 showed that storage duration does not have a strong effect on $\Delta^{14}C_{respired}$, at least within a period of 5–14 years (**Figure 2-4**). Nearly all of the soils incubated were from forests soils collected before 2019, and these all exhibited depletion of $\Delta^{14}C_{respired}$ following air-drying/rewet + storage treatment (**Figure 2-3**, **Figure 2-4**). However, the depletion in the forest soils was greatest in the samples from Oak Ridge (magenta triangles, **Figure 2-3**), which had been substantially enriched in $\Delta^{14}C$ above background levels through release of enriched ^{14}C from a nearby incinerator four years prior to sample collection. This and a subsequent manipulation experiment resulted in ^{14}C enrichment of both surface litter and root inputs (at levels between +400‰ and + 1,000‰) that persisted until the time of sample collection (Cisneros-Dozal et al., 2006).

One explanation for the greater shift observed for the Oak Ridge soils as compared to the nonlabeled forest soils is that for these labeled soils there is a greater difference in $\Delta^{14}C$ between the carbon fixed in the two decades prior to sampling ($\sim$80–200‰) and the labeled carbon (+400‰–1,000‰) introduced to the soil in the four years prior to sampling. The consistently lower $\Delta^{14}C_{respired}$ for samples incubated after air-drying and rewetting adds further support to the idea that C being mobilized comes primarily from CO_2 made available for decomposition from C fixed from the atmosphere >4 years previously. Alternatively, the greater difference observed in the Oak Ridge samples could indicate that the most recently fixed carbon in archived soils is lost over the storage

period. However, given that storage of air-dried samples has not been linked to substantial loss of soil C in previous studies (Blake et al., 2000), this seems unlikely.

Thus, our major finding is that incubation of archived soils can provide useful information on the dynamics of soil carbon and, in particular, be helpful for constraining models of soil carbon. As it is clear that the process of air-drying and rewetting likely mobilizes and increases the contribution of older soil C to respiration in incubations, we recommend that modern soil comparisons use the same treatment (air-drying and rewetting) when creating a time series using newly collected soils from the same location.

2.8. Conclusion

Measuring $\Delta^{14}C_{respired}$ in incubations of air-dried and archived soils is a promising technique for constructing time series of respired $\Delta^{14}C_{respired}$ and constraining soil carbon models. Air-drying and rewetting of soils led to small but significant differences in the $\Delta^{14}C$ of respired CO_2 in laboratory incubations when compared to incubations of the same soils without air-drying. The magnitudes of these differences do not appear to be affected by the duration of storage and are within 25‰ for the majority of forest soils and 40‰ for the more limited number of grassland samples studied. Samples collected and analyzed in the same laboratory had smaller differences of 12.1‰, and 20.4‰, for forest and grasslands, respectively. (For context, $\Delta^{14}C$ of atmospheric CO_2 has declined by ca. 5‰ per year between 2000 and 2015 (Graven et al., 2017).

Overall, our results demonstrate that differences in $\Delta^{14}C_{respired}$ between archived soils and what might have been observed in samples incubated prior to air-drying and rewetting depend on two key variables: the year of sample collection and the carbon dynamics of the system being studied. Determining the exact mechanism driving the differences in $\Delta^{14}C_{respired}$ is beyond the scope of this study, but our results suggest that the CO_2 released upon rewetting air-dried soils is fueled predominantly by older carbon, specifically through the mobilization of substrate from soil organic matter pools dominated by carbon fixed years to decades previously. Furthermore, this shift in $\Delta^{14}C_{respired}$ persists beyond the rewetting pulse, suggesting that simply excluding the rewetting pulse CO_2 when measuring $\Delta^{14}C_{respired}$ does not eliminate the bias introduced by air-drying and rewetting. Finally, we recommend that when comparing $\Delta^{14}C_{respired}$ between recently collected soils and archived soils, both samples should undergo the same air-drying and rewetting procedure to minimize bias.

Acknowledgments

2.9.   Supplemental Information

2.9.1 Methods: Linear mixed models

We compared the results of the paired mean difference analysis approach discussed in the main text with a linear mixed modeling (LMM) framework. For the first set of models, we set $\Delta^{14}C_{respired}$ observed in the second enclosure period as the response variable, and used sample ID as a random intercept term to account for the imbalance in the number of laboratory replicates analyzed for control versus treatment incubations. For fixed effects, we assessed the interaction of ecosystem type with treatment, as well as the three-way interaction of treatment, ecosystem type, and experiment for the combine dataset of Experiment 1 and Experiment 2 samples. We evaluated the significance of the treatment effect by looking at the contrasts between control and treatment samples across experiments but within ecosystem types. These models were also run for $\delta^{13}C$-CO_2.

We also used the LMM framework to assess changes in $\Delta^{14}C_{respired}$ and $\delta^{13}C$-CO_2 between enclosure periods. For these models we extended our initial model by adding enclosure period as an additional dependent variable. These models were restricted to the experiments and treatments where we measured the response variable in both enclosure periods (Experiment 1 treatment samples, and all Experiment 2 samples). We looked at the overall significance of the parameter estimates as well as the contrasts from this model by each experiment, treatment, and ecosystem type.

We tested the effect of storage duration on observed $\Delta^{14}C_{respired}$ using a combined dataset of Experiments 1 and Experiment 3 samples. We used $\Delta^{14}C_{respired}$ observed in the second enclosure period for all samples except the Experiment 3 treatment samples for which only a single enclosure period was observed. We constructed a linear mixed model with storage duration, treatment, and the interaction of these two variables as fixed effects. As with the previous models we allowed for a random intercept term for each sample. We did not include ecosystem type in this model as all of the grassland samples were collected at the same point in time. We also excluded the effect of experiment, since this could lead to a spurious relationship due to the change in $\Delta^{14}C$ of atmospheric CO_2 over time and the fact that samples were collected and analyzed at different times. This model was run first with and then without the Oak Ridge samples, as we considered these samples to be a separate population as they contain ^{14}C from a labelling experiment in addition to atmospheric ^{14}C.

All statistical analyses were performed in R (R Core Team 2019). We used the package lme4 (Bates et al., 2015) to perform the mixed modeling, and for contrast analysis we used the package 'emmeans'

(Lenth, 2021). We employed Tukey's honestly significant difference test to account for multiple comparisons and the Kenward-Roger method for estimating degrees of freedom, an approach which has shown to perform well for small sample sizes (Kenward and Roger, 1997).

2.9.2 Results: Linear mixed models

Contrast analysis of the LMM output shows that control-treatment differences are not significant for the forest samples, but are significant for the grassland samples in both Experiment 1 and Experiment 2 (first two columns of **Supplemental Figure 2-1**). While the results are similar to the paired difference approach used in the main text, the paired difference approach found both forest and grassland differences to be significant.

Comparing the differences observed over time when samples were treated the same at both timepoints (columns "Δ/t Ctl" and "Δ/t Trt", **Supplemental Figure 2-1**)we see significant differences for both the samples that were never air-dried ("Δ/t Ctl") and the samples that were air-dried and rewet ("Δ/t Trt"). Both differences are positive, i.e., $\Delta^{14}C_{respired}$ declined for both control and treatment samples over the period 2011 to 2019. However, we see that the difference over time appear smaller for the forest samples when comparing the difference between the treatment samples (26‰) to the difference between the control samples (49‰), although the confidence intervals overlap substantially. We believe this provides support for reliability of the archived technique when looking at changes in $\Delta^{14}C_{respired}$ over time across samples that have been air-dried and rewetted.

Finally, when comparing treatment samples that have never been air-dried (final two columns of figure), the estimated differences are skewed higher or are no longer significant. Specifically, we fail to detect a significant change in the grassland $\Delta^{14}C_{respired}$ over time when comparing control samples from 2011 to air-dried and rewet samples from 2019 (penultimate column, "Δ/t Ex1 Ctl - Ex2 Trt"). Looked at the other way, i.e., treatment $\Delta^{14}C_{respired}$ from the 2011 grassland samples compared to control grassland samples in 2019, the difference is substantially exaggerated (last column): 58‰ vs. 27‰ (ctl-ctl) or 38‰ (trt-trt). The difference is also greater for forest samples for both of these cross-treatment comparisons. These differences imply it is important to treat the soils from all time points the same in regards to air-drying and rewetting when constructing a time series using $\Delta^{14}C_{respired}$ measured on archived soils in order to minimize bias.

2.9.3 Effect of initial soil moisture contents on 2nd enclosure period $\Delta^{14}C_{respired}$

Differences in field moisture content of samples could be related to the magnitude of the shift in $\Delta^{14}C_{respired}$ observed between control and treatment sample, as control sample field moisture content varied. All treatment samples were air-dried in the laboratory prior to rewetting: a change in moisture content of zero percent water holding capacity (%WHC) to 60 %WHC. In contrast, moisture adjustment of control samples was made from field moisture, thus, for example, control samples with lower field moisture contents received a correspondingly greater water addition than wetter control samples.

In order to control for the variance in field moisture content of control samples, we looked at the relationship of the difference in the second enclosure period $\Delta^{14}C_{respired}$ observed between control and treatment samples and the change in moisture content of the control samples. If the shift in $\Delta^{14}C_{respired}$ observed in response to the air-drying and rewetting treatment were a linear function of the change in moisture content, the differences between control and treatment $\Delta^{14}C_{respired}$ should be smaller for samples with lower field moisture. However, we did not observe any consistent relationship between the difference in $\Delta^{14}C_{respired}$ in the and field moisture (**Supplemental Figure 2-8**).

We observed the strongest trend in the Experiment 2 grassland samples, but the trend was opposite to what we expected: differences in $\Delta^{14}C_{respired}$ between treatment samples and control samples were greater for drier samples than wetter samples (**Supplemental Figure 2-8**). Experiment 2 forest samples showed the expected trend, but it did not appear to be linear (**Supplemental Figure 2-8**). Given the relatively low sample number when considered within treatment and ecosystem groups (Experiment 1 n = 6, Experiment 2 n = 3), we do not consider these trends to be significant, but the data from Experiment 2 suggest that the relationship between the change in $\Delta^{14}C_{respired}$ and the magnitude of rewetting warrants further study.

2.10. Tables

Table 2-1. Mean soil properties by sampling region

| | | | | | | Nutrients | | | | Particle size | | | | | |
| | | | | | | Organic C | | Total N | | Sand | | Silt | | Clay | |
Experiment	Region[a]	Ecosystem[b]	n[c]	MAT	MAP	Mean	sd	Mean	sd	Mean	sd	Mean	sd	Mean	sd
			sites	°C	mm yr^{-1}					g kg^{-1}					
1, 2	Central Germany 1	forest	3	8.3	550	22.1	8.1	1.1	0.3	861	44	92	27	47	20
1, 2	Central Germany 1	grassland	3	8.3	550	22.8	1.5	2.2	0.1	731	99	158	75	111	31
1, 2, 3	Central Germany 2	forest	3	7.3	650	23.7	0.5	1.7	0.1	54	18	754	7	193	15
1, 2, 3	Central Germany 2	grassland	3	7.3	650	41.8	1.9	3.9	0.1	32	17	553	78	414	65
3	Oak Ridge, USA	forest	2	14.1	1360	24.9	0	1.1	0.1	-	-	-	-	-	-
3	Sierra Nevada, USA	forest	2	9.8	960	28.4	1.4	1.1	0.1	700	141	210	85	100	71
3	Harvard Forest, USA	forest	1	7.9	1075	60.0	-	-	-	-	-	-	-	-	-
3	Duke FACE, USA	forest	1	15.5	1140	16.6	-	0.8	-	-	-	-	-	-	-

[a]The Central Germany regions are from the Biodiversity Exploratory project: Schorheide-Chorin (region 1) and Hainich-Dün (region 2). Climate data for these sites are from Fischer et al. (2010). Harvard Forest nutrient data from Gaudinski et al. (2000); climate data are the ten-year averages from 1991 to 2000 (Boose and Gould, 2021); all Oak Ridge data are from Cisneros-Dozal et al. (2006); Duke FACE data are from Hopkins et al. (2012); Sierra Nevada data are from Koarashi et al. (2012). Note that not all data were available for all sites. [b]Central Germany 2, Harvard Forest, and Oak Ridge forest sites are mixed deciduous; Central Germany 2 forest sites include both coniferous and deciduous stands; Sierra Nevada and Duke FACE forest sites are exclusively coniferous. Grasslands were all cool-season grasses (C3 photosynthetic pathway). [c]See Table 2-2 for the total number of samples per experiment, and Table 2-3 for the number of samples per site per experiment.

Table 2-2. Experimental design

Experiment	n	Treatment	Reps[a]	Sampling date	Incubation date	Moisture content[b]		Enclosure period[c]					
								1st (rewetting pulse)			2nd		
						Initial	Adjusted	Time	Δ14C	δ13C	Time	Δ14C	δ13C
				year	year	% grav	% grav	days			days		
1	12	control-1	1	2011	2011	24-55 (11)	24-61 (13)	4	no	no	14	yes	yes
	12	air-dry/rewet + storage	2	2011	2018	<1	24-61 (13)	4	yes	yes	5-45	yes	yes
2	6	control-2	2	2019	2019	17-40 (10)	22-42 (9)	4	yes	yes	10-38	yes	yes
	6	air-dry/rewet	2	2019	2019	<1	22-42 (9)	4	yes	yes	7	yes	yes
3	29	control-3	1-3	1999-2011	1999-2011	6-95 (18)	18-95 (17)	1-10	no	no	5-14	yes	no
	29	storage duration	1-3	2018	2009, 2018	<1	18-95 (17)	-	-	-	5-45	yes	no

[a]Laboratory incubation replicates. [b]Min. and max. values given for control samples, with standard deviations in parentheses. Initial moisture content for treatment samples was <1% following air-drying. Moisture content was adjusted to 60% of water holding capacity for all Experiment 1 and Experiment 2 samples (Methods), but as WHC was not determined for all of Experiment 3 samples the gravimetric (grav) data is provided instead. [c]First enclosure period duration range is only taken from a subset of the samples where it was explicitly reported (n = 4, Hopkins et al., 2012 and Koarashi et al., 2012). The duration was reported as an estimate for some samples (1 week, n = 20, Cisneros-Dozal et al., 2006) or not reported at all for other samples (n = 4, Gaudinski et al., 2000). Δ14C-CO$_2$ and respiration rates from the first enclosure period were only measured for 2 of the 29 control-3 samples (Koarashi et al., 2012). As we did not find significant differences between Δ14C-CO$_2$ of the 1st and 2nd enclosure periods (Results), we decided to incubate the storage duration samples in Experiment 3 for single enclosure period in order to better control the total amount of CO$_2$ respired.

Table 2-3. $\Delta^{14}C$ and $\delta^{13}C$ of respired CO_2 in the second enclosure period[a]

				$\Delta^{14}C_{respired}$			$\delta^{13}C\text{-}CO_2$		$\Delta^{14}C_{respired}$		$\delta^{13}C\text{-}CO_2$	
Experiment[b]	Ecosystem	Treatment	n	Mean	Mean ΔΔ	sd[c]	Mean	sd[c]	Mean	CI95[c]	Mean	CI95[c]
				‰								
1	forest	air-dry/rewet + storage	6	82.2	44.9	8.8	-24.2	1.1				
1	forest	control-1	6	93.8	56.5	7.7	-26.8	0.2	-11.6	[-15.7, -7.5]	2.38	[1.83, 2.92]
1	grassland	air-dry/rewet + storage	6	77.8	40.5	11.4	-27.2	0.5				
1	grassland	control-1	6	54.5	17.2	16.8	-27.7	0.4	23.3	[16.7, 29.9]	0.51	[0.18, 0.83]
2	forest	air-dry/rewet only	3	51.8	62.9	24.9	-24.5	1.4				
2	forest	control-2	3	39.1	50.2	17.9	-26.1	0.8	12.7	[4.2, 21.2]	1.56	[0.41, 2.72]
2	grassland	air-dry/rewet only	3	39.8	50.9	19.9	-27.5	0.4				
2	grassland	control-2	3	20.2	31.4	9.6	-28.6	0.3	19.6	[9.3, 29.9]	1.11	[0.57, 1.66]
3a	forest	storage duration	9	-	-	-	-	-				
3a	forest	control-3	9	-	-	-	-	-	-24.2	[-37.4, -11.0]	-	-
3a	grassland	storage duration	3	-	-	-	-	-				
3a	grassland	control-3	3	-	-	-	-	-	-29.3	[-58.4, -0.2]	-	-
3b	forest	storage duration	17	-	-	-	-	-				
3b	forest	control-3	17	-	-	-	-	-	-44.0	[-52.0, -35.9]	-	-

[a]Experiment 3 storage duration treatment samples were only incubated for a single enclosure period and so data were measured following this period. [b]Results from Experiment 3 reported separately for the enriched samples from Oak Ridge (3b) and the nonenriched samples (3a). Mean control and treatment $\Delta^{14}C\text{-}CO_2$ are only reported for Experiments 1 and 2 where the aggregated data are representative of one site at one point in time. [c]The ΔΔ notation denotes the difference from the atmosphere at the time of sampling.

Supplemental Table 2-1. Linear mixed model marginal means for enclosure period $\Delta^{14}C_{respired}$

Period	Treatment	Experiment	Type	mean	SE	df	lower.CL	upper.CL
2nd	control	1	forest	93.8	7.8	24.4	77.7	109.9
2nd	treatment	1	forest	82.2	6.9	15.7	67.5	96.9
1st	treatment	1	forest	91.4	8.1	26.7	74.8	108.0
2nd	control	2	forest	44.0	8.2	27.2	27.3	60.8
1st	control	2	forest	20.2	8.2	27.2	3.5	37.0
2nd	treatment	2	forest	56.7	8.2	27.2	40.0	73.5
1st	treatment	2	forest	55.3	8.2	27.2	38.6	72.0
2nd	control	1	grassland	54.5	7.8	24.4	38.4	70.6
2nd	treatment	1	grassland	77.8	6.9	15.7	63.1	92.4
1st	treatment	1	grassland	75.0	7.0	16.5	60.2	89.9
2nd	control	2	grassland	20.8	8.1	26.9	4.2	37.4
1st	control	2	grassland	10.4	8.1	26.9	-6.3	27.0
2nd	treatment	2	grassland	40.3	8.1	26.9	23.7	57.0
1st	treatment	2	grassland	39.6	8.1	26.9	23.0	56.2

Supplemental Table 2-2. Linear mixed model marginal means for control and treatment $\Delta^{14}C_{respired}$ (2nd enclosure period only)

Treatment	Experiment	Type	mean	SE	df	lower.CL	upper.CL
control	1	forest	93.8	6.0	18.8	81.3	106.3
treatment	1	forest	82.2	5.4	13.0	70.6	93.9
control	2	forest	43.0	6.3	21.3	29.9	56.0
treatment	2	forest	55.7	6.3	21.3	42.6	68.7
control	1	grassland	54.5	6.0	18.8	42.0	67.0
treatment	1	grassland	77.8	5.4	13.0	66.1	89.4
control	2	grassland	21.8	6.3	21.3	8.8	34.8
treatment	2	grassland	41.4	6.3	21.3	28.3	54.4

Supplemental Table 2-3. Storage duration effect in linear mixed models (including Oak Ridge samples)

Estimated Trends					
Treatment	Duration	SE	df	lower.CL	upper.CL
control	12.18	4.46	44.7	3.205	21.2
treatment	8.46	4.48	45.8	-0.569	17.5

Degrees-of-freedom method: Kenward-Roger

Confidence level: 0.95

Contrasts					
Contrast	Estimate	SE	df	t ratio	*p*
control - treatment	3.73	1.31	61.4	2.855	0.0059

Degrees-of-freedom method: Kenward-Roger

Supplemental Table 2-4. Storage duration effect in linear mixed models (excluding Oak Ridge samples)

Estimated Trends					
Treatment	Duration	SE	df	lower.CL	upper.CL
control	8.59	4.63	36.9	-0.786	18.0
treatment	5.61	4.54	34.4	-3.605	14.8

Degrees-of-freedom method: Kenward-Roger

Confidence level: 0.95

Contrasts					
Contrast	Estimate	SE	df	t ratio	p
control - treatment	2.98	3.9	44.5	0.765	0.4485

Degrees-of-freedom method: Kenward-Roger

Supplemental Table 2-5. Site data, soil properties, and supporting references for all samples (Experiments 1, 2, and 3)

Experiment	Collection date (year)	Treatment incubation date (year)	Control incubation laboratory	Treatment incubation laboratory	Control AMS facility	Treatment AMS facility	Latitude	Longitude	Region	Site	Ecosystem	ID	Incubation replicates	Soil order (WRB name)	Sieved (<2mm)	Top (cm)	Bottom (cm)	Field moisture (gravimetric)	Incubation moisture (gravimetric)	% water holding capacity	Organic C (g kg⁻¹)	Total N (g kg⁻¹)	Sand (g kg⁻¹)	Silt (g kg⁻¹)	Clay (g kg⁻¹)	Reference
1	2011	2018	MPI-BGC	MPI-BGC	P	P	53.09	13.63	Central Germany	Schorfheide-Chorin	forest	SEW11	2	Cambisol	Yes	0	10	0.26	0.26	60	31.3	1.3	884	85	31	Solly et al. 20
1	2011	2018	MPI-BGC	MPI-BGC	P	P	52.90	13.85	Central Germany	Schorfheide-Chorin	forest	SEW34	2	Albeluvisol	Yes	0	10	0.24	0.24	60	16.4	0.7	889	69	42	Solly et al. 20
1	2011	2018	MPI-BGC	MPI-BGC	P	P	52.90	13.93	Central Germany	Schorfheide-Chorin	forest	SEW43	2	Cambisol	Yes	0	10	0.30	0.30	60	18.4	1.1	810	121	69	Solly et al. 20
1	2011	2018	MPI-BGC	MPI-BGC	P	P	53.12	13.68	Central Germany	Schorfheide-Chorin	grassland	SEG38	2	Cambisol	Yes	0	10	0.25	0.27	60	22.8	2.2	838	72	89	Solly et al. 20
1	2011	2018	MPI-BGC	MPI-BGC	P	P	53.12	13.84	Central Germany	Schorfheide-Chorin	grassland	SEG40	2	Luvisol	Yes	0	10	0.26	0.27	60	21.3	2.0	710	192	98	Solly et al. 20
1	2011	2018	MPI-BGC	MPI-BGC	P	P	52.98	13.83	Central Germany	Schorfheide-Chorin	grassland	SEG46	2	Cambisol	Yes	0	10	0.31	0.34	60	24.3	2.3	644	210	146	Solly et al. 20
1	2011	2018	MPI-BGC	MPI-BGC	P	P	51.34	10.36	Central Germany	Hainich-Dün	forest	HEW22	2	Luvisol	Yes	0	10	0.38	0.37	60	23.3	1.7	68	747	184	Solly et al. 20
1	2011	2018	MPI-BGC	MPI-BGC	P	P	51.11	10.45	Central Germany	Hainich-Dün	forest	HEW41	2	Luvisol	Yes	0	10	0.40	0.42	60	23.4	1.9	34	754	210	Solly et al. 20
1	2011	2018	MPI-BGC	MPI-BGC	P	P	51.10	10.46	Central Germany	Hainich-Dün	forest	HEW42	2	Stagnosol	Yes	0	10	0.34	0.36	60	24.3	1.7	60	760	184	Solly et al. 20
1	2011	2018	MPI-BGC	MPI-BGC	P	P	51.28	10.45	Central Germany	Hainich-Dün	grassland	HEG10	2	Vertisol	Yes	0	10	0.47	0.61	60	43.7	4.0	30	532	436	Solly et al. 20
1	2011	2018	MPI-BGC	MPI-BGC	P	P	51.08	10.57	Central Germany	Hainich-Dün	grassland	HEG32	2	Cambisol	Yes	0	10	0.52	0.54	60	40.0	3.8	17	640	340	Solly et al. 20
1	2011	2018	MPI-BGC	MPI-BGC	P	P	51.29	10.38	Central Germany	Hainich-Dün	grassland	HEG48	2	Cambisol	Yes	0	10	0.55	0.56	60	41.6	4.0	50	488	465	Solly et al. 20
2	2019	2019	MPI-BGC	MPI-BGC	P	P	51.34	10.36	Central Germany	Hainich-Dün	forest	HEW22	2	Luvisol	Yes	0	10	0.38	0.37	60	23.3	1.7	68	747	184	Solly et al. 20
2	2019	2019	MPI-BGC	MPI-BGC	P	P	51.11	10.45	Central Germany	Hainich-Dün	forest	HEW41	2	Luvisol	Yes	0	10	0.40	0.42	60	23.4	1.9	34	754	210	Solly et al. 20
2	2019	2019	MPI-BGC	MPI-BGC	P	P	51.10	10.46	Central Germany	Hainich-Dün	forest	HEW42	2	Stagnosol	Yes	0	10	0.34	0.36	60	24.3	1.7	60	760	184	Solly et al. 20
2	2019	2019	MPI-BGC	MPI-BGC	P	P	51.28	10.45	Central Germany	Hainich-Dün	grassland	HEG10	2	Vertisol	Yes	0	10	0.23	0.22	60	43.7	4.0	30	532	436	Solly et al. 20
2	2019	2019	MPI-BGC	MPI-BGC	P	P	51.08	10.57	Central Germany	Hainich-Dün	grassland	HEG32	2	Cambisol	Yes	0	10	0.17	0.23	60	40.0	3.8	17	640	340	Solly et al. 20
2	2019	2019	MPI-BGC	MPI-BGC	P	P	51.29	10.38	Central Germany	Hainich-Dün	grassland	HEG48	2	Cambisol	Yes	0	10	0.19	0.22	60	41.6	4.0	50	488	465	Solly et al. 20
3	2011	2018	MPI-BGC	MPI-BGC	P	P	51.34	10.51	Central Germany	Hainich-Dün	forest	HEW26	2	Luvisol	Yes	0	10	0.34	0.36	60	24.4	1.6	54	796	150	Solly et al. 20
3	2011	2018	MPI-BGC	MPI-BGC	P	P	51.18	10.38	Central Germany	Hainich-Dün	forest	HEW47	2	Stagnosol	Yes	0	10	0.43	0.45	60	32.5	2.4	46	632	323	Solly et al. 20
3	2011	2018	MPI-BGC	MPI-BGC	P	P	51.22	10.37	Central Germany	Hainich-Dün	grassland	HEG20	3	Stagnosol	Yes	0	10	0.47	0.45	60	27.2	2.3	102	661	239	Solly et al. 20
3	2011	2018	MPI-BGC	MPI-BGC	P	P	51.11	10.43	Central Germany	Hainich-Dün	grassland	HEG33	3	Cambisol	Yes	0	10	0.47	0.47	60	40.1	3.8	29	618	353	Solly et al. 20
3	2011	2018	MPI-BGC	MPI-BGC	P	P	51.21	10.39	Central Germany	Hainich-Dün	grassland	HEG6	3	Stagnosol	Yes	0	10	0.41	0.45	60	20.8	2.0	45	698	257	Solly et al. 20
3	2008	2018	UCI	UCI	UCI	P	35.98	-79.09	Duke FACE	Duke FACE control	forest	120	1	Ultic Alfisol	Yes	5	15	0.95	0.95		16.6	0.8				Hopkins et al.
3	1999	2009	UCI	UCI	UCI	UCI	42.54	-72.18	Harvard Forest	Harvard Forest	forest	NWN-1 Ap (bag)	1	Inceptisol	Yes	0	16				60.0					Gaudinski et
3	1999	2009	UCI	UCI	UCI	UCI	42.54	-72.18	Harvard Forest	Harvard Forest	forest	NWN-1 Ap #27	1	Inceptisol	Yes	0	16				60.0					Gaudinski et
3	1999	2009	UCI	UCI	UCI	UCI	42.54	-72.18	Harvard Forest	Harvard Forest	forest	NWN-2 Ap #34	1	Inceptisol	Yes	0	16				60.0					Gaudinski et
3	1999	2009	UCI	UCI	UCI	UCI	42.54	-72.18	Harvard Forest	Harvard Forest	forest	NWN-1 Ap #44	1	Inceptisol	Yes	0	16				60.0					Gaudinski et
3	2004	2018	UCI	UCI	UCI	P	35.94	-84.33	Oak Ridge	TVA	forest	TVA 6E C	1	Inceptisol	No	0	5	0.28	0.28		24.9	1.2				Cisneros-Doz
3	2004	2018	UCI	UCI	UCI	P	35.94	-84.33	Oak Ridge	TVA	forest	TVA 2B C	1	Inceptisol	No	0	5	0.30	0.30		24.9	1.2				Cisneros-Doz
3	2004	2018	UCI	UCI	UCI	P	35.94	-84.33	Oak Ridge	TVA	forest	TVA 3B C	1	Inceptisol	No	0	5	0.49	0.49		24.9	1.2				Cisneros-Doz
3	2004	2018	UCI	UCI	UCI	P	35.94	-84.33	Oak Ridge	TVA	forest	TVA 5B C	1	Inceptisol	No	0	5	0.26	0.26		24.9	1.2				Cisneros-Doz
3	2004	2018	UCI	UCI	UCI	P	35.97	-84.27	Oak Ridge	Walker Branch	forest	WB 4B C	1	Ultisol	No	0	5	0.34	0.34		24.9	1.0				Cisneros-Doz
3	2004	2018	UCI	UCI	UCI	P	35.97	-84.27	Oak Ridge	Walker Branch	forest	WB 5B C	1	Ultisol	No	0	5	0.25	0.25		24.9	1.0				Cisneros-Doz
3	2004	2018	UCI	UCI	UCI	P	35.97	-84.27	Oak Ridge	Walker Branch	forest	WB 8B C	1	Ultisol	No	0	5	0.34	0.34		24.9	1.0				Cisneros-Doz
3	2004	2018	UCI	UCI	UCI	P	35.97	-84.27	Oak Ridge	Walker Branch	forest	WB 3E C	1	Ultisol	No	0	5	0.36	0.36		24.9	1.0				Cisneros-Doz
3	2004	2018	UCI	UCI	UCI	P	35.97	-84.27	Oak Ridge	Walker Branch	forest	WB 7E C	1	Ultisol	No	0	5	0.18	0.18		24.9	1.0				Cisneros-Doz
3	2004	2018	UCI	UCI	UCI	P	35.94	-84.33	Oak Ridge	TVA	forest	TVA 4E	1	Inceptisol	No	0	5	0.26			24.9	1.2				Cisneros-Doz
3	2004	2018	UCI	UCI	UCI	P	35.94	-84.33	Oak Ridge	TVA	forest	TVA 6E	1	Inceptisol	No	0	5	0.30			24.9	1.2				Cisneros-Doz
3	2004	2018	UCI	UCI	UCI	P	35.94	-84.33	Oak Ridge	TVA	forest	TVA 8E	1	Inceptisol	No	0	5	0.22			24.9	1.2				Cisneros-Doz
3	2004	2009	UCI	USGS Menlo Park	UCI	UCI	35.94	-84.33	Oak Ridge	TVA	forest	TVA2B-C_iT2	1	Inceptisol	No	0	5	0.30			24.9	1.2				Cisneros-Doz
3	2004	2009	UCI	USGS Menlo Park	UCI	UCI	35.94	-84.33	Oak Ridge	TVA	forest	TVA3-C_iT1	1	Inceptisol	No	0	5	0.49			24.9	1.2				Cisneros-Doz
3	2004	2009	UCI	USGS Menlo Park	UCI	UCI	35.97	-84.27	Oak Ridge	Walker Branch	forest	WB4B-C_iT2	1	Ultisol	No	0	5	0.34			24.9	1.0				Cisneros-Doz
3	2004	2009	UCI	USGS Menlo Park	UCI	UCI	35.97	-84.27	Oak Ridge	Walker Branch	forest	WB5-C_iT2	1	Ultisol	No	0	5	0.25			24.9	1.0				Cisneros-Doz
3	2004	2009	UCI	USGS Menlo Park	UCI	UCI	35.97	-84.27	Oak Ridge	Walker Branch	forest	WB8-C_iT2	1	Ultisol	No	0	5	0.34			24.9	1.0				Cisneros-Doz
3	2009	2018	UCI	UCI	UCI	P	37.03	-119.27	Sierra Nevada	Musick	forest	MA	3	Ultic Haploxeralf	Yes	5	20	0.07	0.33	50	27.4	1.0	600	270	150	Koarashi et a
3	2009	2018	UCI	UCI	UCI	P	37.03	-119.19	Sierra Nevada	Shaver	forest	SA	3	Pachic Xerumbrept	Yes	5	20	0.07	0.31	50	29.4	1.2	800	150	50	Koarashi et a

2.11. Figures

Figure 2-1. Respiration rates for Experiment 1 (Air-dry/rewet + storage) and Experiment 2 (Air-dry/rewet only) samples. a) Experiment 1 samples; b) Experiment 2 samples. Vertical gray line at day 4 demarcates the end of the first enclosure period (rewetting pulse). Points show measurements and lines show trends in mean respiration rate. Shaded ribbons represent one standard error of the mean. The final measurement points for a few samples which took >18 days to reach CO_2 targets are excluded for display reasons; respiration rates for those samples remained constant. Note that headspace CO_2 concentrations for control-1 samples (panel a) were only measured once during the first enclosure period (day 4) in contrast to daily measurements for all other samples.
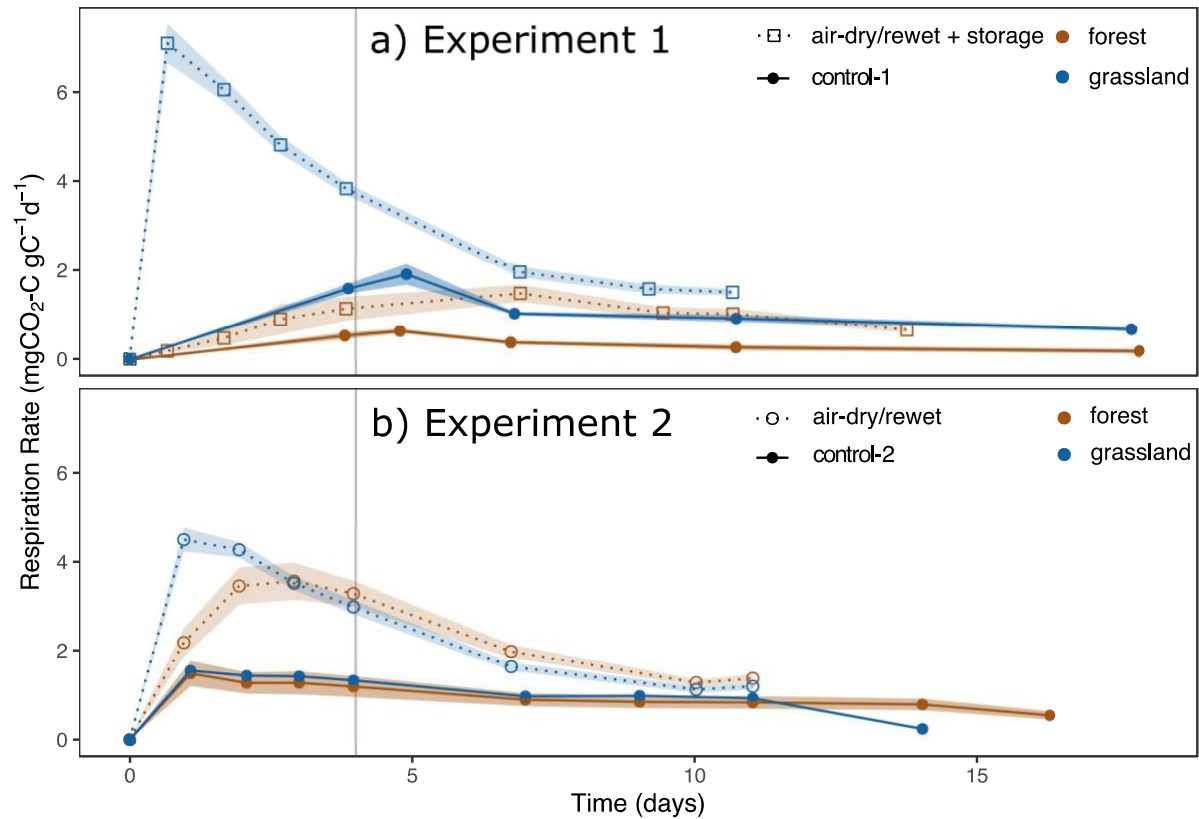
Figure 2-2. $\Delta^{14}C$-CO_2 ($\Delta^{14}C_{respired}$) for the rewetting pulse (first enclosure period) versus the second enclosure period. Points are means of laboratory duplicates and error bars are the minimum and maximum. Note that $\Delta^{14}C$-CO_2 was not measured for the first enclosure period (rewetting pulse) in control-1 samples; additionally samples from three of the forest plots of the air-dry/rewet + storage samples from Experiment 1 failed to accumulate enough CO_2 during this period to measure $\Delta^{14}C$-CO_2.
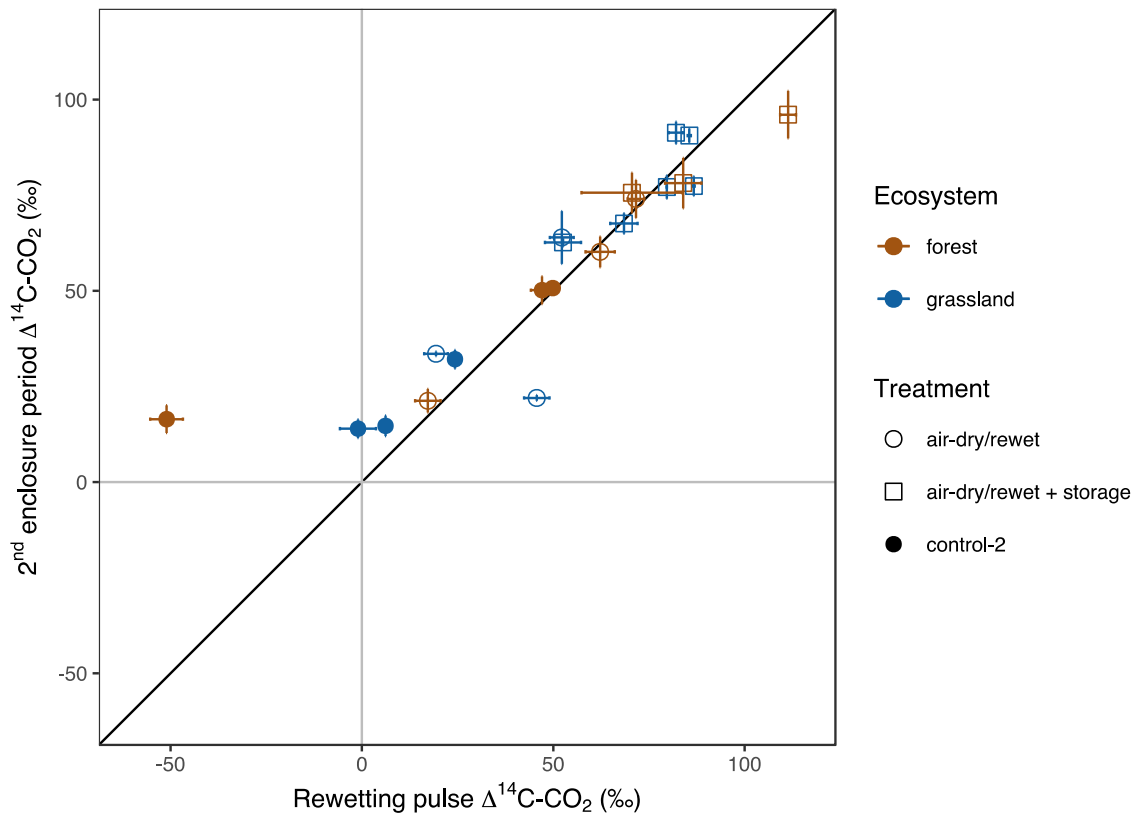
Figure 2-3. Overall treatment effect on $\Delta^{14}C_{respired}$. Points show data from all three experiments and are the mean of laboratory replicates (for replicated samples); error bars are standard deviation of replicates. Solid line is 1:1. For context, the dashed and dotted lines show differences of ±20‰ and ±40‰, respectively. Location names are followed by the corresponding experiment number in parentheses. The samples from both Central Germany sites (Hainich-Dün and Schorfheide-Chorin) behaved similarly in Experiment 1, so samples analyzed in the same experiment are coded with the same colors in the above figure. Oak Ridge soils were part of a whole ecosystem ^{14}C label experiment (Cisneros-Dozal et al., 2006), where the label occurred within four years of original sample collection.
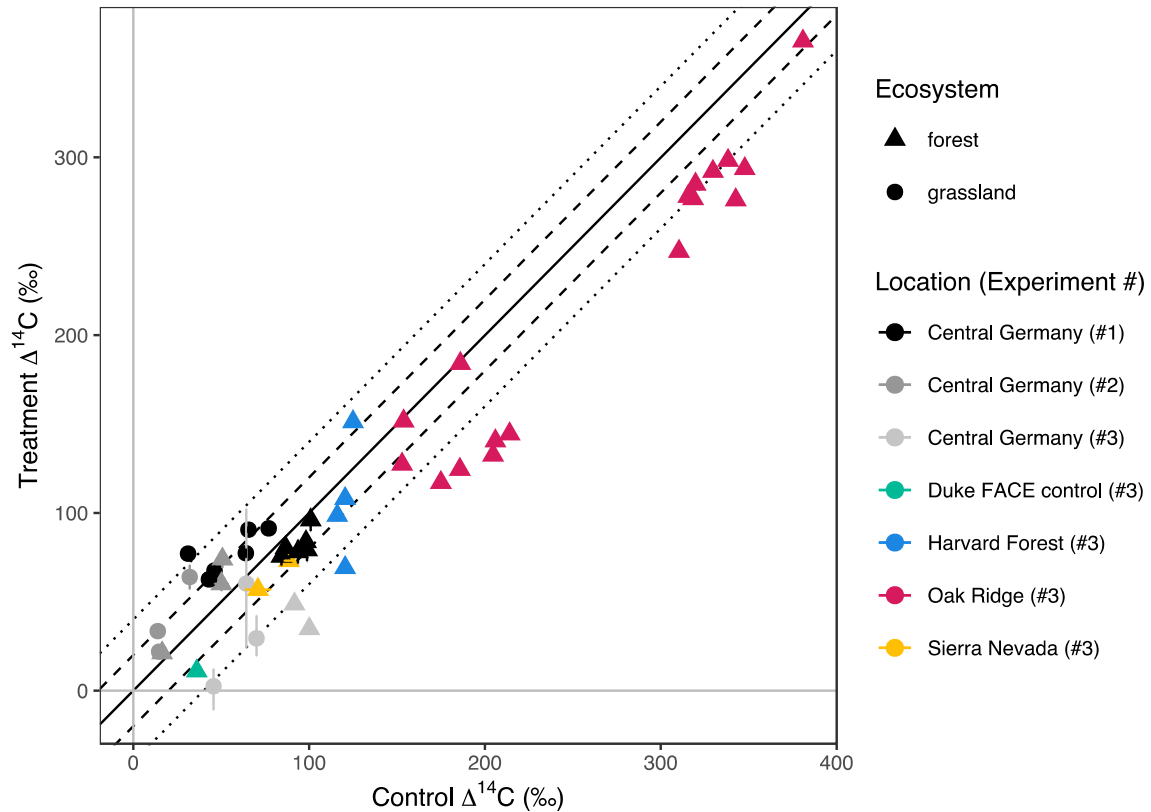
Figure 2-4. Treatment effect on $\Delta^{14}C_{respired}$ in relation to storage duration. Points show data from Experiments 1 and 3. Data are averaged by site (some regions had multiple sites, Table 2-3) and error bars show the standard deviation for the site mean. Note that Central Germany samples from Experiments 1 and 3 are averaged together here. For context, the dashed and dotted lines show differences of ±20‰ and ±40‰, respectively. The Oak Ridge sample points with the greater treatment-control difference at both 5 and 14 years of storage are from the Tennessee Valley site, which received more ^{14}C label than did the other Oak Ridge site, Walker Ridge.
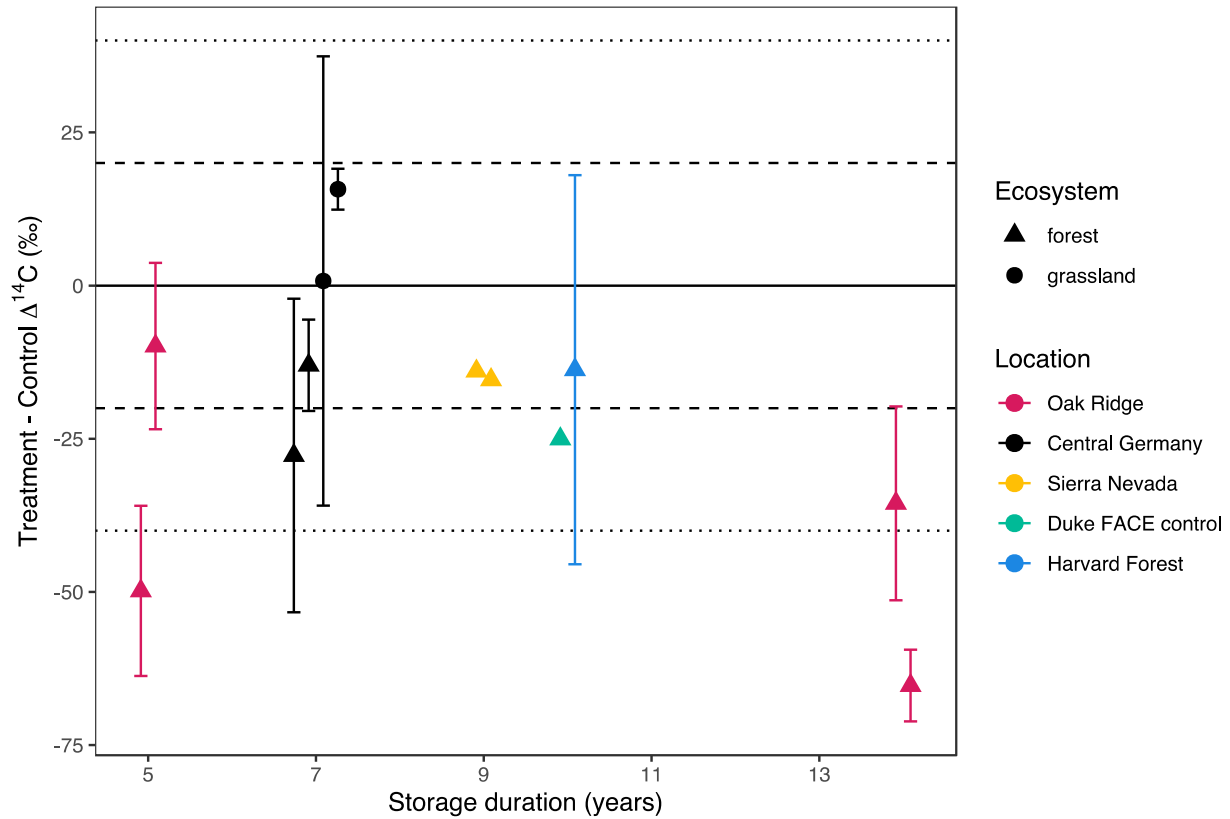
Figure 2-5. Time series of control and treatment Δ^{14}C-CO$_2$ (Δ^{14}C$_{respired}$) in Experiments 1 and 2. (a) forest sites, (b) grassland sites. Points show mean Δ^{14}C$_{respired}$ within ecosystem and treatment groups; error bars show the standard deviation. Atmospheric Δ^{14}C-CO$_2$ data (black line) are from Graven et al. (2017) up to the year 2015, while data points from 2015 to 2019 are extrapolated (Sierra, 2018). All atmospheric radiocarbon data are for the northern hemisphere (zone 2).
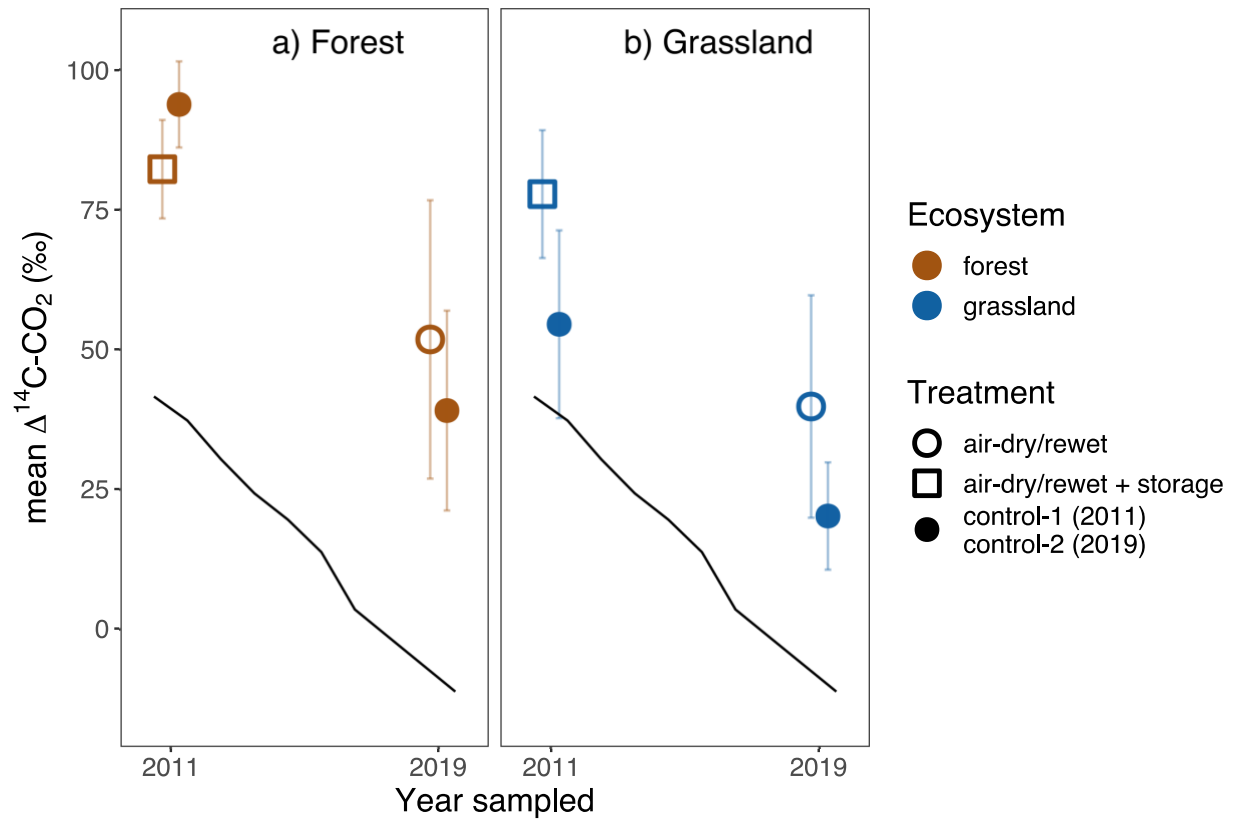
Figure 2-6. Conceptual model fit and observed $\Delta^{14}C_{respired}$ for the Hainich-Dün forest sites (Central Germany 2). (a) $\Delta^{14}C$ of soil pools and heterotrophically respired CO_2 predicted by the model adapted from Schrumpf and Kaiser (2015) alongside atmospheric $\Delta^{14}C$ for the bomb-C period (1950–2020) and $\Delta^{14}C_{respired}$ observed in this study (black points) (b) (inset) Zoom to study period. Blue arrows show the shift in $\Delta^{14}C_{respired}$ following air-drying and rewetting. Note that $\Delta^{14}C_{respired}$ shifts toward the slow pool in both 2011 and 2019, but the direction of the shift depends on sampling year. Points are jittered to prevent over plotting; error bars show standard deviations. Note that the model was not fit to the $\Delta^{14}C_{respired}$ observed in this study. Atmospheric $\Delta^{14}C\text{-}CO_2$ data are from Graven et al. (2017) up to the year 2015, while atmospheric points from 2015 to 2019 are extrapolated (Sierra, 2018). All atmospheric radiocarbon data is for the northern hemisphere (zone 2).
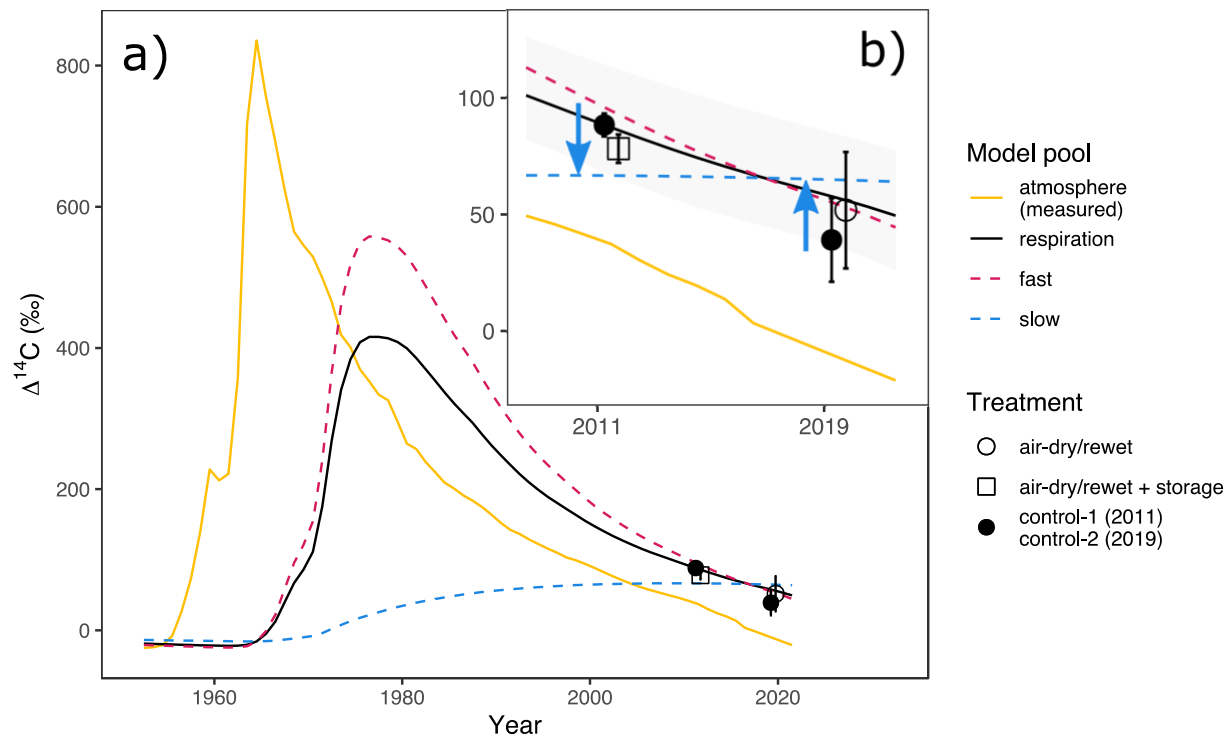
Supplemental Figure 2-1. 95% confidence intervals for linear mixed model contrasts of Hainich-Dün forest time series data
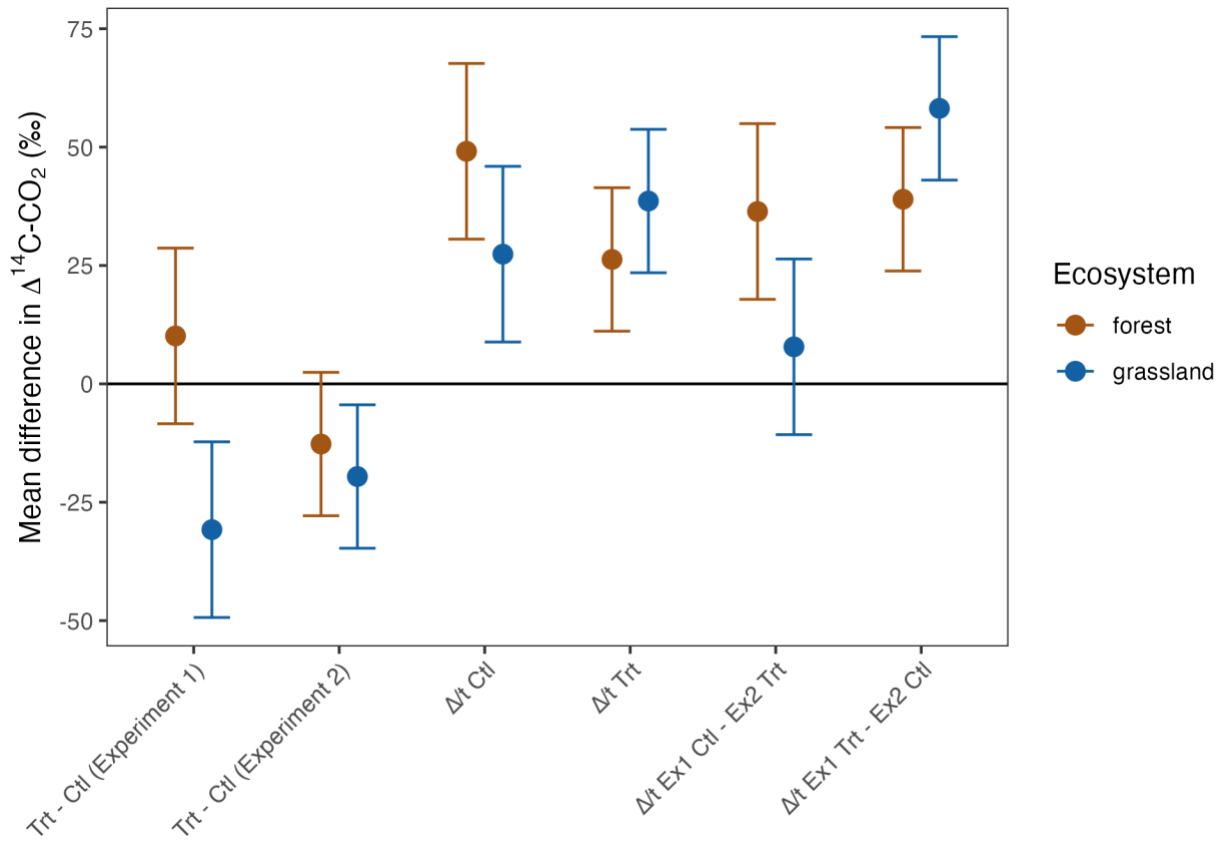
Supplemental Figure 2-2. Time series of control and treatment Δ^{14}C-CO_2 ($\Delta^{14}C_{respired}$) in Experiments 1 and 2, with error bars showing 95% confidence intervals estimated from the linear mixed model instead of pooled standard deviations (cf. Figure 2-5). Points show mean Δ^{14}C-CO_2 within ecosystem and treatment groups. Atmospheric Δ^{14}C-CO_2 data (black line) are from Graven et al. (2017) up to the year 2015, while data points from 2015 to 2019 are extrapolated (Sierra, 2018). All atmospheric radiocarbon data are for the northern hemisphere (zone 2).
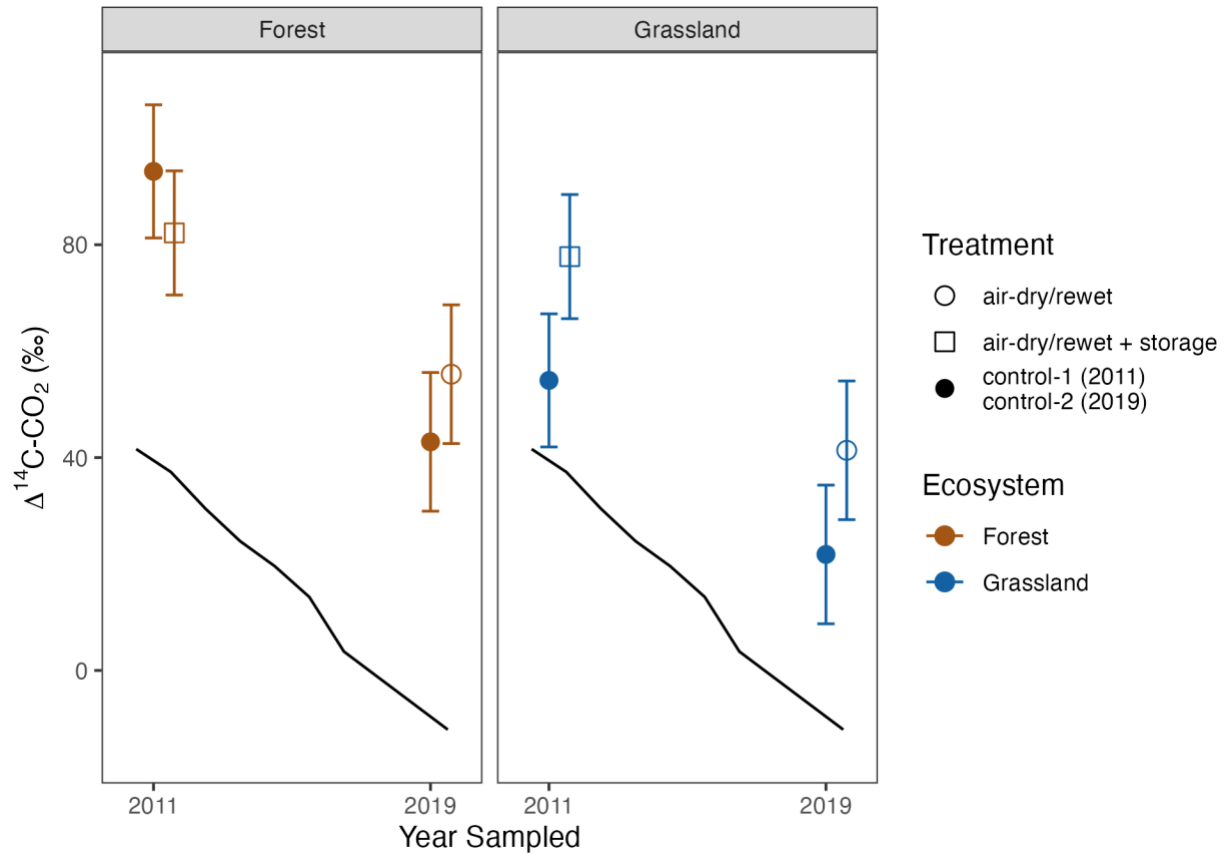
Supplemental Figure 2-3. Respiration rates for Experiment 1 and Experiment 2 (rewetting pulse respiration rates shown as a cumulative average for all samples). CO_2 concentrations for Experiment 1 control samples were only measured once during the pre-incubation period, in contrast to daily measurements for all other samples. Pre-incubation respiration rates are shown here calculated as cumulative averages for the whole pre-incubation period for ease of comparison across all treatments in both Experiment 1 and Experiment 2.
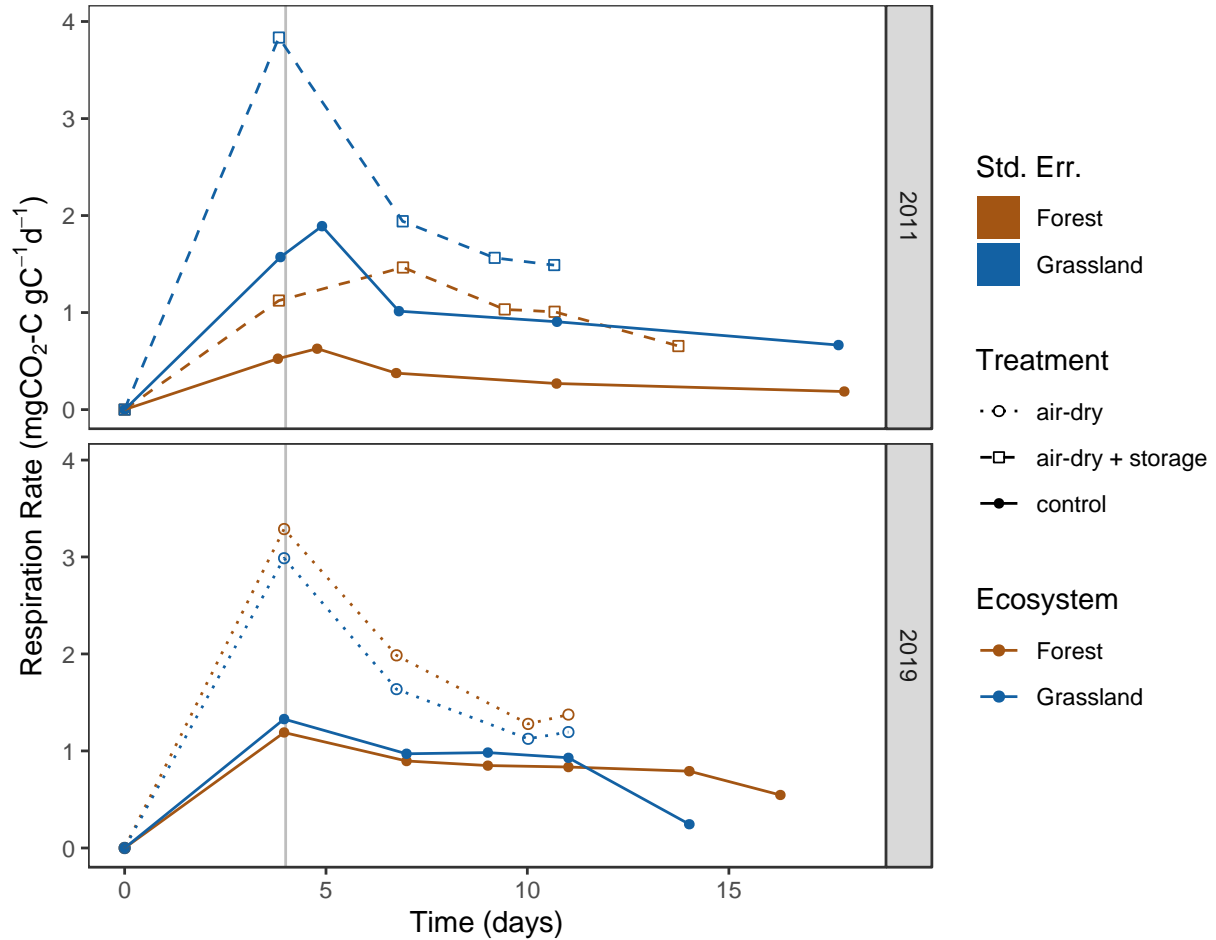
Supplemental Figure 2-4. Respiration rates for Experiment 3. Experiment 3 storage duration treatment samples were only incubated for a single enclosure period, as the results of Experiment 1 and Experiment 2 showed no significant difference in $\Delta^{14}C_{respired}$ between the rewetting pulse CO_2 released during the pre-incubation period and the CO_2 respired during the second enclosure period. The grassland storage duration treatment samples (blue dotted line) respired an equivalent amount of CO_2 in just 3 d as the corresponding control-3 samples respired during the rewetting pulse period and the second enclosure period combined. Consequently those incubations were stopped after the first CO_2 measurement point.
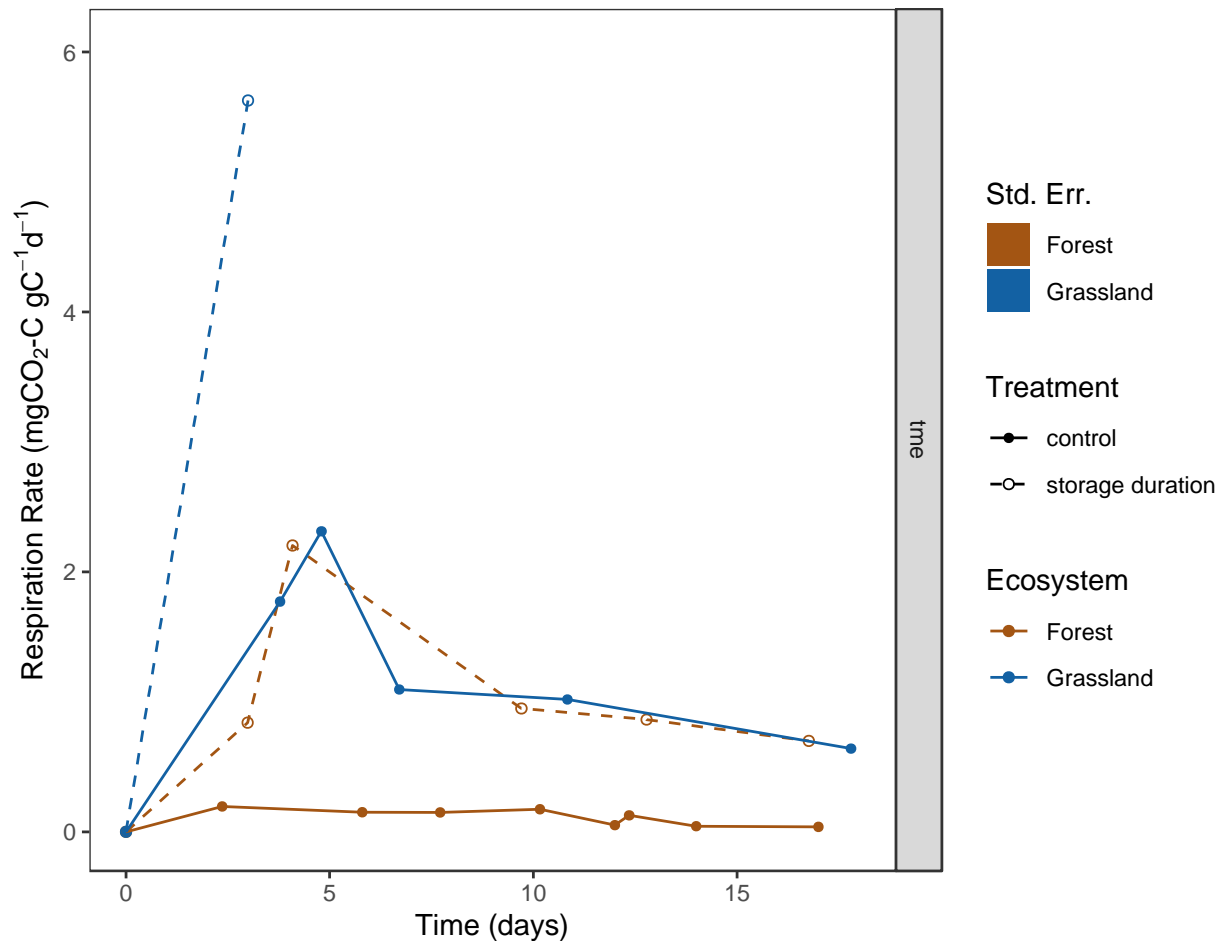
Supplemental Figure 2-5. $\delta^{13}C$-CO_2 of rewetting pulse and 2nd enclosure period. Points are means; error bars show the minimum and maximum of laboratory duplicates.
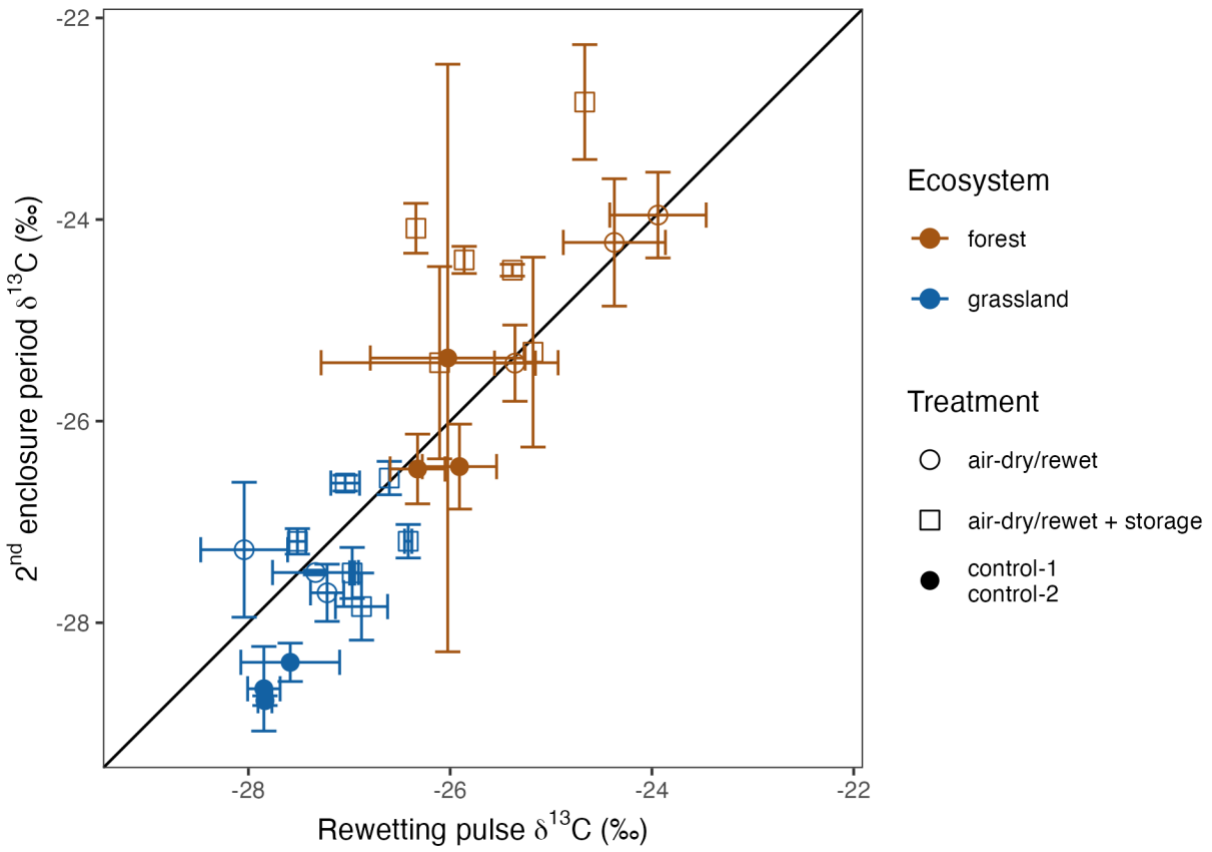
Supplemental Figure 2-6. Time series of control and treatment δ^{13}C-CO_2 (Experiments 1 and 2). Points are means; error bars show pooled standard deviations.
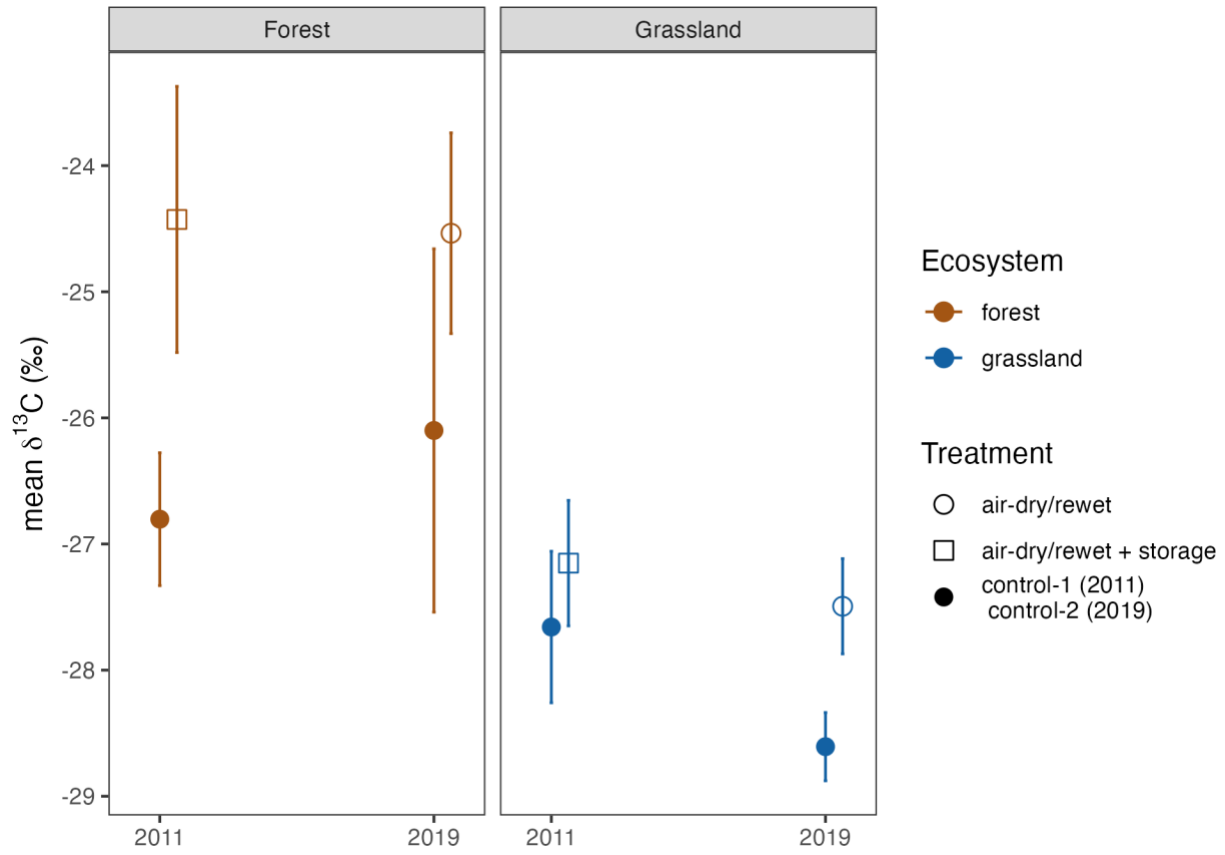
Supplemental Figure 2-7. Change in $\Delta^{14}C_{respired}$ in relation to cumulative soil carbon respired. Error bars show minimum and maximum values measured for laboratory duplicates, while points show the mean. Lines connect mean pre-incubation and second enclosure period observations for a single sample. Lines parallel to the x-axis indicate a lack of trend in $\Delta^{14}C_{respired}$ with the amount of carbon respired, while differences between open and filled symbols show the impact of treatments on both the amount of carbon respired and $\Delta^{14}C_{respired}$. Note that pre-incubation $\Delta^{14}C_{respired}$ was not measured for the control-1 samples in 2011. Plot limits exclude outlier point (HEW22 control-2, pre-incubation) for improved legibility.
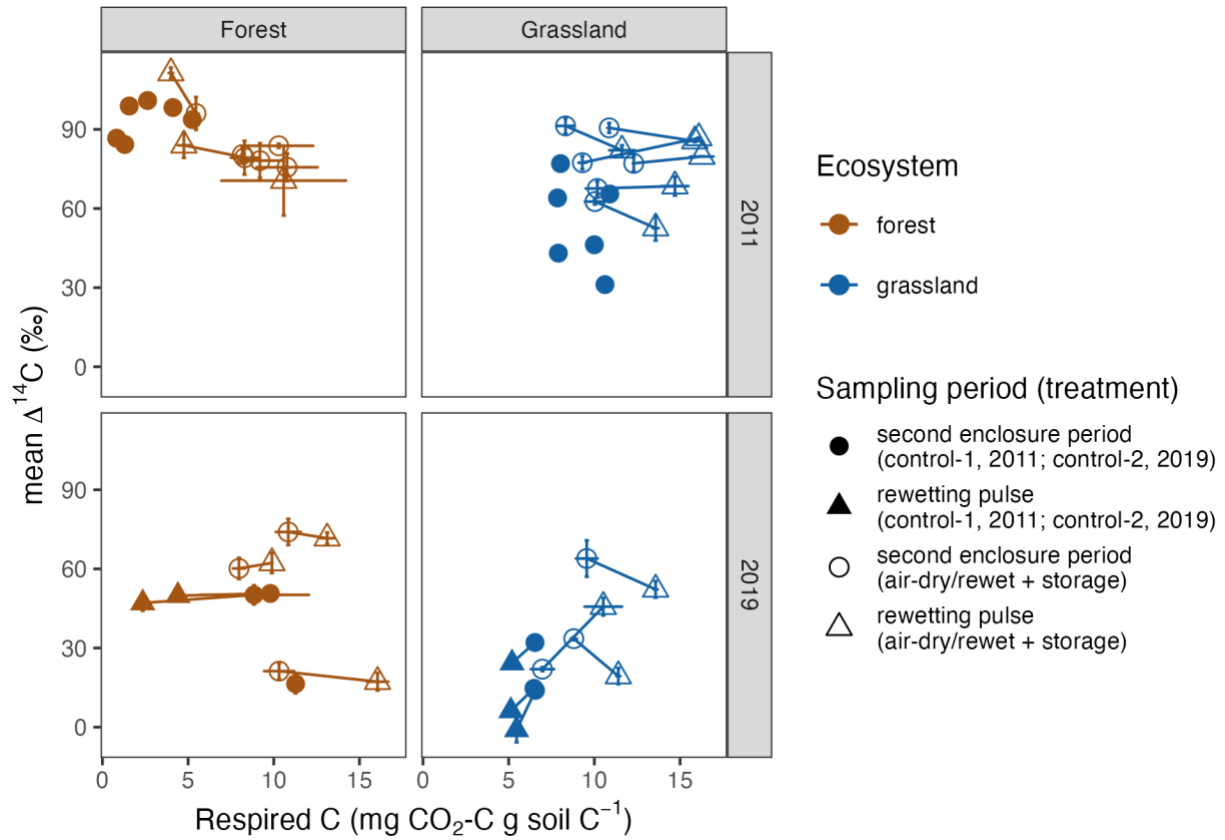
Supplemental Figure 2-8. Change in $\Delta^{14}C_{respired}$ relative to the change in moisture content (control - treatment). Differences in $\Delta^{14}C_{respired}$ are shown as means; error bars show pooled standard deviations. All samples were rewetted to 60% of water holding capacity (WHC) prior to incubation, but control samples were rewetted from field moisture whereas treatment samples were rewetted after air-drying. Data from Experiment 3 are not shown as field moisture content was unknown for the majority of samples (Supplemental Table 2-5).
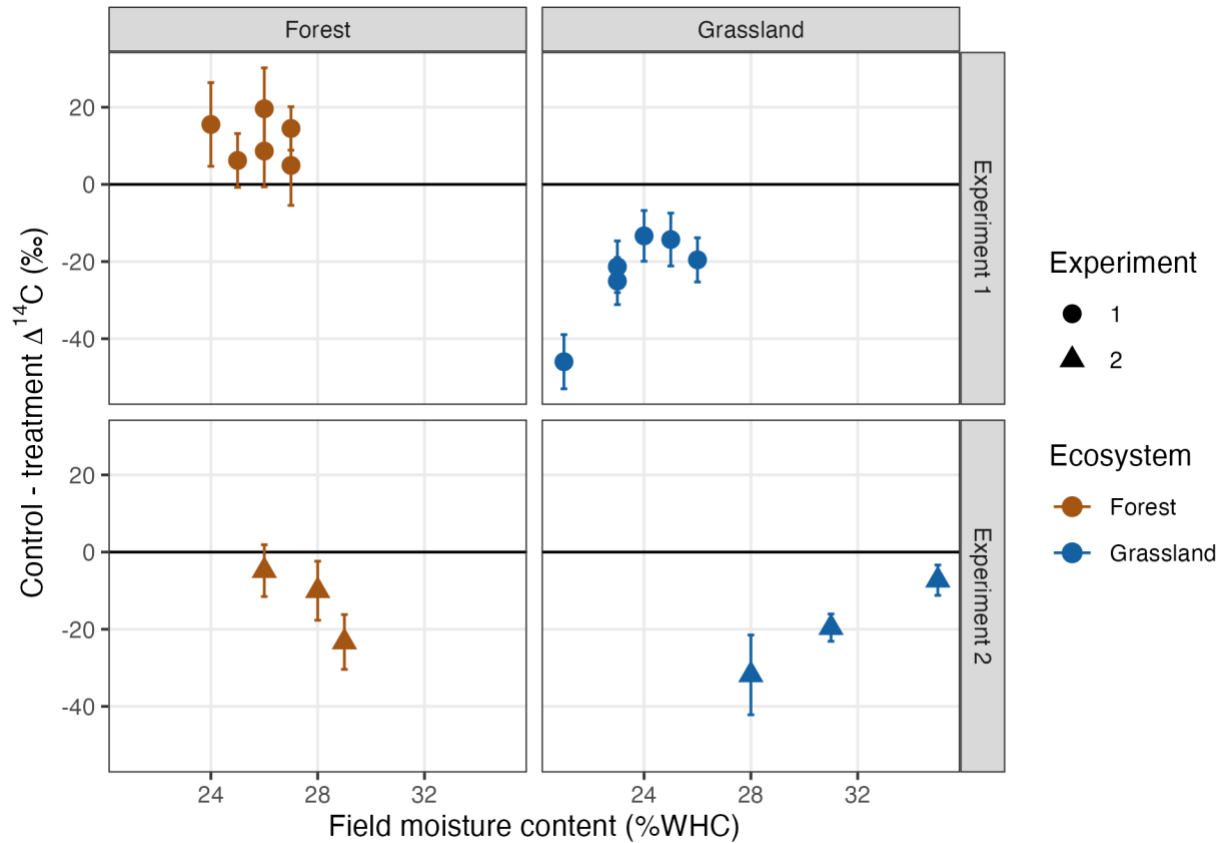
2.12. References

Baisden, W. T., Parfitt, R. L., Ross, C., Schipper, L. A., and Canessa, S.: Evaluating 50 years of time-series soil radiocarbon data : towards routine calculation of robust C residence times, Biogeochemistry, 112, 129–137, https://doi.org/10.1007/s10533-011-9675-y, 2013.

Bartlett, R. and James, B.: Studying Dried, Stored Soil Samples — Some Pitfalls, Soil Sci. Soc. Am. J, 44, 721–724, 1980.

Bates, D., Mächler, M., Bolker, B., and Walker, S.: Fitting linear mixed-effects models using lme4, Journal of Statistical Software, 67, 1–48, https://doi.org/10.18637/jss.v067.i01, 2015.

Birch, H. F.: The effect of soil drying on humus decomposition and nitrogen availability, Plant and Soil, 10, 9–31, https://doi.org/10.1007/BF01343734, 1958.

Blake, L., Goulding, K., Mott, C., and Poulton, P.: Temporal changes in chemical properties of air-dried stored soils and their interpretation for long-term experiments, European Journal of Soil Science, 51, 345–353, 2000.

Boose, E. and Gould, E.: Harvard forest climate data since 1964, Harvard Forest Data Archive: HF300, 2021.

Borken, W. and Matzner, E.: Reappraisal of drying and wetting effects on C and N mineralization and fluxes in soils, Global Change Biology, 15, 808–824, https://doi.org/10.1111/j.1365-2486.2008.01681.x, 2009.

Brödlin, D., Kaiser, K., Kessler, A., and Hagedorn, F.: Drying and rewetting foster phosphorus depletion of forest soils, Soil Biology and Biochemistry, 128, 22–34, https://doi.org/10.1016/j.soilbio.2018.10.001, 2019.

Cisneros-Dozal, L. M., Trumbore, S., and Hanson, P. J.: Partitioning sources of soil-respired CO_2 and their seasonal variation using a unique radiocarbon tracer, Global Change Biology, 12, 194–204, https://doi.org/10.1111/j.1365-2486.2005.001061.x, 2006.

Dungait, J. A. J., Hopkins, D. W., Gregory, A. S., and Whitmore, A. P.: Soil organic matter turnover is governed by accessibility not recalcitrance, Global Change Biology, 18, 1781–1796, https://doi.org/10.1111/j.1365-2486.2012.02665.x, 2012.

Fierer, N. and Schimel, J. P.: A Proposed Mechanism for the Pulse in Carbon Dioxide Production Commonly Observed Following the Rapid Rewetting of a Dry Soil, Soil Science Society of America Journal, 67, 798–805, https://doi.org/10.2136/sssaj2003.0798, 2003.

Fischer, M., Bossdorf, O., Gockel, S., Hänsel, F., Hemp, A., Hessenmöller, D., Korte, G., Nieschulze, J., Pfeiffer, S., Prati, D., Renner, S., Schöning, I., Schumacher, U., Wells, K., Buscot, F., Kalko, E. K. V., Linsenmair, K. E., Schulze, E. D., and Weisser, W. W.: Implementing large-scale and long-term functional biodiversity research: The Biodiversity Exploratories, Basic and Applied Ecology, 11, 473–485, https://doi.org/10.1016/j.baae.2010.07.009, 2010.

Franzluebbers, A. J., Haney, R. L., Honeycutt, C. W., Schomberg, H. H., and Hons, F. M.: Flush of Carbon Dioxide Following Rewetting of Dried Soil Relates to Active Organic Pools, Soil Science Society of America Journal, 64, 613–623, https://doi.org/10.2136/sssaj2000.642613x, 2000.

Gaudinski, J. B., Trumbore, S. E., Davidson, E. A., and Zheng, S.: Soil carbon cycling in a temperate forest: radiocarbon-based estimates of residence times, sequestration rates and partitioning of fluxes, Biogeochemistry, 51, 33–69, https://doi.org/10.1023/A:1006301010014, 2000.

Graven, H., Allison, C. E., Etheridge, D. M., Hammer, S., Keeling, R. F., Levin, I., Meijer, H. A. J., Rubino, M., Tans, P. P., Trudinger, C. M., Vaughn, B. H., and White, J. W. C.: Compiled records of carbon isotopes in atmospheric CO2 for historical simulations in CMIP6, Geoscientific Model Development, 10, 4405–4417, https://doi.org/10.5194/gmd-10-4405-2017, 2017.

Hopkins, F. M., Torn, M. S., and Trumbore, S. E.: Warming accelerates decomposition of decades-old carbon in forest soils (SI), Proceedings of the National Academy of Sciences, 1–6, https://doi.org/10.1073/pnas.1206575109, 2012.

Jones, A. R., Gupta, V. V. S. R., Buckley, S., Brackin, R., Schmidt, S., and Dalal, R. C.: Drying and rewetting effects on organic matter mineralisation of contrasting soils after 36 years of storage, Geoderma, 342, 12–19, https://doi.org/10.1016/j.geoderma.2019.01.053, 2019.

Kaiser, M., Kleber, M., and Asefaw, A.: How air-drying and rewetting modify soil organic matter characteristics : An assessment to improve data interpretation and inference, Soil Biology and Biochemistry, 80, 324–340, https://doi.org/10.1016/j.soilbio.2014.10.018, 2015.

Kenward, M. G. and Roger, J. H.: Small sample inference for fixed effects from restricted maximum likelihood, Biometrics, 983–997, 1997.

Koarashi, J., Hockaday, W. C., Masiello, C. a., and Trumbore, S. E.: Dynamics of decadally cycling carbon in subsurface soils, Journal of Geophysical Research G: Biogeosciences, 117, G03033, https://doi.org/10.1029/2012JG002034, 2012.

Lehmann, J. and Kleber, M.: The contentious nature of soil organic matter, Nature, 528, 60–68, https://doi.org/10.1038/nature16069, 2015.

Lehmann, J., Hansel, C. M., Kaiser, C., Kleber, M., Maher, K., Manzoni, S., Nunan, N., Reichstein, M., Schimel, J. P., Torn, M. S., Wieder, W. R., and Kögel-Knabner, I.: Persistence of soil organic carbon caused by functional complexity, Nature Geoscience, 13, 529–534, https://doi.org/10.1038/s41561-020-0612-3, 2020.

Lenth, R. V.: emmeans: Estimated Marginal Means, aka Least-Squares Means, 2021.

Lützow, M. v, Kögel-Knabner, I., Ekschmitt, K., Matzner, E., Guggenberger, G., Marschner, B., and Flessa, H.: Stabilization of organic matter in temperate soils: mechanisms and their relevance under different soil conditions–a review, European journal of soil science, 57, 426–445, 2006.

MacFadyen, A.: Inhibitory effects of carbon dioxide on microbial activity in soil, Pedobiologia, 1973.

Marschner, B., Brodowski, S., Dreves, A., Gleixner, G., Gude, A., Grootes, P. M., Hamer, U., Heim, A., Jandl, G., Ji, R., Kaiser, K., Kalbitz, K., Kramer, C., Leinweber, P., Rethemeyer, J., Schäffer, A., Schmidt, M. W. I., Schwark, L., and Wiesenberg, G. L. B.: How relevant is recalcitrance for the stabilization of organic matter in soils?, Journal of Plant Nutrition and Soil Science, 171, 91–110, https://doi.org/10.1002/jpln.200700049, 2008.

O'Neill, B.: Some Useful Moment Results in Sampling Problems, American Statistician, 68, 282–296, https://doi.org/10.1080/00031305.2014.966589, 2014.

R Core Team: R: A language and environment for statistical computing, 2020.

Šantrůčková, H. and Šimek, M.: Soil microorganisms at different CO 2 and O 2 tensions, Folia microbiologica, 39, 225–230, 1994.

Schimel, J. P.: Life in Dry Soils: Effects of Drought on Soil Microbial Communities and Processes, Annual Review of Ecology, Evolution, and Systematics, 49, 409–432, https://doi.org/10.1146/annurev-ecolsys-110617-062614, 2018.

Schlichting, E., Blume, H., and Stahr, K.: Bodenkundliches praktikum. Blackwall wissenschaftsverlag, Berlin, Wien, 1995.

Schmidt, M. W. I., Torn, M. S., Abiven, S., Dittmar, T., Guggenberger, G., Janssens, I. a., Kleber, M., Kögel-Knabner, I., Lehmann, J., Manning, D. a. C., Nannipieri, P., Rasse, D. P., Weiner, S., and Trumbore, S. E.: Persistence of soil organic matter as an ecosystem property, Nature, 478, 49–56, https://doi.org/10.1038/nature10386, 2011.

Schrumpf, M. and Kaiser, K.: Large differences in estimates of soil organic carbon turnover in density fractions by using single and repeated radiocarbon inventories, Geoderma, 239–240, 168–178, https://doi.org/10.1016/j.geoderma.2014.09.025, 2015.

Schrumpf, M., Kaiser, K., Guggenberger, G., Persson, T., Kögel-Knabner, I., and Schulze, E. D.: Storage and stability of organic carbon in soils as related to depth, occlusion within aggregates, and attachment to minerals, Biogeosciences, 10, 1675–1691, https://doi.org/10.5194/bg-10-1675-2013, 2013.

Sierra, C. A.: Forecasting atmospheric radiocarbon decline to pre-bomb values, Radiocarbon, 60, 1055–1066, https://doi.org/10.1017/RDC.2018.33, 2018.

Sierra, C. A., Müller, M., and Trumbore, S. E.: Modeling radiocarbon dynamics in soils: SoilR version 1.1, Geoscientific Model Development, 7, 1919–1931, https://doi.org/10.5194/gmd-7-1919-2014, 2014.

Sierra, C. A., Hoyt, A. M., He, Y., and Trumbore, S. E.: Soil Organic Matter Persistence as a Stochastic Process: Age and Transit Time Distributions of Carbon in Soils, Global Biogeochemical Cycles, 32, 1574–1588, https://doi.org/10.1029/2018GB005950, 2018.

Slessarev, E. W., Lin, Y., Jiménez, B. Y., Homyak, P. M., Chadwick, O. A., D'Antonio, C. M., and Schimel, J. P.: Cellular and extracellular C contributions to respiration after wetting dry soil, Biogeochemistry, 147, 307–324, https://doi.org/10.1007/s10533-020-00645-y, 2020.

Solly, E., Schöning, I., Boch, S., Kandeler, E., Marhan, S., Michalzik, B., Müller, J., Zscheischler, J., Trumbore, S. E., and Schrumpf, M.: Factors controlling decomposition rates of fine root litter in temperate forests and grasslands, Plant and Soil, 382, 203–218, https://doi.org/10.1007/s11104-014-2151-4, 2014.

Steinhof, A.: Data Analysis at the Jena 14C Laboratory, Radiocarbon, 55, 282–293, https://doi.org/10.2458/azu_js_rc.55.16350, 2013.

Stuiver, M. and Polach, H. A.: Reporting of 14C Data, Radiocarbon, 19, 355–363, https://doi.org/10.1017/S0033822200003672, 1977.

Trumbore, S.: Age of soil organic matter and soil respiration: Radiocarbon constraints on belowground C dynamics, Ecological Applications, 10, 399–411, https://doi.org/10.1890/1051-0761(2000)010[0399:AOSOMA]2.0.CO;2, 2000.

Trumbore, S.: Radiocarbon and Soil Carbon Dynamics, Annual Review of Earth and Planetary Sciences, 37, 47–66, https://doi.org/10.1146/annurev.earth.36.031207.124300, 2009.

Vaughn, L. J. S. and Torn, M. S.: C evidence that millennial and fast-cycling soil carbon are equally sensitive to warming, Nature Climate Change, 9, https://doi.org/10.1038/s41558-019-0468-y, 2019.

Warren, C. R.: Do microbial osmolytes or extracellular depolymerisation products accumulate as soil dries?, Soil Biology and Biochemistry, 98, 54–63, https://doi.org/10.1016/j.soilbio.2016.03.021, 2016.

Williams, M. A. and Xia, K.: Characterization of the water soluble soil organic pool following the rewetting of dry soil in a drought-prone tallgrass prairie, Soil Biology and Biochemistry, 41, 21–28, https://doi.org/10.1016/j.soilbio.2008.08.013, 2009.

Wu, J. and Brookes, P. C.: The proportional mineralisation of microbial biomass and organic matter caused by air-drying and rewetting of a grassland soil, Soil Biology and Biochemistry, 37, 507–515, https://doi.org/10.1016/j.soilbio.2004.07.043, 2005.

Wynn, J. G., Bird, M. I., and Wong, V. N. L.: Rayleigh distillation and the depth profile of 13C/ 12C ratios of soil organic carbon from soils of disparate texture in Fe Range National Park, Far North Queensland, Australia, Geochimica et Cosmochimica Acta, 69, 1961–1973, https://doi.org/10.1016/j.gca.2004.09.003, 2005.

Xiang, S., Doyle, A., Holden, P. A., and Schimel, J. P.: Drying and rewetting effects on C and N mineralization and microbial activity in surface and subsurface California grassland soils, Soil Biology and Biochemistry, 40, 2281–2289, https://doi.org/10.1016/j.soilbio.2008.05.004, 2008.

Xu, X., Trumbore, S. E., Zheng, S., Southon, J. R., McDuffee, K. E., Luttgen, M., and Liu, J. C.: Modifying a sealed tube zinc reduction method for preparation of AMS graphite targets: Reducing background and attaining high precision, Nuclear Instruments and Methods in Physics Research, Section B: Beam Interactions with Materials and Atoms, 259, 320–329, https://doi.org/10.1016/j.nimb.2007.01.175, 2007.

3. Study 2

"Soil minerals mediate climatic control of soil C cycling on annual to centennial timescales"

Contribution: I conceived the idea for the study, conducted the study, visualized the results, and wrote the manuscript with inputs from Susan Trumbore, Marion Schrumpf, Alison Hoyt, and Georg Guggenberger, and Craig Rasmussen. Archived samples and mineralogical data were originally collected and prepared by Craig Rasmussen (see text for details).

Keywords: soil carbon, radiocarbon, time series, parent material, climate, incubation, soil archives

Under review in: SOIL

DOI: 10.5194/egusphere-2022-1083

Soil minerals mediate climatic control of soil C cycling on annual to centennial timescales

Jeffrey Beem-Miller[1], Craig Rasmussen[2], Alison M. Hoyt[1,3], Marion Schrumpf[1], Georg Guggenberger[4], & Susan Trumbore[1]

[1] Department of Biogeochemical Processes, Max Planck Institute for Biogeochemistry, Jena, Germany

[2] Department of Environmental Science, The University of Arizona, Tucson, AZ, USA

[3] Department of Earth System Science, Stanford University, Stanford, CA, USA

[4] Institute of Soil Science, Leibniz University Hannover, Hannover, Germany

Correspondence: J. Beem-Miller; email: jbeem@bgc-jena.mpg.de

3.1. Abstract

Climate and parent material both affect soil C persistence, yet the relative importance of climatic versus mineralogical controls on soil C dynamics remains unclear. To test this, we collected soil samples in 2001, 2009, and 2019 along a combined gradient of parent material (andesite, basalt, granite) and climate (mean annual soil temperature (MAST): 6.5 °C "cold", 8.6 °C "cool", 12.0 °C "warm"). We measured the radiocarbon of heterotrophically respired CO_2 ($\Delta^{14}C_{respired}$) and bulk soil C ($\Delta^{14}C_{bulk}$) as proxies for transient and persistent soil C, and characterized mineral assemblages using selective dissolution. Using linear regression, we observed that MAST was not a significant predictor of either $\Delta^{14}C_{bulk}$ or $\Delta^{14}C_{respired}$, yet climate was highly significant as a categorical variable. Climate explained more variance in $\Delta^{14}C_{bulk}$ and $\Delta^{14}C_{respired}$ over 0–0.1 m, but parent material explained more from 0.1–0.3 m. Cool site soil C was more persistent (lower $\Delta^{14}C_{bulk}$) than cold or warm climate sites, and also more persistent on andesitic soils, followed by basaltic and then granitic soils. Poorly crystalline (oxy) hydroxides of Al and Fe (PCMs), but not crystalline Fe oxides (CRM), were significantly ($p < 0.1$) correlated with $\Delta^{14}C_{bulk}$, $\Delta^{14}C_{respired}$, and $\Delta^{14}C_{respired}$ - $\Delta^{14}C_{bulk}$, indicating their importance for soil C cycling on both short and long timescales. The change in $\Delta^{14}C_{respired}$ observed over the study period was linearly related to MAST for the granite soils with the lowest PCM content, but not in the andesitic and basaltic soils with higher PCM content. This link between PCM abundance and the decoupling of MAST and soil C cycling rates suggests PCMs may attenuate the temperature sensitivity of decomposition.

3.2. Introduction

Understanding the response of soil carbon stocks to current and future changes in climate requires insight into the environmental factors governing soil carbon dynamics. Climate, and in particular temperature, has been found to be the most important variable for explaining the age of soil carbon in topsoil at local to global scales (Frank et al., 2012; Mathieu et al., 2015; Shi et al., 2020). Yet our current understanding of soil organic matter decomposition underscores the importance of mechanisms that may control the temperature sensitivity of this process, such as the interaction between soil organic matter and minerals (Davidson et al., 2000; Rasmussen et al., 2005; Davidson and Janssens, 2006; Lehmann and Kleber, 2015). The effect of mineral-organic associations on the temperature sensitivity of soil organic matter has been addressed in several modeling studies (Tang and Riley, 2014; Abramoff et al., 2019; Woolf and Lehmann, 2019; Ahrens et al., 2020). These models typically invoke Michaelis Menten kinetics in addition to an Arrhenius-type temperature response in

order to account for energy and substrate limitations on decomposition rates of soil organic matter found in association with minerals (Tang and Riley, 2019; Ahrens et al., 2020). In situ studies comparing the role of soil mineral assemblages and temperature in explaining soil C dynamics over time are scarce, yet are critical for testing model-based findings. We designed the current study to quantify the relative importance of climatic versus mineralogical mechanisms of soil organic C persistence across time scales ranging from annual to centennial and beyond.

The relevance of soil minerals for mediating soil organic matter protection has been found to be a function of the specific minerals present, rather than the amount of clay or total mineral surface area (Kramer and Chadwick, 2018; Rasmussen et al., 2018a). Soil mineral assemblages are dynamic, developing over time as primary minerals inherited from parent material weather to form reactive, poorly crystalline secondary minerals, which in turn eventually weather or ripen into increasing stable crystalline species (Mikutta et al., 2010; Slessarev et al., 2022). The relative abundance of PCMs and CRMs in soils is directly related to parent material, but is also a function of mineral weathering rates (Rasmussen et al., 2018a; Slessarev et al., 2022). This is relevant for soil C dynamics, as soils enriched in PCMs are known to be of particular importance for the accumulation and persistence of soil C (Torn et al., 1997; Masiello et al., 2004). Due to the strong effect of climate on weathering, different soil mineral assemblages can form from the same parent material under different climatic regimes (Kramer and Chadwick, 2016; Rasmussen et al., 2018b). Conversely, similar mineral assemblages can be found among soils developed on different parent materials given adequate time for weathering and similar vegetation and climate (Graham and O'Geen, 2010; Rasmussen, 2004; Rasmussen et al., 2010a, 2010b). These complex interactions demonstrate that climatic and mineralogical controls on soil C cycling are not independent, but interact over the centennial to millennial time scales of soil development.

The potential for ligand exchange is a key determinant of the strength and sorptive capacity of soil minerals. This potential is a function of surface area, charge, and in particular, the density of accessible hydroxyl groups (Kaiser and Guggenberger, 2003; Kleber et al., 2015; Rasmussen et al., 2018a). Poorly crystalline Al and Fe (oxy) hydroxides are particularly enriched in hydroxyl groups, and batch sorption/desorption experiments have shown that the mineral-organic interactions between pedogenic metal oxide-rich clays are stronger than those with siloxane-rich phyllosilicate clays (Kahle et al., 2004). Furthermore, the reactive properties of pedogenic metal (oxy) hydroxides/oxides can also facilitate lower strength interactions with soil organic matter through multivalent cation bridging (Kleber et al., 2007). The high reactivity of poorly crystalline Fe (oxy)

hydroxides in particular is also implicated in the observations that these Fe mineral phases are correlated with aggregate stability but crystalline Fe oxide content is not (Duiker et al., 2003).

Rasmussen et al. (2018b) observed that oxalate extractable Fe, which extracts poorly crystalline Fe (oxy) hydroxides, was the best predictor both soil C concentration and $\Delta^{14}C_{bulk}$ across soils with mixed mineralogies. In contrast, crystalline Fe oxides, as represented by the difference between dithionite-citrate extractable Fe and ammonium-oxalate extractable Fe, were not as well correlated with $\Delta^{14}C_{bulk}$ or SOC as PCMs in this study (Rasmussen et al., 2018b). Yet other studies have demonstrated that the strength of the correlations between PCM or CRM abundance and SOC or $\Delta^{14}C_{bulk}$ may be depth dependent, with CRMs more relevant in the A horizon and PCMs in the B horizon (Masiello et al., 2004). In spite of much study, the relevance of mineral-organic associations with specific mineral phases such as poorly crystalline Fe and Al (oxy) hydroxides or crystalline Fe oxides for shorter timescales of soil C cycling remains an open question (Heckman et al., 2018).

Radiocarbon (^{14}C) is a useful tracer for soil C dynamics over annual to millennial time scales (Trumbore, 2000). The use of ^{14}C to measure timescales of soil carbon decomposition is reliant on our knowledge of the $^{12}C/^{14}C$ ratio of atmospheric CO_2. Once CO_2 is fixed into organic matter via photosynthesis this ratio starts to shift, as ^{14}C is preferentially lost due to radioactive decay. Changes in the $^{12}C/^{14}C$ ratio due to radioactive decay are detectable at timescales of hundreds to thousands of years. However, we can detect changes in ^{14}C with nearly annual resolution for the so-called "bomb-C" period, which began with the atmospheric testing of nuclear weapons in the mid-20th century (Trumbore, 2000). This pulse of "bomb-C" led to a doubling of atmospheric ^{14}C concentration prior to the ban on above-ground nuclear tests in 1963 (Hua et al., 2021). The level of ^{14}C in the atmosphere returned to pre-bomb levels around 2020, thus archived samples now represent the best opportunity to construct a high-resolution time series of the bomb-C pulse as it moves through different soil organic matter pools (Trumbore, 2009).

Soil is an open system, and this has important implications for the interpretation of radiocarbon measurements of soil C. For most soils, the majority of carbon that enters the soil leaves quickly, with only a small fraction persisting on time scales > 10 y (Sierra et al., 2018; Crow and Sierra, 2022). The signal from these persistent pools typically dominate measurements of $\Delta^{14}C_{bulk}$, while the signal from more transient pools dominate measurements of $\Delta^{14}C_{respired}$ (Trumbore, 2000). Here we define "transient" for C cycling on annual to decadal timescales, while we use "persistent" to refer to C cycling on centennial to millennial timescales. A diagnostic feature of $\Delta^{14}C_{bulk}$ and $\Delta^{14}C_{respired}$ is that

when these two metrics are the same, this indicates all of the C in the soil has an equal probability of being decomposed by microbes, i.e., the system is homogenous (Sierra et al., 2017). However, when $\Delta^{14}C_{bulk}$ and $\Delta^{14}C_{respired}$ are substantially different, this indicates the presence of both labile and persistent pools of soil C (Ewing et al., 2006; Hopkins et al., 2012).

We turned to the western slope of the Sierra Nevada Mountains, USA to compare and contrast the effects of climate and mineral assemblage on soil C dynamics. Drawing on earlier studies in this region (Jenny et al., 1949; Harradine and Jenny, 1958; Trumbore et al., 1996, p.199; Dahlgren et al., 1997; Rasmussen, 2004), we selected soils similar in age and vegetation along a combined gradient of parent material (granite, andesite, basalt) and MAST (6.5 °C, 8.6 °C, 12.0 °C). The climate gradient also represents a weathering gradient, with poorly developed soils at the cold climate sites, intermediately developed soils at the cool climate sites, and highly weathered soils at the warm climate sites (Rasmussen, 2004; Rasmussen et al., 2010a, 2010b). Previous work at these sites (Rasmussen, 2004; Rasmussen et al., 2010a, 2010b, 2018b) and nearby locations (Trumbore et al., 1996; Dahlgren et al., 1997; Castanha et al., 2008; Koarashi et al., 2012) confirmed strong differences in mineral assemblages along both the parent material and climate gradients, making these sites an ideal setting for probing the relative influence of climatic and mineralogical factors (and their interactions), on soil C dynamics.

We were able to construct a time series of both $\Delta^{14}C_{bulk}$ and $\Delta^{14}C_{respired}$ at these sites by combining data from samples newly collected in 2019 with data from archived samples collected in 2001 and 2009-2010 (referred to subsequently as 2009). Such a time series provides a crucial constraint for determining the trajectory of bomb-derived ^{14}C concentrations over time (Baisden et al., 2002; Stoner et al., 2021). Whether bomb-C concentrations are increasing or decreasing in bulk or respired CO_2 over time depends on both on the distribution of soil C among pools with different cycling rates as well as the year in which the soil was sampled (Beem-Miller et al., 2021). Given this, the trajectory of ^{14}C cannot be easily determined from observations at a single point in time (Baisden et al., 2013). Using the radiocarbon time series in combination with previously determined mineralogical data, we were able to test several hypotheses regarding the roles of mineralogical versus climatic factors in determining both overall cycling rates and the dynamics of transiently cycling soil C.

We can expect soils with large stocks of persistent soil C to have depleted values of $\Delta^{14}C_{bulk}$ relative to soils dominated by fast cycling soil C. If climate proves more important than parent material for determining soil C persistence, than we would expect to see large differences in $\Delta^{14}C_{bulk}$ among

climate regimes when comparing soils within a given parent material, but minimal differences among parent materials when comparing soils within the same climate regime. However, if parent material proves more important than climate for soil C persistence, we would expect the opposite trends in $\Delta^{14}C_{bulk}$: differences would be greater among parent materials within a given climate regime than among climate regimes within a given parent material. Alternatively, if persistent soil C were associated with specific soil minerals, we would expect an interactive effect of parent material and climate on $\Delta^{14}C_{bulk}$. For example, if soil C persistence is due to the association of soil organic matter with PCMs, we would expect to observe the most depleted $\Delta^{14}C_{bulk}$ values where the combination of parent material and climate factors has led to the greatest abundance of these specific soil minerals.

Soil C found in association with minerals is typically older than organic matter found in free particulate forms (Lavallee et al., 2020). Accordingly, we might expect climate to be the dominant factor controlling the amount and cycling rates of C in transiently cycling soil C pools, with mineral factors being less relevant at these shorter timescales. If this hypothesis is correct, we would expect to see greater differences in $\Delta^{14}C_{respired}$ among different climate regimes and within a given parent material than we would among different parent materials within the same climate regime. Furthermore, given sufficient moisture, we would expect warmer climate soils to have $\Delta^{14}C_{respired}$ values closer to the atmosphere than colder climate soils, due to faster decomposition rates in the actively cycling soil C pools. Accordingly, we would also expect $\Delta^{14}C_{respired}$ to change more over time at the warmer climate sites than at the colder climate sites.

3.3. Methods

3.3.1 Site descriptions

We collected samples from nine sites in the Sierra Nevada Mountains of California (see Rasmussen et al., 2018b for a map of sampling locations). Parent material changes from basalt to andesite to granite along the north-south axis of the cordillera, while MAST decreases as a function of increasing elevation along the east-west axis (**Table 3-1**). Total mean annual precipitation (MAP) ranges from 910 to 1400 mm yr^{-1} across the sites. Precipitation increases slightly with elevation (**Table 3-1**), and falls mainly as rain at lower elevations (< 1400 m), but mainly as snow at higher elevations (> 1800 m) (Rasmussen, 2004). The andesitic and basaltic parent materials receive slightly more precipitation on average than the granitic soils, with MAP of 1330 (± 75) mm yr^{-1}, 1160 (± 175) mm yr^{-1}, and 1000 (± 85) mm yr^{-1} averaged across the andesite, basalt, and granite transects, respectively.

Vegetation at the study sites is typical of the Sierran Mixed Conifer habitat (Parker and Matyas, 1981). All of the sites are forested and dominated by conifers. The species composition changes along the elevation and climate gradient, but not along the parent material gradient. Tree species at the lowest elevation warm climate sites are predominantly *Pinus ponderosa* mixed with lesser amounts of *Quercus* spp. The canopy species at the mid-elevation cool climate sites consist primarily of *Abies concolor* and *Pinus lambertiana*, while *Abies magnifica* dominates at the high elevation cold climate sites. Species present at all sites include *Calocedrus decurrens* in the canopy, the shrubs *Arctostaphylos* spp., *Chamaebatia foliolosa*, and *Ceanothus* spp. in the understory, and variable ground cover of grasses and forbs.

3.3.2 Sample collection

Site locations were initially established in 2001 by Rasmussen (2004) and resampled in 2009 (Rasmussen et al., 2018b) and 2019 (this study). Three replicate pits were dug at each site. Only samples collected from the A horizon were available from 2001, so we focus on the upper mineral soil layers in this study (0 to ca. 0.3 m) despite availability of sample from deeper soil layers in 2009 and 2019. Sampling was done from pit sidewalls by horizon in 2001 and 2009, and by 0.1 m increments in 2019. We located the sites for the 2019 sampling using GPS and geospatial coordinates recorded during site establishment. Prior to sample collection we compared the soil profiles to the pedon descriptions from the 2001 sampling campaign to confirm the profiles matched.

3.3.3 Incubations

Laboratory soil incubations were performed on composite samples from the three replicate profiles sampled at each site in 2001 and 2019. We omitted the 2009 samples from the incubation experiment because sample material was only available from a single profile at each site. We composited and incubated each depth increment separately in 1 L glass mason jars fitted with airtight sampling ports in the lids. Incubations were performed in duplicate. Prior to the start of incubations, we adjusted the soil moisture content to 60% of water holding capacity (WHC). Samples from 2001 were air-dried prior to archiving, and therefore we also air-dried the freshly collected soils from 2019 in order to control for the known effects of air-drying and rewetting on $^{14}C_{respired}$ (Beem-Miller et al., 2021). We defined WHC as the gravimetric water content of water-saturated soil placed in mesh-covered (50μm) tubes (50ml) weighed after draining for 30 minutes on a bed of fine sand. Following rewetting we allowed the soils to respire for one week before closing the jars.

Incubations proceeded until CO_2 concentrations in the jar headspace reached approximately 10,000 ppm, at which point we collected a 400 ml gas subsample for radiocarbon analysis. While differences in incubation duration can lead to substrate depletion, potentially affecting $\Delta^{14}C_{respired}$, we do not believe this would impact the results presented here due to the relatively short duration of all of these incubations (**Supplemental Figure 3-2**).

Gas samples were collected with pre-evacuated stainless-steel vacuum canisters (Restek GmbH, Bad Homburg, Germany). All incubations were performed in the dark at 20°C.

3.3.4 Soil Physical Analyses and Mineral Characterization

Data on soil particle size distribution, bulk density, and mineral characterization were obtained from previously published analyses of samples collected at the study sites in 2001 and 2009 (Rasmussen, 2004; Rasmussen et al., 2005, 2007, 2010a, b, 2018b). Both qualitative and quantitative approaches were used to characterize soil mineral assemblages, including X-ray diffraction (XRD) for the clay (<2 μm) fraction, and non-sequential selective dissolution. These previous analyses revealed that the dominant mineral species in the soils of the highly weathered warm climate zone were similar across parent materials, but differed substantially across parent materials at the less weathered cool and cold climate sites. Mineral assemblages at the warm climate sites are dominated by 1:1 clays and large accumulations of crystalline Fe oxides (Dahlgren et al., 1997; Rasmussen et al., 2010a, b). In contrast, the cool and cold climate andesitic soils contain high concentrations of short-range order minerals such as allophane and Fe oxyhydroxides. The cool and cold climate basaltic soils contain intermediate amounts of reactive secondary minerals, while the granitic soils lack reactive secondary minerals almost entirely, but are rich in quartz and contain relatively more hydroxyl-interlayered vermiculite than soils from the other lithologies (Rasmussen, 2004).

The previous work at these sites showed that the oxalate extractable Fe was the best predictor of both C abundance and $^{14}C_{bulk}$, but that oxalate extractable Al was also strongly correlated with these metrics (Rasmussen et al., 2018b). Accordingly, our analyses focus on the relationship between radiocarbon measurements and the abundance of PCMs (sum of ammonium-oxalate extractable Al and half of the ammonium-oxalate extractable Fe selectively dissolved from bulk soils). We also compared the relationship between $\Delta^{14}C$ (bulk and respired) and CRM abundance (difference of dithionite-citrate extractable Fe and ammonium-oxalate extractable Fe) (Masiello et al., 2004; Kleber et al., 2005). A caveat for the use of CRM as defined here as a proxy for crystalline (oxy) hydroxides

is that this excludes crystalline forms of Al. The dithionite-citrate extraction also excludes gibbsite, however as gibbsite was quantified by Rasmussen et al. (2018), we were able to assess the effect of gibbsite separately and did not find it to explain a significant amount of the variance in $\Delta^{14}C_{bulk}$ or $\Delta^{14}C_{respired}$.

3.3.5 Carbon, Nitrogen, and Radiocarbon Analysis

Total carbon content was determined by dry combustion (2019 samples: Vario Max, Elementar Analysensysteme GmbH, Langenselbold, Germany) on finely ground soils (2019 samples: MM400, Retsch GmbH, Haan, Germany). For radiocarbon analysis of 2001 and 2019 samples, we first purified CO_2 from combusted soil samples (bulk soils) and incubation flask samples (respired CO_2) on a vacuum line using liquid N_2. Following purification, samples were graphitized with an Fe catalyst under an H_2 enriched atmosphere at 550 °C. Radiocarbon content was then measured by accelerator mass spectrometry (Micadas, Ionplus, Zurich, Switzerland) at MPI-BGC (Steinhof et al., 2017). See Rasmussen et al. (2018b) for details of C and radiocarbon analysis of the 2009 samples.

We report radiocarbon values using units of $\Delta^{14}C$, defined as the deviation in parts per thousand of the ratio of $^{14}C/^{12}C$ from that of the oxalic acid standard measured in 1950. This unit also contains a correction for the potential effect of mass-dependent fractionation by normalizing sample ^{13}C to a common value of -25 ‰ (Stuiver and Polach, 1977). Values of $\Delta^{14}C > 0$ indicate the presence of 'bomb' C produced by atmospheric weapons testing in the early 1960s; values of $\Delta^{14}C < 0$ indicate radioactive decay of ^{14}C, which has a half-life of 5730 years.

3.3.6 Spline fitting

We used a spline function to compare soil properties from samples collected from different depth intervals in different years and at different sites. We were motivated to use consistent depth increments across sites when resampling in 2019 because of the strong correlation between depth and $\Delta^{14}C$ observed in the 2009 dataset, a correlation also noted in numerous other studies (Mathieu et al., 2015; Shi et al., 2020). We fit a mass-preserving quadratic spline to the 2001 and 2009 profiles in order to convert soil property data to the equivalent depth increments sampled in 2019 (Bishop et al., 1999). We performed the spline fitting with the 'mpspline' function of the GSIF package in R, using a value of 0.1 (Hengl, 2019).

3.3.7 Statistical analysis

We used a linear modeling approach to assess the relative explanatory power of climate versus parent material on the observed variation in $\Delta^{14}C$, as well as potential interactions between these two factors. We constructed separate models for $\Delta^{14}C_{bulk}$ and $\Delta^{14}C_{respired}$ but with the same equation structure (Eq. 3-1). For each model we considered the two-way interaction between parent material and climate as well as the three-way interaction with time. For ease of interpretation, we considered the effect of depth by modeling each depth layer separately (0–0.1 m, 0.1–0.2 m, 0.2–0.3 m). We also made pairwise comparisons of $\Delta^{14}C_{bulk}$ and $\Delta^{14}C_{respired}$ across sites and within years, and across years for individual sites. We assessed the significance of the temporal trend for pairwise combinations of parent material and climate using the 'emmtrends' function of the emmeans package (Lenth, 2021). We corrected for multiple comparisons using Tukey's honestly significant mean difference.

$$\Delta^{14}C = \alpha + \beta_1(Parent_{material}) \times \beta_2(Climate) \times \beta_3(Year) + \varepsilon, \quad (3\text{-}1)$$

where α is the intercept term, the β terms are coefficients, and ε is random error.

We also considered the relationship between $\Delta^{14}C_{bulk}$ and $\Delta^{14}C_{respired}$ in order to gain insight into potential differences in soil C dynamics and persistence mechanisms across our sites (Sierra et al. 2018). We modeled the effects of parent material (Eq. 3-2) and climate (Eq. 3-3) on this relationship separately, as we did not have an adequate number of observations to consider the interactions. For this analysis, we used $\Delta^{14}C$ measurements made on samples collected in 2001 and 2019, and data from all depths. We excluded both depth and time from the models as the three-way interactions between depth or time, $\Delta^{14}C_{bulk,}$ and the explanatory variable (parent material in Eq. 3-2, or climate in Eq. 3-3) were not significant.

$$\Delta^{14}C_{respired} = \alpha + \beta_1(\Delta^{14}C_{bulk}) \times \beta_2(Parent\_material) + \epsilon \quad (3\text{-}2)$$

$$\Delta^{14}C_{respired} = \alpha + \beta_1(\Delta^{14}C_{bulk}) \times \beta_2(Climate) + \epsilon \quad (3\text{-}3)$$

We assessed the relative importance of PCMs versus CRMs in protecting soil C from microbial decomposition by regressing $\Delta^{14}C$ against the concentrations of ammonium-oxalate extractable Fe, ammonium-oxalate extractable Al, pyrophosphate extractable Al, and dithionite-citrate extractable Fe (Eq. 3-4). We fit the model for $\Delta^{14}C_{bulk}$, $\Delta^{14}C_{respired}$, and the difference between $\Delta^{14}C_{respired}$ and $\Delta^{14}C_{bulk}$

($\Delta^{14}C_{\text{bulk-respired}}$). We used ^{14}C data from 2001, 2009, and 2019 for the $^{14}C_{\text{bulk}}$ model, but only data from 2001 and 2019 for the $\Delta^{14}C_{\text{respired}}$ and $\Delta^{14}C_{\text{bulk-respired}}$ models (as $^{14}C_{\text{respired}}$ data were not available for the 2009 samples). Selective dissolution was only performed on the soils collected in 2001, but these data were assumed to be comparable for the other time points as they reflect weathering processes operating at timescales much beyond the 18-year duration of this study. The regression analysis conducted with Eq. 3-4 was done for the combined depth increment of 0–0.3 m, as extracted metal concentrations did not change substantially over this depth (Rasmussen et al., 2018b). Combining depth increments allowed us to control for the depth dependence of $\Delta^{14}C$ as well as to simplify interpretation of the data. In order to obtain values for the necessary data over the 0 to 0.3 m depth increment we computed mass-weighted estimates of extractable metal concentrations, carbon mass-weighted means of $\Delta^{14}C_{\text{bulk}}$, and flux-weighted means of $\Delta^{14}C_{\text{respired}}$; these calculations were made prior to determining $\Delta^{14}C_{\text{bulk-respired}}$.

$$\Delta^{14}C = \alpha + \beta_1(Metal_x) + \beta_2(time) + \varepsilon, \qquad (3\text{-}4)$$

where α is the intercept term, β is the coefficient for each factor in the model, $Metal_x$ is the concentration of selectively dissolved metal oxides, $time$ is the year of sampling, and ε is random error.

We present the results of regression analyses looking at PCMs versus CRMs in the main text (**Figure 3-5**). Results for specific relationships between the concentration of Fe or Al extracted with ammonium-oxalate, Fe extracted with dithionite-citrate, and Al extracted with sodium-pyrophosphate, and $\Delta^{14}C_{\text{bulk}}$, $\Delta^{14}C_{\text{respired}}$, and the difference between $\Delta^{14}C_{\text{respired}}$ and $\Delta^{14}C_{\text{bulk}}$ ($\Delta^{14}C_{\text{respired-bulk}}$) are provided in the supplemental information (**Supplemental Figure 3-4**, **Supplemental Figure 3-5**, **Supplemental Figure 3-6**, **Supplemental Figure 3-7**, **Supplemental Figure 3-8**).

3.4. Results

3.4.1 Soil carbon concentrations and flux rates

We observed both parent material and climate effects on soil organic C (SOC) concentration (**Figure 3-1**, **a–c**). Concentrations of SOC were similar among parent materials for the warm climate sites (Fig. 1a), while at the cool and cold climate sites (**Figure 3-1**, **b** and **c**) the andesitic soils had higher SOC concentrations than either the basaltic or granitic soils. The basaltic and granitic soils had similar SOC concentrations across climate zones, while the cool and cold climate andesitic soils were

enriched in C relative to the warm climate soils. Soils showed a similar decrease in SOC concentration with depth across all sites (**Figure 3-1**). We did not calculate SOC stocks for the 2019 samples as we did not measure bulk density or coarse fragment content for these samples (Schrumpf et al., 2013; Beem-Miller et al., 2016). However, measurements of SOC stocks made in 2001 and 2009 showed similar overall trends as SOC concentration, with the highest SOC stocks observed in the andesitic soils, followed by the basalt and granitic soils for which SOC stocks were similar (**Figure 3-1**, **d–f**, see also Rasmussen et al., 2018b).

Soil organic C concentrations did not change significantly over time at the majority of our sites (**Supplemental Figure 3-1**). We saw the most substantial variation in SOC concentration between 2001, 2009, and 2019 in the surface mineral layers (0–0.1 m). We observed significant differences between years for the 0–0.1 m layer at the warm climate andesitic and basaltic sites, and for 0–0.1 m, 0.1–0.2 m, and 0.2–0.3 m layers at the cold climate andesitic site (**Supplemental Table 3-1**).

Flux rates of heterotrophic respiration differed among parent materials and among climate zones. When compared on a carbon basis (mg CO_2 g C^{-1} d^{-1}), flux rates tended to be higher for the andesitic soils than soils from either basaltic or andesitic soils, particularly at depth (**Supplemental Figure 3-2**). The exceptions to this trend were the surface (0–0.1 m, 2001 and 2019) and near-surface (0.1–0.2 m, 2019) soils from the warm climate sites (**Supplemental Figure 3-2**). Respiration rates for granitic and basaltic soils tended to decrease with decreasing MAST (warm > cool > cold); however, we did not see any clear trend in respiration rates with respect to climate for the andesitic soils (**Supplemental Figure 3-2**).

3.4.2 Radiocarbon depth profiles
3.4.2.1.   Bulk soil.

$\Delta^{14}C_{bulk}$ covaried with both parent material and climate. We observed the most enriched $\Delta^{14}C_{bulk}$ at the warm climate sites, indicating a preponderance of relatively young, fast-cycling C in these soils. However, contrary to what would be expected from the decomposition-temperature relationship, we observed the oldest soil C (i.e., most depleted $\Delta^{14}C_{bulk}$ values) at the cool climate sites with intermediate MAST (**Figure 3-2**, **b**) rather than at the cold climate sites (**Figure 3-2**, **c**). When comparing $\Delta^{14}C_{bulk}$ from different parent materials within a given climate zone, $\Delta^{14}C_{bulk}$ of andesitic soils tended to be the most depleted, while the granitic soils tended to be the most enriched (**Figure 3-2**, **a–c**; **Supplemental Table 3-2**, **Supplemental Table 3-3**, **Supplemental Table 3-4**). We focus

here on the 2019 data for simplicity, but $\Delta^{14}C_{bulk}$ profiles showed similar patterns in both 2001 (**Supplemental Figure 3-3**, **a**) and 2009 (Rasmussen et al., 2018b).

Analysis of variance for $\Delta^{14}C_{bulk}$ revealed significant two-way interactions between parent material and climate at all depths (**Table 3-2**). This interaction was evident in the differences in $\Delta^{14}C_{bulk}$ that we observed among parent materials within each climate zone. We observed the greatest differences in $\Delta^{14}C_{bulk}$ among parent materials at the warm and cool sites (**Figure 3-2**, **a-b**), while $\Delta^{14}C_{bulk}$ was similar among parent materials at the coldest sites (**Figure 3-2**, **c**). We also found depth to be an important factor influencing the relative importance of climate versus parent material effects on $\Delta^{14}C_{bulk}$. Although $\Delta^{14}C_{bulk}$ declined with depth for all sites, climate explained more of the variance in $\Delta^{14}C_{bulk}$ in the uppermost soil layer (0–0.1 m) whereas parent material explained more in the bottom two layers (0.1–0.2 m, 0.2–0.3 m) (**Table 3-2**).

3.4.2.2.   Heterotrophically respired CO_2.

The patterns we observed in $\Delta^{14}C_{respired}$ were similar to those we observed in $\Delta^{14}C_{bulk}$ (**Figure 3-2**, **d–f**). We found climate to the only significant factor for explaining the variance observed in $^{14}C_{respired}$ in the uppermost soil layer (0–0.1 m), while at the deepest depth (0.2–0.3 m) parent material was more important than climate (**Table 3-2**). Overall, we found the two-way interaction between parent material and climate explained more of the variance in $\Delta^{14}C_{respired}$ than it did in $\Delta^{14}C_{bulk}$ (**Table 3-2**).

The effect of climate on $\Delta^{14}C_{respired}$ was moderated by parent material. Accordingly, we did not observe significant differences in $\Delta^{14}C_{respired}$ among the andesitic soils when compared across climate zones at any depth (**Supplemental Table 3-2**, **Supplemental Table 3-3**, **Supplemental Table 3-4**). In contrast, $\Delta^{14}C_{respired}$ diverged substantially between climate zones for the basaltic and granitic soils, particularly for the 0.1–0.2 m and 0.2–0.3 m depth layers (**Figure 3-2**, **d–f**). Overall, $\Delta^{14}C_{respired}$ values across sites were most similar at the soil surface (0–0.1 m), and most divergent at the intermediate depth (0.1–0.2 m) (**Figure 3-2**, **d–f**).

3.4.3 Radiocarbon time series

Temporal trends in bulk and respired $\Delta^{14}C$ reflect the degree to which soil C is exchanging with C fixed from the atmosphere. The average annual decline in $\Delta^{14}C$ atmospheric CO_2 between 2001 and 2009 for the northern hemisphere was -5.13 ‰ y^{-1} (Graven et al., 2017; Sierra, 2018) (**Figure 3-3**,

dotted lines). Therefore, changes in Δ^{14}C of soil C that parallel the atmospheric trend must be exchanging relatively rapidly compared to those that change little over the same time period.

3.4.3.1.   Bulk soil

We observed a significant three-way interaction between parent material, climate, and time at all three depths in the linear models (Eq. 3-1) for $\Delta^{14}C_{bulk}$ (**Table 3-2**). The change over time in $\Delta^{14}C_{bulk}$ was also affected by depth, with greater differences seen between 2001 and 2019 in the uppermost soil layer than in the deeper layers (**Figure 3-3**, **a–f**). We observed a significant decrease in $\Delta^{14}C_{bulk}$ over time in both warm and cool climate granitic soils for the uppermost soil layer (0–0.1 m), and additionally for the warm climate andesitic soils (**Figure 3-3**, **a** and **c**; **Supplemental Table 3-5**). In the deeper soil layers (0.1–0.2 m and 0.2–0.3 m), we only observed a significant change over time in $\Delta^{14}C_{bulk}$ for the cool climate basalt and granite soils (**Figure 3-3**, **d**; **Supplemental Table 3-5**). $\Delta^{14}C_{bulk}$ of the cool climate andesitic soils remained essentially unchanged between 2001 and 2019 for all depths (**Figure 3-3**, **c-d**; **Supplemental Table 3-5**), underscoring the importance of the interaction between parent material and climate for explaining temporal trends in $\Delta^{14}C_{bulk}$.

The relationship of $\Delta^{14}C_{bulk}$ to atmospheric Δ^{14}C also depended on the combination of parent material and climate. In 2001, the warm climate sites were the only sites where the basaltic and andesitic soils were enriched relative to the atmosphere, and this enrichment was only observed for the uppermost soil layer (**Figure 3-3**, **a**). In contrast, 0–0.1 m layer granitic soils at both the warm and cool climate sites were enriched relative to the atmosphere in 2001 (**Figure 3-3**, **a** and **c**). For the cold climate sites, where $\Delta^{14}C_{bulk}$ was most similar across all three lithologies, $\Delta^{14}C_{bulk}$ was depleted relative to atmospheric in both surface and subsoil layers in 2001 (**Figure 3-3**, **e-f**).

We observed that $\Delta^{14}C_{bulk}$ remained either unchanged or tended to decrease between 2001 and 2019 across sites. In the latter case, the rates of change in $\Delta^{14}C_{bulk}$ were typically smaller than the corresponding change in atmospheric Δ^{14}C over the same period. Accordingly, $\Delta^{14}C_{bulk}$ measured in 2019 tended to be enriched relative to the atmosphere at more sites, and also more enriched at depth than in 2001. We observed surface soil $\Delta^{14}C_{bulk}$ (0–0.1 m) in 2019 to be enriched relative to the atmosphere at all sites except for the cool climate andesite soils (**Figure 3-3**; **Figure 3-2**, **d–f**). Furthermore, $\Delta^{14}C_{bulk}$ was enriched relative to the atmosphere down to 0.3 m at two of the sites in 2019: the warm climate granite soil (**Figure 3-2**, **d**) and cold climate basalt soil (**Figure 3-2**, **f**).

$\Delta^{14}C_{bulk}$ at the cool climate andesite site was the most depleted relative to the atmosphere at all time points (**Figure 3-3**, **c-d**).

3.4.3.2. Heterotrophically respired CO_2.

Temporal trends in $\Delta^{14}C_{respired}$ (**Figure 3-3**, **g–l**) tended to be of greater magnitude than what we observed for $\Delta^{14}C_{bulk}$ (**Figure 3-3**, **a–f**). However, changes in $\Delta^{14}C_{respired}$ between 2001 and 2019 still tended to be smaller in magnitude than the change observed in the atmosphere over this period (**Figure 3-3**, **g–l**). In contrast to $\Delta^{14}C_{bulk}$, $\Delta^{14}C_{respired}$ values of both surface and near surface soils (0–0.2 m) were close to atmospheric levels in 2001, while in 2019, $\Delta^{14}C_{respired}$ tended to be enriched relative to the atmosphere, even for the deeper soil layers (**Figure 3-3**, **g–l**).

We saw significant decreases in $\Delta^{14}C_{respired}$ over time for surface (0–0.1 m) soils at seven of the nine sites, with the only exceptions being the cool climate andesitic and cold climate granitic sites (**Figure 3-3**, **g–l**; **Supplemental Table 3-6**). In absolute terms, the changes in $\Delta^{14}C_{respired}$ over time in the uppermost soil layer were greatest at the warm sites (-4 ±2‰ y^{-1}), while changes were similar for the cool and cold sites (-2.7 ±1.2‰ y^{-1}, and -2.2 ±2.1‰ y^{-1}, respectively). When considered within parent materials, granitic soils showed the greatest decrease in $\Delta^{14}C_{respired}$ over time at the warm climate site and the least change at the cold climate site. In contrast, the andesitic soils showed the least amount of change over time at the cool climate sites, and changes over time in the basaltic soils were similar across all three of the climate zones (**Figure 3-3**, **g–l**).

The magnitude of the change in $\Delta^{14}C_{respired}$ over time tended to decrease with depth for all soils (**Figure 3-3**, **g–l**). For the 0.1–0.2 m layer, we observed significant negative trends over time for $\Delta^{14}C_{respired}$ at only four of the nine sites (warm andesite, cool basalt, cool granite, and cold basalt) (**Figure 3-3**, **h, j**, **l**; **Supplemental Table 3-6**), and only one site for the 0.2–0.3 m layer (cold basalt) (**Supplemental Table 3-3**). $\Delta^{14}C_{respired}$ at the cool andesitic soils remained unchanged at all depths over the study period (**Figure 3-3**, **g–l**; **Supplemental Table 3-6**).

We observed a significant increase in $\Delta^{14}C_{respired}$ from 2001 to 2019 at only one site: the cold climate granitic soil (**Figure 3-3**, **l**).; **Supplemental Table 3-6**). This was also the only soil for which $\Delta^{14}C_{respired}$ was more depleted than $\Delta^{14}C_{bulk}$. We observed this anomaly for the deeper soil layers in both 2001 and 2019. We measured $\Delta^{14}C_{respired}$ values of -469 and -127‰ for the 0.08–0.27 m layer in 2001, compared to $\Delta^{14}C_{bulk}$ values of -31 and -11‰ in the same year. Similarly, we observed $\Delta^{14}C_{respired}$ values of -397 and -24‰ for the 0.1–0.2 m layer in 2019, compared to -18 and 0‰ for

$\Delta^{14}C_{bulk}$. However, these anomalous values of $\Delta^{14}C_{respired}$ were restricted to the deeper soil layers from this one site, and were consistent over time, thus the response appears to be artifact that is unique to these soils. If old soil C dominated the release flux in situ, it would indicate the C dynamics of the system were not in equilibrium, which we think unlikely. We suspect this phenomenon is related to the specific response of these soils to the disturbance of the soil during sample extraction and preparation, and accordingly, we have excluded these highly depleted samples from the statistical analyses. This may be due to the lower pH of these soils (5.1) relative to the other sites (cf. Table S1 in Rasmussen et al., 2018b), which promotes increased desorption of organic matter (Chadwick and Chorover, 2001; Masiello et al., 2004).

3.4.4 Relationship of bulk soil and respired CO_2 ^{14}C

We assessed the relationship between $\Delta^{14}C_{bulk}$ and $\Delta^{14}C_{respired}$ using linear regression models for parent material Eq. (3-3) and climate Eq. (3-4). We observed that while $\Delta^{14}C_{respired}$ was enriched relative to $\Delta^{14}C_{bulk}$ for almost all sites and all depths, the magnitude of the difference depended on both parent material and climate. Accordingly, y-intercepts for all models were indistinguishable from or greater than zero, indicating that CO_2 respired by these soils is predominantly modern (i.e., < 60 years old) in all but the deepest soil layers, regardless of parent material or climate regime. We found the largest y-intercept values for the soils developed on andesitic parent material (72‰), and for soils in the cool climate zones (65‰), values indicating that CO_2 respired from these soils is relatively enriched in decadally cycling bomb-C.

Slope values less than one in these models indicate that every ‰ change in $\Delta^{14}C_{bulk}$ is associated with a correspondingly smaller change in $\Delta^{14}C_{respired}$. This suggests that the process regulating persistence of soil C on long time scales is distinct from that which regulates more transiently cycling soil C. Similar to what we found for the y-intercepts, modeled slopes for the parent material-only model (Eq. 3-2) were smallest for the andesitic soils: slope = 0.51, 95% CI = [0.22, 0.80]) (**Figure 3-4**, **a**), and for cool climate soils in the climate-only model (Eq. 3-3): slope = 0.61, 95% CI = [0.30, 0.91]) (**Figure 3-4**, **b**). While we could not test the interaction of parent material and climate factors in these models directly owing to the limited number of observations, we observed that mean differences in $\Delta^{14}C_{bulk}$ and $\Delta^{14}C_{respired}$ were substantially greater for the cool climate soils developed on andesitic parent material than for the other sites.

3.4.5 Mineral assemblages and radiocarbon

Mineral assemblage data is reported fully in Rasmussen et al. (2018b). Here we focus on the selective dissolution data with respect to the trends we observed in $\Delta^{14}C_{bulk}$, $\Delta^{14}C_{respired}$, and $\Delta^{14}C_{respired-bulk}$. We observed a significant negative correlation between $\Delta^{14}C_{bulk}$ and the concentration of oxalate extractable Fe, oxalate extractable Al, and pyrophosphate extractable Al (**Supplemental Figure 3-4**, **Supplemental Figure 3-5**, **Supplemental Figure 3-6**). However, for simplicity we focus here on the abundance of PCMs (the sum of ½ oxalate extractable Fe and oxalate extractable Al) and CRMs (the difference of dithionite-citrate extractable Fe and oxalate extractable Fe).

The relationship between PCM abundance and $\Delta^{14}C_{bulk}$ was highly significant (p <0.001), but the relationship between CRM abundance and $\Delta^{14}C_{bulk}$ was not (**Supplemental Figure 3-7**). For $\Delta^{14}C_{respired}$, we observed a significant relationship with PCM abundance for the 2001 samples (p = 0.04), but not for the 2019 samples (**Supplemental Figure 3-8**). Accordingly, the combined set of 2001 and 2019 data was only marginally significant (p = 0.07). However, we did see a highly significant relationship between PCM abundance and $\Delta^{14}C_{respired-bulk}$ (**Figure 3-5, a**). As with $\Delta^{14}C_{bulk}$, there was no relationship with CRM abundance for either $\Delta^{14}C_{respired}$ (**Supplemental Figure 3-8**) or $\Delta^{14}C_{respired-bulk}$ (**Figure 3-5**, **b**).

3.5.   Discussion

Climatic and mineralogical factors both play key roles in soil carbon persistence. However, the relevance of parent material for explaining soil organic matter persistence in soils with mixed mineralogies is still poorly explained. In the current study we illuminate how parent material interactions with climate lead to the development of distinct mineral assemblages, which in turn control the dynamics of soil C cycling at timescales ranging from annual to centennial. Our key findings are: 1) soil mineral characteristics mediate climatic controls on soil C cycling, and 2) mineralogical controls on soil C cycling are not limited to soil C persistence on centennial timescales, but are relevant for C cycling on shorter timescales as well.

Our results challenge the primacy of climatic controls on soil carbon persistence, insofar as we observed the most depleted $\Delta^{14}C_{bulk}$ in soils of the cool climate zone, not the cold climate zone. However, we found that as a categorical predictor, climate is critical for explaining the dynamics of both persistent and more transient soil C pools (as measured by proxy with $\Delta^{14}C_{bulk}$ and $\Delta^{14}C_{respired}$, respectively). Interestingly, our results indicate that soil mineral characteristics moderate the

strength of the climate effect. This is particularly apparent at depth. These findings are supported by a recent study in which the authors used a depth-resolved model with energy and substrate limitation prescribed by Michalis Menten kinetics to model profiles of $\Delta^{14}C_{bulk}$ (Ahrens et al., 2020). The authors found that mean annual temperature could only explain a minimal amount of variation in the observed radiocarbon profiles, while varying sorption potential in the model (a function of the soil mineral assemblage) allowed for a superior fit.

Previous work at our study sites showed that PCMs were key to explaining both soil C accumulation and $\Delta^{14}C_{bulk}$ values in these soils (Rasmussen et al., 2018b). Our results confirm these findings and extend them to demonstrate a highly significant correlation between PCM abundance and $\Delta^{14}C_{respired-bulk}$ (p = 0.001), and a significant correlation with $\Delta^{14}C_{respired}$ (p = 0.1). We focus here on $\Delta^{14}C_{respired-bulk}$, as this metric offers a unique insight into the magnitude of the difference between the cycling rates of persistent and more transiently cycling soil C.

We would expect the greatest differences between $\Delta^{14}C_{respired}$ and $\Delta^{14}C_{bulk}$ to be found in soils with a pool of old soil C protected from decomposition, and another pool of soil C that is readily decomposed. In contrast, the smallest differences should occur in soils lacking strong soil C protection mechanisms, in which the majority of soil C has an equal probability of being decomposed by microbes. Accordingly, we observed the smallest differences between $\Delta^{14}C_{respired}$ and $\Delta^{14}C_{bulk}$ in the soils with the lowest abundance of PCMs, while we observed the largest differences in the soils with the highest concentrations of these minerals (**Figure 3-5**). We interpret these findings as direct evidence of a key role for PCMs in protecting soil organic matter from decomposition. The values of $\Delta^{14}C_{bulk}$ in the subsurface layers (0.1–0.3 m) of the soils lacking substantial concentration of PCMs (e.g., granitic soils) were depleted relative to the atmosphere, indicating the presence of persistent soil C, yet we also observed similarly depleted values of $\Delta^{14}C_{respired}$ in these soils. Given that respiration rates were of the same magnitude across all soils (**Supplemental Figure 3-2**), this suggests that soil C persistence in these soils may be due to physical constraints on decomposition that are alleviated under laboratory incubation conditions, for example transport or isolation (Gleixner, 2013).

The soils with the greatest differences between $\Delta^{14}C_{respired}$ and $\Delta^{14}C_{bulk}$ were those that had both strongly depleted values of $\Delta^{14}C_{bulk}$ and values of $\Delta^{14}C_{respired}$ that were enriched relative to the atmosphere. If we employ a theoretical compartmental model to interpret this finding, a possible scenario would involve one pool of centennial to millennially cycling soil C whose signal dominates

the $\Delta^{14}C_{bulk}$ signal, and second pool of soil C enriched with C fixed from the atmosphere in the years immediately following the bomb-C spike, e.g., 1964 to 1990, whose signal dominates the $\Delta^{14}C_{respired}$ signal. More complex model structures could potentially be fit to these data, but the data provide clear evidence for the presence of at least two distinct pools: one with strongly depleted C largely inaccessible to the microbial community, and another pool enriched with decadally cycling C that is preferentially respired. This scenario can be contrasted to the soils with $\Delta^{14}C_{respired}$ values close to that of the atmosphere, in which the respired signal is likely dominated by close to annually cycling C.

Laboratory studies on mineral-organic matter associations show that only a portion of the organic matter is so tightly bound as to resist desorption (Kaiser and Guggenberger, 2003). Further studies have demonstrated that a portion of the sorbed organic matter can easily be mobilized by exchange with dissolved organic C (DOC) (Leinemann et al., 2018; Liebmann et al., 2022). In such a scenario, the highly depleted $\Delta^{14}C_{bulk}$ values observed in this study for the soils with a high abundance of PCMs may derive from organic matter that is strongly sorbed to mineral surfaces or trapped in micropores, while the bomb-C enriched decadally cycling C observed in the respiration flux could derive from a more microbially accessible and DOC-exchangeable mineral associated soil C pool that is in some way facilitated by PCMs (e.g., organo-metal complexes, cf. Lawrence et al., 2015; Heckman et al., 2018). However, the rates of change over time that we observed for $\Delta^{14}C_{respired}$ indicate that annually cycling C is also an important component of soil organic matter at all of our sites.

Our finding that parent material explains more of the variation in $\Delta^{14}C_{respired}$ at depth than climate suggests that the role of soil minerals in regulating annually to decadally cycling soil C is of particular importance in deeper soil layers. Dissolved organic C has been shown to move downward through the soil profile via preferential sorption of new soil C inputs and corresponding desorption of older DOC, which is then made available to the microbial community (Kaiser and Kalbitz, 2012). This process is mineral controlled, and while we did not test it directly, such a process could explain why we see an increase in the importance of parent material, and the interaction between climate and parent material, for explaining $\Delta^{14}C_{respired}$ trends with depth.

In contrast to what we observed for PCMs, the lack of correlation we observed between CRMs and soil radiocarbon suggests that these minerals do not play an important role in explaining soil C persistence on either short or long time scales, at least in these soils. Other studies have shown that crystalline Fe oxides do protect soil C from microbial decomposition, but that the overall sorption

capacity of these mineral species is low (Kahle et al., 2003). We observed a large increase in the amount of Fe dissolved from CRMs at the warm sites relative to the cool or cold sites, coinciding with a decrease in soil C concentration, and relative enrichment in both $\Delta^{14}C_{bulk}$ and $\Delta^{14}C_{respired}$. The increase in CRM abundance was also associated with a corresponding decrease in PCMs. Together, these trends suggest that these soils have lost PCMs through leaching and transformation into CRM species. Overall, the patterns of C concentrations, associated SOC stocks, $\Delta^{14}C_{bulk}$, and $\Delta^{14}C_{respired}$ observed across the climate/weathering gradient suggest that weathering and crystallization of PCMs leads to a reduction in soil carbon stocks caused by losses of old $\Delta^{14}C$-depleted carbon associated with these minerals, and that this process is relevant across a range of igneous parent materials.

The sensitivity of decomposition to temperature is of particular interest for understanding how soil C dynamics may change under a warming climate. Comparing the change in $\Delta^{14}C_{respired}$ over time for the different climate zones across different lithologies provides insight into this question. Focusing on the near surface soils (0–0.1 m), where climate effects are strongest, we observed that the rate of change in $\Delta^{14}C_{respired}$ over time was correlated with PCM abundance. We observed a linear relationship between MAST and the rate of change in $\Delta^{14}C_{respired}$ over time for the granitic soils, which had low abundances of PCMs in all three climate zones. This relationship was absent for the basalt and andesitic soils, which had higher concentrations of PCMs in the cool climate zone than in the cold climate zone. Furthermore, the change in $\Delta^{14}C_{respired}$ over time was similar in all of the warm climate zone soils lacking substantial PCM content. These findings provide evidence that the presence of PCMs is associated with a decoupling of MAST and soil C cycling rates, suggesting in turn that PCMs may attenuate the temperature sensitivity of soil organic matter decomposition. If this is true, we would expect that potential increases in decomposition rates and accompanying carbon losses due to climate warming would be greater in soils lacking PCMs than in soils enriched in these mineral phases.

3.6.   Conclusion

Our study shows clearly that parent material and climate interact to control soil C dynamics. This interaction is the key to explain trends in $\Delta^{14}C_{bulk}$, which is a proxy for the mean age of soil C, and additionally in $\Delta^{14}C_{respired}$, which reveals the relative contributions of faster or more slowly cycling soil C to respiration. We were unable to explain the trends in $\Delta^{14}C_{bulk}$, or $\Delta^{14}C_{respired}$ across all sites

with MAST, demonstrating the limits of relying on the temperature-decomposition relationship in determining soil C persistence, and the importance of considering soil mineral assemblages.

The results of this study imply that parent material and soil development rates can be equal in importance to temperature when determining soil C persistence. Specifically, intermediate aged soils developed on parent materials with the potential for substantial PCM development, such as basalt or andesite, can be expected to accumulate more C than soils lacking this potential, such as granite. Furthermore, changes in environmental conditions that accelerate the loss of PCMs via leaching or crystallization, e.g., low redox potential, low pH, warm temperatures and adequate moisture, can be expected to lead to SOC stock losses and a lower capacity to store soil C once the system returns to steady-state. Finally, the signal from decadally cycling soil C in $\Delta^{14}C_{respired}$ observed at the sites most enriched with PCMs provides preliminary evidence that the association of soil organic matter with these mineral phases may attenuate the temperature sensitivity of decomposition.

Code/Data availability

All data and code required to reproduce the analyses are available on Zenodo (Beem-Miller, 2022).

Acknowledgements

Financial support

3.7. Supplemental Information

3.7.1 Temporal trends in soil carbon

We did not observe clear trends in soil carbon concentration over time for the majority of sites, making us confident that most sites are at steady-state with regards to carbon stock changes (**Supplemental Figure 3-1**). Although we did observe substantial variation in some sites, this is likely due to spatial heterogeneity in soil C concentration that cannot be avoided when destructively resampling the same sites over time (**Supplemental Figure 3-1**). However, we did observe significant trends in soil C concentration with time for a few of the sites when considered by specific depth increments. A caveat is that we did not account for potential differences in the mass of soil sampled over time, as we only considered depth-based increments. We observed significant changes at two sites for the surface layer (0-0.1 m), and at two additional sites in the intermediate depth layer (0.1-0.2 m), but C concentration changes were only significant at a single site showed changes for the deepest depth layer (0.2-0.3 m) (**Supplemental Table 3-1**). The soil at the cold climate andesite site was an outlier in that the soil C concentration showed a consistently significant increase in the two deeper depth layers over the study period, while the other soils with significant changes showed decreases in C concentrations (**Supplemental Table 3-1**).

3.7.2 Radiocarbon depth profiles: 2001 data

Depth profiles of $\Delta^{14}C_{bulk}$ were similar in 2001 (**Supplemental Figure 3-2**) as to what we observed in 2019. We observed the most depleted $\Delta^{14}C$ overall in the cool climate sites, where we also observed the clearest differences among parent materials. Parent material differences were least apparent for the cold climate sites, as we also observed in 2019. Within climate zones andesitic soils tended be most depleted and the granitic soils most enriched, with the basaltic parent material intermediate between the other two.

3.7.3 Parent material and climate effects on $\Delta^{14}C_{bulk}$ and $\Delta^{14}C_{respired}$

We saw more significant contrasts in the change over time in $\Delta^{14}C_{respired}$ than we did for $\Delta^{14}C_{bulk}$ (**Supplemental Table 3-7**). When considered within climate zones, trends for the basaltic and granitic soils were more similar to one another overall than were either to the andesitic soils. We observed parent material trend contrasts more commonly in the cool and cold climate sites than in the warm sites; however, we only observed significant trend contrasts for the cold climate sites in

the $\Delta^{14}C_{respired}$ data, and not for $\Delta^{14}C_{bulk}$. When considered within parent materials, we saw more significant trend contrasts for the granitic and basaltic soils than for the andesitic soils (**Supplemental Table 3-7**).

3.7.4 Mineral assemblages

We simplified the data in the main text to consider the relationship between $\Delta^{14}C_{respired}$-$\Delta^{14}C_{bulk}$ and either PCMs or CRMs. We present here the individual regression plots for $\Delta^{14}C_{bulk}$ (**Supplemental Figure 3-7**) and $\Delta^{14}C_{respired}$ (**Supplemental Figure 3-8**).

We also present here the results of the individual regression analyses for $\Delta^{14}C_{bulk}$ (**Supplemental Figure 3-5**) $\Delta^{14}C_{respired}$ (**Supplemental Figure 3-6**), and $\Delta^{14}C_{respired-bulk}$ vs. Al selectively dissolved with ammonium oxalate (Al_o) or sodium pyrophosphate (Al_p), and Fe selectively dissolved with ammonium oxalate (Fe_o), or dithionite citrate (Fe_d) (**Supplemental Figure 3-4**). The relationships between Al_o, Al_p, and Fe_o and $\Delta^{14}C_{respired-bulk}$ in the models derived from Eq. (3-4) were all highly significant ($p < 0.001$). P-values for the metal oxide concentration coefficients in the $\Delta^{14}C_{respired-bulk}$ and $\Delta^{14}C_{bulk}$ models were highly significant (< 0.001 at alpha = 0.1) for Al_o, Al_p, and Fe_o. The coefficient for Al_o in the $\Delta^{14}C_{respired}$ model also had a p-value of < 0.001. While still significant at $\alpha = 0.1$, p-values were larger for Al_p and Fe_o than Al_o in the $\Delta^{14}C_{respired}$ models: 0.028, 0.086 respectively.

In contrast, the concentration of Fe_d was not significant in any of the models.

3.8. Tables

Table 3-1. Soil and climate data by site

Parent Material	Climate Zone	MAT	MAP	Elev	pH[a] mean	pH[a] range	Sand[a] mean	Sand[a] range	Clay[a] mean	Clay[a] range	Soil Taxonomy[b]
		°C	*mm yr^{-1}*	*masl*			*g kg^{-1}*		*g kg^{-1}*		*USDA-NRCS*
andesite	warm	11.5	1250	1167	6.4	(6.3, 6.4)	384	(352, 410)	323	(264, 342)	fine, parasesquic, mesic, Andic Palehumult
	cool	8.5	1400	1737	6.2	(6.1, 6.3)	608	(589, 617)	58	(43, 64)	medial-skeletal, amorphic, mesic Humic Haploxerand
	cold	6.0	1350	2240	5.8	(5.7, 6.0)	613	(605, 618)	52	(47, 64)	medial-skeletal, amorphic, frigid Humic Vitrixerand
basalt	warm	13.3	990	1167	5.9	(5.8, 6.2)	354	(343, 367)	272	(263, 280)	fine, kaolinitic, mesic Xeric Haplohumult
	cool	8.3	1150	1737	6.5	(6.4, 6.6)	797	(670, 853)	104	(70, 116)	loamy-skeletal, mixed, superactive, mesic Typic Haploxerept
	cold	6.5	1340	2240	6.0	(5.9, 6.3)	768	(680, 930)	57	(37, 65)	sandy-skeletal, mixed, superactive, frigid Typic Xerorthent
granite	warm	11.1	910	1385	5.8	(5.6, 5.8)	615	(601, 622)	153	(143, 160)	fine-loamy, mixed, semiactive, mesic Ultic Haploxeralf
	cool	9.1	1010	1789	6.1	(6.0, 6.1)	824	(800, 829)	62	(47, 67)	coarse-loamy, mixed, superactive, mesic Humic Dystroxerept
	cold	7.2	1080	2317	5.5	(5.4, 5.5)	810	(810, 811)	40	(40, 40)	mixed, superactive, frigid Dystric Xeropsamment

Abbreviations: MAP—mean annual precipitation; MAT—mean annual temperature; Elev—elevation; masl—meters above sea level. [a]pH and particle size data are from samples collected in 2009 and aggregated over the depth increment 0–0.3 m. Data were aggregated using a mass-weighted spline function (see text for details). [b]Soil taxonomy previously reported in Rasmussen et al. (2018b).

Table 3-2. ANOVA for $\Delta^{14}C_{bulk}$ and $\Delta^{14}C_{respired}$[1]

Depth	Predictor	Bulk soil			Respiration		
		df	*F*	*p*	*df*	*F*	*p*
0–0.1 m	Parent material	2	12.00	**< 0.001**	2	0.04	0.958
	Climate	2	32.34	**< 0.001**	2	14.02	**< 0.001**
	Year	1	32.03	**< 0.001**	1	75.29	**< 0.001**
	Parent material:Climate	4	8.75	**< 0.001**	4	7.9	**0.001**
	Parent material:Year	2	2.38	0.105	2	1.93	0.177
	Climate:Year	2	6.61	**0.003**	2	2.26	0.137
	Parent material:Climate:Year	4	5.19	**0.002**	4	3.75	**0.024**
	Residuals	44			44		
0.2–0.3 m	Parent material	2	15.58	**< 0.001**	2	0.92	0.421
	Climate	2	11.61	**< 0.001**	2	0.77	0.483
	Year	1	1.30	0.260	1	0.65	0.434
	Parent material:Climate	4	1.71	0.165	4	4.33	**0.019**
	Parent material:Year	2	1.56	0.222	2	0.86	0.446
	Climate:Year	2	4.04	**0.024**	2	1.41	0.278
	Parent material:Climate:Year	4	0.98	0.430	2	0.37	0.698
	Residuals	44			44		

[1]Bold text indicates significance at $\alpha < 0.05$.

Supplemental Table 3-1. Changes in soil C concentration (%), 2001-2019. (Only significant trends shown).

Depth	Site	Trend	SE	df	95% CI lower	95% CI upper
0-10cm	andesite (warm)	-0.20	0.09	62	-0.38	-0.02
	andesite (cold)	0.20	0.10	62	0.01	0.40
	basalt (cold)	-0.27	0.09	62	-0.45	-0.09
10-20cm	andesite (cold)	0.23	0.06	62	0.12	0.35
	granite (warm)	0.16	0.05	62	0.05	0.26
20-30cm	andesite (cold)	0.21	0.04	62	0.13	0.29

Supplemental Table 3-2. Contrasts of $\Delta^{14}C_{bulk}$ and $\Delta^{14}C_{respired}$ for parent material and climate factors, 0-0.1 m (all pairs). P-value adjustment: Tukey method for comparing a family of 3 estimates.

Year	Group	Contrast	Bulk Est.	SE	p	Respired Est.	SE	p
2001	cool	andesite - basalt	-62.0	18.8	**0.011**			
		andesite - granite	-124.5	18.8	**< .001**			
		basalt - granite	-62.4	18.8	**0.011**			
	cold	andesite - granite				84.0	22.1	**0.016**
		basalt - granite				82.1	18.1	**0.006**
	andesite	warm - cool	126.6	18.8	**< .001**			
		cool - cold	-82.1	21.0	**0.003**			
	basalt	warm - cool	48.7	18.8	**0.048**			
		warm - cold	66.1	18.8	**0.007**			
	granite	warm - cold	107.3	18.8	**< .001**	114.5	18.1	**< .001**
		cool - cold	83.6	18.8	**< .001**	104.1	18.1	**0.002**
2019	warm	andesite - basalt	-56.5	16.3	**0.007**			
		andesite - granite	-79.8	16.3	**< .001**			
	cool	basalt - granite				-43.6	18.0	0.089
	andesite	cool - cold	-42.0	16.3	**0.047**			
	basalt	warm - cool	52.3	16.3	**0.013**			
	granite	warm - cool	65.0	16.3	**0.002**			
		warm - cold	58.5	16.3	**0.006**	47.1	18.0	0.066
		cool - cold				49.0	18.0	0.056

Supplemental Table 3-3. Contrasts of $\Delta^{14}C_{bulk}$ and $\Delta^{14}C_{respired}$ for parent material and climate factors, 0.1-0.2 m (all pairs). P-value adjustment: Tukey method for comparing a family of 3 estimates.

Year	Group	Contrast	Bulk			Respired		
			Est.	SE	p	Est.	SE	p
2001	warm	andesite - granite	-47.8	20.1	0.072			
	cool	andesite - basalt	72.2	20.1	0.006			
		andesite - granite	-99.5	20.1	< .001			
	cold	andesite - granite				162.8	31.4	0.005
		basalt - granite				227.2	27.2	< .001
	andesite	warm - cool	65.0	20.1	0.013			
		cool - cold	-57.2	22.5	0.052			
	granite	warm - cold	70.4	20.1	0.007	165.1	27.2	0.002
		cool - cold	57.2	20.1	0.029	163.9	27.2	0.002
2019	warm	andesite - basalt	-62.6	20.1	0.016			
		andesite - granite	-124.9	20.1	< .001	-52.4	13.7	0.013
		basalt - granite	-62.3	20.1	0.016	-35.2	13.7	0.078
	cool	andesite - basalt				74.2	13.7	0.002
		andesite - granite				87.3	13.7	< .001
	cold	andesite - granite				62.2	16.8	0.015
		basalt - granite				70.8	16.8	0.007
	basalt	warm - cool	74.8	20.1	0.004	63.0	13.7	0.004
		cool - cold	-63.5	20.1	0.014	-54.2	13.7	0.011
	granite	warm - cool	118.2	20.1	< .001	111.3	13.7	< .001
		warm - cold	105.3	20.1	< .001	114.7	16.8	< .001

Supplemental Table 3-4. Contrasts of $\Delta^{14}C_{bulk}$ and $\Delta^{14}C_{respired}$ for parent material and climate factors, 0.2-0.3 m (all pairs). P-value adjustment: Tukey method for comparing a family of 3 estimates.

Year	Group	Contrast	Bulk			Respired		
			Est.	*SE*	*p*	Est.	*SE*	*p*
2001	warm	andesite – granite	-70.2	21.0	**0.01**			
	cool	andesite – granite	-106.5	21.0	**< .001**			
		basalt – granite	-62.9	21.0	**0.021**			
	granite	warm – cold	51.8	21.0	0.061			
2019	warm	andesite – granite	-51.9	19.6	**0.042**			
		basalt – granite	-51.3	19.6	**0.044**			
	cool	andesite – basalt				93.9	20.6	**0.005**
		basalt – granite	-53.5	19.6	**0.035**	-61.0	20.6	**0.043**
	cold	andesite – basalt	-46.3	19.6	0.073			
	andesite	warm – cool	57.6	19.6	**0.023**			
	basalt	warm – cool	75.7	19.6	**0.003**	64.7	20.6	**0.033**
		cool – cold	-106.5	19.6	**< .001**	-86.8	25.3	**0.022**
	granite	warm – cool	73.5	19.6	**0.004**			
		warm – cold	51.5	19.6	**0.043**	57.8	20.6	0.054

Supplemental Table 3-5. Change in $\Delta^{14}C_{bulk}$, 2001-2019. Degrees of freedom = 44; confidence level used = 0.95.

Climate	Parent material	0-10cm		10-20cm		20-30cm	
		Trend	SE	Trend	SE	Trend	SE
warm	andesite	**-5.8**	1.0	-1.9	1.3	1.1	1.3
	basalt	-1.8	1.0	-0.1	1.3	-1.1	1.3
	granite	**-2.5**	1.0	2.4	1.3	0.2	1.3
cool	andesite	0.1	1.0	0.4	1.3	0.3	1.3
	basalt	-2.1	1.0	**-3.2**	1.3	**-3.3**	1.3
	granite	**-4.9**	1.0	**-3.5**	1.3	**-3.6**	1.3
cold	andesite	-2.2	1.1	-0.9	1.4	0.4	1.5
	basalt	0.9	1.0	0	1.3	1.4	1.3
	granite	0.1	1.0	0.3	1.3	0.1	1.3

Supplemental Table 3-6. Change in $\Delta^{14}C_{respired}$, 2001-2019. Degrees of freedom = 44; confidence level used = 0.95.

Climate	Parent material	0-10cm		10-20cm		20-30cm	
		Trend	SE	Trend	SE	Trend	SE
warm	andesite	**-6.2**	1.0	-2.1	1.0	1.4	2.0
	basalt	**-2.3**	1.0	-0.9	1.0	0.4	2.0
	granite	**-3.7**	1.0	2	1.0	3.2	2.0
cool	andesite	-1.4	1.2	-1	1.2	-1.5	2.5
	basalt	**-3.7**	1.0	**-5.9**	1.0	NA	
	granite	**-3**	1.0	**-4.1**	1.0	0	2.0
cold	andesite	**-2.9**	1.2	-0.8	1.2	1.4	2.5
	basalt	**-3.9**	1.0	**-3.9**	1.0	-3.5	2.5
	granite	0.1	1.0	**4.8**	1.4	NA	

Supplemental Table 3-7. Contrasts for $\Delta^{14}C_{bulk}$ and $\Delta^{14}C_{respired}$ temporal trends. P-value adjustment: Tukey method for comparing a family of 3 estimates.

Depth	Group	Contrast	Bulk			Respired		
			Est.	SE	p	Est.	SE	p
0-10cm	warm	andesite - basalt	-4.0	1.4	**0.021**	-3.9	1.4	**0.036**
	warm	andesite - granite	-3.3	1.4	0.068			
	cool	andesite - granite	5.0	1.4	**0.004**			
	cold	basalt - granite				-4.0	1.4	**0.031**
	andesite	warm - cool	-5.9	1.4	**< .001**	-4.8	1.6	**0.021**
	andesite	warm - cold	-3.6	1.5	0.06			
	granite	warm - cold				-3.7	1.4	**0.045**
	granite	cool - cold	-5.0	1.4	**0.004**			
10-20cm	warm	andesite - granite	-4.3	1.8	0.051	-4.1	1.4	**0.03**
	cool	andesite - basalt				4.9	1.6	**0.019**
	cool	andesite - granite	4.0	1.8	0.08			
	cold	andesite - granite				-5.6	1.9	**0.024**
	cold	basalt - granite				-8.7	1.7	**< .001**
	basalt	warm - cool				5.0	1.4	**0.008**
	granite	warm - cool	5.9	1.8	**0.005**	6.1	1.4	**0.002**
	granite	cool - cold	-3.8	1.8	0.094	-8.9	1.7	**< .001**
20-30cm	basalt	cool - cold	-4.7	1.9	**0.04**			

3.9.   Figures

Figure 3-1. Profiles of SOC concentration (a–c) and stocks (d–f). Points show mean of 2001, 2009, and 2019 data for SOC concentration, and 2001 and 2009 data for SOC stocks (bulk density was not measured in 2019); error bars show ±2SE.
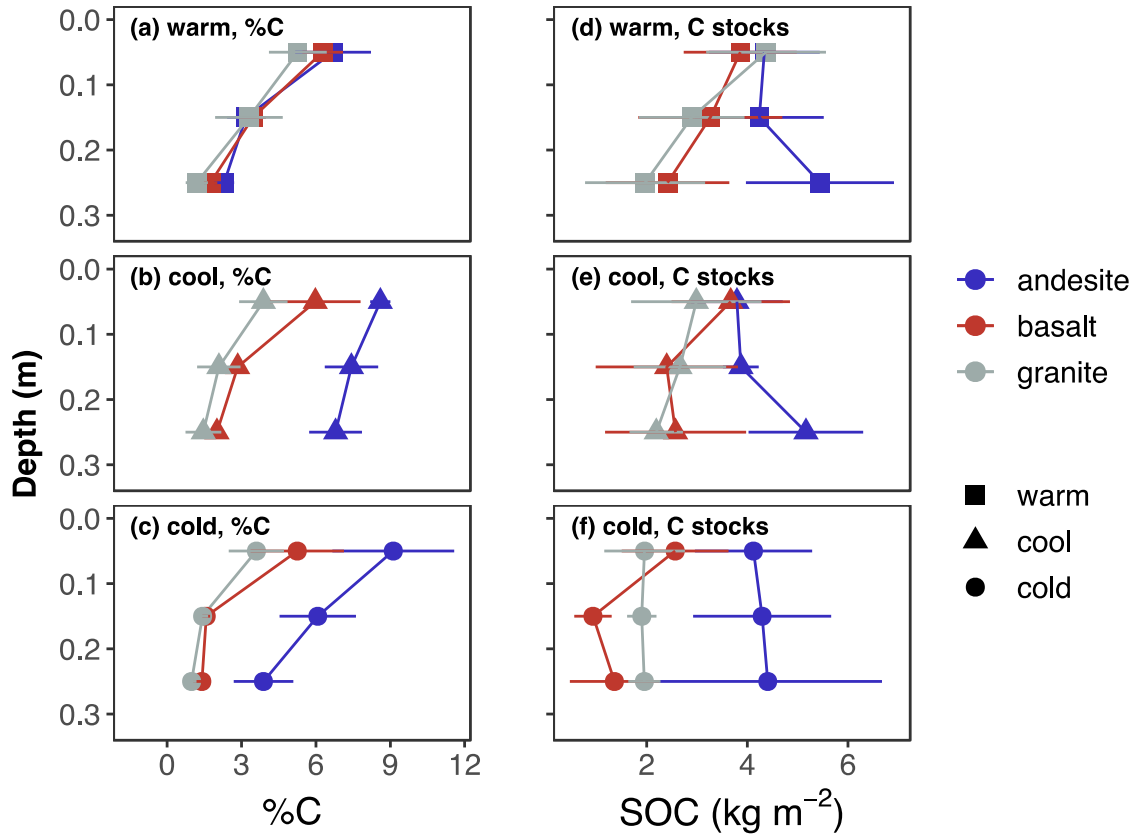
Figure 3-2. Depth profiles of $\Delta^{14}C_{bulk}$ (a–c) and $\Delta^{14}C_{respired}$ (d–f) in 2019. Points show the mean of three replicate profiles for bulk soil, and the mean of laboratory duplicates for respired CO_2. Error bars show ±1 SD for bulk soils and the minimum and maximum for respired CO_2. Dotted gray vertical line shows $\Delta^{14}C$ of the atmosphere in the year of sampling, 2019 (data from Graven et al. 2017, forecasted to 2019 using the method of Sierra 2018).
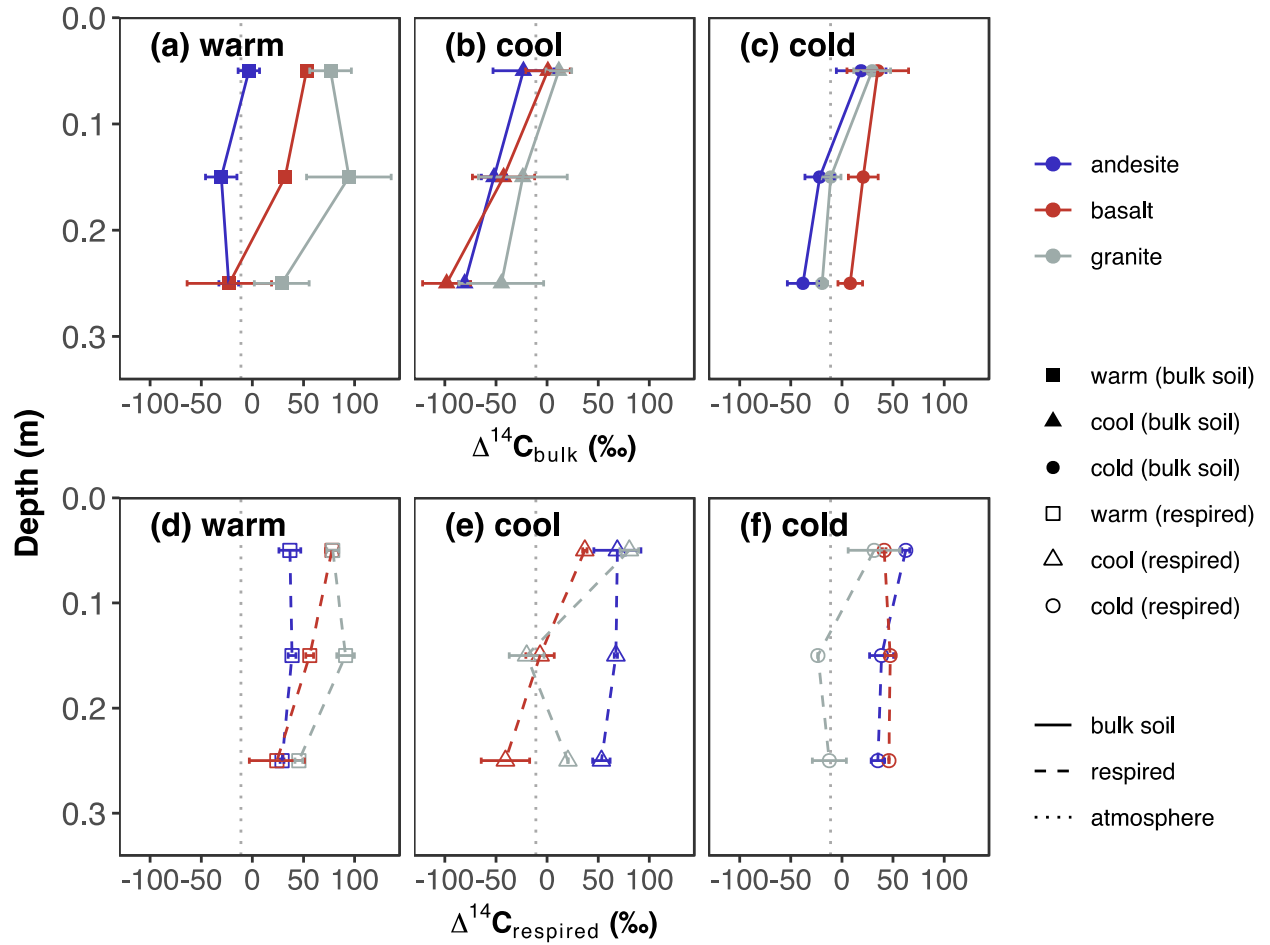
Figure 3-3. Temporal trends in $\Delta^{14}C$ for 0–0.1 m and 0.1–0.2 m depth layers. Panels (a–f) show $\Delta^{14}C_{bulk}$ data. The first column from left—panels (a), (c), and (e)—shows 0–0.1 m data; the second column—panels (b), (d), and (f)—shows 0.1–0.2 m data. Panels (g–l) show $\Delta^{14}C_{respired}$ data; the third column—panels (g), (i), and (k)—shows 0–0.1 m data; the rightmost column—panels (h), (j), and (l)—shows 0.1–0.2 m data. Points show observed data; lines show linear trend estimates for marginal means; ribbons show 95% confidence intervals for trends. Dotted line shows atmospheric $\Delta^{14}C$ (data from Graven et al. 2017, forecasted to 2019 using the method of Sierra 2018).
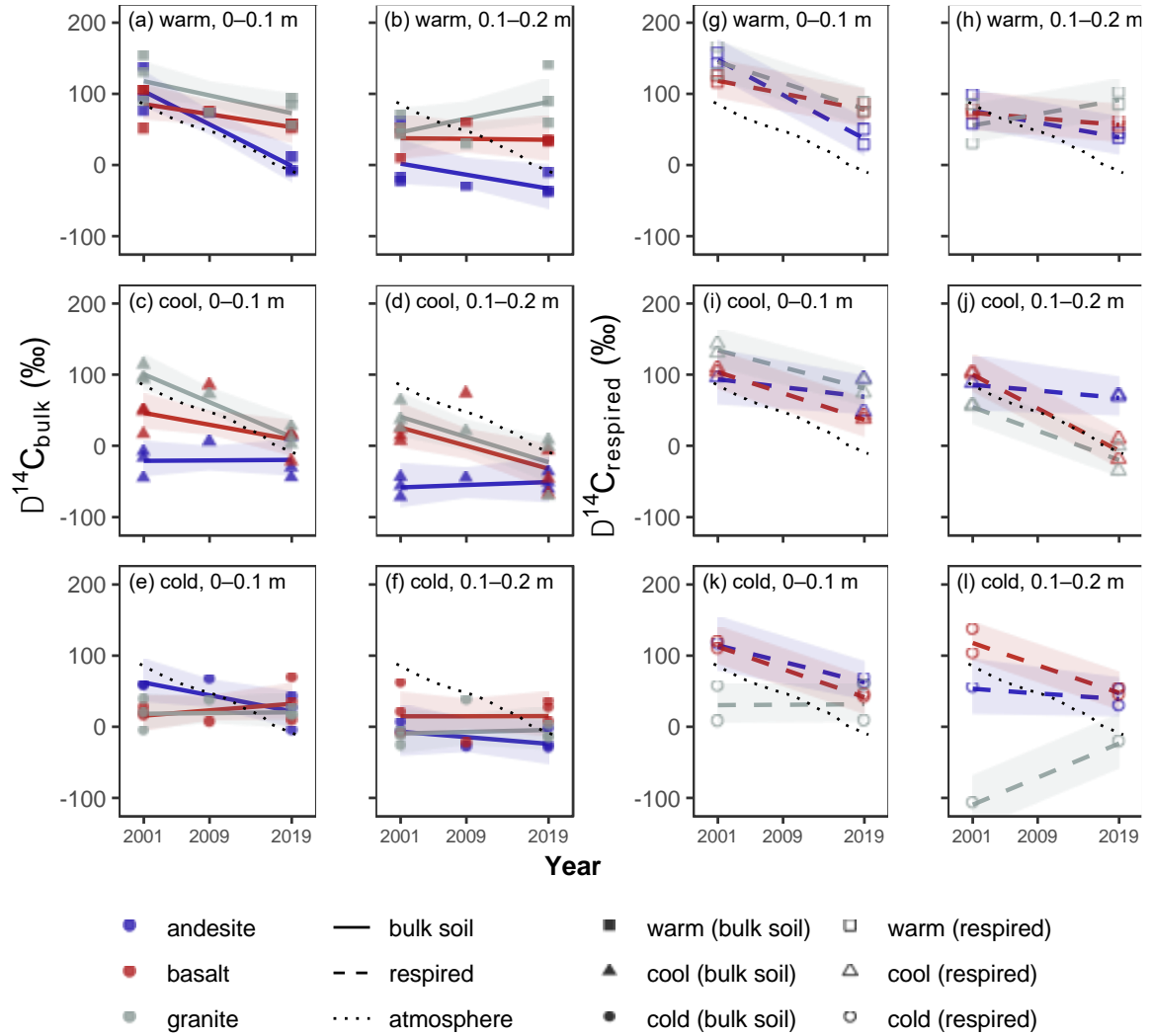
Figure 3-4. Parent material and climate effects on the relationship of $\Delta^{14}C_{bulk}$ and $\Delta^{14}C_{respired}$. (a) Parent material model, Eq. (3-3) and (b) Climate model, Eq. (3-4). Dotted line shows 1:1 relationship. Points show the mean of three replicate profiles for $\Delta^{14}C_{bulk}$, and the mean of laboratory duplicates for $\Delta^{14}C_{respired}$. Error bars show ±1 SD for $\Delta^{14}C_{bulk}$, and the minimum and maximum for $\Delta^{14}C_{respired}$. The cold granite site in 2001 had extremely depleted in $\Delta^{14}C_{respired}$ values and thus was from the models.
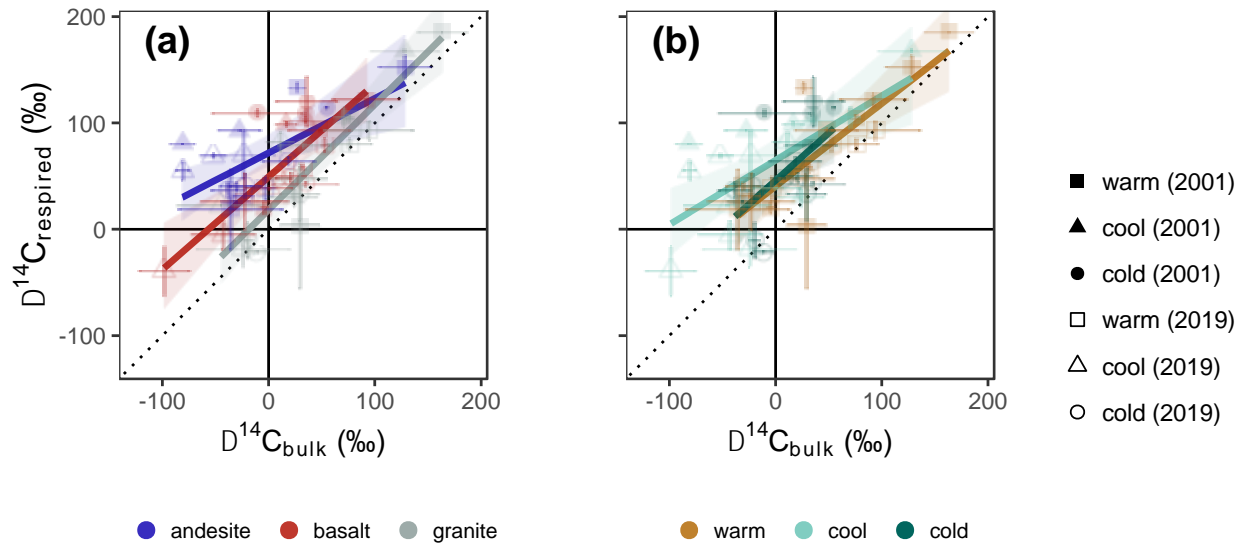
Figure 3-5. Relationship of poorly crystalline and crystalline metal oxides to the difference of $\Delta^{14}C_{respired}$ and $\Delta^{14}C_{bulk}$ ($\Delta^{14}C_{respired-bulk}$). (a) PCM = poorly crystalline metal oxide content (oxalate-extractable Al + 1/2 oxalate-extractable Fe), (b) CRM = crystalline metal oxide content (dithionite-extractable Fe - oxalate-extractable Fe). Points show mass-weighted metal oxide concentrations and carbon-weighted values of $\Delta^{14}C_{respired-bulk}$ for 0–0.3 m profiles. Lines show partial slopes for 2001 and 2019 from the linear model fit (Eq. 3-5). P-values indicate significance of metal concentration coefficient estimate for predicting $\Delta^{14}C_{respired-bulk}$.
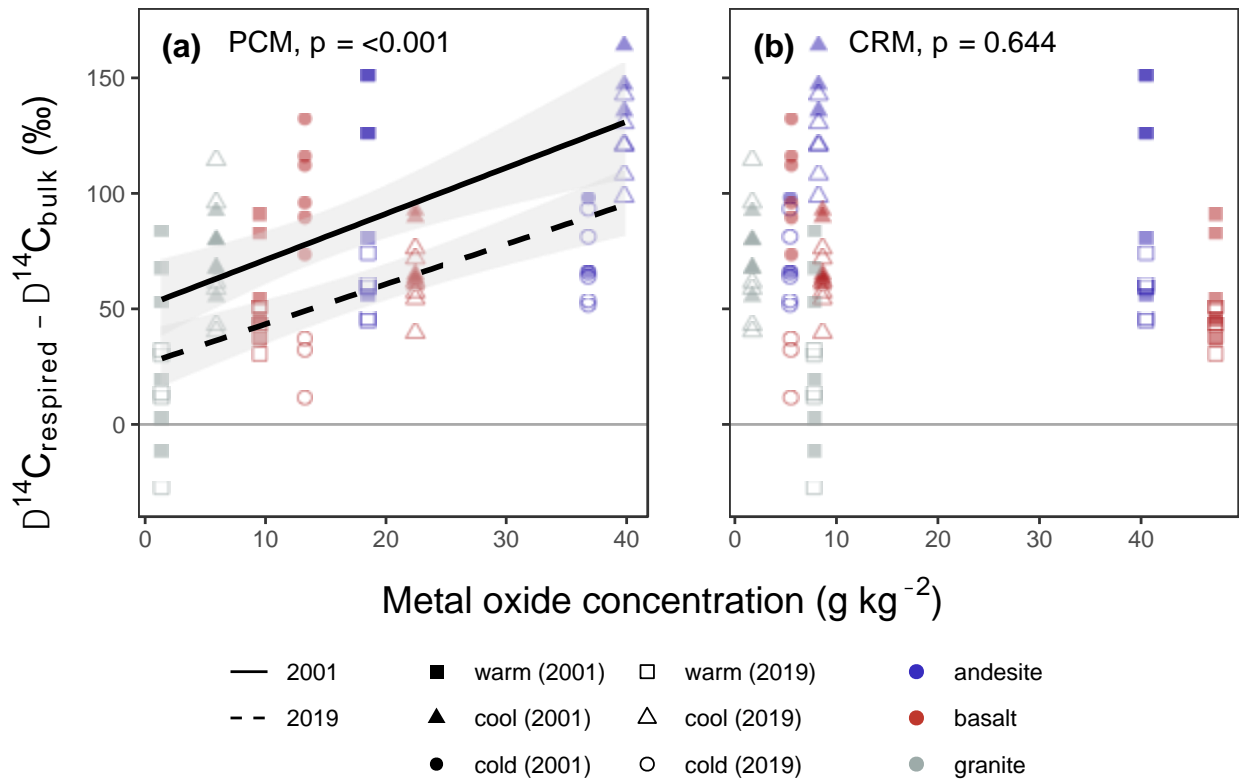
Supplemental Figure 3-1. Changes in soil C concentration, 2001-2019. Points show replicate profiles (*n* = 3); lines show marginal mean estimates of linear trends in soil C concentration with time; ribbons show 95% CIs around trend estimates.
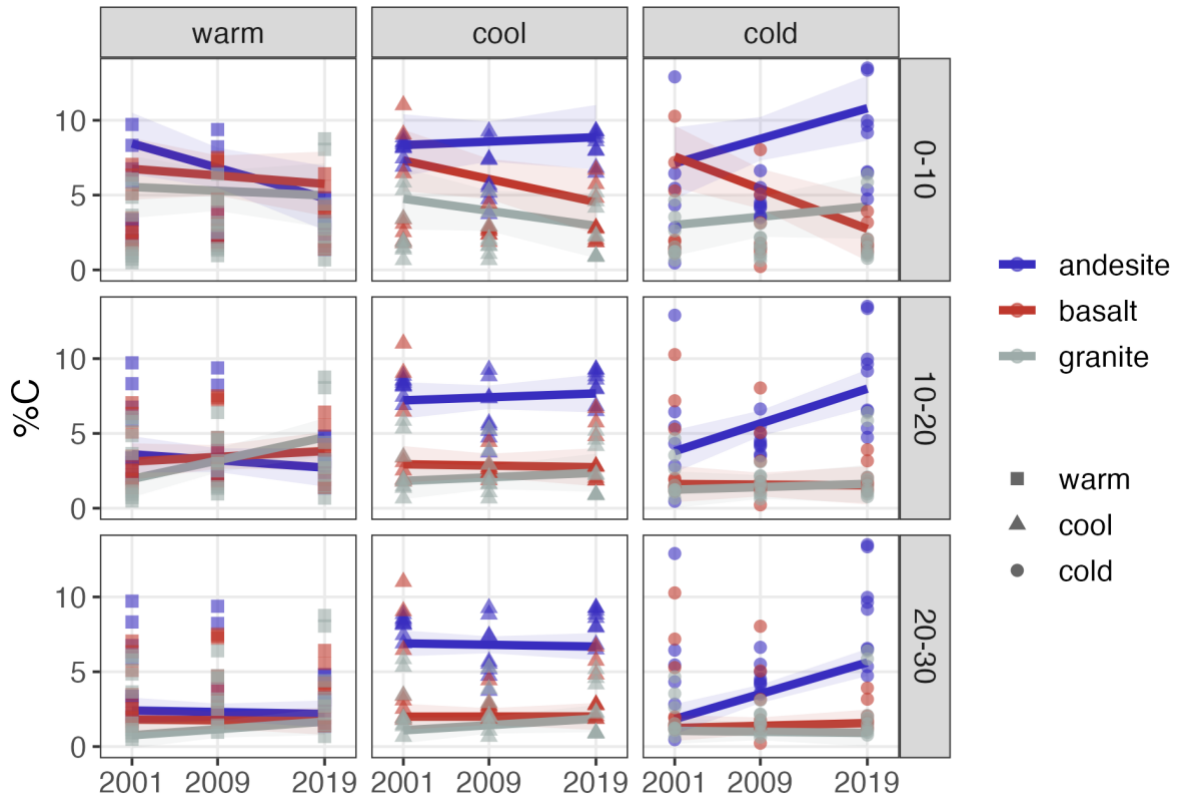
Supplemental Figure 3-2. Heterotrophic respiration rates from incubations of 2019 and 2001 samples. Panels a-c show 2019 data, and panels d-f show 2001 data. Panels in the top row (a, d) show the first depth increment for each year, middle row shows the second depth increment (b, e), and the bottom row shows the third depth increment (c, f). Bars show means for laboratory duplicates averaged over the whole incubation period; error bars ± 1 standard error of the mean. NB: Total CO_2 respired was controlled to be within 10,000 ppm (±1,000 ppm) for all samples; incubation duration varied between 4 and 40 days.
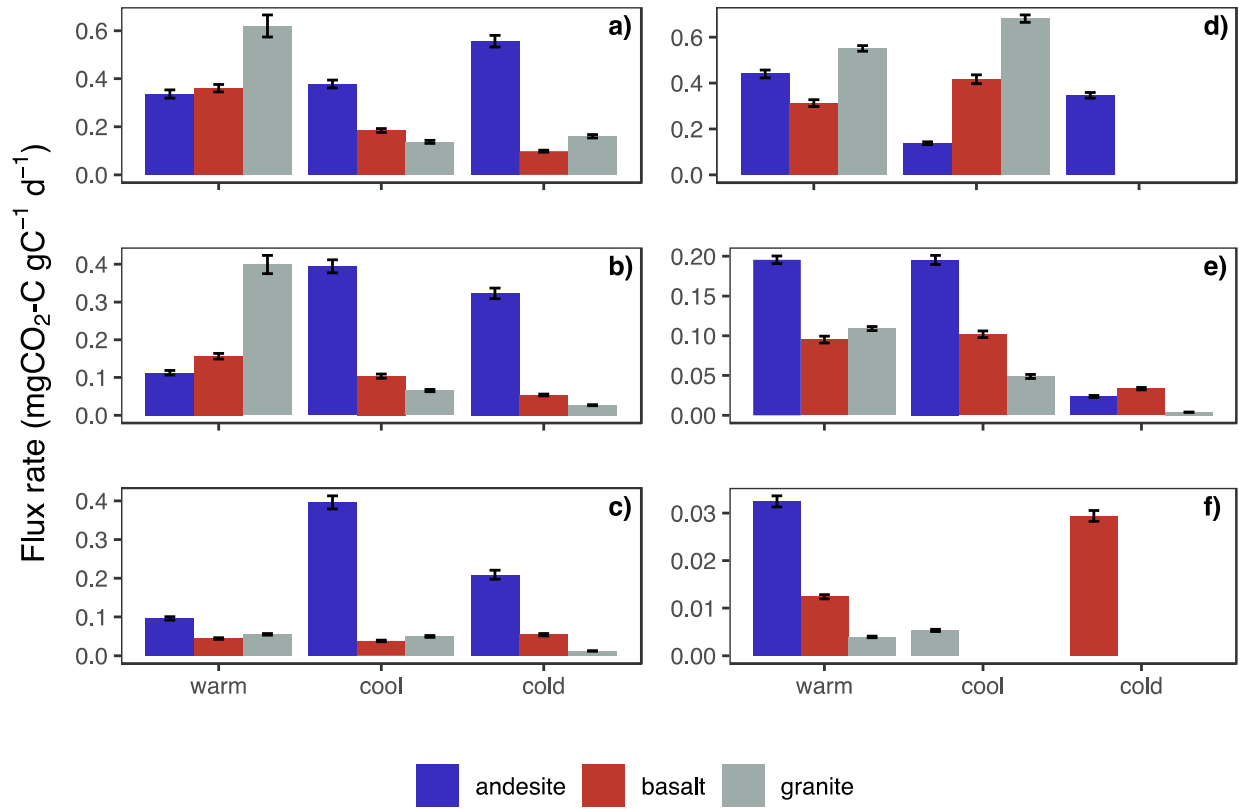
Supplemental Figure 3-3. Depth profiles of $\Delta^{14}C_{bulk}$ and $\Delta^{14}C_{respired}$ for 2001 data. Top panels show bulk data, bottom panels respired data. Dotted vertical lines show $\Delta^{14}C$ of the atmosphere in the year of sampling. Points show the mean of three replicate profiles for bulk soil, and the mean of laboratory duplicates for respired CO_2. Error bars show ±1 SD for bulk soils and the minimum and maximum for respired CO_2. Respired CO_2 from the cold granite site (bottom left panel) was extremely depleted in $\Delta^{14}C$ and thus is excluded for display purposes.
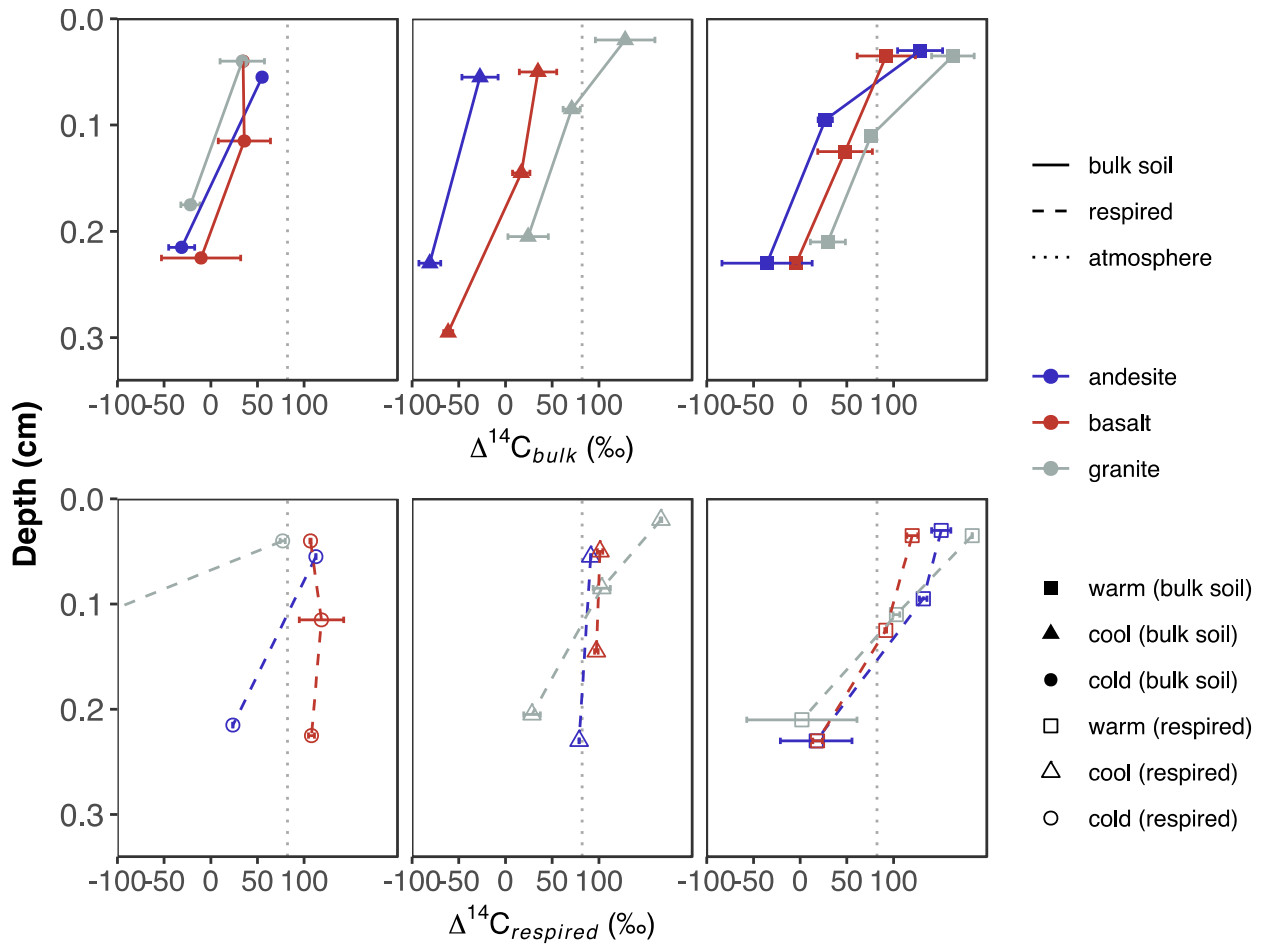
Supplemental Figure 3-4. Relationship of selectively dissolved Fe and alumnimum to the difference between $\Delta^{14}C_{respired}$ and $\Delta^{14}C_{respired}$ ($\Delta^{14}C_{respired-bulk}$). a) Oxalate-extractable Al (Al_o), b) Pyrophosphate-extractable Al (Al_p), c) Oxalate-extractable Fe (Fe_o), d) Dithionite extractable Fe (Fe_d). Points show mass-weighted mineral concentrations and carbon-weighted values of $\Delta^{14}C_{respired-bulk}$ for 0-30cm profiles. Lines show linear model fits from Eq. 3-5.
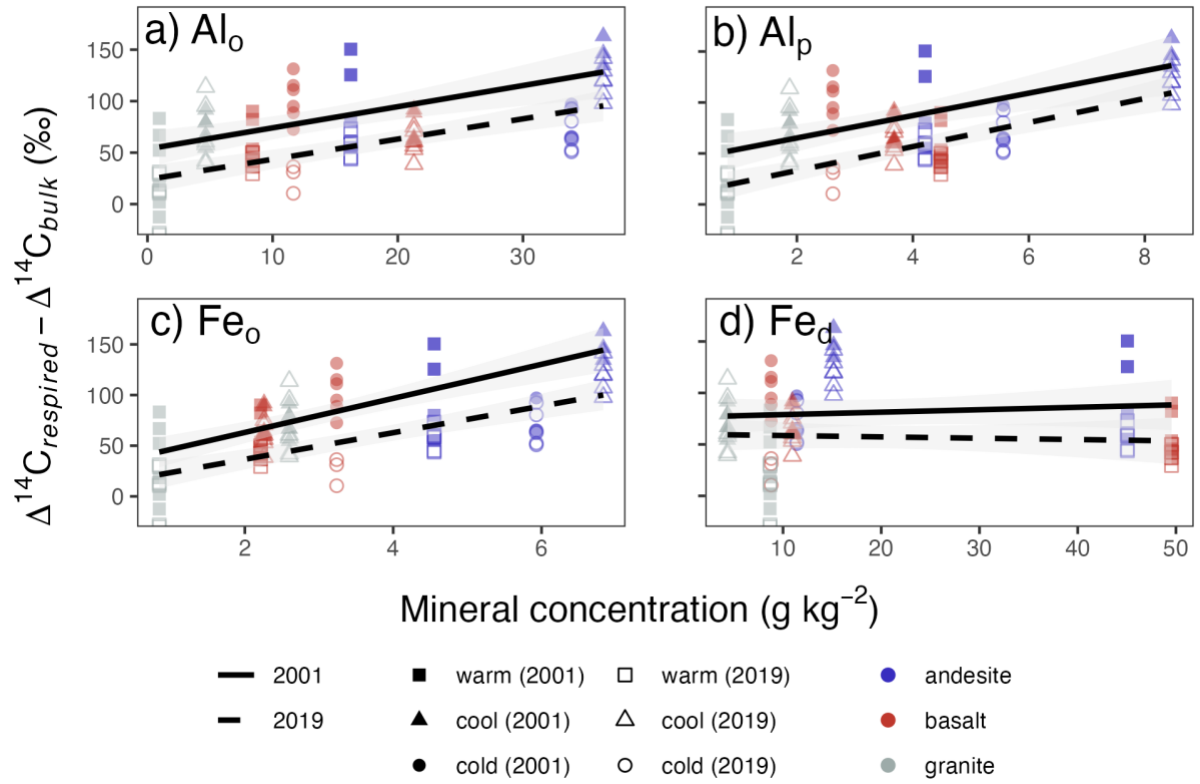
Supplemental Figure 3-5. Relationship of selectively dissolved Fe and alumnimum to $\Delta^{14}C_{bulk}$. a) Oxalate-extractable Al (Al_o), b) Pyrophosphate-extractable Al (Al_p), c) Oxalate-extractable Fe (Fe_o), d) Dithionite extractable Fe (Fe_d). Points show mass-weighted mineral concentrations and carbon-weighted values of $\Delta^{14}C_{bulk}$ for 0-30cm profiles. Lines show linear model fits from Eq. 3-5.
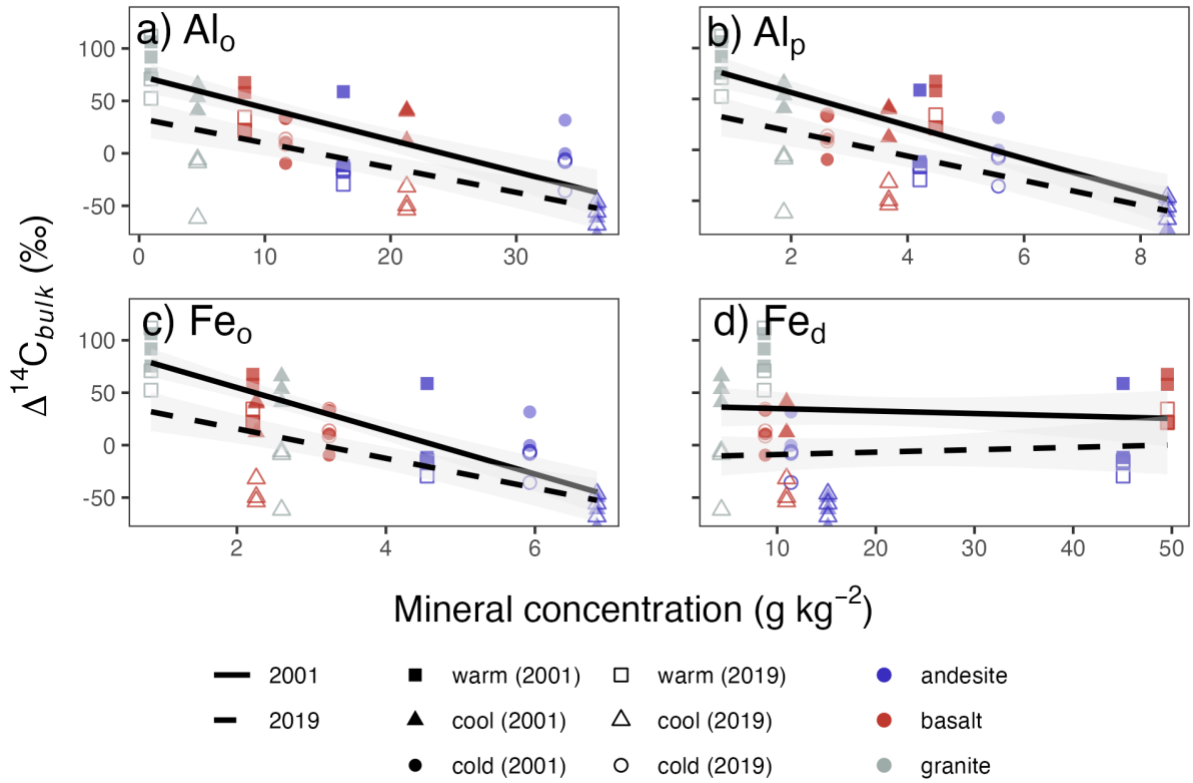
Supplemental Figure 3-6. Relationship of selectively dissolved Fe and alumnimum to $\Delta^{14}C_{respired}$. a) Oxalate-extractable Al (Al$_o$), b) Pyrophosphate-extractable Al (Al$_p$), c) Oxalate-extractable Fe (Fe$_o$), d) Dithionite extractable Fe (Fe$_d$). Points show mass-weighted mineral concentrations and carbon-weighted values of $\Delta^{14}C_{respired}$ for 0-30cm profiles. Lines show linear model fits from Eq. 3-5.
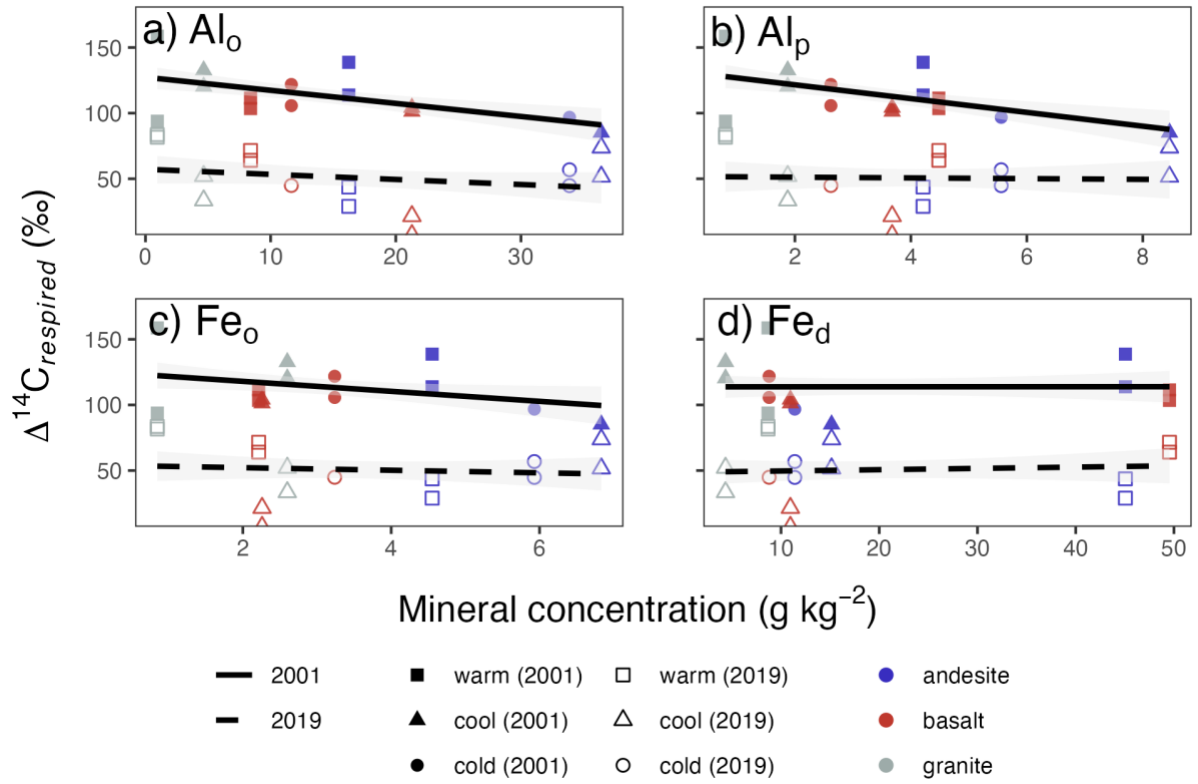
Supplemental Figure 3-7. Relationship of poorly crystalline and crystalline minerals to $\Delta^{14}C_{bulk.}$ (a) Poorly crystalline mineral content (oxalate-extractable Al + 1/2 oxalate-extractable Fe), (b) Crystalline mineral content (dithionite-extractable Fe - oxalate-extractable Fe). Lines show linear model fits from Eq. 3-5.
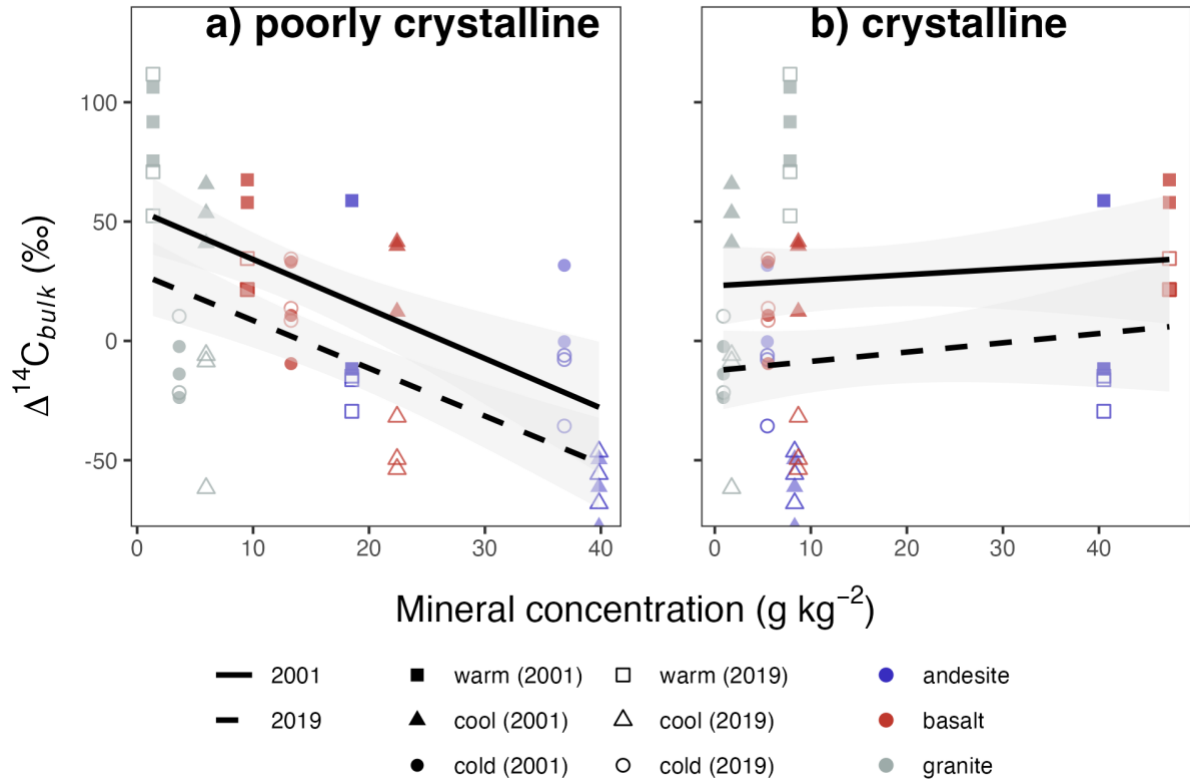
Supplemental Figure 3-8. Relationship of poorly crystalline and crystalline minerals to $\Delta^{14}C_{respired.}$ (a) Poorly crystalline mineral content (oxalate-extractable Al + 1/2 oxalate-extractable Fe), (b) Crystalline mineral content (dithionite-extractable Fe - oxalate-extractable Fe). Lines show linear model fits from Eq. 3-5.
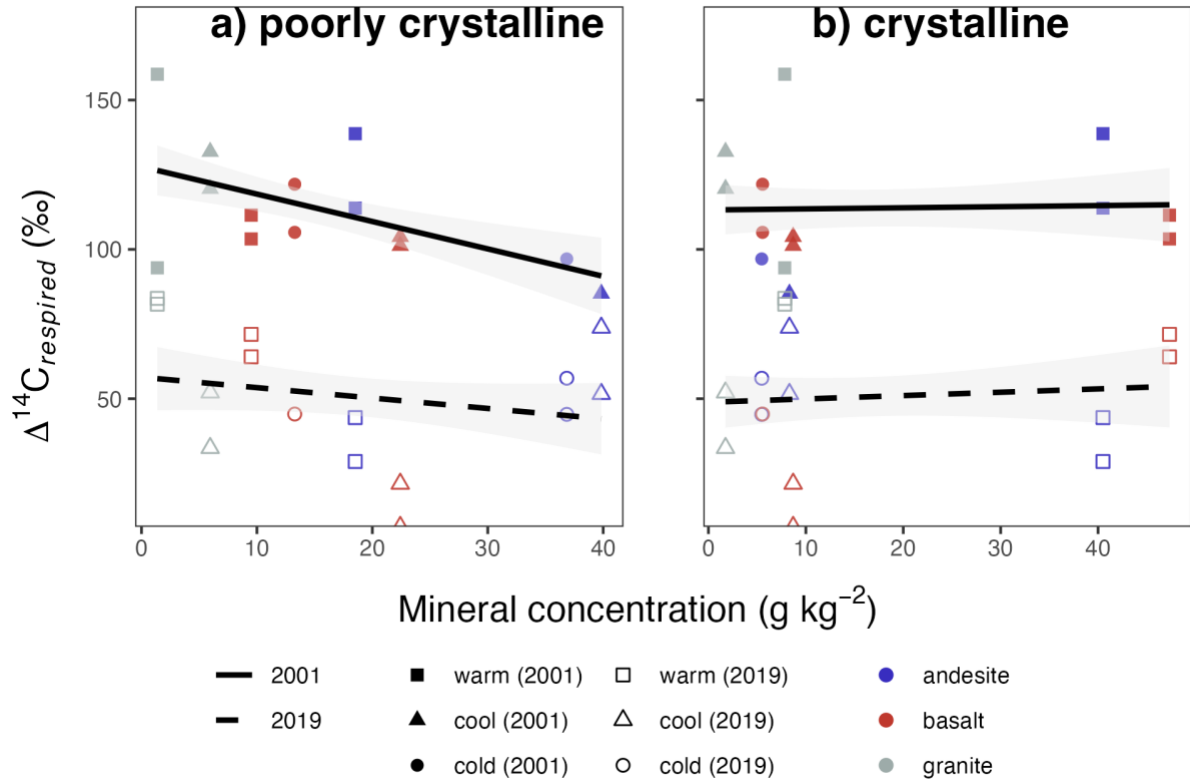
3.10. References

Abramoff, R. Z., Torn, M. S., Georgiou, K., Tang, J., and Riley, W. J.: Soil Organic Matter Temperature Sensitivity Cannot be Directly Inferred From Spatial Gradients, Global Biogeochemical Cycles, 33, 761–776, https://doi.org/10.1029/2018GB006001, 2019.

Ahrens, B., Guggenberger, G., Rethemeyer, J., John, S., Marschner, B., Heinze, S., Angst, G., Mueller, C. W., Kögel-Knabner, I., Leuschner, C., Hertel, D., Bachmann, J., Reichstein, M., and Schrumpf, M.: Combination of energy limitation and sorption capacity explains 14C depth gradients, Soil Biology and Biochemistry, 148, https://doi.org/10.1016/j.soilbio.2020.107912, 2020.

Baisden, W. T., Amundson, R., Cook, A. C., and Brenner, D. L.: Turnover and storage of C and N in five density fractions from California annual grassland surface soils, Global Biogeochemical Cycles, 16, 64-1-64–16, https://doi.org/10.1029/2001gb001822, 2002.

Baisden, W. T., Parfitt, R. L., Ross, C., Schipper, L. A., and Canessa, S.: Evaluating 50 years of time-series soil radiocarbon data : towards routine calculation of robust C residence times, Biogeochemistry, 112, 129–137, https://doi.org/10.1007/s10533-011-9675-y, 2013.

Beem-Miller, J.: v1.0 jb388/sra-ts: Submission to SOIL (Copernicus) 11 Oct 2022, 2022. https://doi.org/10.5281/zenodo.7186755

Beem-Miller, J., Schrumpf, M., Hoyt, A. M., Guggenberger, G., and Trumbore, S.: Impacts of Drying and Rewetting on the Radiocarbon Signature of Respired CO2 and Implications for Incubating Archived Soils, Journal of Geophysical Research: Biogeosciences, 126, 1–17, https://doi.org/10.1029/2020JG006119, 2021.

Beem-Miller, J. P., Kong, A. Y. Y., Ogle, S., and Wolfe, D.: Sampling for soil carbon stock assessment in rocky agricultural soils, Soil Science Society of America Journal, 80, https://doi.org/10.2136/sssaj2015.11.0405, 2016.

Bishop, T. F., McBratney, B., and Laslett, G. M.: Modeling soil attribute depth functions with equal-area quadratic smoothing splines, Geoderma, 91, 27–45, https://doi.org/10.1016/S0016-7061(99)00003-8, 1999.

Castanha, C., Trumbore, S., and Amundson, R.: Methods of separating soil carbon pools affect the chemistry and turnover time of isolated fractions, Radiocarbon, 50, 83–97, https://doi.org/10.1017/S0033822200043381, 2008.

Chadwick, O. A., and J. Chorover: The chemistry of pedogenic thresholds, Geoderma, 100, 321– 353, 2001, https://doi.org/10.1016/S0016-7061(01)00027-1, 2001.

Crow, S. E. and Sierra, C. A.: The climate benefit of sequestration in soils for warming mitigation, Biogeochemistry, https://doi.org/10.1007/s10533-022-00981-1, 2022.

Dahlgren, R. A., Boettinger, J. L., Huntington, G. L., and Amundson, R. G.: Soil development along an elevational transect in the western Sierra Nevada, California, Geoderma, 78, 207–236, https://doi.org/10.1016/S0016-7061(97)00034-7, 1997.

Davidson, E. A. and Janssens, I. A.: Temperature sensitivity of soil carbon decomposition and feedbacks to climate change, Nature, 440, 165–173, https://doi.org/10.1038/nature04514, 2006.

Davidson, E. A., Trumbore, S. E., and Amundson, R.: Soil warming and organic carbon content, Nature, 408, 789–790, https://doi.org/10.1038/35048672, 2000.

Duiker, S. W., Rhoton, F. E., Torrent, J., Smeck, N. E., and Lal, R.: Fe (Hydr)Oxide Crystallinity Effects on Soil Aggregation, Soil Science Society of America Journal, 67, 606–611, https://doi.org/10.2136/sssaj2003.6060, 2003.

Ewing, S. A., Sanderman, J., Baisden, W. T., Wang, Y., and Amundson, R.: Role of large-scale soil structure in organic carbon turnover: Evidence from California grassland soils, Journal of Geophysical Research: Biogeosciences, 111, 1–9, https://doi.org/10.1029/2006JG000174, 2006.

Frank, D. A., Pontes, A. W., and McFarlane, K. J.: Controls on Soil Organic Carbon Stocks and Turnover Among North American Ecosystems, Ecosystems, 15, 604–615, https://doi.org/10.1007/s10021-012-9534-2, 2012.

Gleixner, G.: Soil organic matter dynamics: A biological perspective derived from the use of compound-specific isotopes studies, Ecological Research, 28, 683–695, https://doi.org/10.1007/s11284-012-1022-9, 2013.

Graham, R. C. and O'Geen, A. T.: Soil mineralogy trends in California landscapes, Geoderma, 154, 418–437, https://doi.org/10.1016/j.geoderma.2009.05.018, 2010.

Graven, H., Allison, C. E., Etheridge, D. M., Hammer, S., Keeling, R. F., Levin, I., Meijer, H. A. J., Rubino, M., Tans, P. P., Trudinger, C. M., Vaughn, B. H., and White, J. W. C.: Compiled records of carbon isotopes in atmospheric CO2 for historical simulations in CMIP6, Geoscientific Model Development, 10, 4405–4417, https://doi.org/10.5194/gmd-10-4405-2017, 2017.

Harradine, F. and Jenny, H.: Influence of parent material and climate on texture and nitrogen and carbon contents of virgin California soils: I. Texture and nitrogen contents of soils, Soil Science, 85, 235–243, https://doi.org/10.1097/00010694-195805000-00001, 1958.

Heckman, K., Lawrence, C. R., and Harden, J. W.: A sequential selective dissolution method to quantify storage and stability of organic carbon associated with Al and Fe hydroxide phases, Geoderma, 312, 24–35, https://doi.org/10.1016/j.geoderma.2017.09.043, 2018.

Hengl, T.: GSIF: Global Soil Information Facilities, 2019. https://CRAN.R-project.org/package=GSIF

Hopkins, F. M., Torn, M. S., and Trumbore, S. E.: Warming accelerates decomposition of decades-old carbon in forest soils (SI), Proceedings of the National Academy of Sciences, 1–6, https://doi.org/10.1073/pnas.1206575109, 2012.

Hua, Q., Turnbull, J. C., Santos, G. M., Rakowski, A. Z., Ancapichún, S., De Pol-Holz, R., Hammer, S., Lehman, S. J., Levin, I., Miller, J. B., Palmer, J. G., and Turney, C. S. M.: Atmospheric radiocarbon for the period 1950-2019, Radiocarbon, 64, https://doi.org/10.1017/RDC.2021.95, 2021.

Jenny, H., Gessel, S. P., and Bingham, F.T.: Comparative Study of Decomposition Rates of Organic Matter in Temperate and Tropical Regions, Soil Science, 68, 419–432, 1949.

Kahle, M., Kleber, M., and Jahn, R.: Retention of dissolved organic matter by illitic soils and clay fractions: Influence of mineral phase properties, Journal of Plant Nutrition and Soil Science, 166, 737–741, https://doi.org/10.1002/jpln.200321125, 2003.

Kahle, M., Kleber, M., and Jahn, R.: Retention of dissolved organic matter by phyllosilicate and soil clay fractions in relation to mineral properties, Organic Geochemistry, 35, 269–276, https://doi.org/10.1016/j.orggeochem.2003.11.008, 2004.

Kaiser, K. and Guggenberger, G.: Mineral surfaces and soil organic matter, European Journal of Soil Science, 54, 219–236, https://doi.org/10.1046/j.1365-2389.2003.00544.x, 2003.

Kaiser, K. and Kalbitz, K.: Cycling downwards - dissolved organic matter in soils, Soil Biology and Biochemistry, 52, 29–32, https://doi.org/10.1016/j.soilbio.2012.04.002, 2012.

Kleber, M., Mikutta, R., Torn, M. S., and Jahn, R.: Poorly crystalline mineral phases protect organic matter in acid subsoil horizons, European Journal of Soil Science, 56, 717–725, https://doi.org/10.1111/j.1365-2389.2005.00706.x, 2005.

Kleber, M., Sollins, P., and Sutton, R.: A conceptual model of organo-mineral interactions in soils: Self-assembly of organic molecular fragments into zonal structures on mineral surfaces, Biogeochemistry, 85, 9–24, https://doi.org/10.1007/s10533-007-9103-5, 2007.

Kleber, M., Eusterhues, K., Keiluweit, M., Mikutta, C., Mikutta, R., and Nico, P. S.: Mineral-Organic Associations: Formation, Properties, and Relevance in Soil Environments, Elsevier Ltd, 1–140 pp., https://doi.org/10.1016/bs.agron.2014.10.005, 2015.

Koarashi, J., Hockaday, W. C., Masiello, C. a., and Trumbore, S. E.: Dynamics of decadally cycling carbon in subsurface soils, Journal of Geophysical Research G: Biogeosciences, 117, G03033, https://doi.org/10.1029/2012JG002034, 2012.

Kramer, M. G. and Chadwick, O. A.: Controls on carbon storage and weathering in volcanic soils across a high-elevation climate gradient on Mauna Kea, Hawaii, Ecology, 97, 2384–2395, https://doi.org/10.1002/ecy.1467, 2016.

Kramer, M. G. and Chadwick, O. A.: Climate-driven thresholds in reactive mineral retention of soil carbon at the global scale, Nature Climate Change, 8, 1104–1108, https://doi.org/10.1038/s41558-018-0341-4, 2018.

Lavallee, J. M., Soong, J. L., and Cotrufo, M. F.: Conceptualizing soil organic matter into particulate and mineral-associated forms to address global change in the 21st century, Global Change Biology, 26, 261–273, https://doi.org/10.1111/gcb.14859, 2020.

Lawrence, C. R., Harden, J. W., Xu, X., Schulz, M. S., and Trumbore, S. E.: Long-term controls on soil organic carbon with depth and time: A case study from the Cowlitz River Chronosequence, WA USA, Geoderma, 247–248, 73–87, https://doi.org/10.1016/j.geoderma.2015.02.005, 2015.

Lehmann, J. and Kleber, M.: The contentious nature of soil organic matter, Nature, 528, 60–68, https://doi.org/10.1038/nature16069, 2015.

Leinemann, T., Preusser, S., Mikutta, R., Kalbitz, K., Cerli, C., Höschen, C., Mueller, C. W., Kandeler, E., and Guggenberger, G.: Multiple exchange processes on mineral surfaces control the transport of dissolved organic matter through soil profiles, Soil Biology and Biochemistry, 118, 79–90, https://doi.org/10.1016/j.soilbio.2017.12.006, 2018.

Lenth, R. V.: emmeans: Estimated Marginal Means, aka Least-Squares Means, 2021. https://CRAN.R-project.org/package=emmeans

Liebmann, P., Mikutta, R., Kalbitz, K., Wordell-Dietrich, P., Leinemann, T., Preusser, S., Mewes, O., Perrin, E., Bachmann, J., Don, A., Kandeler, E., Marschner, B., Schaarschmidt, F., and Guggenberger, G.: Biogeochemical limitations of carbon stabilization in forest subsoils, Journal of Plant Nutrition and Soil Science, 185, 35–43, https://doi.org/10.1002/jpln.202100295, 2022.

Masiello, C. A., Chadwick, O. A., Southon, J., Torn, M. S., and Harden, J. W.: Weathering controls on mechanisms of carbon storage in grassland soils C, Global Biogeochemical Cycles, 2004.

Mathieu, J. A., Hatté, C., Balesdent, J., and Parent, É.: Deep soil carbon dynamics are driven more by soil type than by climate: a worldwide meta-analysis of radiocarbon profiles, Global Change Biology, n/a-n/a, https://doi.org/10.1111/gcb.13012, 2015.

Mikutta, R., Kaiser, K., Dörr, N., Vollmer, A., Chadwick, O. A., Chorover, J., Kramer, M. G., and Guggenberger, G.: Mineralogical impact on organic nitrogen across a long-term soil chronosequence (0.3-4100 kyr), Geochimica et Cosmochimica Acta, 74, 2142–2164, https://doi.org/10.1016/j.gca.2010.01.006, 2010.

Parker, I. and Matyas, W. J.: CALVEG: A Classification of Californian Vegetation, U.S. Dep. Agric., For. Serv., Reg. Ecol. Group, San Francisco, CA, USA, 1981.

Rasmussen, C.: Pedogenesis, Soil Mineralogy, and Soil Carbon Dynamics in Sierra Nevada Conifer Systems of California, 246, 2004.

Rasmussen, C., Torn, M. S., and Southard, R. J.: Mineral Assemblage and Aggregates Control Carbon Dynamics in a California Conifer Forest, Soil Science Society of America Journal, 69, 1711–1721, https://doi.org/10.2136/sssaj2005.0040, 2005.

Rasmussen, C., Southard, R. J., and Horwath, W. R.: Soil Mineralogy Affects Conifer Forest Soil Carbon Source Utilization and Microbial Priming, Soil Science Society of America Journal, 71, 1141, https://doi.org/10.2136/sssaj2006.0375, 2007.

Rasmussen, C., Dahlgren, R. A., and Southard, R. J.: Basalt weathering and pedogenesis across an environmental gradient in the southern Cascade Range, California, USA, Geoderma, 154, 473–485, https://doi.org/10.1016/j.geoderma.2009.05.019, 2010a.

Rasmussen, C., Matsuyama, N., Dahlgren, R. A., Southard, R. J., and Brauer, N.: Soil Genesis and Mineral Transformation Across an Environmental Gradient on Andesitic Lahar, Soil Science Society of America Journal, 71, 225, https://doi.org/10.2136/sssaj2006.0100, 2010b.

Rasmussen, C., Heckman, K., Wieder, W. R., Keiluweit, M., Lawrence, C. R., Berhe, A. A., Blankinship, J. C., Crow, S. E., Druhan, J. L., Hicks Pries, C. E., Marin-Spiotta, E., Plante, A. F., Schädel, C., Schimel, J. P., Sierra, C. A., Thompson, A., and Wagai, R.: Beyond clay: towards an improved set of variables for predicting soil organic matter content, Biogeochemistry, 137, 297–306, https://doi.org/10.1007/s10533-018-0424-3, 2018a.

Rasmussen, C., Throckmorton, H., Liles, G., Heckman, K., Meding, S., and Horwath, W. R.: Controls on Soil Organic Carbon Partitioning and Stabilization in the California Sierra Nevada, Soil Systems, 2018b.

Schrumpf, M., Kaiser, K., Guggenberger, G., Persson, T., Kögel-Knabner, I., and Schulze, E. D.: Storage and stability of organic carbon in soils as related to depth, occlusion within aggregates, and attachment to minerals, Biogeosciences, 10, 1675–1691, https://doi.org/10.5194/bg-10-1675-2013, 2013.

Shi, Z., Allison, S. D., He, Y., Levine, P. A., Hoyt, A. M., Beem-Miller, J., Zhu, Q., Wieder, W. R., Trumbore, S., and Randerson, J. T.: The age distribution of global soil carbon inferred from radiocarbon measurements, Nature Geoscience, 13, 555–559, https://doi.org/10.1038/s41561-020-0596-z, 2020.

Sierra, C. A.: Forecasting atmospheric radiocarbon decline to pre-bomb values, Radiocarbon, 60, 1055–1066, https://doi.org/10.1017/RDC.2018.33, 2018.

Sierra, C. A., Müller, M., Metzler, H., Manzoni, S., and Trumbore, S. E.: The muddle of ages, turnover, transit, and residence times in the carbon cycle, Global Change Biology, 23, 1763–1773, https://doi.org/10.1111/gcb.13556, 2017.

Sierra, C. A., Hoyt, A. M., He, Y., and Trumbore, S. E.: Soil Organic Matter Persistence as a Stochastic Process: Age and Transit Time Distributions of Carbon in Soils, Global Biogeochemical Cycles, 32, 1574–1588, https://doi.org/10.1029/2018GB005950, 2018.

Slessarev, E. W., Chadwick, O. A., Sokol, N. W., Nuccio, E. E., and Pett-Ridge, J.: Rock weathering controls the potential for soil carbon storage at a continental scale, Biogeochemistry, 157, 1–13, https://doi.org/10.1007/s10533-021-00859-8, 2022.

Steinhof, A., Altenburg, M., and Machts, H.: Sample Preparation at the Jena 14C Laboratory, Radiocarbon, 59, 815–830, https://doi.org/10.1017/RDC.2017.50, 2017.

Stoner, S. W., Hoyt, A. M., Trumbore, S., Sierra, C. A., Schrumpf, M., Doetterl, S., Baisden, W. T., and Schipper, L. A.: Soil organic matter turnover rates increase to match increased inputs in grazed grasslands, Biogeochemistry, 156, 145–160, https://doi.org/10.1007/s10533-021-00838-z, 2021.

Stuiver, M. and Polach, H. A.: Reporting of 14C Data, Radiocarbon, 19, 355–363, https://doi.org/10.1017/S0033822200003672, 1977.

Tang, J. and Riley, W. J.: Weaker soil carbon–climate feedbacks resulting from microbial and abiotic interactions, Nature Clim Change, 5, 56–60, https://doi.org/10.1038/nclimate2438, 2014.

Tang, J. and Riley, W. J.: Competitor and substrate sizes and diffusion together define enzymatic depolymerization and microbial substrate uptake rates, Soil Biology and Biochemistry, 139, 107624, https://doi.org/10.1016/j.soilbio.2019.107624, 2019.

Torn, M. S., Trumbore, S. E., Chadwick, O. A., Vitousek, P. M., and Hendricks, D. M.: Mineral control of soil organic carbon storage and turnover, Nature, 389, 170–173, 1997.

Trumbore, S.: Age of soil organic matter and soil respiration: Radiocarbon constraints on belowground C dynamics, Ecological Applications, 10, 399–411, https://doi.org/10.1890/1051-0761(2000)010[0399:AOSOMA]2.0.CO;2, 2000.

Trumbore, S.: Radiocarbon and Soil Carbon Dynamics, Annual Review of Earth and Planetary Sciences, 37, 47–66, https://doi.org/10.1146/annurev.earth.36.031207.124300, 2009.

Trumbore, S. E., Chadwick, O. A., and Amundson, R.: Rapid Exchange between Soil Carbon and Atmospheric Carbon Dioxide Driven by Temperature Change, Science, 272, 393–396, 1996.

Woolf, D. and Lehmann, J.: Microbial models with minimal mineral protection can explain long-term soil organic carbon persistence, Scientific Reports, 9, 1–8, https://doi.org/10.1038/s41598-019-43026-8, 2019.

4. Study 3

"Mineralogical and climatic controls on age and transit time distributions of soil C"

Contribution: I conceived the idea for the study, conducted the study, visualized the results, and wrote the manuscript with inputs from Susan Trumbore, Marion Schrumpf, and Georg Guggenberger. Archived samples and mineralogical data were originally collected and prepared by Craig Rasmussen (see text for details).

Status: To be submitted

Keywords: soil carbon, radiocarbon, time series, parent material, climate, incubation, soil archives

4.1.   Abstract

The response of soil C to rising temperatures is uncertain, with the potential for gains or losses in the coming decades. Insight into these dynamics can be obtained from model-derived probability distributions of soil C ages and transit times. The aims of this study were two-fold: 1) assess the relationship between climatic and mineralogical factors and soil C age and transit time distributions, and 2) quantify the effect of soil mineral assemblages on the temperature response of soil C age and transit time distributions. I adopted a comparative modeling approach, with the models constrained by time series of $\Delta^{14}C_{respired}$ and $\Delta^{14}C_{bulk}$ observed at the sites described in Ch. 3: 0-0.3 m soil profiles developed on andesitic, basaltic, and granitic parent materials, spanning a MAST gradient from 6.0 to 13.3 °C. Pre-aging of soil C was quantified by fitting a lag time parameter in the models, while inputs were estimated using observed soil C stocks and modeled transit times. Parameter uncertainty was assessed with a Markov Chain Monte Carlo approach, while relationships among climatic and mineralogical variables and model outputs were quantified in a Bayesian linear modeling framework.

Two pool models (2p) performed better than the one or three pool models. Internal model dynamics did not affect the age and transit time distributions or model performance, with similar results for the 2p models with inputs processed in parallel (2pp) versus serially (2ps). Root mean square error (RMSE) for the 2p model fits ranged from 9.1 to 36.3 ‰ole (n = 27), indicating a good fit to the data. Trends in ages and transit times mirrored those in $\Delta^{14}C_{bulk}$ and $\Delta^{14}C_{respired}$ (Ch. 3). Soil C ages and transit times increased with depth, and were oldest in the soils developed on andesite, then basalt, and then granite. The warm climate sites had the youngest ages and transit times. Transit times were similar between the cool and cold sites, but C ages were older at the cool sites than the cold sites. Mean soil C ages showed no response to MAST in the linear models. Median C ages decreased with increasing MAST in the granitic and basaltic soils, but not in the andesitic soils. In contrast, mean C ages increased exponentially with PCM content across all parent materials. Transit times did not vary in response to PCM content, but the response of transit time to MAST varied by parent material, suggesting mineralogical control. Mean and median transit times of soil C decreased strongly with increasing MAST for the granite soils, but not the basaltic or andesitic soils.

Inputs increased along with MAST, suggesting the potential for changes in inputs under predicted future temperature increases. Both inputs and lag times increased with soil depth. Lag time increased at an average rate of 20 y per 0.1 m, indicating pre-aging of soil C is an important mechanism for older apparent C ages in deeper soil layers. Neither parent material nor PCM content were related to inputs or lag times in the models.

The results of this study demonstrate that mineral assemblages attenuate the temperature sensitivity of soil C ages and transit times in soils with mixed mineralogies. Mineral control of soil C ages is strong, particularly PCM abundance, while the effect of parent material on transit time suggests mineral control may be important for annual to decadally cycling soil C as well. These findings underscore the importance of future studies identifying the specific mineralogical mechanisms controlling soil C cycling on short time scales. Going beyond mean C ages and transit times and characterizing their full distributions will be key for predicting the response of soil C reservoir to a changing climate, and this work shows that time series of $\Delta^{14}C_{bulk}$ and $\Delta^{14}C_{respired}$ can provide the necessary constraints to do so.

4.2. Introduction

Soils have the potential to be a sink or a source for atmospheric CO_2 in the coming decades (Friedlingstein et al., 2014; Todd-Brown et al., 2018). This potential is a function of both the quantity of C stored in soils and the duration of storage (Sierra et al., 2021). Soil C storage capacity is related to the average age of C in the soil (system age), while the duration of storage (transit time) is equivalent to the mean age of C leaving the system (Sierra et al., 2017). Both mineralogical and climatic factors are strongly correlated with soil C storage and persistence on a global scale (Heckman et al., 2022), yet the influence of these factors on the time scales of C cycling in different soil C pools is poorly quantified. Here we extend the findings of Ch. 2 by using the time series of $\Delta^{14}C_{bulk}$ and $\Delta^{14}C_{respired}$ from the combined parent material and climate gradient to constrain simple compartmental models. We use these models to calculate the age distribution of soil C ages and transit times, and assess the relationship between these distributions and both climatological and mineralogical factors in order to gain novel insight into future soil C stock changes.

The majority of topsoil (0 to 0.3 m depth) C cycles on annual to decadal time scales, but a small proportion can persist for centuries to millennia, resulting in an age distribution with a mean that is much older than the median (Sierra et al., 2018; Schimel, 2006). Due to the skewness of age and transit time distributions, the median of these distributions can be a better measure of the central tendency than the mean. In a heterogeneous system, i.e., characterized by multiple pools of soil C, a skewed distribution arises from the superposition of pool age distributions shaped by soil C persistence mechanisms operating on different time scales (Sierra et al., 2018; Lehmann and Kleber, 2015). A consequence of the typical long-tailed age distribution (mean >> median) is that the radiocarbon content of bulk soil C is biased toward the signal from more slowly cycling soil C pools, owing to the fact that faster cycling C is preferentially lost and therefore tends to make up a smaller proportion of the bulk organic matter mass. In contrast, the $\Delta^{14}C$ signal in the release flux, e.g., from heterotrophic respiration, skews younger and is dominated by faster cycling soil C (Sierra et al., 2018).

Radiocarbon is well suited for constraining soil C models because it can be used to quantify C cycling rates across time scales ranging from annual to millennial (Trumbore, 2009, 2000). Radioactive decay of ^{14}C (half-life = 5730 y) is used to quantify soil C cycling on centennial to millennial time scales. This quantification relies on a ^{14}C calibration curve created by measuring the ^{14}C content of known-age samples going back millennia (Reimer et al., 2020). In contrast, the fraction of "bomb-C"

derived from nuclear weapons testing in the mid-20th century can be used to quantify cycling rates of soil C on annual to decadal timescales. The concentration of ^{14}C in the atmosphere nearly doubled prior to the ban of above ground testing in 1963, after which it rapidly declined, enabling the use of this "bomb-C" pulse as a tracer for decadally cycling soil C (Broecker et al., 1982).

A key benefit of using the radiocarbon content of bulk soil C and respired CO_2 as model constraints is that they can be measured empirically as well as generated as an output of a linear dynamical model (Metzler et al., 2018). However, because ^{14}C of bulk soil C is more sensitive to the age distribution, and ^{14}C of respired CO_2 is more sensitive to the transit time distribution, these constraints are most useful when measured in tandem (Trumbore, 2000). Another feature of these measurements is that they are independent of any assumptions about the internal dynamics of the system, i.e., the sizes and cycling rates of soil C pools. This confers an advantage of flexibility but also carries the risk of model equifinality: an outcome where the same data support multiple model solutions (Beven, 2006).

Mechanistic constraints on decomposition, such as bonding environments, the chemical makeup of soil organic matter, or its physical arrangement, are critical for determining the time scales of soil C persistence. For example, consider a soil with a portion of the organic matter ionically bound to soil minerals via multivalent cation bridging. Assuming this material all has the same mean turnover rate, we can treat it as a distinct pool with a characteristic distribution of C ages. In turn, we could expect that this turnover rate would be distinct from the turnover rate of the organic matter covalently bonded to permanently charged silicate clay minerals, or electrostatically bonded to metal (oxy) hydroxides with variable charge. In such a scenario, the overall system age distribution of soil C would result from the superposition of the characteristic age distributions of each distinct pool.

Empirical approaches of partitioning soil organic matter into distinct pools have the advantage of clear physical definitions, such as with density or size fractionation. However, these laboratory-defined pools may not correspond to actual pools in situ (Abramoff et al., 2018; Lehmann and Kleber, 2015), i.e., they may be mixtures of soil organic matter with different sensitivities to decomposition. This pitfall is illustrated with the example presented above, in which different pools of mineral-associated organic matter are defined by bond type, all of which would likely be categorized as "heavy" material in a density fractionation. A conceptual model-based approach provides an alternative method which can be used to test simplified hypotheses about soil C dynamics without relying on potentially heterogeneous empirical pools.

Given our current understanding of the mechanisms of soil organic matter persistence, a single pool model is unlikely to be able to reproduce the C dynamics observed in actual soils (Baisden et al., 2002). However, adding additional pools to a model requires adding more parameters, which in turn requires more data for parameterization. For example, increasing the complexity of a model to two pools from one introduces a minimum of two additional parameters. The simplest of the two pool model structures can be characterized as parallel systems or serial systems (Sierra et al., 2015). In a parallel system the inputs are partitioned between the pools, while a serial system has the inputs entering the first pool before being transferred to the second pool. A two-pool system could be made more complex by adding a feedback mechanism, with C flowing from pool one to pool two and also from pool two back to pool one, but at the cost of a fourth parameter. Importantly, even the simplest two-pool models, e.g., parallel (2pp) and serial (2ps), are tractable for testing useful hypotheses about soil C dynamics (Stoner et al., 2021).

In Chapter 2, we used a time series of $\Delta^{14}C_{bulk}$ and $\Delta^{14}C_{respired}$ data from to demonstrate that: (1) climate controls on $\Delta^{14}C_{bulk}$ and $\Delta^{14}C_{respired}$ dominate at the soil surface, but mineral control increases with depth, (2) $\Delta^{14}C_{bulk}$, $\Delta^{14}C_{respired}$ and $\Delta^{14}C_{respired}$-$\Delta^{14}C_{bulk}$ were all significantly correlated with the abundance of oxalate extractable Fe/Al phases, indicating a role for mineral protection in determining cycling rates of both fast and more slowly cycling soil C.

Here, we use the previously described time series of radiocarbon measurements of $\Delta^{14}C_{bulk}$ and $\Delta^{14}C_{respired}$ to constrain compartmental models of soil C dynamics at nine sites across a combined gradient of parent material and climate, resolved by depth. Under the steady-state assumption, we estimate below ground inputs from the models using measured soil C stocks. We also introduce a lag time to account for pre-aging of C inputs, i.e., in plant tissues or in upper depth layers, which may be required to explain the evolution of $\Delta^{14}C_{bulk}$ and $\Delta^{14}C_{respired}$ over the last two decades. Using the models, we derive distributions of soil C ages and transit times in order to address the following questions regarding climatological and mineralogical controls on the different time scales of soil C persistence:

1. Does parent material or mineral assemblage affect transit time distributions of soil C?
2. Are climatic controls on soil C age or transit time distributions independent of mineralogical controls? Does the relative importance of climate and mineralogical factors change with depth, as observed with $\Delta^{14}C_{bulk}$ and $\Delta^{14}C_{respired}$?

3. Do lag times improve model fits? How do lag times vary with soil depth and across the climatological and mineralogical gradients?

4. Are inputs estimated from fitted models comparable to those estimated from flux measurements at nearby sites?

4.3. Materials & Methods

4.3.1 Data

4.3.2 Field setting and soil sampling

The soils used in this study come from a combined gradient of parent material and climate located on the western slope of the Sierra Nevada mountains, USA. Parent materials consisted of granite, andesite, and basalt, while the climate gradient is defined by MAST, MAP, and potential evapotranspiration (PET). Mean annual soil temperature at the study sites ranged from 6.0 to 13.3 °C, MAP ranged from 910 to 1400 mm yr^{-1}, and PET ranged from 950 to 1140 mm yr^{-1}. Overstory vegetation at the sites consisted of mixed conifer species. Full site details are provided in Ch. 2 and in Rasmussen (2004)

Soil samples were collected at three time points over approximately two decades: 2001, 2009-2010, and 2019. Three replicate pits were dug at each site, with samples collected from the sidewalls of all three pits. Samples in 2001 and 2009–2010 were collected by genetic soil horizon. However, due to the strong dependence of $\Delta^{14}C$ on depth, we adopted a depth-based sampling strategy in 2019 (0.1 m increments). Samples were collected from the A horizons only in 2001, but from the A, B and C horizons in 2009–2010 and 2019. We focus here on the A horizons (ca. 0–0.3 m) in order to leverage the whole time series as constraints for the soil carbon modeling. Note that the 2009-2010 samples will be referred to as "2009 samples" going forward, as the majority of the samples were collected in 2009.

Site descriptions and geospatial coordinates were recorded in 2001, allowing us to relocate the sites with confidence in subsequent re-samplings (2009, 2019). For the 2019 sampling we compared the soil profiles to the pedon descriptions made in earlier sampling campaigns to confirm we were in the right locations and that the profiles matched.

4.3.3 Soil analyses

Laboratory analyses of soils were performed on both fresh soils and archived air-dried subsamples. Mineralogical assays, including selective dissolution and X-ray diffraction, were conducted on the 2001 and 2009–2010 samples. Bulk density and soil particle distributions were also determined from these samples, along with organic carbon and total nitrogen concentrations. Data from these analyses are used here with permission; methodological details are available in Rasmussen (2004) and Rasmussen et al. (2018). Concentrations of C and N were also measured for the 2019 samples (Ch. 2). The mineralogical data used in this chapter are described in more detail in Ch 2. Full details of the analytical methodology are provided in Rasmussen (2004) and Rasmussen et al. (2018).

Soil organic C stocks were calculated using Eq. 4-1. We used the 2009 bulk density values for calculating SOC stocks in 2019, as we did not observe substantial changes in soil C concentrations between 2009 and 2019 for the majority of sites (Ch. 2), and soil moisture content was assumed to be similar as most samples were collected at the same time of year.

$$SOC_{stock} = \rho \cdot C \cdot FE \cdot d, \hspace{2cm} (\,4\text{-}1\,)$$

where SOC is soil organic C, ρ is bulk density (g m^{-2}), FE is the fine earth proportion (<2mm), and d is depth (m).

We incubated the soils collected in 2001 and 2019 in the laboratory. Soils were only available from a single profile at each site for the 2009 samples, so we excluded these samples from the incubation experiment to avoid spatial bias. Incubations for both years were performed in 2020. All soils were air-dried prior to remoistening at 60% of WHC for consistency across the freshly collected samples (2019) and archived samples (2001) (Beem-Miller et al., 2021). See Ch. 2 for details of the incubation procedure and CO_2 collection protocol. Prior to incubation we composited the soils from the three replicate pits at each site by depth. Each composite sample was then incubated in duplicate.

We measured the radiocarbon content of both bulk soils and CO_2 respired during the laboratory incubations. Details of the bulk soil radiocarbon analysis for the 2009 samples are reported in Rasmussen et al. (2018), while details of both the bulk soil radiocarbon analysis for 2019 samples and respired CO_2 radiocarbon analysis for 2001 and 2019 samples are provided in Ch. 2.

Radiocarbon data are reported in units of $\Delta^{14}C$ (see Ch. 2 for details) (Stuiver and Polach, 1977). The $\Delta^{14}C$ unit is particularly useful for samples that contain substantial enrichment from bomb-C, which derives from atmospheric testing of nuclear weapons in the early 1960s. Values of $\Delta^{14}C > 0$ indicate the presence of bomb-C, while values < 0 are due to radioactive decay of ^{14}C (half-life $\sim$ 5730 y).

We used a mass-preserving quadratic spline function to compare soil properties from samples collected from different depth intervals in different years and at different sites (Bishop et al., 1999). We performed this operation with the 'mpspline' function from the R package mpspline2, using the default λ value of 0.1 (Hengl, 2019; O'Brien, 2022).

4.3.4 Climate data

The climate data used in this study comes from a combination of downscaled gridded global climate data including MAP (mm yr^{-1}) and MAST (°C), gridded PET (mm yr^{-1}) from a hydrological model developed for the state of California and adjacent watersheds (California Basin Characterization Model, CBCM), and water balance measurements made at flux tower sites adjacent to soil sampling locations (volumetric soil moisture). Rasmussen et al. (2006) calculated MAST and MAP as the 30-year average over the period 1971–2001 using PRISM (Parameter-elevation Regressions on Independent Slopes Model) data. CBCM runs on a monthly timestep, and the available data covers the period 1895 to 2010 (Flint et al., 2013). We calculated PET as the sum of monthly CBCM output, and averaged these annual sums over the time period 1991 to 2010 to determine mean annual PET.

We also acquired depth-resolved soil moisture data from two of the National Ecological Observatory Network (NEON) (Keller et al., 2008) flux towers located along the granitic parent material transect. The Soaproot Saddle site (SOAP) is located at (37.0° N, -119.26° W) at an elevation of (1160 m), corresponding to the warm climate granite site from our transect. The Lower Teakettle site (TEAK) is located at (37.0° N, -119.01° W) at an elevation of 2147 m, which places it in between the cool and cold climate sites on the granite transect. The sampling depths for soil moisture varied between the SOAP and TEAK sites, and also diverged from the sampling depths used in our study. Accordingly, we used the same mass preserving spline technique as for the other soil data in order to estimate volumetric soil moisture content over the same depth increments sampled in our study (0-0.1 m, 0.1-0.2 m, 0.2-0.3 m).

4.3.5 Modeling framework

4.3.5.1.   Model structures and assumptions

We used a compartmental modeling framework to estimate ages and transit times of soil C. Modeling was carried out with the R package SoilR (Sierra et al., 2014), and models were constrained with the time series of $\Delta^{14}C_{bulk}$ and $\Delta^{14}C_{respired}$. We implemented first-order decay kinetics in all models and assumed that all systems were at steady-state. The balance of C in such models (Eq. 4-2), and by extension ^{14}C (Eq. 4-3), can be treated as a system of linear differential equations with the form

$$\frac{dC}{dt} = \mathbf{u} + \mathbf{B} \cdot \mathbf{C}\,(t) \tag{4-2}$$

$$\frac{d^{14}C}{dt} = \mathbf{u} + \mathbf{B} \cdot {}^{14}\mathbf{C}\,(t) \; - \; \lambda^{14}C(t) \tag{4-3}$$

where $\mathbf{u}$ is an n dimensional vector of inputs, $\mathbf{B}$ is an n x n matrix giving the decomposition rates of each pool on the diagonal and transfers between pools on the off-diagonal, $\mathbf{C}$(t) and $^{14}\mathbf{C}$(t) are the n dimensional vector of C stocks and ^{14}C in each pool at time t, and λ is the radioactive decay constant.

We compared the performance of a one pool model system to more complex multiple pool systems. Multiple pool models can be structured differently with respect to the amount of C transferred between pools and also in the partitioning of inputs among pools. We only considered both parallel and series type models, as these models require fewer parameters and therefore fewer data constraints than more complex structures, e.g., feedback type models. In a parallel type model, inputs (I) are partitioned between the fast and slow pools according to the partitioning coefficient γ_{fast}, and there is no transfer of C from one pool to another. The input vector, model matrix, and C stock vector for the two pool parallel models are shown in Eq. 4-4. In contrast to the parallel model, all of the inputs in a series type model first enter the "fast" pool and are then transferred sequentially to the other pools. The input vector, model matrix, and C stock vector for the two pool series models are shown in Eq. 4-5. Note that for the two pool models we have adopted the convention of labeling the model pools "fast" and "slow".

$$\mathbf{u} = I \, \cdot \begin{pmatrix} \gamma_{fast} \\ 1 - \gamma_{fast} \end{pmatrix}, \mathbf{B} = \begin{pmatrix} -k_{fast} & 0 \\ 0 & -k_{slow} \end{pmatrix}, \mathbf{C}\,(t) = \begin{pmatrix} x_{fast} \\ x_{slow} \end{pmatrix} \tag{4-4}$$

$$\mathbf{u} = I \cdot \begin{pmatrix} 1 \\ 0 \end{pmatrix}, \mathbf{B} = \begin{pmatrix} -k_{fast} & 0 \\ \alpha_{fast}k_{fast} & -k_{slow} \end{pmatrix}, \mathbf{C}(t) = \begin{pmatrix} x_{fast} \\ x_{slow} \end{pmatrix} \qquad (4\text{-}5)$$

For the parallel models, we fit decomposition constants (k) for each model pool and input partitioning coefficients (γ) that determine the amount of C entering each pool. We fit a single partitioning coefficient (γ_{fast}) for the two pool parallel models (2pp), defined as the proportion of the total system inputs partitioned to the fast pool; accordingly, the proportion of the total system inputs entering the slow pool in the 2pp model is 1-γ_{fast}. We fit an additional partitioning coefficient (γ_{slow}) for the three pool parallel (3pp) models, defined as the proportion of total system inputs partitioned to the slow pool (γ_{slow}). The input to the third pool in the 3pp system is 1-(γ_{fast}+γ_{slow}).

The parameters fit for the series model structures include decomposition rate constants for each model pool, and transfer coefficients (α) giving the proportion of the output flux from each pool transferred sequentially to the next pool in the system. We fit a single alpha coefficient (α_{fast}) for the two pool series models (2ps), defined as the proportion of the output flux from the fast pool transferred to the slow pool. We fit an additional alpha coefficient (α_{slow}) for the three pool series models (3ps), defined as the proportion of the output flux from the slow pool that is transferred to the third model pool.

We also fit a lag time parameter for each of the models considered (1p, 2pp, 2ps, 3pp, 3ps). Fitting the lag time parameter enabled us to separate the potential effects of pre-aging of soil C inputs, e.g., in vegetation or via vertical transport, from other mechanisms of soil C persistence. We report this lag time as a model parameter of interest, including how it varies with climatological and mineralogical factors. Lag times are implemented in SoilR by shifting the radiocarbon signature of C inputs along the atmospheric radiocarbon curve according to the supplied lag time: for example, if we fit a 10-year lag time, inputs to the soil in 2019 would have the Δ^{14}C signature of C fixed in 2009.

4.3.5.2.   Parameter optimization

We determined the initial parameter values by adjusting the values manually until we achieved reasonably good fits for $\Delta^{14}C_{bulk}$ and $\Delta^{14}C_{respired}$ with respect to the observed data. The exception was the lag time parameter, for which we used an initial value of 10 y based on lag times and root ^{14}C content observed for other temperate forest sites (Gaudinski et al., 2000; Koarashi et al., 2012; Solly et al., 2013). The initial parameters were then used as inputs for an optimization algorithm. We enforced steady-state during the parameter fitting procedure by finding the steady-state solution for

soil C stocks for each candidate set of model parameters (Eq. 4-6), and then initializing C stocks in the model using these values. The initial timepoint for our model runs was set to 1900, allowing us to use the candidate decomposition rate parameters to determine the initial $\Delta^{14}C$ values of the model pools (Eq. 4-7) (cf. Eq. 3.25 in Trumbore et al., 2016).

$$\mathbf{C} = -\mathbf{B^{-1}} \cdot \mathbf{u} \qquad\qquad (4\text{-}6)$$

$$F = \frac{k}{k+\lambda} \qquad\qquad (4\text{-}7)$$

We used the Nelder-Mead algorithm for optimization, which is the default from the R package optim (R Core Team, 2020). This is a direct search method that performs well for optimization problems over a small number of variables with minimal iterations (Sierra et al., 2015; McKinnon, 1998). We increased the number of algorithm iterations from a default value (n = 500) as needed, i.e., when the initial search did not converge. In a few cases, specifically for the 3p models with a larger number of parameters, we observed degeneracy of the Nelder-Mead simplex. When this occurred, we used the conjugate gradient method "BFSG" in optim, as we observed the results from this method to be similar to those achieved with the Nelder-Mead algorithm when we compared the two algorithms at sites where both algorithms converged successfully.

The optimized parameter set and covariance matrix were then used to initialize a constrained Markov Chain Monte Carlo (MCMC) simulation with 10,000 iterations. The MCMC approach is useful for avoiding local minima that can confound conventional optimization algorithms when searching for the global minimum. Furthermore, when the model system is under constrained, multiple parameter combinations may be equally valid, and the MCMC approach is useful for quantifying the uncertainty that results from this problem of equifinality (Sierra et al., 2015; Stoner et al., 2021). We used the function 'modMCMC' in the R package FME to perform MCMC simulations (Soetaert and Petzoldt, 2010). We constrained both the decomposition rate parameters and the α/γ parameters to the interval (0, 1) and the lag time parameter to the interval (0, 100) in order to ensure realistic results but still allow for flexibility during the MCMC simulation. We set the delayed rejection parameter to 2 to improve fitting for sites with high variance in the model constraint dataset.

4.3.5.3.   Model selection

We identified the best-fit parameter set from the MCMC simulation as the parameter combination that returned the lowest sum of squared residuals against the empirically measured values for

$\Delta^{14}C_{bulk}$ and $\Delta^{14}C_{respired}$. We then selected the best-performing MCMC model among the candidate model structures (1p, 2pp, 2ps, 3pp, 3ps) using Aikaike's Information Criterion (AIC) (Eq. 4-8), corrected for small sample sizes (AIC_c) (Eq. 4-9) (Hurvich and Tsai, 1989). We considered models with AIC_c scores within two AIC_c points to be equally valid (Burnham, 2002).

$$AIC = -2\log\left(\mathcal{L}(\hat{\theta}|y)\right) + 2K \tag{4-8}$$

where the first part of the righthand side of the equation is the maximum value for the log-likelihood of the unknown parameter θ given data y, and the second part is a bias correction term that increases with the number of parameters, K.

$$AIC_c = AIC + \frac{2K\,(K+1)}{n-K-1} \tag{4-9}$$

where n is the sample size.

4.3.6 Model output

4.3.6.1. Ages & transit times

We calculated probability distributions for soil C ages and transit times using the modeling framework outlined above (Metzler et al., 2018; Sierra et al., 2018). The probability distribution functions for C ages and transit times are given by

$$f(a) = -1^T \cdot \mathbf{B} \cdot e^{a \cdot \mathbf{B}} \cdot \frac{\mathbf{C}}{\sum \mathbf{C}} \tag{4-10}$$

and

$$f(\tau) = -1^T \cdot \mathbf{B} \cdot e^{\tau \cdot \mathbf{B}} \cdot \frac{\mathbf{u}}{\sum \mathbf{u}} \tag{4-11}$$

where a is the random variable age, τ is the random variable transit time, T is the transpose operator, $\mathbf{B}$ is the model matrix defined in Eq. 4-2, $\sum\mathbf{C}$ is the sum of soil C stocks in all model pools at steady-state, and $\sum\mathbf{u}$ is the total input. We report the quantiles of these distributions in addition to the means in order to better assess the central tendency as well as the shape of the distributions. The mean age of soil C is given by

$$\mathbb{E}\,(a) = \, -1^T \, \cdot \, \mathbf{B}^{-1} \, \cdot \, \frac{\mathbf{c}}{\sum \mathbf{c}} \tag{4-12}$$

and the mean transit time by

$$\mathbb{E}\,(\tau) = \, -1^T \, \cdot \, \mathbf{B}^{-1} \, \cdot \, \frac{\mathbf{u}}{\sum \mathbf{u}} \tag{4-13}$$

where $\mathbb{E}$ symbolizes the expected value.

Probability distributions for system age and transit time typically decrease exponentially with increasing time. The relationship between the mean and median of an exponential distribution can be expressed by the ratio in Eq. 4-14; and the degree to which this ratio diverges from one is a useful metric for assessing the degree of skewness in the distribution. We use this ratio to identify long-tailed age distributions of ages that could be expected to develop in soils with persistence mechanisms operating on multi-century timescales, or transit time distributions with substantial contributions from pools with strongly divergent turnover rates.

$$median : mean = \frac{\ln(2) \cdot median}{mean} \tag{4-14}$$

4.3.6.2. Inputs

Belowground inputs of C to soils are challenging to measure (Rasse et al., 2005; Schmidt et al., 2011; Sokol and Bradford, 2019; Peixoto et al., 2022), and were not available for our sites. However, we did measure SOC stocks. Under a steady-state assumption, inputs to the compartmental model system are related to SOC stocks by the model matrix (Eq. 4-6). We first fit the models using an arbitrary initial input value in order to derive the parameters for the model matrix. Once we obtained the optimized parameter values from the MCMC algorithm, we used an exhaustive search method to perturb the input values until modeled SOC stocks were equal to measured SOC stocks. We used this approach for a random subset of the MCMC parameter sets (n = 200) in order to generate a distribution of inputs for each site.

We compared the model-estimated inputs to CO_2 flux data measured at adjacent sites along the andesitic and granitic parent material transects in order to determine whether our estimates were realistic. The measured data we considered included chamber, gas well, and flux tower data. Chamber data came from measurements made by Wang et al. (2000) at sites which correspond to the warm,

cool, and cold climate granite soils, and by Tang et al. (2005), who measured soil respiration at the Blodgett Forest Ameriflux tower site, which is located at an intermediate elevation between the warm and cool climate sites of the andesite climate gradient in this study. The gas well data also came from the Blodgett Forest site (Soong et al., 2021). Finally, we drew on eddy covariance-derived gross primary production data from Goulden et al. (2012), measured at sites adjacent to the granite climate gradient sites. In order to estimate the proportion of total CO_2 fluxes contributed per 0.1 m depth increment, we fit an exponential model to the depth-resolved CO_2 fluxes (combined autotrophic and heterotrophic components) measured by Soong et al. (2021) at Blodgett Forest. We used the empirically derived parameters from this model (Eq. 4-15) to predict CO_2 fluxes at the mid-depth point of each depth increment for which we collected samples in 2019 (0.05 m, 0.15 m, 0.25 m).

$$CO_2 \ (gC \ m^{-3} \ h^{-1}) = \ e^{(\beta_0 + \beta_d \cdot d)} \qquad\qquad (\ 4\text{-}15\ )$$

where β_0 and β_d are the intercept and depth coefficients.

4.3.7 Bayesian linear modeling

We employed a generalized Bayesian linear modeling framework to assess the relationship of selected mineralogical and climatological variables to ages and transit times of soil C. The choice of this modeling framework enabled us to use the variance observed in ages and transit times from the MCMC parameter optimization output to inform the model priors. Additionally, considering the posterior distribution of the model parameters can improve uncertainty estimates for sparse datasets (Gelman et al., 2013).

We used mean and median system C age and transit time as the response variables in the models. For the climatological variables we focused on MAST, and for the mineralogical variables we considered the sum of oxalate extractable Al and half of the oxalate extractable Fe (OX) as a proxy for the abundance of reactive minerals. Wetness index and MAP were strongly correlated with parent material, so we excluded both of these variables from the regression analysis. We based the choice of model on the distribution of the data from preliminary model runs.

The response of mean age to OX appeared to be exponentially distributed from the exploratory data analysis, so we modeled the relationship using the Gamma distribution with the log link (Eq. 4-16). We assumed normally distributed priors for model coefficients with the exception of the response error, which we assumed to be exponential. We used the default values for the prior distributions

employed by the function 'stan_glm' in the R package rstanarm (Goodrich et al., 2023) for all parameters but the intercept term, for which we set the mean to zero and the standard deviation equal to the log-transformed standard deviation of mean ages from MCMC parameter optimization output.

We fit a hierarchical mixed model for the effect of MAST on ages and transit times, with intercepts varying by parent material, parent material specific slopes for MAST, and a global interaction between depth and MAST (Eq. 4-17). The hierarchical mixed model also permits the specification of a decomposition of covariance model (Σ), which enables the use of prior knowledge about the expected relationship among model coefficients. Details on the specification of the decomposition of covariance model are provided in the Supplemental Information (section 4.7.3). As with the GLM model for OX, we assumed normally distributed priors for model coefficients with the exception of the response error, which we assumed to be exponential. We also used the default values for the priors of all parameters but the intercept term, for which we set the mean to zero and the standard deviation equal to the log-transformed standard deviation of mean ages from MCMC parameter optimization output.

$$Y_i \mid \beta_{ox}, \beta_d, \beta_{ox}\beta_d = Gamma\ (\mu_i, \sigma^2) \qquad\qquad (\ 4\text{-}16\ )$$

$$\ln(\mu_i) = \beta_0 + \beta_{ox} \cdot OX_i + \beta_d \cdot d_i + \beta_{ox}\beta_d \cdot OX_i \cdot d_i$$

$$\sigma \sim Exp\ (1)$$

$$\beta_p \sim N(\mu_p, \sigma_p^2)$$

where Y_i is the ith mean or median age, or mean or median transit time with a mean value equal to the natural log of μ_i, σ^2 is the exponentially distributed global residual error with a standard deviation of 1, d_i is depth in m, β_0 is the intercept term, OX_i is the vector of reactive mineral abundances (g Al_{ox} + ½ Fe_{ox} kg^{-1} soil), β_{OX} is the coefficient for the effect of reactive mineral abundance, $\beta_{OX}\beta_d$ is the coefficient for the change in the rate parameter β_{OX} with depth, and β_p is the Gaussian normal distributed prior for model coefficient p with mean μ_p and standard deviation σ_p^2.

$$Y_i \mid \beta_{0j}, \beta_{Tj}, \beta_d, \beta_d\beta_T = N\left(\mu_{ij}, \sigma_y^2\right) \tag{4-17}$$

$$\mu_{ij} = \beta_{0j} + \beta_{Tj} \cdot T_i + \beta_d \cdot d_i + \beta_d\beta_T \cdot T_i \cdot d_i$$

$$\sigma \sim Exp\left(\frac{1}{s_y}\right)$$

$$\beta_{pj} \mid \beta_p, \dots, \beta_{p+1} \sim N\begin{pmatrix} \beta_p, \dots, \\ \beta_{p+1} \end{pmatrix}, \Sigma$$

where Y_{ij} is i[th] mean or median age, or mean or median transit time for parent material j with a Gaussian normal distributed mean of μ_{ij} and standard deviation of $\sigma_y{}^2$, β_{0j} is the intercept term for parent material j, which is normally distributed around the global intercept term β_0, β_{Tj} is the coefficient for the effect of MAST for parent material j, which is normally distributed around the global intercept term β_T, β_{dT} is the coefficient for the change in the global coefficient β_T with depth, d is a vector of depths in m, T is a vector of mean annual soil temperatures in °C, β_d is the normally distributed global coefficient for depth, β_{pj} is the conditional distribution of the parent material specific coefficient β_p given the global coefficients, and is the decomposition of covariance model (Supplemental Information section 4.7.3).

We summarized the estimates from the output of each model by calculating the median and 95% uncertainty intervals, and considered coefficient estimates to be significant only when the 95% credible interval for the parameter estimate excluded zero.

4.4. Results

4.4.1 Compartmental model performance and selection

The two-pool models performed better than the one-pool model structures for the majority of our study sites, with smaller values for both AIC$_c$ and RMSE (**Table 4-1**, best-fit model in **bold**). However, the 2pp and 2ps model structures performed equally well (i.e., AIC$_c$ values were within 2 points) at most of the sites, indicating that either model could be used to fit the time series of observed bulk and respired Δ^{14}C. The results from the 0-0.1 m depth of the cold climate andesitic soil serves as a typical example of the equivalency of the 2pp and 2ps model structures, which can be seen from the time series fits, parameterizations, system ages, and transit times (**Figure 4-1**). The 2pp model fits are shown for the uppermost depth layer of all sites in **Figure 4-2**. In some of the granitic soils, and

for the deepest depth layer in the warm climate andesite and basaltic soils, the one-pool model performed better than either of the two-pool models (**Table 4-1**). Mean bulk soil and respired $\Delta^{14}C$ values overlapped in these soils, supporting the assumption of homogeneity that underlies the one-pool model structure.

We were unable to achieve convergence when running the parameter optimization for the three pool models at the majority of the sites. Additionally, the parameters returned by the optimization algorithm were highly collinear, indicating that the models were over-parameterized for the data constraints (Sierra et al., 2015). At the sites where we were able to successfully fit the three-pool models, we observed that the additional parameters did not substantially improve the model fits, as indicated by lower AIC_c values for the two-pool models. Given these factors, we did not consider the three-pool models further.

We will focus our results and discussion on the 2pp models on the basis of: 1) improved estimates of inputs for these models compared to the 2ps models, and 2) otherwise similar performance in terms of AIC, and distributions of system C ages and transit times (See Supplemental Information section 4.7.1 for a more detailed comparison of the 2pp and 2ps models).

4.4.2 Fitting issues

There was one site, cool climate basalt, for which the 2pp (and 2ps) models could not be fitted for the two deepest soil layers (0.1-0.2 m, 0.2-0.3 m) with a realistic mean age or transit time. This site had to be moved ca. 1 km in 2019 from the GPS coordinates recorded in 2001 due to an ongoing timber harvest operation. This may have contributed to the fact that the $\Delta^{14}C_{bulk}$ data from the 2009 sampling was much more enriched than either the 2001 or 2019 data, and that $\Delta^{14}C_{respired}$ data from this site shifted from being enriched relative to the atmosphere in 2001 to being depleted relative to the atmosphere in 2019 (**Figure 4-2**, **Supplemental Figure 4-7**). Given that these temporal trajectories are not in line with the steady state assumption assumed in this study, we have removed the results from this site at these depths from all other analyses.

The deeper layers at the cold climate granite site (0.1-0.2 m, 0.2-0.3 m) also presented challenges when fitting the models. Specifically, $\Delta^{14}C_{respired}$ in these soil layers was highly depleted, suggesting the respiration flux was dominated by C in excess of 200 years in age. This also is not commensurate with a steady-state assumption, as this would suggest the soil is losing C. We removed these highly depleted $\Delta^{14}C_{respired}$ data points as model constraints, and instead fit the model with the time series

of $\Delta^{14}C_{bulk}$ data only. With this approach we were able to get acceptable fits for the 0.1-0.2 m depth. However, the age and transit time distributions, as well as the estimated inputs from the 0.2-0.3 m layer remained unrealistic, so we have removed these data from this site and depth layer from the results.

4.4.3 Soil C model parameters

Optimized parameter values for the two-pool parallel model structure returned from the accepted set of MCMC iterations (n = 10,000) are given in **Table 4-2**. Mean C ages for the model pools ranged from 1 to 119 years for the fast pool (τ_{fast}) and from 76 to 3700 years in the slow pool (τ_{slow}), while the proportion of inputs entering the fast pool (γ_{fast}) ranged from 0.21 to 0.99. Both pool turnover rates and the proportion of inputs entering the fast pool varied in response to climatological and mineralogical variables, yet these trends tended to be weak or inconsistent when considered over all sites and depths. When considered within parent materials, the granitic soils were an exception in that turnover times for the slow pool tended to decrease with increasing MAST, particularly in the two deeper soil layers (0.1-0.3 m), and we also observed a strong increase in γ_{fast} with increasing MAST in the upper depth layers (0-0.2 m). The clearest trend was the increase in slow pool turnover rates with increasing reactive mineral content, which was most apparent in the deeper soil layers (**Table 4-2**).

Estimated mean lag time ranged from 0 to 50 years, and in contrast to the other model parameters, lag times varied strongly in response to climate and depth (**Figure 4-3**, **Table 4-2**). However, soils developed on different parent materials showed similar lag times for a given climate zone and depth. Lag time increased with depth at a rate of approximately 20 y per 0.1 m at both the warm and the cold climate sites. Lag times were substantially shorter (≤ 4 y) at the cool climate sites, however, and did not change with depth.

4.4.4 Ages of soil C

System ages varied with both climate and mineralogical factors, as well as depth. System C age distributions skewed right, with older mean than median values (**Figure 4-4**, **Figure 4-5**, **Figure 4-6**, **Table 4-3**), which indicates the presence of small amounts of C with ages on the order of hundreds of years. This distribution shape can be characterized by the ratio between median and mean C ages (**Table 4-3**). This ratio converged on a value of around 0.45 for the majority of sites. The andesitic soils were an exception to this pattern in the median:mean ratio, with much smaller values of 0.03

and 0.07 in the surface layer (0-0.1 m) of the cool and warm climate sites. The median:mean C age ratio tended to decline with increasing MAST in the surface soils of all three lithologies, with the strongest decrease in the andesitic soils, followed by the granitic and then the basaltic soils. However, we did not observe a relationship between MAST and median:mean C age in the deeper soil layers.

The andesitic soils tended to have the oldest mean and median C ages, and the granitic soils had the youngest when compared across all climate zones and all depths (**Figure 4-4**, **Figure 4-5**, **Figure 4-6**, **Table 4-3**). Mean and median system C ages were most similar among parent materials in the surface layer (0-0.1 m) of the cold climate sites (**Figure 4-4**). Both mean and median system C ages tended to increase with depth, and at a similar rate of approximately 80 y per 0.1 m, with the exception of the cool climate andesitic soils, which had similar mean C ages at all depths (**Figure 4-7**).

System C ages in the granitic soils showed the strongest overall temperature response (**Figure 4-8**, **Table 4-4**). Both mean and median system C ages tended to decrease with increasing MAST, but decreases were only significant for the median, not the mean. The average rate at which median system C age declined with MAST was similar across parent materials, but the posterior distribution of the slope term indicated a stronger response for the granitic soils than the basaltic soils, and for the andesitic soils the 95% uncertainty interval included zero (**Table 4-4**). For the granitic and basaltic soils, the decrease in median system C age was 16.8 (7, 33.8) y per °C and 15.4 (0.8, 27.7) y per °C, respectively (95% uncertainty intervals in parentheses). Although the trend in median age with MAST did not appear to be as strong in the deeper soil layers, there was no increase in model performance when including an interaction between MAST and depth.

We found the strongest relationship between C ages and mineralogical variables with the proxy measurement for (oxy) hydroxide abundance, i.e., the sum of oxalate extractable Al and half of the oxalate extractable Fe (OX). Mean system age increased exponentially with increasing OX abundance across all three lithologies (**Figure 4-10**, **Table 4-5**), at a rate of 1 y per g kg^{-1} m^{-2} OX.

4.4.5 Transit times of soil C

System transit time distributions also varied in response to climatic and mineralogical factors, but showed different patterns than system C age distributions. The response of system transit time to MAST was notably stronger than that of system C age (**Figure 4-9**, **Table 4-5**), and the relationship between system transit time and reactive mineral content was weak. Mean transit time increased

with depth at a similar rate as mean and median C ages, ca. 8 y per 0.1 m, but the increase in median transit time with depth was slower, ca. 4 y per 0.1 m (**Figure 4-7**).

Mean system C transit times tended to be older than median transit times, as with the means and medians of system C age distributions. However, both mean and median system C transit times were notably younger than mean and median system C ages (**Table 4-3**). In contrast to system C ages, the median:mean ratio for the transit time distributions varied widely across both climate zones and lithologies. In general, the median:mean transit time ratio was higher in the granitic soils than in the andesitic or basaltic soils, which we attribute to relatively fast median transit times with respect to mean transit times in the andesitic and basaltic soils. We observed a small amount of very fast (< 1 y) cycling soil C in a few of the models (cold climate basaltic soils and the 0.1-0.2 m depth of the cool climate granitic soils) (**Figure 4-4**, **Figure 4-5**, **Figure 4-6**, **Table 4-3**), which correspond to models with less than 1% of the total soil C pool allocated to the fast cycling soil C pool along with fast pool turnover rates ≤ 1 y (**Supplemental Figure 4-8**, **Supplemental Figure 4-3**).

We observed a strong interaction between MAST and parent material in the models for both mean and median system C transit time (**Figure 4-9**), with transit time tending to decrease with increasing MAST. These trends were strongest in the granitic parent materials (**Figure 4-9**, **Table 4-4**), as with system C ages. Mean system C transit time decreased at a rate of 17.7 y per °C increase in MAST (95% uncertainty interval: 10.5, 55.1 y per °C) in the granitic soils, and at slightly lower rates in the basaltic and andesitic soils. However, the uncertainty intervals for the slope estimates in the basaltic and andesitic soils overlapped with zero. We also observed an interaction between depth and the rate of change in mean system C transit time with MAST, with a trend towards flatter slopes with increasing depth, however, the uncertainty interval for this interaction term was large and overlapped with zero.

The relationship between transit time and OX was inconsistent when considered over all sites and depths. Mean system C transit time appeared to show a similarly exponential increase with increasing OX as did mean system C ages when the data were restricted to the two deepest depth layers (0.1-0.3 m), and to the cool and cold climate basaltic and andesitic soils. However, mean transit time did not appear to be affected by OX in the remaining soils, i.e., granitic soils, surface soils, and the warm climate soils, indicating a weak relationship overall.

4.4.6 Inputs

Estimated soil C inputs varied in response to depth and climate, but did not vary among parent materials. We estimated the highest inputs in the surface layer (0-0.1 m) of the warm climate sites andesitic and granitic soils. Inputs at these sites were substantially higher than in the upper layer of the warm climate basaltic soils, and were also a full order of magnitude greater than in the corresponding surface layer of the cool or cold climate soils for all three lithologies (**Figure 4-11**, **Supplemental Table 4-1**). Excluding the anomalously high inputs from these two soil layers, inputs tended to decrease with increasing depth at a similar rate across parent materials, ca. 11 g C m^{-2} per 0.1 m (**Figure 4-11**).

4.5.   Discussion

The focus of this chapter was the parameterization of models to quantify the effect of climatic and mineralogical factors on distributions of soil C ages and transit times. We accomplished this by using the time series of bulk soil and respired radiocarbon from the combined parent material and climate gradient introduced in Ch. 3. The age and transit time distributions are the key output from these models, but we also fit a lag time parameter to account for pre-aging of soil C inputs in vegetation or via vertical transfers between soil layers. Under the steady-state assumption, soil C inputs are related to soil C stocks by the transit time (Eq. 4-6), so using our prior knowledge of soil C stocks at the study sites we were able to use the fitted models to estimate belowground C inputs.

4.5.1 System C ages, transit times, and climatic vs. mineralogical controls

A central question motivating this study was how mineralogical factors, including parent material and reactive mineral content, affect transit time distributions. In the previous chapter, we established that both bulk soil radiocarbon and the radiocarbon signature of heterotrophically respired CO_2 varied among study sites with distinct mineral assemblages and climatic regimes. These results confirmed prior research showing that bulk soil radiocarbon values are strongly correlated with parent material, and more specifically, the abundance of reactive secondary minerals such as (oxy) hydroxides. We also demonstrated a relationship between the radiocarbon signature of respired CO_2 and reactive mineral content, indicating the potential for mineral control of soil C cycling on annual to decadal time scales.

Using the compartmental models developed in this study we were able to demonstrate a significant interaction between parent material and MAST on transit time, which to our knowledge has not been previously demonstrated in situ. These results suggest that soil mineral assemblages can reduce the temperature sensitivity of soil C transit times. Transit time is a measure of the average age of C in the release flux, which is normally expected to derive from relatively unprotected or otherwise easy to decompose material such as particulate organic matter. Decomposition of particulate organic matter has been shown to be strongly dependent on temperature, but our finding that mineral assemblages affect the temperature sensitivity of transit time indicates that a significant portion of the respiration flux may be coming from pools of mineral-associated organic matter in soils rich in reactive minerals.

Earlier work at our study sites (Rasmussen et al., 2006), as well as in other studies (Karhu et al., 2019, 2010; Doetterl et al., 2015), provide laboratory evidence that reactive mineral species may reduce the temperature sensitivity of decomposition. In a follow up study, Rasmussen et al. (2018) observed higher concentrations of reactive secondary minerals in the andesitic and basaltic soils than in the granitic soils, and increased partitioning of the soil C pool to the mineral-associated fraction in the andesite soils relative to the other lithologies. Although we did not observe strong relationships between mean transit time and any proxy measurements for reactive mineral species, when compared to the granitic soils the basaltic and andesitic soils had either shallower slopes for the relationship between transit time and MAST or failed to exhibit a significant relationship at all. Even for the andesitic soils with a significant trend in age or transit time with respect to MAST, we observed the oldest mean C ages and longest transit times at the cool climate site (8.5 °C), not the cold climate site (6.0 °C). Taken together, we interpret our results as providing field-based evidence that parent material can moderate temperature sensitivity of decomposition.

 In line with the findings of Rasmussen et al. (2018), we found that mean C ages varied strongly in response to oxalate extractable Fe and Al content, unlike transit times, and that mineral assemblages played a more important role than MAST in determining mean C age. Soils with more abundant oxalate extractable metals not only had older mean C ages, but also smaller ratios of median to mean C ages. This indicates that the abundance of Al and Fe (oxy) hydroxides is associated with more asymmetric C age distributions, and also suggests the older C ages in these soils is a function of small amounts of centennial to millennial cycling C that may persist through association with soil minerals.

4.5.2 Interactions between climate and mineral assemblages

Previous research at our study sites demonstrated that lithology determines the potential for (oxy) hydroxide formation, but that the observed abundance of these reactive minerals for a given parent material is largely determined by the effects of temperature and soil moisture on weathering rates. We observed a positive correlation between MAP and mean C age at our sites, and an even stronger positive correlation between wetness index and mean C ages. However, we also observed strong collinearity between parent material and both MAP and wetness index, as well as between the abundance of oxalate extractable metals and both MAP and wetness index. This presents a challenge for disentangling the direct effect of precipitation and wetness index on soil C ages from potentially indirect effects via enhanced weathering and the development of reactive secondary minerals.

High soil moisture is associated with old C ages in some soils, which has been attributed to anoxic conditions in poorly drained soils (Wickland and Neff, 2008; Harden et al., 1997). However, in lighter textured soils, such as those at our sites, anoxic conditions are not common. Increased throughflow of water through soils accelerates weathering rates, which in young soils leads to the development of reactive secondary mineral species. Comparing the cold climate andesitic and basaltic soils, we observe the same wetness index value but much higher abundances of oxalate extractable metals and older C ages in the andesitic soils. We interpret this as evidence that the correlation of C age and wetness index is more of an indirect effect at these sites: wetter conditions lead to enhanced weathering, which in turn favors the development of reactive secondary minerals with high potential for slowing decomposition through the formation of mineral-organic associations.

The importance of climate in controlling both C ages and transit times decreased with depth across all lithologies, corresponding to an increase in importance of mineralogical factors. These findings support our results for the climatic and mineralogical control of $\Delta^{14}C_{bulk}$ and $\Delta^{14}C_{respired}$. Temperature influences both enzymatic reaction rates and microbial activity, with faster reaction rates and more microbial activity observed at warmer temperatures than colder temperatures. However, the insulating effect of soil increases with depth, potentially leading to decoupling between air temperature and decomposition rates.

4.5.3 Pre-aging of soil C

The potential pre-aging of soil C inputs confounds the direct interpretation of soil C ages from $\Delta^{14}C$ data alone. There are multiple mechanisms that could lead to pre-aging of inputs, including pre-aging

of C within vegetation (Gaudinski et al., 2000; Joslin et al., 2006; Herrera-Ramírez et al., 2020) and vertical transport of pre-aged soil C between soil layers (Leinemann et al., 2018; Ahrens et al., 2020). Earlier studies from sites adjacent to our granitic parent material sites found that the $\Delta^{14}C$ of fine roots was elevated relative to the atmosphere in the year of sampling, with mean ages ranging between 1 to 20 y (Koarashi et al., 2012). This divergence between the $\Delta^{14}C$ of fine roots and the atmosphere has also been corroborated in other forested ecosystems (Gaudinski et al., 2000; Solly et al., 2013, 2018).

We addressed this issue by fitting a lag time parameter in our soil C models. The strongest control on lag time was depth, which is commensurate with the hypothesis that deeper soil layers receive pre-aged inputs from the upper soil layers. We did not measure $\Delta^{14}C$ of roots, nor did we model root dynamics, so we are unable to separate potential pre-aging of C in vegetation from vertical transport. However, we observed that the depth dependence of the lag time parameter was weakest at the wettest sites. Although lag times at the cool climate sites with the highest wetness index values did not change with depth, they did increase strongly with depth at the relatively dry warm climate sites. We interpret this as possible evidence for reduced transport of fresh soil C inputs to deeper soil layers in response to drying of the upper soil layers during the spring and summer months (Supplemental Information section 4.7.2, **Supplemental Figure 4-5**).

Seasonal drying of upper soil layers and reduced transport of recent C inputs to deeper soil layers does not explain the increase in lag times with increasing depth that we observed at the cold climate sites. However, there are two additional explanations for this. During the winter months, soils at the cold climate sites freeze, leading to reduced transport of water through the soil profile. Although a portion of this water is flushed through the soil during spring snowmelt, preferential flow is likely given the coarse texture of these soils (Rasmussen, 2004), and not all of this snowmelt enters the soil due to runoff processes (Flint et al., 2013). In combination, the cryic regime and coarse textures could lead to reduced delivery of fresh C inputs to deeper layers in the cold climate sites, which gives a hydrological explanation for the increased lag times.

Alternatively, a potentially more likely explanation is increased in root ages with depth, a phenomenon that is well-documented (Hendrick and Pregitzer, 1996; Gaudinski et al., 2000; Wells et al., 2002; Baddeley and Watson, 2005; Joslin et al., 2006). Root ages tend to be older overall at colder sites than at warmer sites (Sah et al., 2011; Solly et al., 2018), and furthermore, the rate of increase in root age with depth has also been shown to increase with decreasing temperature

(Kengdo et al., 2023). Taken together, the evidence suggests that the increase in lag time seen with depth at the cold climate sites would be driven mainly by the effect of temperature on pre-aging of soil C inputs in vegetation (root age), and less so by hydrology, while at the warm climate sites, the increase is likely driven more by the development of a seasonal moisture gradient with depth and its corresponding impact on vertical transport processes.

4.5.4 Model-estimated soil C inputs

The use of soil C models to estimate belowground inputs is not a new idea, and in fact was one of the original applications of the Rothamsted soil C model (Jenkinson et al., 1992). A key advantage of the model-based approach is that it yields an estimate of inputs that integrates variation in annual inputs over time, in contrast to the time-consuming and challenging work of measuring annual inputs over multiple years (Jenkinson et al., 1992). The inputs we estimated from our 2pp models decreased with both soil depth and MAST, which is commensurate with observations of soil CO_2 fluxes reported from nearby sites in other studies (Wang et al., 2000; Tang et al., 2005; Soong et al., 2021).

The decrease in inputs observed with depth matches the decrease observed by Soong et al. (2021) for depth profiles of soil air CO_2 concentrations at the Blodgett Forest Ameriflux tower site, located at an intermediate elevation between the warm and cool climate andesitic soils in this study. The data from Soong et al. (2021) estimates the relative contribution of the total soil profile CO_2 concentration from the 0–0.1 m, 0.1-0.2 m, and 0.2-0.3 m depth layers to be 47%, 32%, and 21%. In comparison, the estimated contribution to total CO_2 fluxes in this study from the same depth layers (across all sites) were 52±29%, 20±11%, and 13±7%. Note that the high standard deviation of the estimates for the uppermost soil layer was driven by notably higher estimates for inputs in the warm climate andesitic and granitic sites compared to the other sites.

We observed substantial decreases in inputs with increasing elevation and MAST in this study, which correlate with the decreases seen in heterotrophic respiration fluxes with increasing elevation reported by Wang et al. (2000) and Tang et al. (2005). A potential mechanism that could explain the decrease in inputs with increasing elevation and MAST is the presence of a thick under canopy shrub layer at both the warm climate andesite and granite soils (dominated by *C. foliolosa* and *Arctostaphylos* spp., respectively), which is also where we estimated the largest inputs. This explanation is supported by the data from basaltic soil transect, where the thick understory

vegetation layer was absent at the warm climate site and where we also did not observe large differences in inputs along the climate gradient.

Our model-estimated fluxes were smaller but of the same order of magnitude as the chamber-based observations of heterotrophic respiration fluxes reported by Wang et al. (2000) and Tang et al. (2005). Wang et al. (2000) estimated annual heterotrophic C fluxes of 460 and 260 g C m^{-2} y^{-1} from sites adjacent to the warm and cold climate granitic sites in this study, respectively, compared to our estimated fluxes of 216 and 102 g C m^{-2} y^{-1} at these sites. Tang et al. (2005) estimated annual heterotrophic C fluxes of 757 g C m^{-2} y^{-1} at the Blodgett Forest site, and we estimated fluxes of 485 and 65 g m^{-2} y^{-1} for the adjacent warm and cool climate andesitic soils, respectively. An important caveat for our data is that our estimates of total inputs/fluxes are inherently biased lower than chamber measurements, because our method does not fully include the inputs from sub-annually cycling C. We sampled soils at the end of the growing season, and therefore our inferred inputs only consider the contribution from roots that persist for a whole growing season or longer.

There are also additional method biases that could explain the differences in inputs between our study and these chamber-based studies. For example, we excluded the organic layer in our estimates of soil C fluxes, but Tang et al. (2005) included it. Wang et al. (2000) also excluded the organic layer, and this could also explain why their flux estimates were lower than those of Tang et al. (2005). Another caveat for interpreting the data from Wang et al. (2000) is that they calculated heterotrophic respiration with the assumption that the Δ^{14}C signal of CO_2 measured from flux chambers during the non-growing season would exclude the contribution from root respiration. While the root contribution is certain to be lower during the non-growing season, it is not likely to be zero, which would contribute to higher flux estimates relative to our findings. Finally, both Wang et al. (2000) and Tang et al. (2005) calculated CO_2 fluxes for the entire soil profile, while we only considered the top 0.3 m of the mineral soil. The contribution to the total heterotrophic CO_2 flux from soil layers below 0.3 m is likely to be relatively small, but this bias in our data would also make our estimates smaller than those from flux chamber measurements.

4.5.5 Model selection and data limitations

The choice of model structure is important for determining soil C persistence as models with different structures can yield divergent results in terms of mean and median ages and transit times (Sierra et al., 2018). However, the 2pp and 2ps model structures assessed in our study performed

equally well with regards to model fit (RMSE, AIC_c). These two model structures also yielded similar results for ages and transit times, indicating that the time series of bulk soil and heterotrophically respired CO_2 was agnostic to the assumptions inherent in model choice. This outcome points to a central challenge of modeling studies: that of model equifinality.

The MCMC approach taken in this study is one solution for dealing with the issue of model equifinality. Using this approach, we were able to quantify the uncertainty associated with the parameter optimization, as well as the correlation between parameters. We emphasized the output from the 2pp model due to the similarity of the output of the two different model structures and the moderately higher confidence in the estimated soil C inputs from the 2pp model. However, we stress that this does not imply overall poorer performance of the 2ps models. Rather, the equivalency of these models indicates that we cannot distinguish the internal dynamics of multiple pool models at these sites with the available data.

The most divergent property between the 2pp and 2ps model structures were the pool turnover rates. While the models performed similarly under the steady-state assumption, violations of that assumption due to changes in inputs or mineral assemblages in response to changing temperature, moisture, or vegetation regimes in the future could lead to divergent estimates for potential soil C gains or losses. In particular, recent work assessing the effect of changes to the size and turnover rate of the fast pool underscore the importance of understanding the internal dynamics of the model pools for accurately predicting future soil C stock changes. The findings of this study indicate that further constraints on pool sizes and turnover rates are needed to assess the response of these systems under a non-steady state assumption. I will return to this point in Ch. 5.

4.6.   Conclusion

The results of this study demonstrate the high value of measuring radiocarbon of both bulk soil and heterotrophically respired CO_2 over time for constraining soil C models. Furthermore, we also make clear the additional power gained from developing models, rather than simply using raw $\Delta^{14}C$ data. The trends in the $\Delta^{14}C_{bulk}$ data align with the mean C ages calculated with the models, while the trends in $\Delta^{14}C_{respired}$ data are closer to what is observed in the mean transit time data. A recommendation from the results of this chapter is that $\Delta^{14}C_{bulk}$ and $\Delta^{14}C_{respired}$ should be applied in tandem as model constraints as they capture different system dynamics. However, while mean C age and mean transit time are important for understanding certain aspects of soil C persistence mechanisms, they are

inadequate for understanding how much C is stored in soils and for how long. The distributions of soil C ages and transit times are essential for answering such questions as how much of the soil C inputs in a given year will remain in the soil over a particular time horizon (Crow and Sierra, 2022). These distributions also reveal biases in the means due to the leveraging effect of small pools of strongly Δ^{14}C-depleted C, which could lead to underestimates of the rate at which C cycles through soils when using Δ^{14}C data without model-based interpretation.

Pre-aging of soil C inputs and a lack of knowledge regarding the size and turnover rate of distinct soil C pools complicates interpretation of Δ^{14}C in soils (Baisden et al., 2013). This study demonstrates that combining $\Delta^{14}C_{bulk}$ and $\Delta^{14}C_{respired}$ time series can provide enough information to estimate pre-aging of inputs as a system parameter. This enables separating the pre-aging component of soil C persistence mechanisms, which in the case of this study adds support to recent findings that the old ^{14}C ages of C in deeper soil layers are due to pre-aging as well as limitations on decomposition. The similarity in system age, transit time, and input estimates from the 2pp and 2ps models indicates that the combination of $\Delta^{14}C_{bulk}$ and $\Delta^{14}C_{respired}$ time series serve as robust constraints for the system absent information about internal pool dynamics. This is an advantage for modeling system C dynamics, as it lessens the importance of selecting the correct model structure and obviates the need for quantifying soil pool sizes or turnover rates empirically, which remains a challenge.

4.7. Supplemental Information

4.7.1 Comparison of 2pp and 2ps models

System ages and transit times of soil C did not vary substantially between the 2pp and 2ps model structures (**Supplemental Figure 4-1**). Mean C ages tend to be older in the 2pp models than in the 2ps models, but the opposite is true for median C ages, which tend to be older in the 2ps models. The age distributions for both model structures have long right tails, making the mean C ages substantially older than the median ages for both model structures.

Inputs and pool sizes calculated for the 2pp and 2ps models were also similar (**Supplemental Table 4-1**). However, inputs for the 2ps models had higher uncertainty. Additionally, the estimated inputs for the 2ps models at a few sites were both substantially higher compared to the inputs estimated for the 2pp models and compared to the inputs estimated for the other sites at the same depth.

Pool turnover times did vary substantially between the 2pp and 2ps models at some sites, leading to greater differences in pool ages between the two model structures than observed for system ages or transit times. Mean ages of the fast pool in the 2ps models tended to be younger than in the 2pp model, particularly for the andesitic soils (**Supplemental Figure 4-3**). Mean ages of the slow pool were more similar between the two model structures, and when different they did not show consistent trends across sites (**Supplemental Figure 4-4**).

These differences in pool turnover did not lead to substantial differences in ages and transit times (**Supplemental Figure 4-1**). However, these differences are relevant in the context of potential changes to turn over rates. Small changes in the decomposition rates of the fast pool, for example, can have substantial impact on the amount of C sequestered in the soil over the next several decades (cf. Crow and Sierra, 2022). In general, the inability to reliably distinguish between the goodness of fit of the 2pp and 2ps models indicates the need for additional constraints on the internal pool dynamics in order to determine how future changes to pool turnover rates may affect future SOC stock changes.

Supplemental Figure 4-6 provides an example of a site for which ages and transit times diverged substantially between the 2pp and 2ps model structures (cool climate andesitic, 0-0.1 m). For panels a) and b): numbers in parentheses give inputs and organic C stocks estimated for each model fit, italicized numbers give transfer rates as a percentage of system inputs, and colored numbers give pool fluxes; units are gC m^{-2}. For panel c): lines show fits using the mean parameter values returned

from the MCMC optimization, ribbons show the estimated 95% confidence interval for the data-constrained pools (bulk soil C, respired CO_2). Note that $\Delta^{14}C$ of respired CO_2 overlaps $\Delta^{14}C$ of the fast pool for the 2-pool parallel model.

4.7.2 Seasonal soil moisture effects on modeled lag times

We assessed the effect of soil moisture on lag times for the sites on the granitic transect (the only sites where these soil moisture data were available). We observed strong seasonal differences in soil moisture between the 0-0.1 m and 0.2-0.3 m depths at the SOAP site (equivalent to the warm climate site from this study), but not at the TEAK site (intermediate in elevation between the cool and cold climate sites) (**Supplemental Figure 4-5**). Soil moisture at the warm climate site analog diverged between 0 and 0.3 m over the course of the year, with similar soil moisture at all depths in winter, diverging in the spring as the surface soil begins to dry out substantially more than the deeper soil layers, and reaching the maximum difference at the end of summer. In contrast, while we observed overall soil moisture fluctuations throughout the year at the cool/cold analog site, these fluctuations were similar at all depths (**Supplemental Figure 4-5**).

4.7.3 Decomposition of covariance model

The decomposition of covariance model is a hypothesis about the relationship among the coefficients in a hierarchical model. The decomposition of covariance model is defined by three hyperparameters, η, δ, and τ each of which defines a separate prior probability distribution (Eq. 4-18). The regularization hyperparameter (η) specifies the correlation between the slope and intercept terms (R), the concentration hyperparameter (δ) gives the proportional contribution to total variance from slope versus intercept terms by group (ζ), while τ describes relative contribution of the slope or intercept terms to the variability between groups (Johnson et al., 2022).

$$\Sigma \sim diag\,(\omega)\,R\,diag\,(\omega) \qquad\qquad (4\text{-}18)$$

$$\omega = \zeta\,\sqrt{\tau}$$

$$R \sim LKJ\,(\eta)$$

$$\zeta \sim Dirichlet\,(2,\delta)$$

$$\tau \sim Gamma\,(s,r)$$

where ω is the vector of standard deviations, R is the correlation matrix for the model covariates described by the Lewandowski-Kurowicka-Joe (LKJ) distributed parameter η, ζ is the simplex vector for the allocation of variance among slope and intercept terms, which is described by a joint symmetric Dirichlet distribution with concentration parameter δ, and τ is the gamma-distributed total variance in intercepts and slopes with scale (s) and shape (r) parameters (Goodrich et al., 2023).

We fit the hyperparameters of the decomposition of covariance models for the response of mean and median ages and transit times to MAST using information from the radiocarbon time series of bulk soil and respired CO_2 at our study sites, as well as an exploratory analysis of variance with the posterior distributions of ages and transit times from the MCMC parameter optimization. We used these data to determine appropriate values for the hyperparameters η and δ separately for each model. However, as we did not have adequate information about the combined variability in slope and intercept terms within each parent material, we used the default value for τ (Goodrich et al., 2023).

Starting with the regularization parameter, we assumed that the parent material specific expected value for mean or median age or transit time in a soil is likely to be correlated with the change in median age in response to temperature for that parent material. This relationship can be modeled with a value of 0.5 for η. We compared the variance among parent materials to the variance among climate zones (warm, cool, cold) as a tool to assess the relative contribution of the intercept and slope terms, respectively, to expected variance in the global response of different parent materials to MAST. Mean and median ages varied more among parent materials than climate zones, but the opposite was true for mean and median transit times. In either case, this relationship can be captured by setting the concentration hyperparameter δ to a value of 0.5.

4.8.   Tables

Table 4-1. Fitting statistics and observed error for 1p, 2pp, 2ps models[1]

| Depth (m) | Climate | Parent material | Data | | Model | | | | | |
| | | | Obs. Err. | n | AIC | | | RMSE | | |
					1*p*	2*pp*	2*ps*	1*p*	2*pp*	2*ps*
0-0.1	warm	andesite	10.6	11	93.7	72.6	73.4	62.4	20.1	23.3
		basalt	7.9	11	71.5	67.8	67.8	22.6	15.5	15.8
		granite	10.1	11	80.6	74.6	74.6	35.0	21.9	23.4
	cool	andesite	12.9	11	95.1	74.8	74.2	63.2	22.2	22.4
		basalt	7.3	11	83.6	77.5	76.8	37.6	23.8	26.1
		granite	6.9	11	80.6	78.6	80.4	32.5	28.6	30.0
	cold	andesite	4.6	10	72.3	64.4	66.9	32.2	17.4	19.5
		basalt	7.3	11	84.5	69.5	69.3	39.4	16.7	17.0
		granite	17.5	11	69.6	73.5	73.2	19.7	21.5	20.3
0.1-0.2	warm	andesite	15.1	11	89.1	80.7	81.0	51.5	28.4	28.8
		basalt	5.3	11	69.0	63.9	63.8	20.1	13.1	13.5
		granite	15.3	11	75.6	79.7	79.6	26.0	27.0	27.1
	cool	andesite	4.3	11	99.2	58.6	57.6	83.3	10.7	10.3
		basalt	10.0	10	95.3	70.1	70.1	64.2	20.3	19.8
		granite	15.7	11	85.0	85.8	82.1	41.1	36.3	35.3
	cold	andesite	7.0	10	80.4	58.5	58.4	35.3	13.2	13.6
		basalt	13.3	11	86.7	76.6	76.3	44.6	23.5	23.5
		granite	5.9	8	62.0	66.0	65.0	18.1	19.8	18.8
0.2-0.3	warm	andesite	20.0	11	81.8	81.7	81.7	52.5	33.6	31.0
		basalt	14.5	11	76.1	77.7	77.9	27.8	26.3	28.4
		granite	8.4	10	77.6	80.0	70.1	28.6	30.2	22.3
	cool	andesite	4.5	11	102.3	56.4	53.7	89.5	9.7	9.1
		basalt	11.0	10	113.2	81.8	81.8	143.9	32.7	33.7
		granite	11.3	11	81.8	83.5	83.5	36.3	33.3	35.8
	cold	andesite	7.2	10	75.1	55.2	55.2	37.4	11.6	11.6
		basalt	9.1	10	90.6	73.9	75.5	77.2	32.0	29.3
		granite	11.2	9	59.8	63.3	62.4	16.2	15.8	16.1

[1] Observed error (Obs. err.) is the overall mean of the standard error calculated for $\Delta^{14}C$ (‰) of observed bulk soil and respired CO_2 across all time points; RMSE units are also $\Delta^{14}C$ (‰)

Table 4-2. Optimized parameters (2pp model)[1]

Depth (m)	Climate	Parent material	τ_{fast} mean	(quartiles)	τ_{slow} mean	(quartiles)	γ_{fast} mean	(quartiles)	Lag mean	(quartiles)
0-0.1	warm	andesite	9	(9, 9, 9)	2697	(1914, 2668, 3884)	1	(1, 1, 1)	0	(0, 0, 0)
		basalt	19	(19, 19, 19)	110	(107, 110, 114)	0.38	(0.39, 0.39, 0.38)	1	(1, 1, 1)
		granite	14	(14, 14, 14)	86	(77, 90, 100)	0.83	(0.87, 0.84, 0.79)	1	(2, 1, 1)
	cool	andesite	90	(86, 90, 94)	3714	(3009, 3713, 4901)	0.99	(0.99, 0.99, 0.99)	1	(1, 1, 1)
		basalt	9	(9, 9, 9)	197	(190, 196, 204)	0.64	(0.65, 0.64, 0.64)	0	(0, 0, 0)
		granite	18	(18, 18, 18)	150	(144, 150, 157)	0.55	(0.6, 0.55, 0.5)	4	(6, 4, 2)
	cold	andesite	17	(16, 17, 17)	161	(155, 161, 167)	0.48	(0.49, 0.48, 0.46)	1	(1, 1, 1)
		basalt	1	(1, 1, 1)	188	(182, 188, 195)	0.66	(0.67, 0.66, 0.64)	11	(11, 11, 10)
		granite	59	(42, 52, 128)	165	(163, 166, 169)	0.09	(0.14, 0.07, 0.03)	11	(17, 10, 4)
0.1-0.2	warm	andesite	14	(12, 14, 17)	347	(332, 348, 365)	0.48	(0.5, 0.49, 0.47)	2	(3, 2, 1)
		basalt	26	(26, 26, 27)	173	(166, 174, 182)	0.25	(0.27, 0.25, 0.23)	1	(1, 1, 1)
		granite	97	(87, 97, 112)	76	(62, 77, 101)	0.72	(0.88, 0.73, 0.57)	27	(27, 27, 27)
	cool	andesite	64	(64, 64, 65)	1002	(976, 1007, 1031)	0.83	(0.83, 0.83, 0.83)	1	(1, 1, 1)
		basalt	-	-	-	-	-	-	-	-
		granite	1	(1, 1, 1)	266	(243, 267, 295)	0.61	(0.68, 0.6, 0.54)	2	(3, 1, 1)
	cold	andesite	38	(37, 38, 39)	393	(378, 393, 411)	0.42	(0.42, 0.42, 0.42)	1	(1, 1, 1)
		basalt	1	(1, 1, 1)	210	(194, 208, 228)	0.61	(0.61, 0.61, 0.61)	14	(14, 14, 14)
		granite	36	(36, 36, 37)	349	(324, 356, 381)	0.05	(0.08, 0.04, 0.02)	13	(20, 12, 6)
0.2-0.3	warm	andesite	58	(49, 55, 67)	307	(238, 310, 424)	0.47	(0.63, 0.47, 0.3)	50	(54, 52, 48)
		basalt	119	(94, 118, 165)	529	(415, 489, 812)	0.6	(0.88, 0.54, 0.37)	22	(26, 23, 18)
		granite	38	(29, 54, 103)	154	(154, 154, 154)	0.21	(0.27, 0.16, 0.09)	36	(37, 36, 36)
	cool	andesite	48	(47, 48, 49)	1043	(1016, 1045, 1073)	0.73	(0.74, 0.73, 0.72)	0	(0, 0, 0)
		basalt	-	-	-	-	-	-	-	-
		granite	102	(74, 104, 187)	278	(251, 306, 364)	0.34	(0.46, 0.29, 0.19)	1	(1, 1, 0)
	cold	andesite	96	(84, 98, 114)	672	(594, 670, 761)	0.64	(0.73, 0.64, 0.56)	26	(28, 27, 25)
		basalt	1	(1, 1, 1)	244	(224, 249, 267)	0.37	(0.49, 0.36, 0.23)	23	(29, 21, 16)
		granite	-	-	-	-	-	-	-	-

[1] Parameter units are: y for τ_{fast}, τ_{slow}, and lag; γ_{fast} is a ratio.

Table 4-3. Summary of ages and transit times (2pp model)[1]

Depth (m)	Climate	Parent material	System age			Transit time			Lag
			mean (sd)	quartiles	median:mean (sd)	mean (sd)	quartiles	median:mean (sd)	mean
0-0.1	warm	andesite	257 (217)	1, 7, 712	0.03 (0.01)	10 (0)	0, 6, 28	0.45 (0.01)	0 (0)
		basalt	102 (5)	4, 66, 320	0.45 (0)	75 (3)	2, 36, 278	0.33 (0.01)	1 (0)
		granite	54 (10)	1, 23, 206	0.31 (0.03)	26 (3)	1, 12, 99	0.33 (0.02)	1 (1)
	cool	andesite	1049 (284)	6, 96, 5970	0.07 (0.02)	118 (7)	5, 63, 284	0.37 (0.02)	1 (0)
		basalt	183 (10)	4, 120, 569	0.46 (0)	76 (3)	1, 12, 383	0.11 (0)	0 (0)
		granite	134 (10)	4, 84, 430	0.43 (0.02)	79 (11)	2, 28, 332	0.25 (0.02)	5 (3)
	cold	andesite	149 (9)	5, 96, 464	0.45 (0)	92 (3)	2, 31, 374	0.24 (0.01)	1 (0)
		basalt	187 (9)	8, 129, 562	0.48 (0)	65 (3)	0, 1, 360	0.02 (0)	11 (0)
		granite	163 (8)	8, 112, 492	0.48 (0.01)	159 (9)	8, 108, 485	0.47 (0.01)	11 (8)
0.1-0.2	warm	andesite	337 (25)	11, 228, 1033	0.47 (0)	189 (16)	1, 38, 816	0.14 (0.04)	2 (2)
		basalt	166 (10)	7, 111, 510	0.47 (0)	137 (5)	4, 76, 467	0.38 (0.02)	1 (0)
		granite	96 (9)	5, 65, 288	0.47 (0.01)	92 (7)	5, 62, 281	0.47 (0.01)	27 (0)
	cool	andesite	786 (37)	12, 432, 2763	0.38 (0.01)	226 (6)	4, 57, 1247	0.18 (0.01)	1 (0)
		basalt	-	-	-	-	-	-	-
		granite	269 (33)	12, 184, 799	0.48 (0)	104 (15)	0, 2, 551	0.02 (0.03)	2 (2)
	cold	andesite	373 (24)	13, 246, 1151	0.46 (0)	247 (14)	4, 91, 965	0.26 (0.01)	1 (0)
		basalt	210 (25)	9, 143, 622	0.48 (0)	83 (10)	0, 2, 428	0.02 (0)	14 (0)
		granite	354 (41)	18, 245, 1066	0.48 (0)	339 (40)	14, 224, 1045	0.46 (0.02)	13 (9)
0.2-0.3	warm	andesite	308 (100)	10, 175, 929	0.41 (0.07)	191 (15)	6, 90, 734	0.33 (0.06)	49 (8)
		basalt	395 (68)	14, 214, 1301	0.39 (0.07)	271 (35)	10, 149, 937	0.38 (0.04)	22 (5)
		granite	149 (7)	7, 102, 453	0.47 (0.01)	141 (12)	7, 95, 441	0.46 (0.03)	36 (1)
	cool	andesite	938 (33)	18, 605, 3015	0.45 (0)	318 (11)	3, 52, 1768	0.11 (0)	0 (0)
		basalt	-	-	-	-	-	-	-
		granite	310 (67)	13, 194, 916	0.46 (0.03)	264 (29)	10, 160, 851	0.42 (0.05)	1 (1)
	cold	andesite	546 (48)	16, 312, 1812	0.4 (0.05)	302 (21)	7, 117, 1290	0.27 (0.02)	26 (2)
		basalt	247 (27)	12, 175, 757	0.48 (0)	161 (42)	0, 64, 664	0.23 (0.16)	23 (8)
		granite	-	-	-	-	-	-	-

[1] Summary statistics calculated from MCMC runs. Quartiles are the median values of a random subsample (n = 200) drawn from the system age distributions returned from each MCMC iteration (n total iterations = 10,000); units are y.

Table 4-4. Mean annual soil temperature (MAST) effect on C ages and transit times (TT)[1]

Depth	Response	Parent material	Estimate	95% CI
0-0.1 m	median age	andesite	-16.8	(-19.6, -15.2)
		basalt	-9.6	(-12.5, -6.8)
		granite	-22.7	(-25.8, -18.7)
	mean TT	andesite	-15.6	(-16.9, -14.6)
		granite	-34.0	(-38.3, -29.3)
	median TT	andesite	-5.0	(-5.5, -4.6)
		basalt	5.1	(4.5, 5.7)
		granite	-24.2	(-28.5, -20.7)
0.1-0.2 m	mean age	granite	-66.2	(-91, -42.7)
	median age	granite	-46.1	(-62.9, -29)
	mean TT	andesite	-10.6	(-18.1, -3.1)
		granite	-62.6	(-83.6, -43.8)
	median TT	andesite	-9.3	(-13.3, -3.1)
		basalt	10.9	(4.4, 15)
		granite	-41.5	(-55.7, -28.1)
0.2-0.3 m	mean age	andesite	-48.8	(-79, -7.6)
		granite	-80.7	(-155.5, -16.3)
	median age	andesite	-28.6	(-42.7, -16)
		granite	-50.5	(-93.8, -14.6)
	mean TT	andesite	-20.9	(-29.9, -11.9)
		granite	-61.6	(-92.6, -30)
	median TT	granite	-32.8	(-48.6, -16.7)

[1] Estimates are the slopes from Figs. 4-8 & 4-9, i.e., change in age or TT per change in °C; 95% CI gives the 2.5th and 97.5th quantiles of the posterior probability distribution of the model coefficients.

Table 4-5. Effect of reactive mineral content (OX) on mean C age[1]

Response	Predictor	Estimate	95%CI
mean age	(Intercept)	66.29	(46.09, 87.25)
	OX	1.06	(1.04, 1.08)
	depth	0.01	(0.01, 0.01)
	OX:depth	0.01	(0.01, 0.01)

[1]Values in the 'estimate' column are the exponentiated coefficients from the model given in Eq. 4-16, therefore the effect of each coefficient is multiplicative; model fits for depth values of 0.1 m, 0.2 m. and 0.3 m are shown in Fig. 4-10. The 95% CI gives the 2.5th and 97.5th quantiles of the posterior probability distribution of the model coefficients.

Supplemental Table 4-1 Comparison of estimated inputs by model structure. Units are g C m^{-2} y^{-1}.

Depth	Climate	Parent Material	2pp model mean	2pp model sd	2ps model mean	2ps model sd
0-0.1	warm	andesite	433	7	3026	431
		basalt	51	2	53	6
		granite	170	17	156	29
	cool	andesite	32	2	16	2
		basalt	48	2	88	76
		granite	39	5	64	30
	cold	andesite	45	2	44	6
		basalt	40	2	41	9
		granite	12	1	15	7
0.1-0.2	warm	andesite	23	2	32	13
		basalt	24	1	26	2
		granite	32	3	32	3
	cool	andesite	17	0	12	1
		basalt	-	-	-	-
		granite	26	4	66	159
	cold	andesite	17	1	17	1
		basalt	11	1	17	16
		granite	6	1	33	18
0.2-0.3	warm	andesite	29	2	244	333
		basalt	9	1	8	1
		granite	14	1	11	2
	cool	andesite	16	1	10	1
		basalt	-	-	-	-
		granite	8	1	8	1
	cold	andesite	15	1	12	1
		basalt	9	3	9	1
		granite	-	-	-	-

4.9. Figures

Figure 4-1. Model schematic (2-pool parallel model). Comparison of parallel and series fits for the cold climate andesite soil (0-0.1 m). For the diagrams in panels a) and b): numbers in parentheses give inputs and organic C stocks estimated for each model fit, italicized numbers give transfer rates as a percentage of system inputs, and colored numbers give pool fluxes; units are g C m^{-2} y^{-1}; values for turnover times (τ), ages, and transit times (TT) are means with medians in parentheses. For panel c): lines show fits using the mean parameter values returned from the MCMC optimization, ribbons show the estimated 95% confidence interval for the data-constrained pools (bulk soil C, respired CO_2).
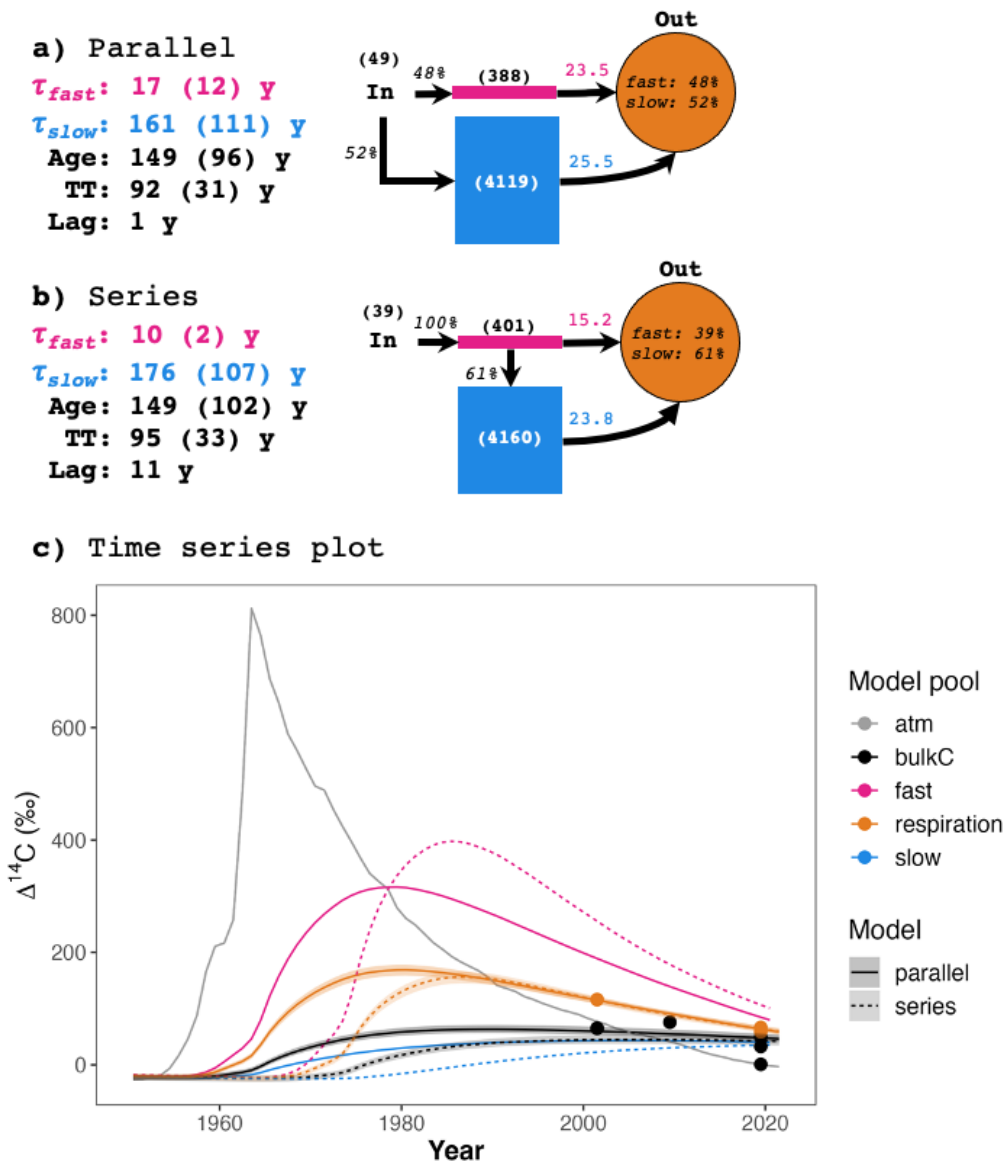
Figure 4-2. Δ^{14}C time series of model fits (2-pool parallel model) and data constraints (0-0.1 m). Note expanded y-axis limits on plots marked with asterisk.
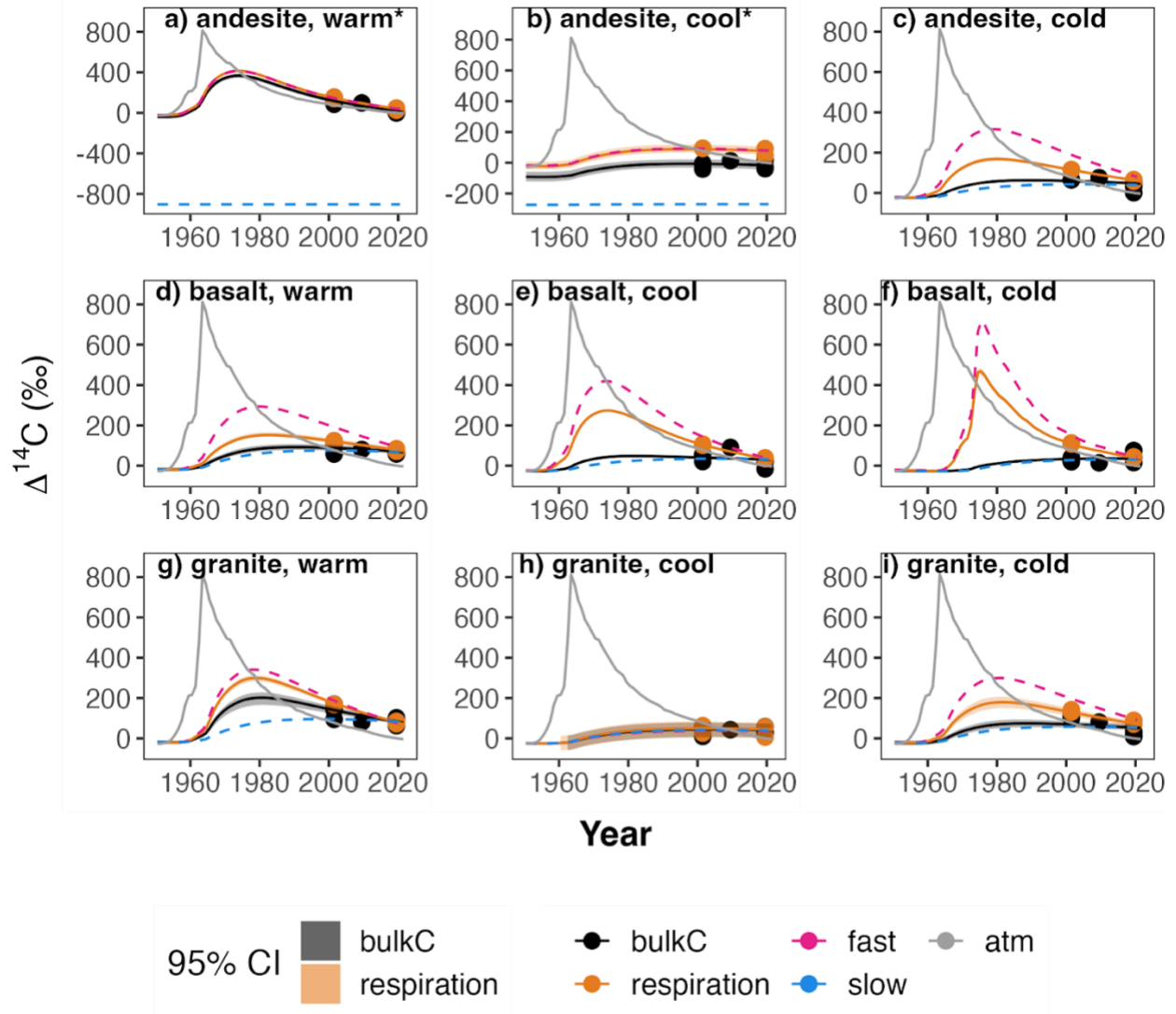
Figure 4-3. Depth and climate effects on modeled lag time. Points show means of 10,000 MCMC runs, error bars show ±SD.
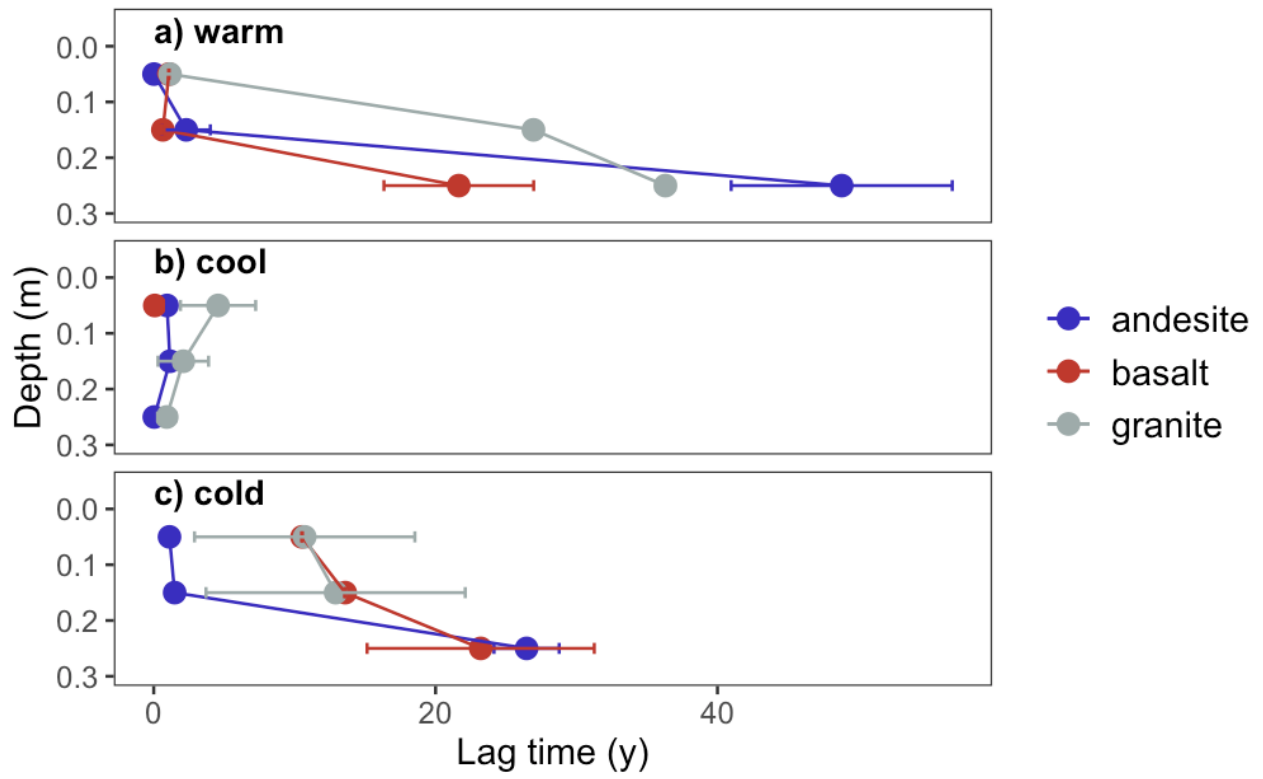
Figure 4-4. System age & transit time distributions, 0-0.1 m
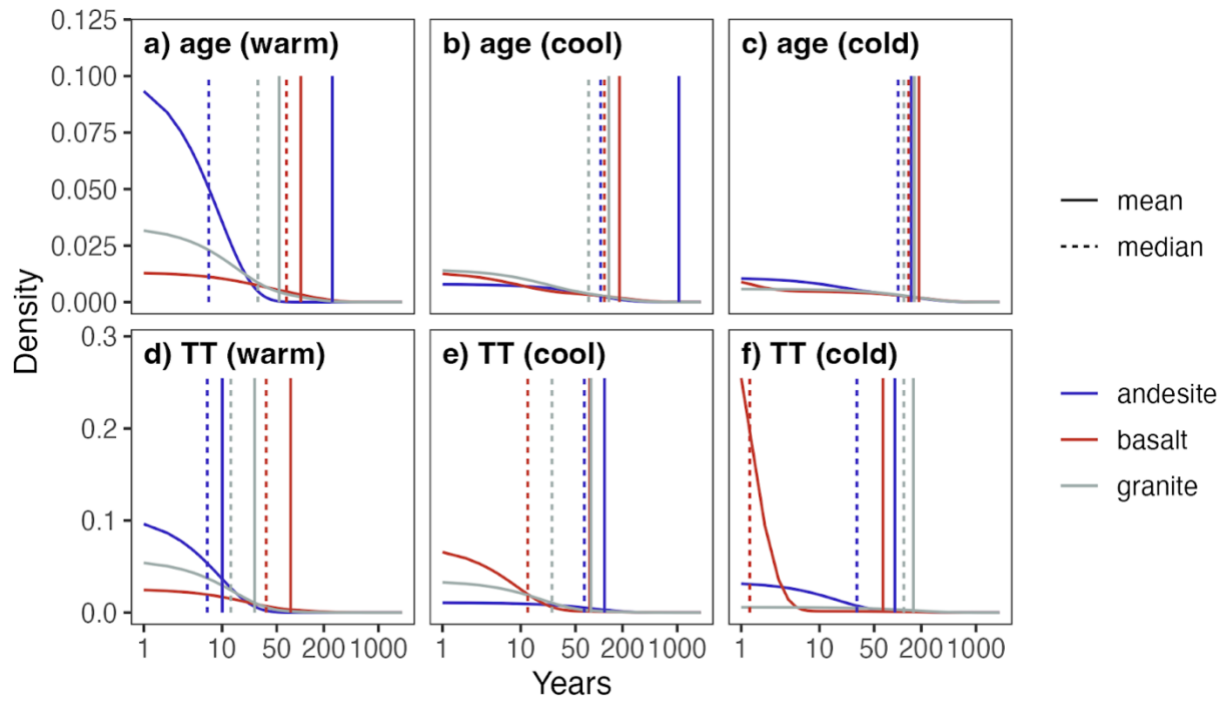
Figure 4-5. System age & transit time distributions, 0.1-0.2 m
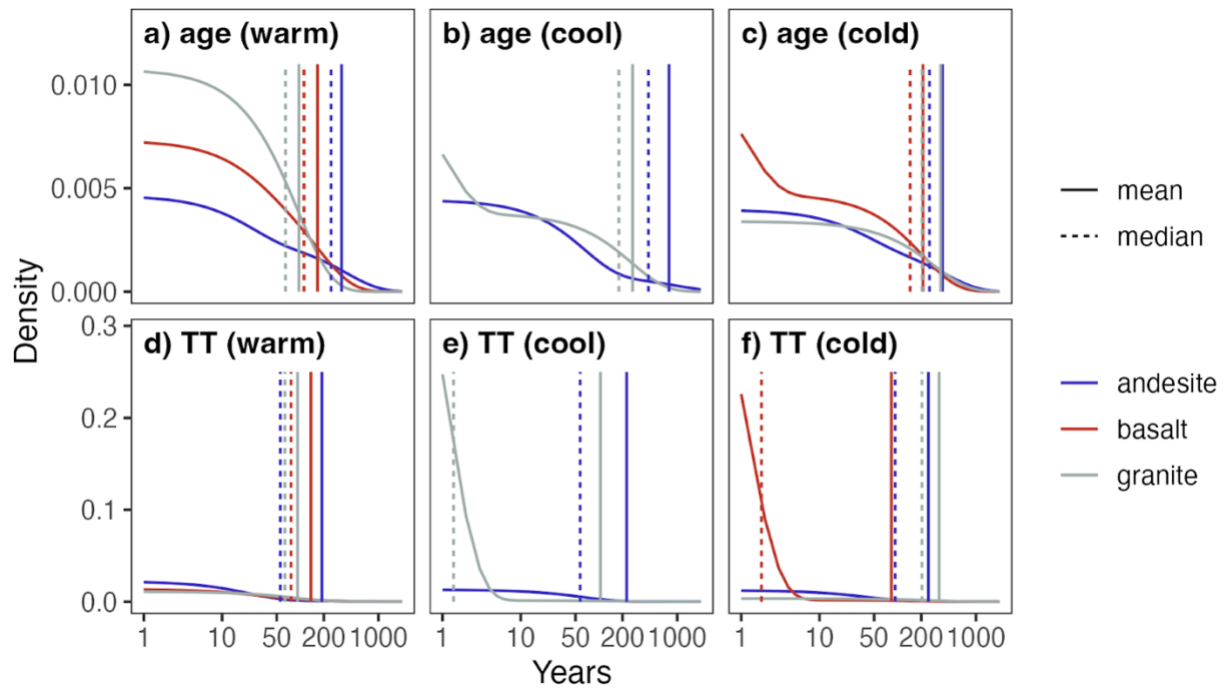
Figure 4-6. System age & transit time distributions, 0.2-0.3 m
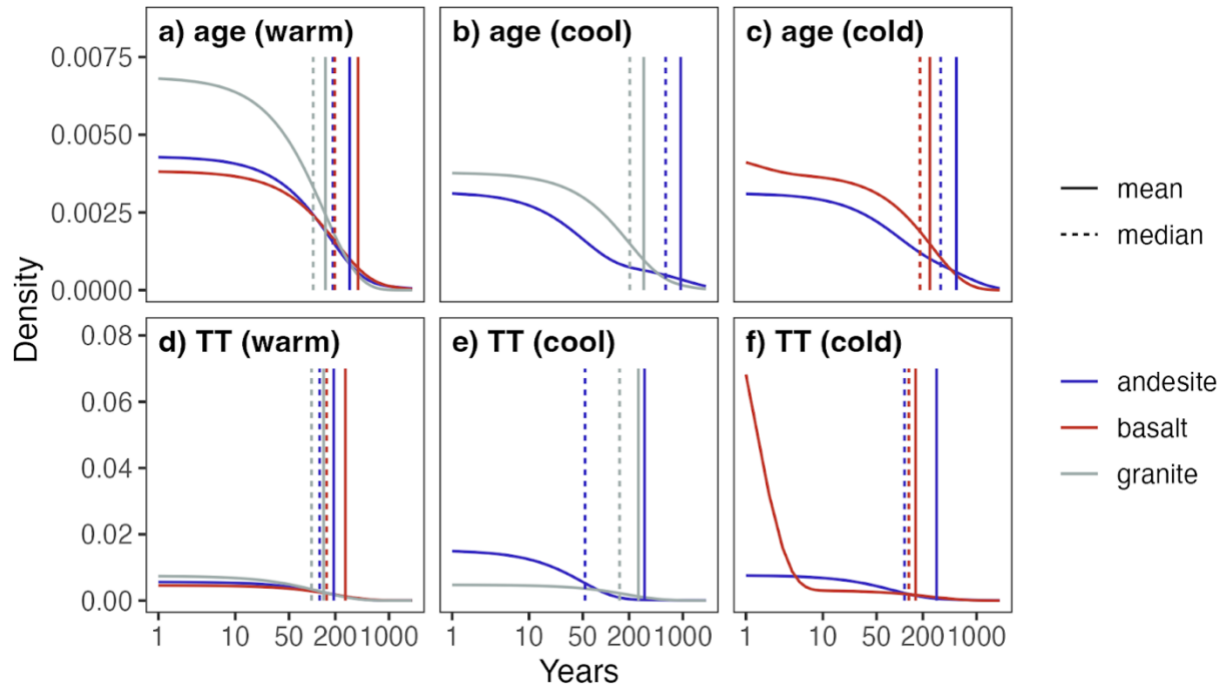
Figure 4-7. Depth dependence of mean and median ages and transit times (TT). Points show means and medians of 10,000 MCMC runs. Error bars for means show ±SD. Error bars for median age and transit time show the median values of the 25th and 75th quartiles of the age and transit time distributions from the total set of MCMC runs. Depth profiles are shown on a log scale to capture the interquartile range of the distribution.
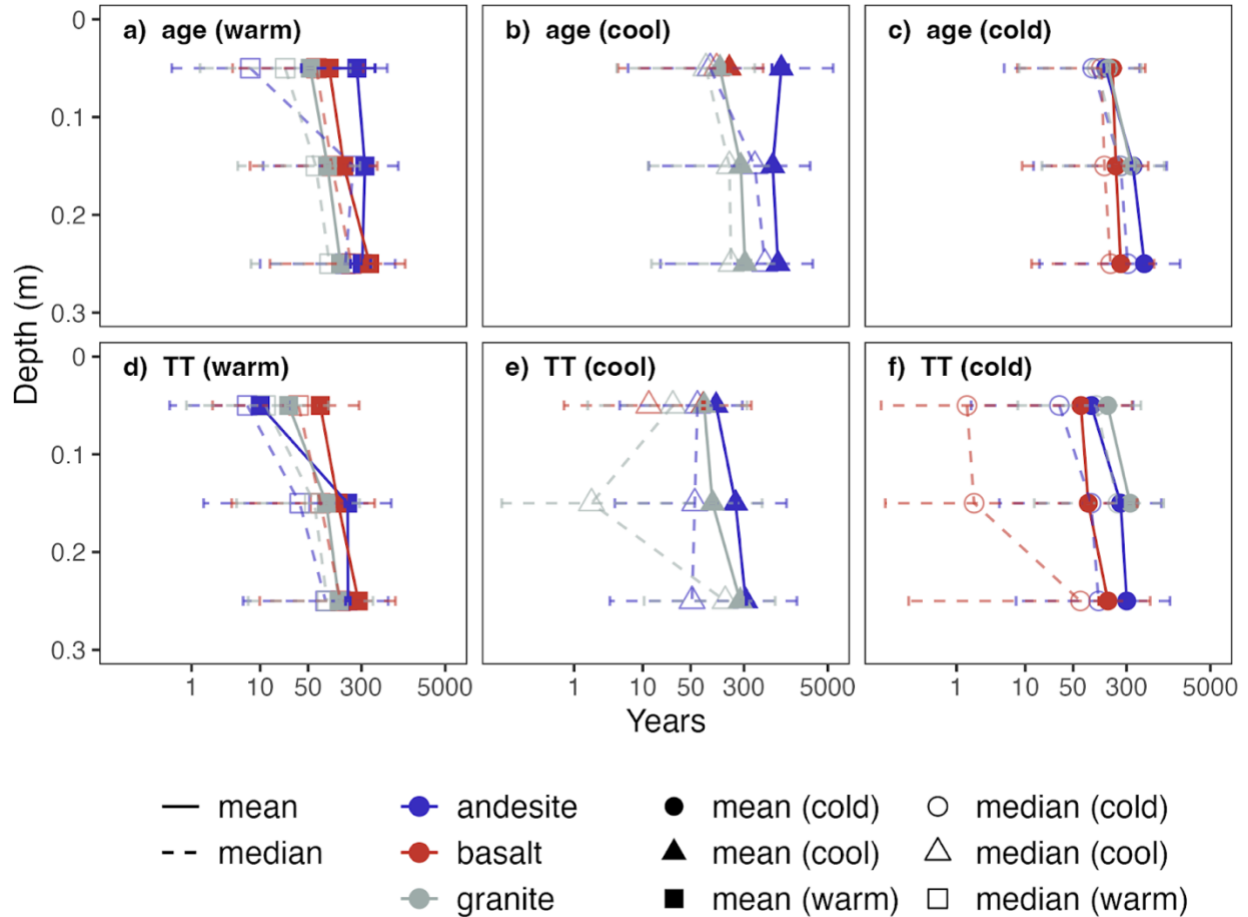
Figure 4-8. Mean annual soil temperature effect on system C ages
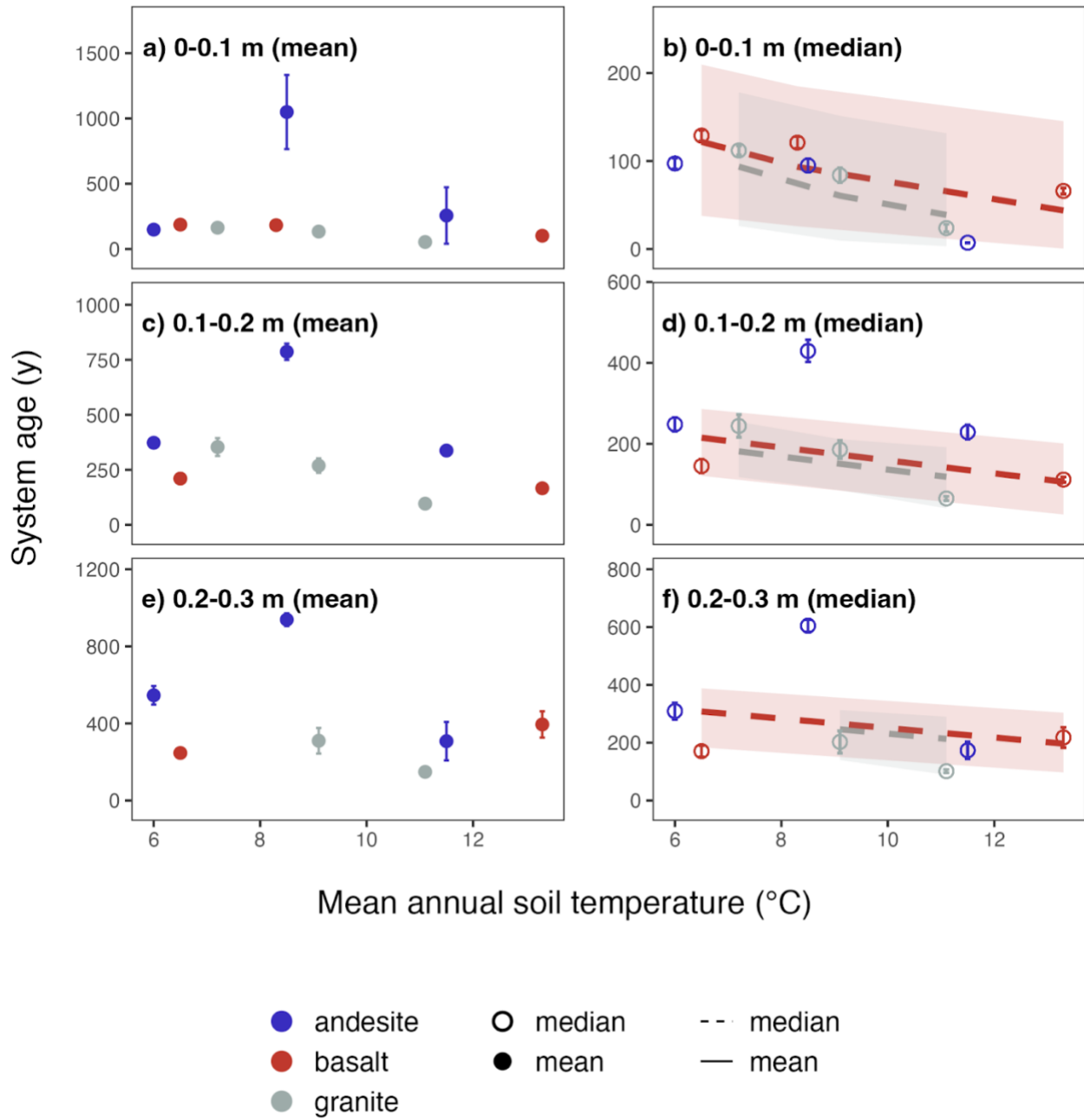
Figure 4-9. Mean annual soil temperature effect on system C transit times
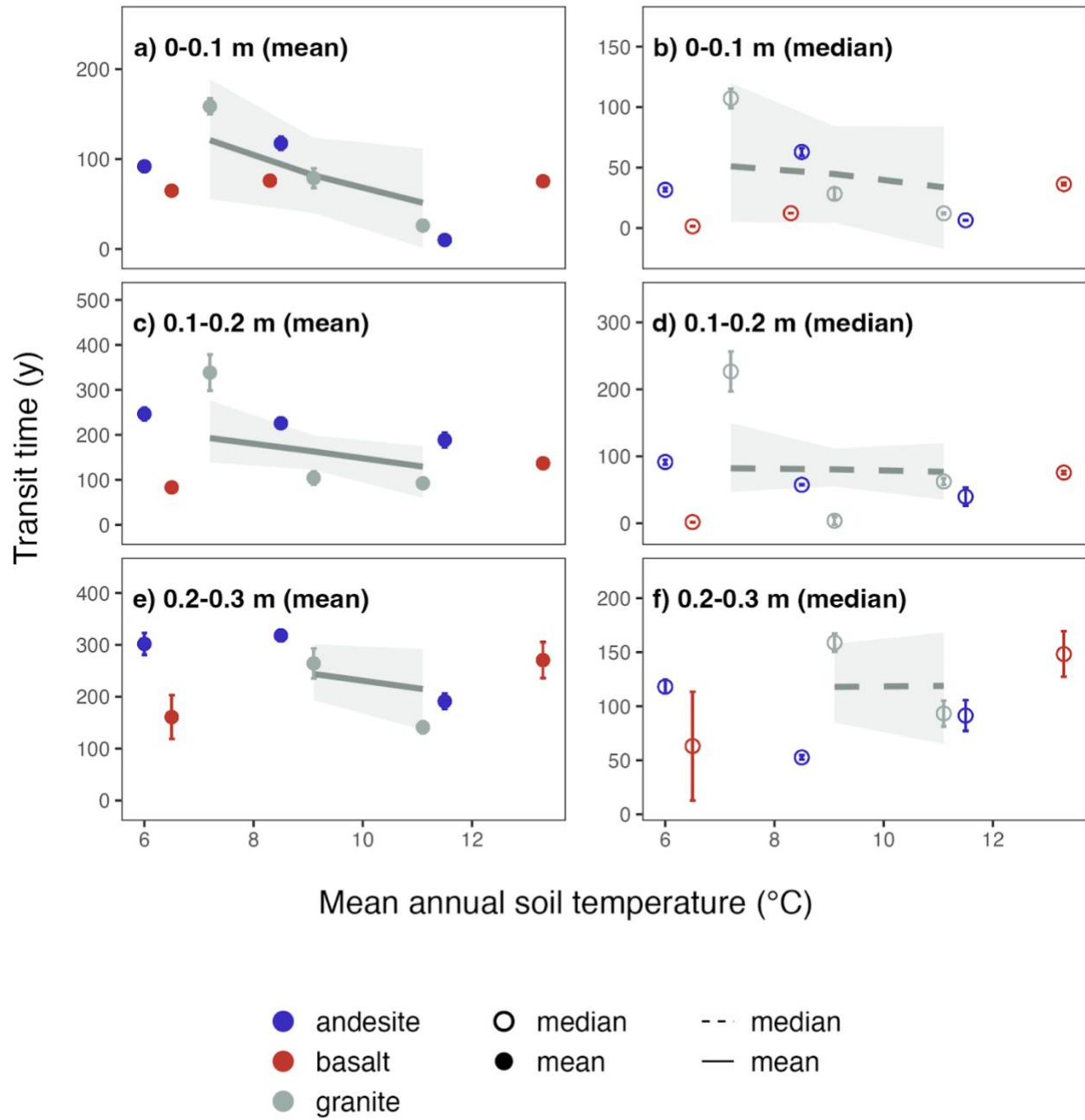
Figure 4-10. Mean C age vs. oxalate extractable Fe and Al abundance. Points show means and error bars standard deviation from MCMC estimates of mean system age, lines and ribbons show Bayesian model fits.
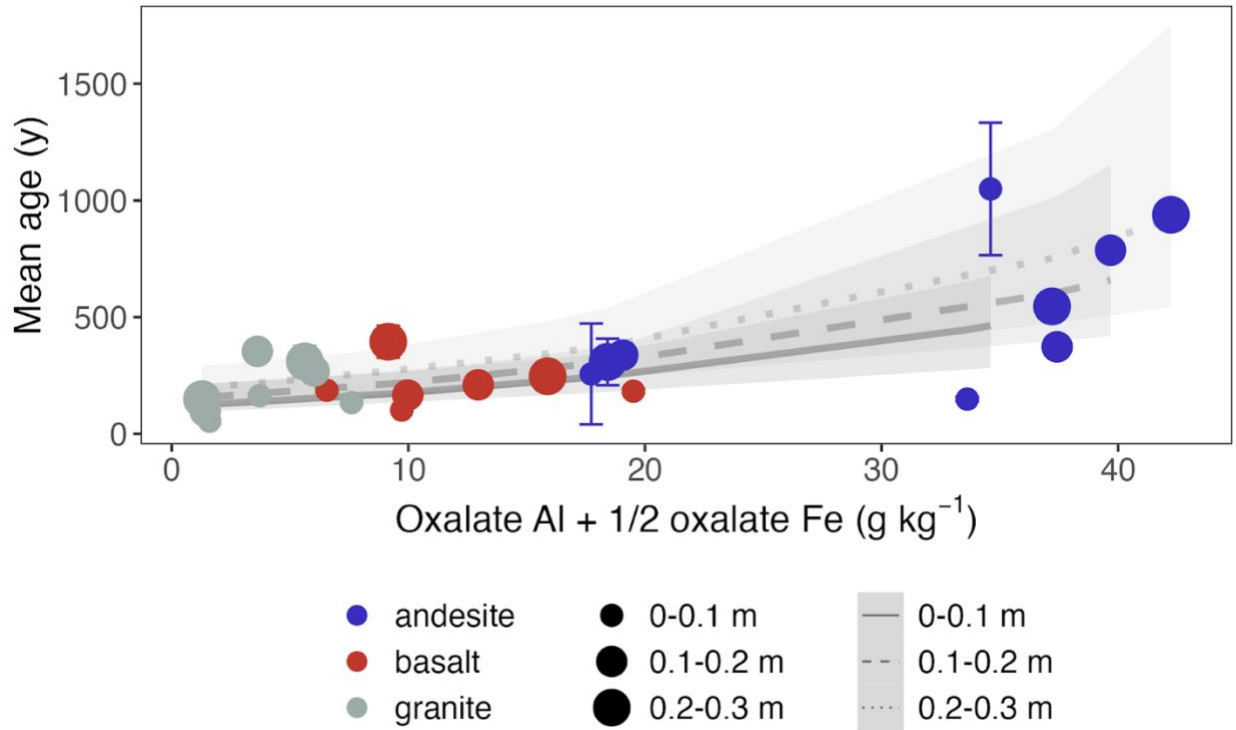
Figure 4-11. Model estimated soil C inputs
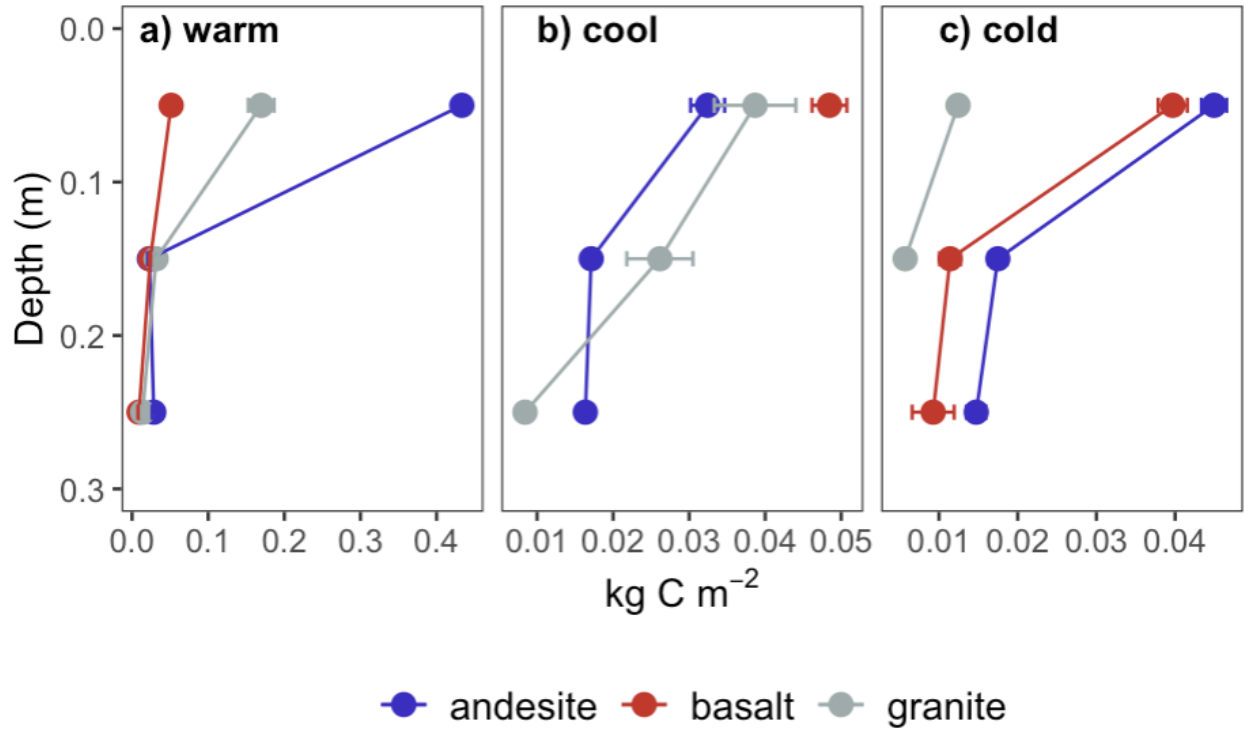
Supplemental Figure 4-1. System ages of 2pp and 2ps models

System ages: 2pp vs. 2ps
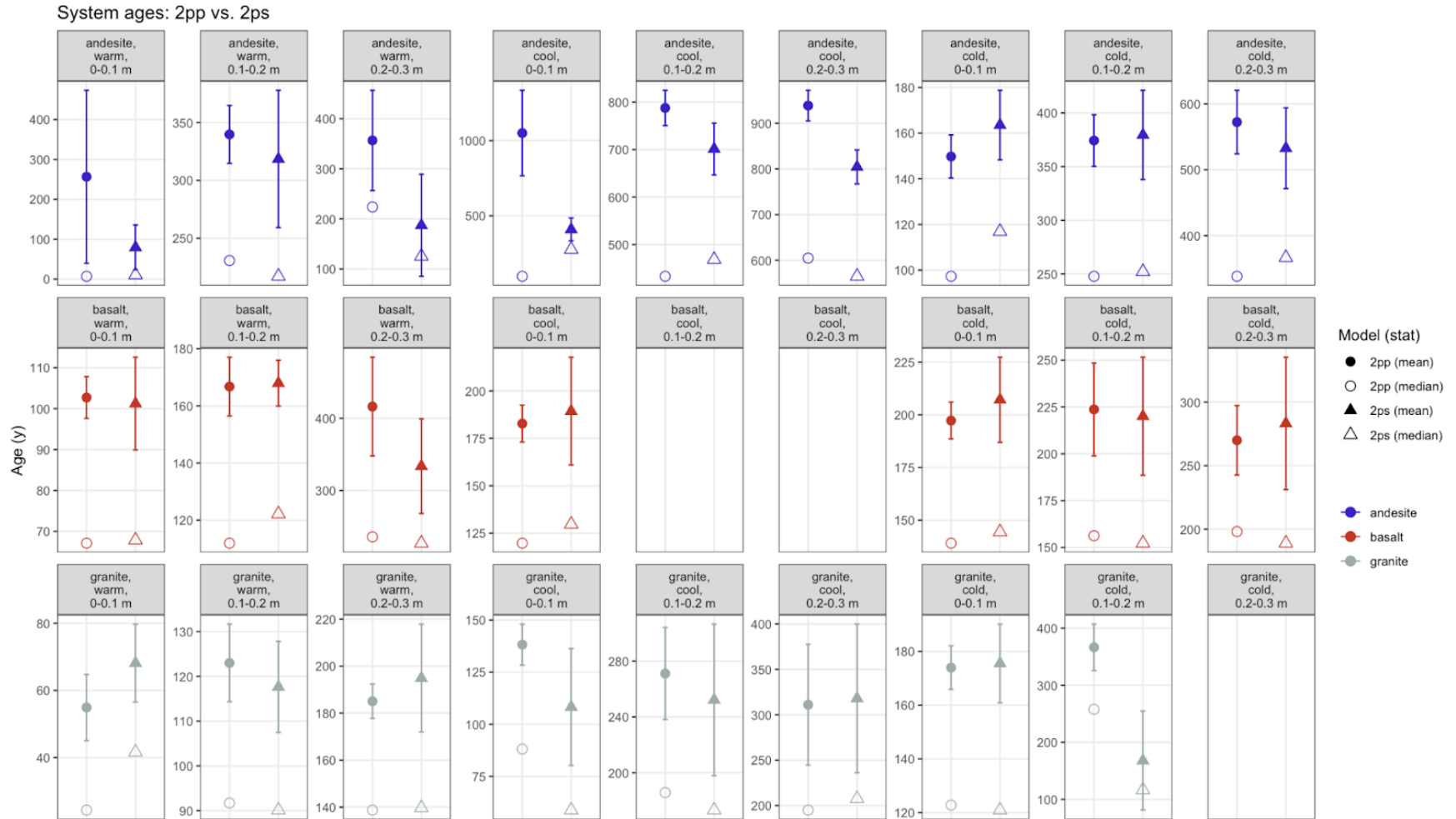
Supplemental Figure 4-2. Transit times of 2pp and 2ps models
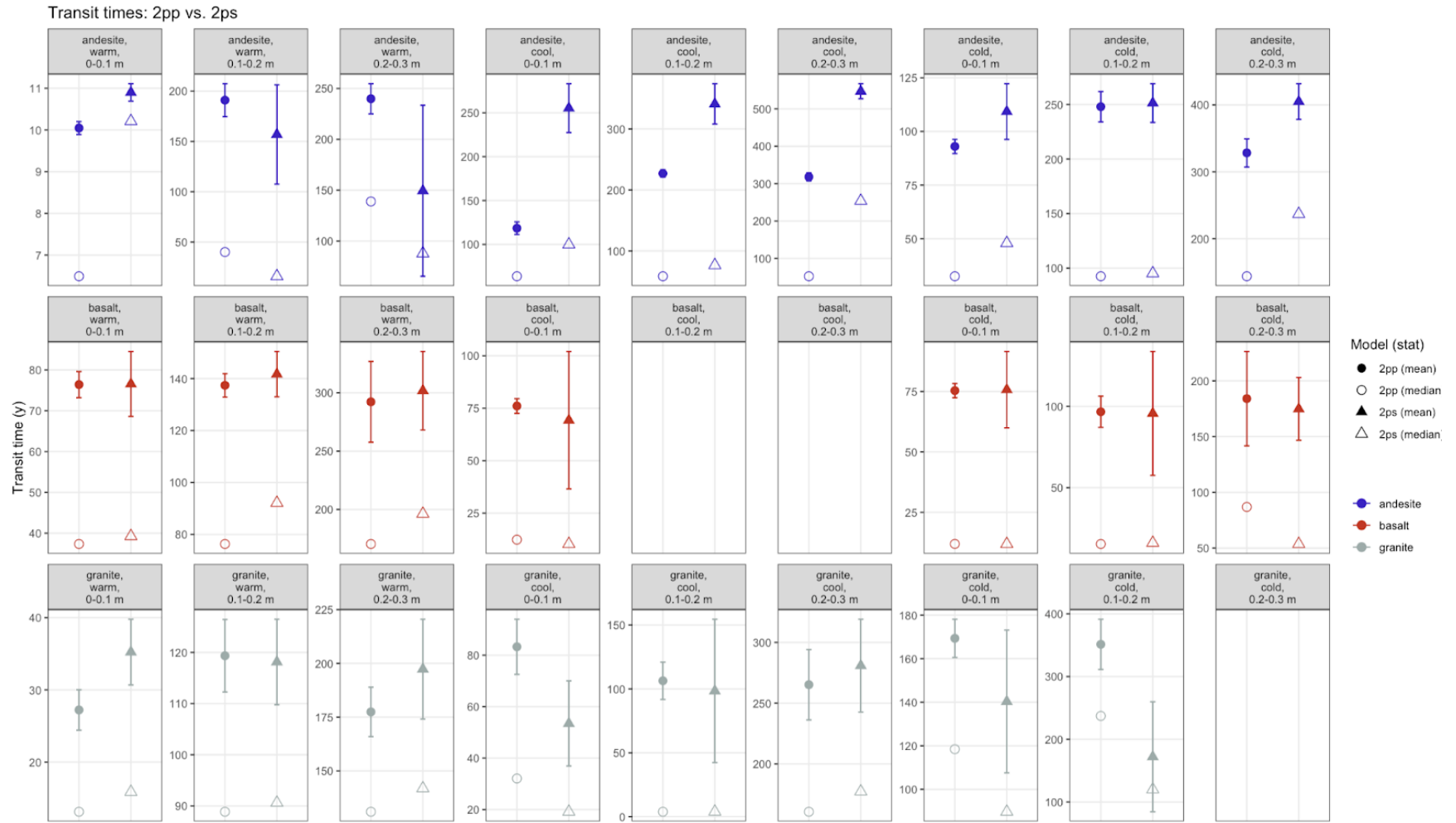
Supplemental Figure 4-3. Fast pool ages for 2pp and 2ps models

Fast pool ages: 2pp vs. 2ps
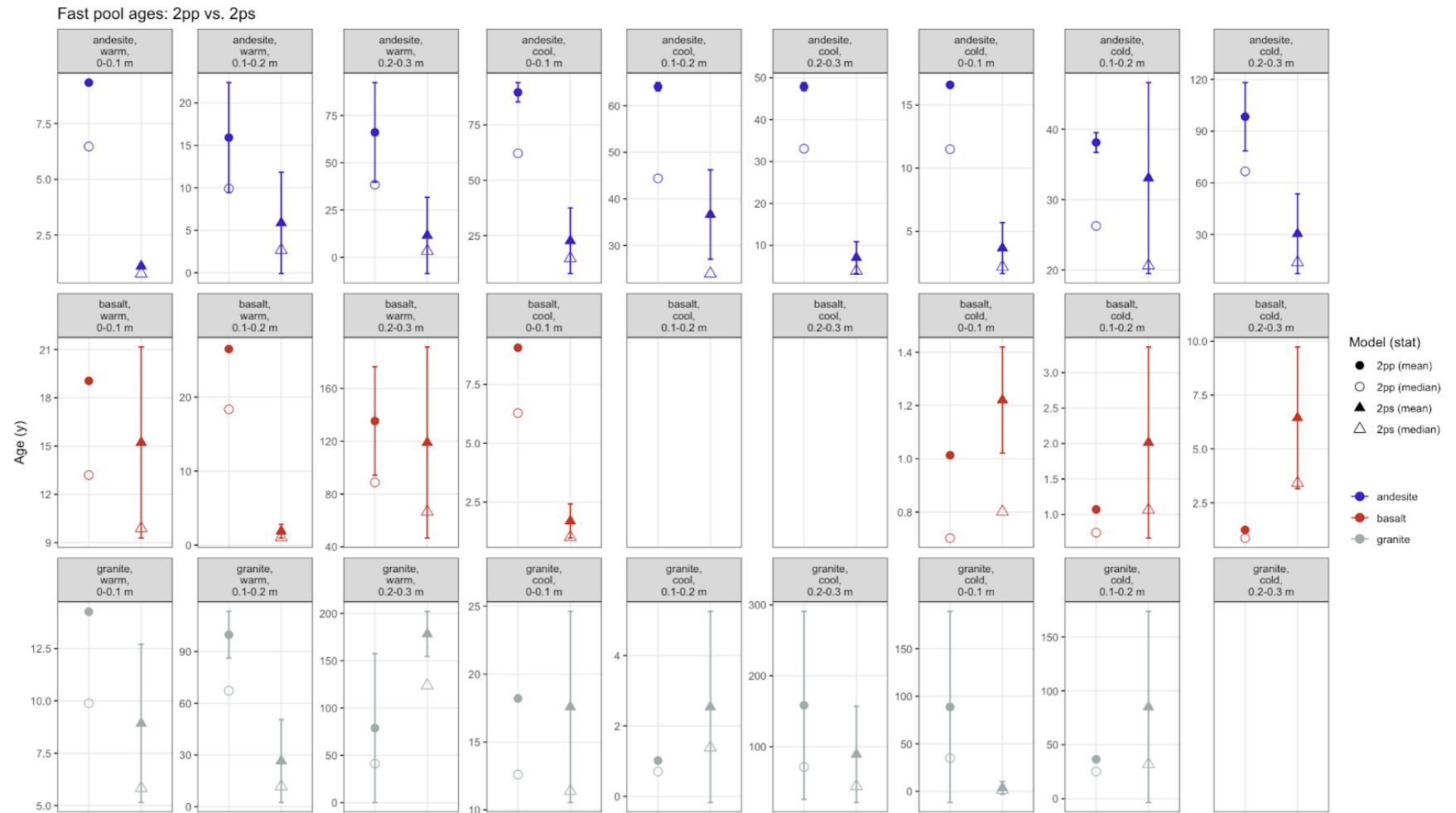
Supplemental Figure 4-4. Slow pool age for 2pp and 2ps models
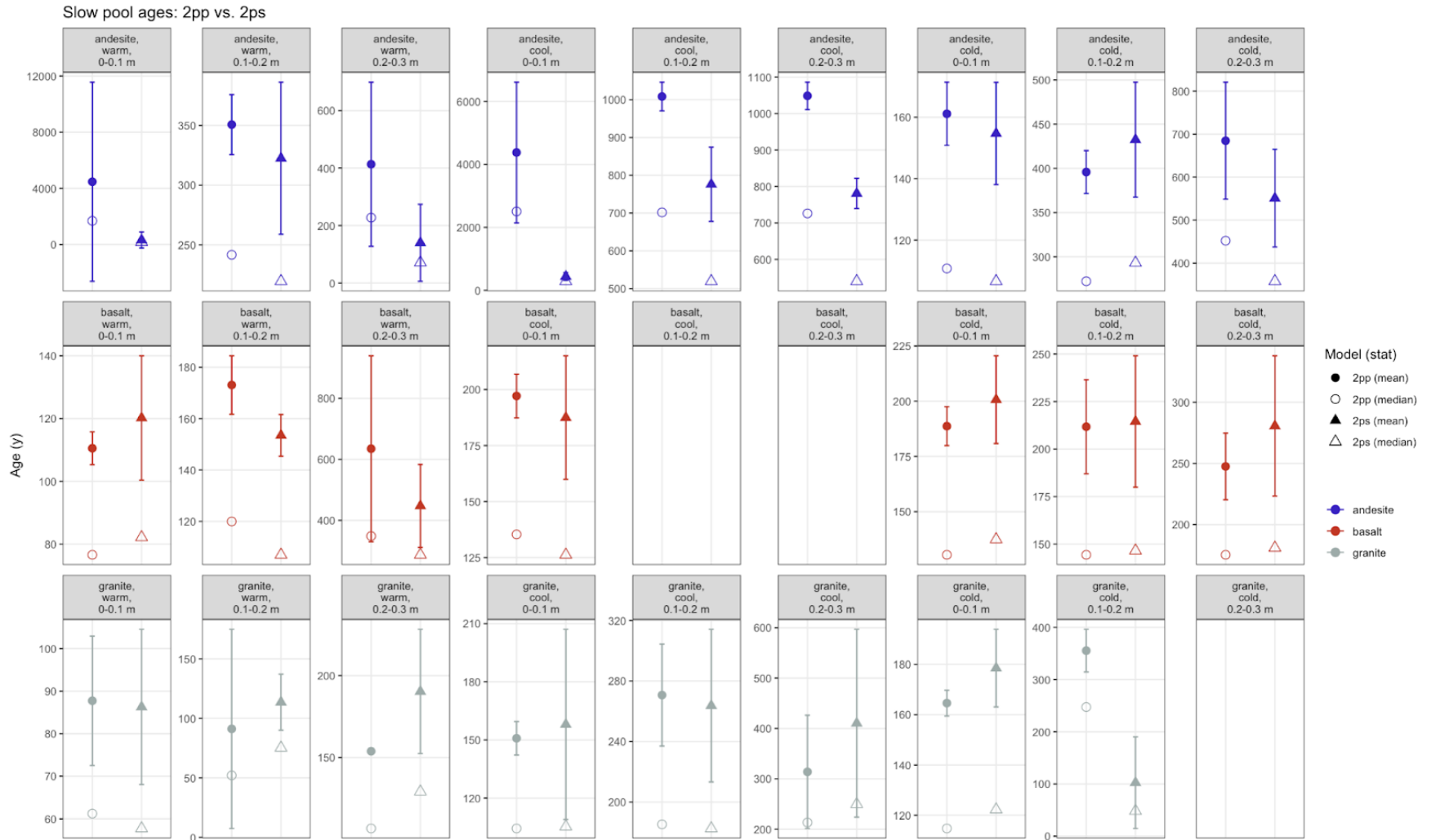
Supplemental Figure 4-5. Seasonal volumetric soil water content along granitic elevation transect
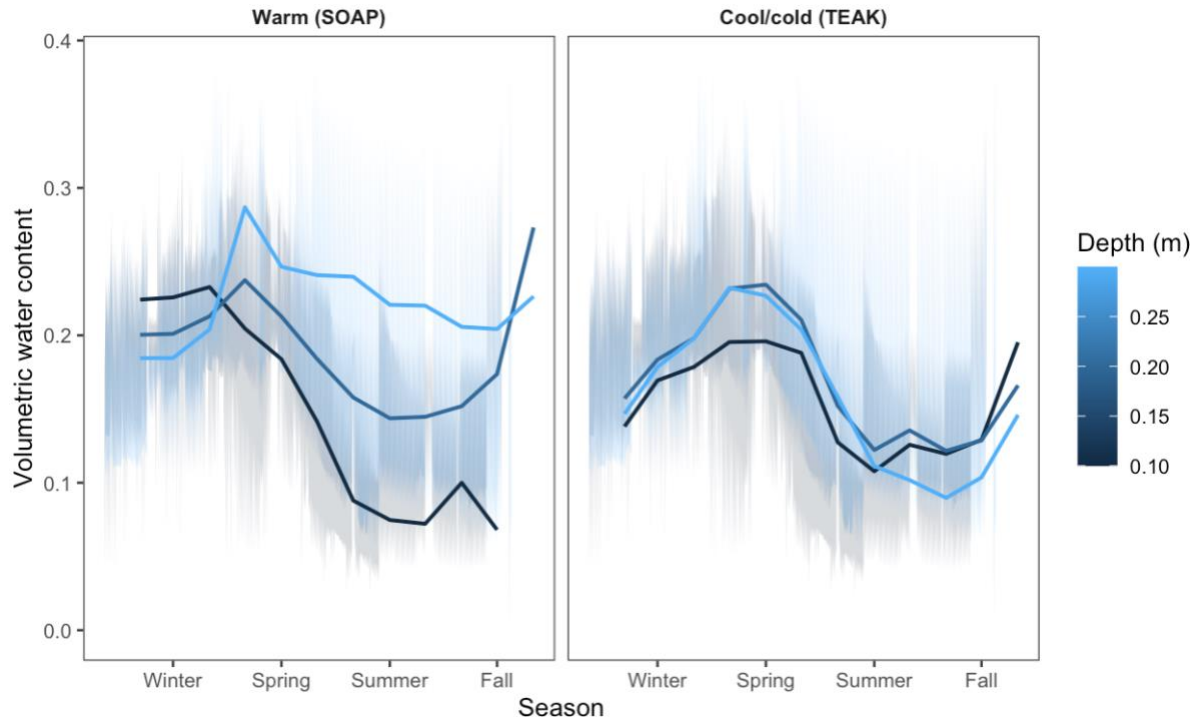
Supplemental Figure 4-6. Model structure comparison for the cool climate andesitic soil (0-0.1 m)
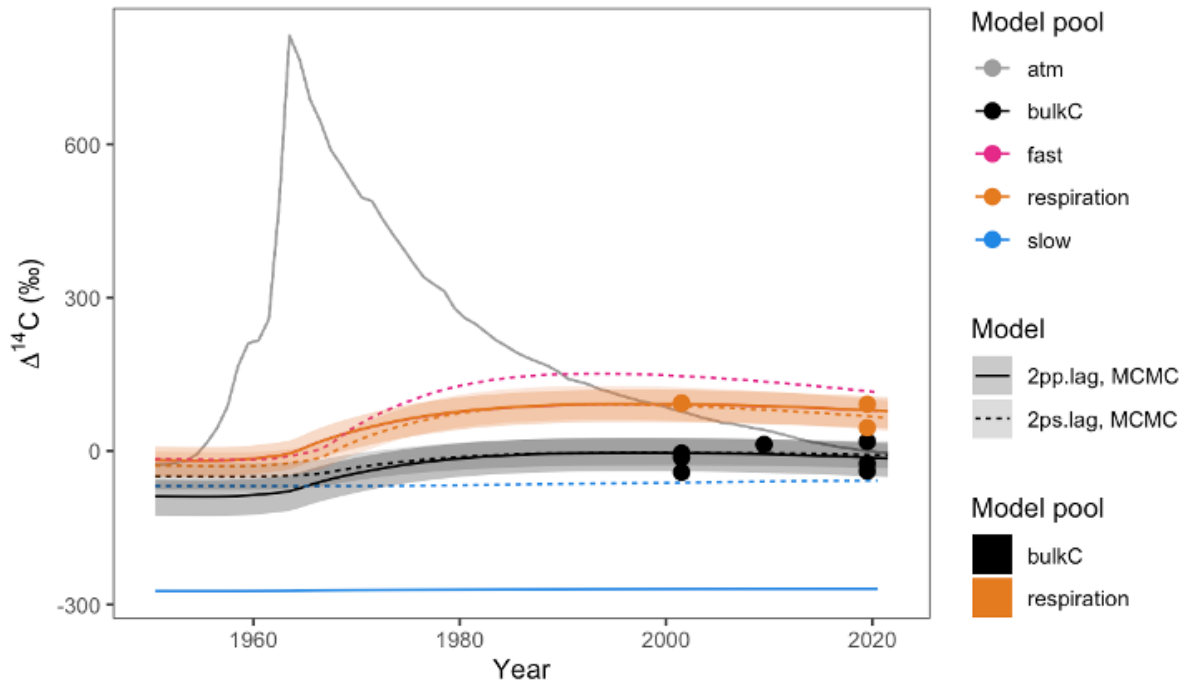
Supplemental Figure 4-7. Time series fits for 0.1-0.2 m and 0.2-0.3 m depths (2-pool parallel models). Note: data not shown for rejected model fits (marked with asterisk).

a) 0.1-0.2 m
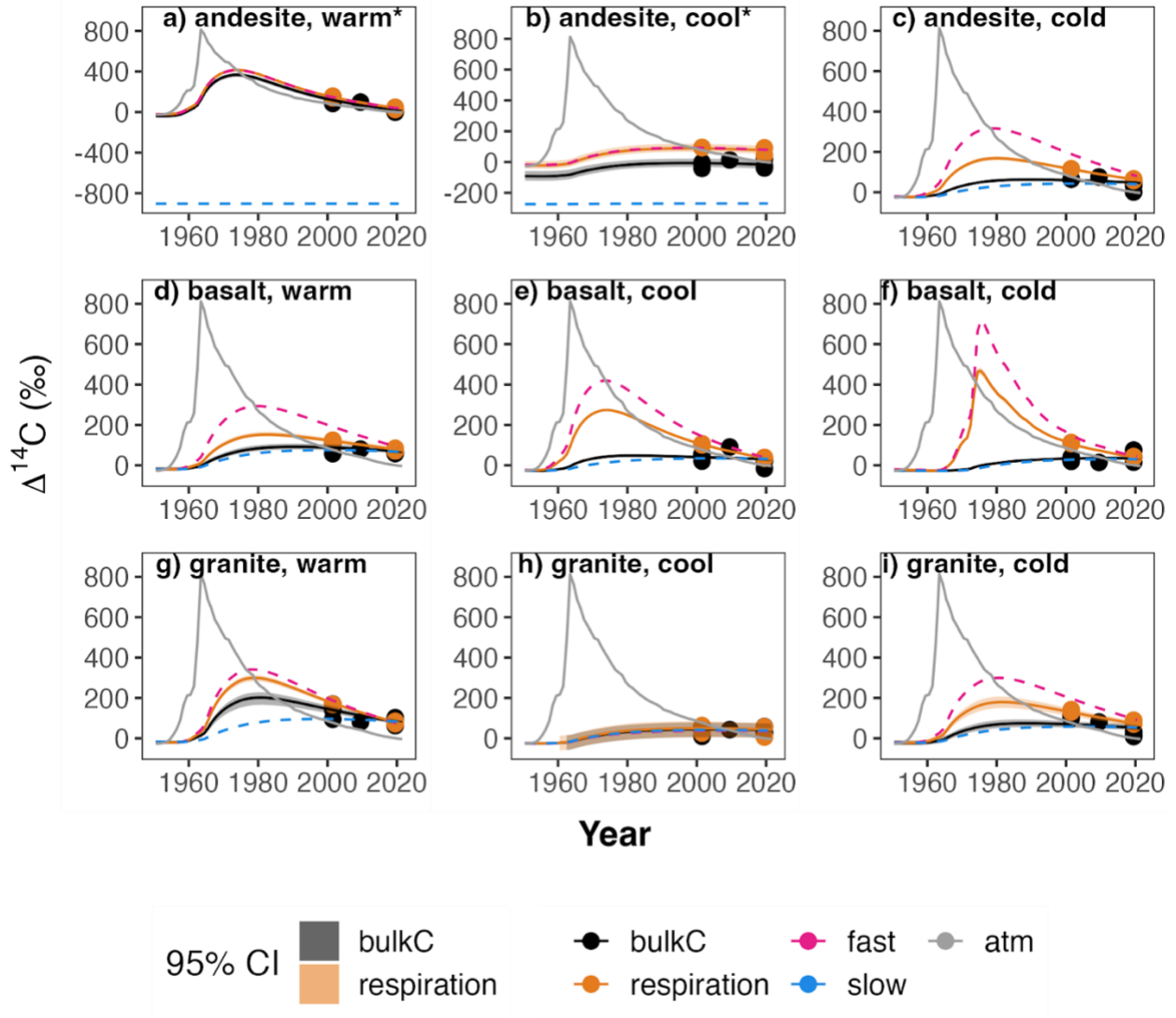
b) 0.2-0.3 m
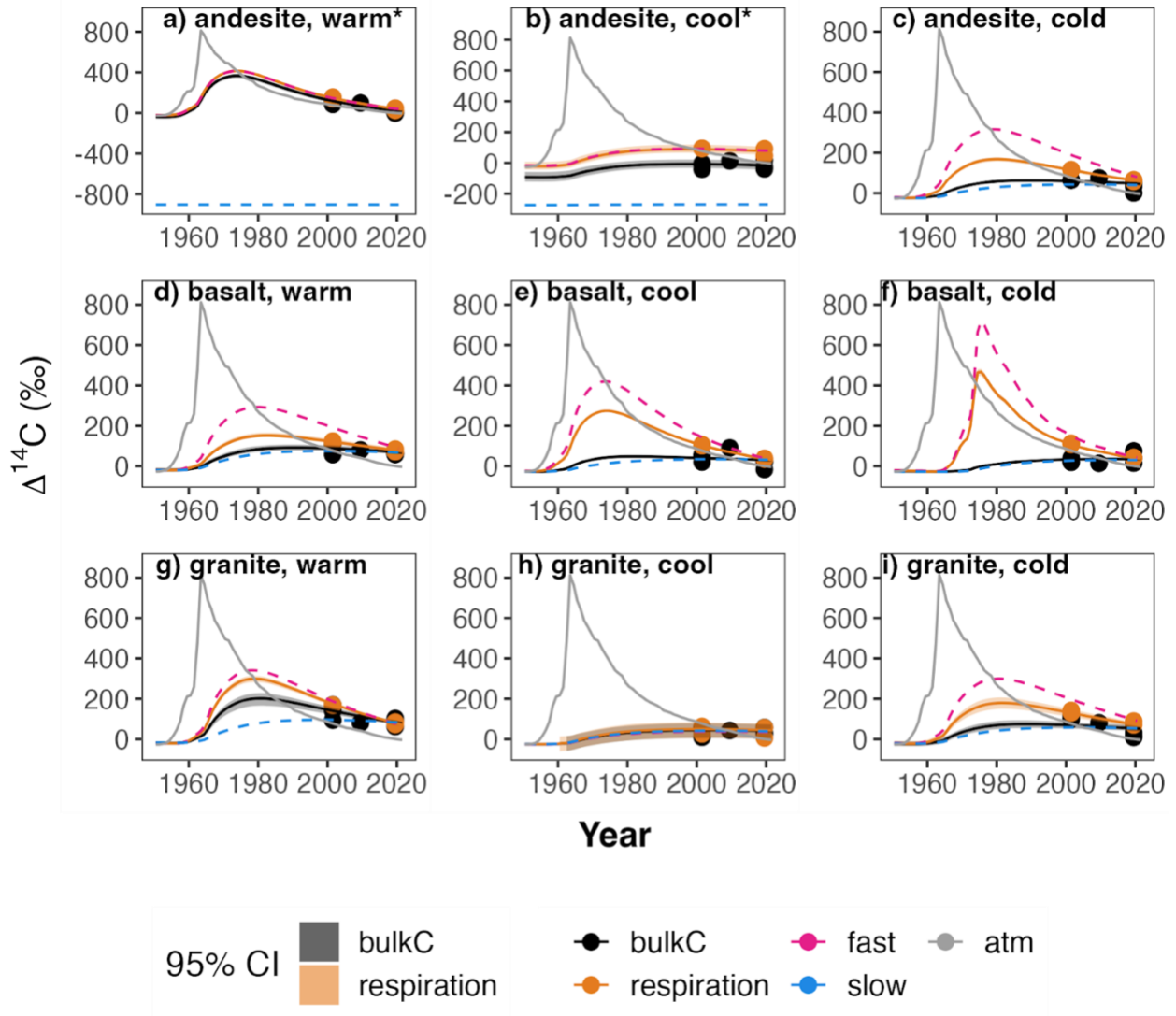
Supplemental Figure 4-8. Partitioning of soil C stocks between fast and slow pools (2-pool parallel models)

4.10. References

Abramoff, R., Xu, X., Hartman, M., O'Brien, S., Feng, W., Davidson, E., Finzi, A., Moorhead, D., Schimel, J., Torn, M., and Mayes, M. A.: The Millennial model: in search of measurable pools and transformations for modeling soil carbon in the new century, Biogeochemistry, 137, 51–71, https://doi.org/10.1007/s10533-017-0409-7, 2018.

Ahrens, B., Guggenberger, G., Rethemeyer, J., John, S., Marschner, B., Heinze, S., Angst, G., Mueller, C. W., Kögel-Knabner, I., Leuschner, C., Hertel, D., Bachmann, J., Reichstein, M., and Schrumpf, M.: Combination of energy limitation and sorption capacity explains 14C depth gradients, Soil Biology and Biochemistry, 148, https://doi.org/10.1016/j.soilbio.2020.107912, 2020.

Baddeley, J. A. and Watson, C. A.: Influences of root diameter, tree age, soil depth and season on fine root survivorship in Prunus avium, Plant and Soil, 276, 15–22, 2005.

Baisden, W. T., Amundson, R., Cook, A. C., and Brenner, D. L.: Turnover and storage of C and N in five density fractions from California annual grassland surface soils, Global Biogeochemical Cycles, 16, 64-1-64–16, https://doi.org/10.1029/2001gb001822, 2002.

Baisden, W. T., Parfitt, R. L., Ross, C., Schipper, L. A., and Canessa, S.: Evaluating 50 years of time-series soil radiocarbon data : towards routine calculation of robust C residence times, Biogeochemistry, 112, 129–137, https://doi.org/10.1007/s10533-011-9675-y, 2013.

Beem-Miller, J., Schrumpf, M., Hoyt, A. M., Guggenberger, G., and Trumbore, S.: Impacts of Drying and Rewetting on the Radiocarbon Signature of Respired CO2 and Implications for Incubating Archived Soils, Journal of Geophysical Research: Biogeosciences, 126, 1–17, https://doi.org/10.1029/2020JG006119, 2021.

Beven, K.: A manifesto for the equifinality dissertation, Journal of hydrology, 320, 18–36, 2006.

Bishop, T. F. a, McBratney, a. B., and Laslett, G. M.: Modeling soil attribute depth functions with equal-area quadratic smoothing splines, Geoderma, 91, 27–45, https://doi.org/10.1016/S0016-7061(99)00003-8, 1999.

Broecker, W. S., Peng, T.-H., and others: Tracers in the sea, Lamont-Doherty Geological Observatory, Columbia University Palisades, New York, 1982.

Burnham, K. P.: Information and likelihood theory: a basis for model selection and inference, Model selection and multimodel inference: a practical information-theoretic approach, 49–97, 2002.

Crow, S. E. and Sierra, C. A.: The climate benefit of sequestration in soils for warming mitigation, Biogeochemistry, https://doi.org/10.1007/s10533-022-00981-1, 2022.

Doetterl, S., Stevens, A., Six, J., Merckx, R., Van Oost, K., Casanova Pinto, M., Casanova-Katny, A., Muñoz, C., Boudin, M., Zagal Venegas, E., and Boeckx, P.: Soil carbon storage controlled by interactions between geochemistry and climate, Nature Geoscience, 2015.

Flint, L. E., Flint, A. L., Thorne, J. H., and Boynton, R.: Fine-scale hydrologic modeling for regional landscape applications: the California Basin Characterization Model development and performance, Ecological Processes, 2, 25, https://doi.org/10.1186/2192-1709-2-25, 2013.

Friedlingstein, P., Meinshausen, M., Arora, V. K., Jones, C. D., Anav, A., Liddicoat, S. K., and Knutti, R.: Uncertainties in CMIP5 climate projections due to carbon cycle feedbacks, Journal of Climate, 27, 511–526, https://doi.org/10.1175/JCLI-D-12-00579.1, 2014.

Gaudinski, J. B., Trumbore, S. E., Davidson, E. A., and Zheng, S.: Soil carbon cycling in a temperate forest: radiocarbon-based estimates of residence times, sequestration rates and partitioning of fluxes, Biogeochemistry, 51, 33–69, https://doi.org/10.1023/A:1006301010014, 2000.

Gelman, A., Carlin, J. B., Stern, H. S., Dunson, D. B., Vehtari, A., and Rubin, D. B.: Bayesian data analysis, CRC press, 2013.

Goodrich, B., Gabry, J., Ali, I., and Brilleman, S.: rstanarm: Bayesian applied regression modeling via Stan., 2023.

Goulden, M. L., Anderson, R. G., Bales, R. C., Kelly, A. E., Meadows, M., and Winston, G. C.: Evapotranspiration along an elevation gradient in California's Sierra Nevada, Journal of Geophysical Research: Biogeosciences, 117, 1–13, https://doi.org/10.1029/2012JG002027, 2012.

Harden, J. W., O'neill, K., Trumbore, S. E., Veldhuis, H., and Stocks, B.: Moss and soil contributions to the annual net carbon flux of a maturing boreal forest, Journal of Geophysical Research: Atmospheres, 102, 28805–28816, 1997.

Heckman, K., Hicks Pries, C. E., Lawrence, C. R., Rasmussen, C., Crow, S. E., Hoyt, A. M., von Fromm, S. F., Shi, Z., Stoner, S., McGrath, C., Beem-Miller, J., Berhe, A. A., Blankinship, J. C., Keiluweit, M., Marín-Spiotta, E., Monroe, J. G., Plante, A. F., Schimel, J., Sierra, C. A., Thompson, A., and Wagai, R.: Beyond bulk: Density fractions explain heterogeneity in global soil carbon abundance and persistence, Global Change Biology, 28, 1178–1196, https://doi.org/10.1111/gcb.16023, 2022.

Hendrick, R. L. and Pregitzer, K. S.: Temporal and depth-related patterns of fine root dynamics in northern hardwood forests, Journal of Ecology, 167–176, 1996.

Hengl, T.: GSIF: Global Soil Information Facilities, 2019.

Herrera-Ramírez, D., Muhr, J., Hartmann, H., Römermann, C., Trumbore, S., and Sierra, C. A.: Probability distributions of nonstructural carbon ages and transit times provide insights into carbon allocation dynamics of mature trees, New Phytologist, 226, 1299–1311, 2020.

Hurvich, C. M. and Tsai, C.-L.: Regression and time series model selection in small samples, Biometrika, 76, 297–307, 1989.

Jenkinson, D. S., Harkness, D. D., Vance, E. D., Adams, D. E., and Harrison, A. F.: Calculating net primary production and annual input of organic matter to soil from the amount and radiocarbon content of soil organic matter, Soil Biology and Biochemistry, 24, 295–308, https://doi.org/10.1016/0038-0717(92)90189-5, 1992.

Johnson, A. A., Ott, M. Q., and Dogucu, M.: Bayes rules!: An introduction to applied Bayesian modeling, CRC Press, 2022.

Joslin, J. D., Gaudinski, J. B., Torn, M. S., Riley, W. J., and Hanson, P. J.: Fine-root turnover patterns and their relationship to root diameter and soil depth in a 14C-labeled hardwood forest, New Phytologist, 172, 523–535, https://doi.org/10.1111/j.1469-8137.2006.01847.x, 2006.

Karhu, K., Fritze, H., Hämäläinen, K., Vanhala, P., Jungner, H., Oinonen, M., Sonninen, E., Tuomi, M., Spetz, P., Kitunen, V., and others: Temperature sensitivity of soil carbon fractions in boreal forest soil, Ecology, 91, 370–376, 2010.

Karhu, K., Hilasvuori, E., Järvenpää, M., Arppe, L., Christensen, B. T., Fritze, H., Kulmala, L., Oinonen, M., Pitkänen, J.-M., Vanhala, P., Heinonsalo, J., and Liski, J.: Similar temperature sensitivity of soil mineral-associated organic carbon regardless of age, Soil Biology and Biochemistry, 136, 107527, https://doi.org/10.1016/j.soilbio.2019.107527, 2019.

Keller, M., Schimel, D. S., Hargrove, W. W., and Hoffman, F. M.: A continental strategy for the national ecological observatory network, The Ecological Society of America: 282-284, 2008.

Kengdo, S. K., Ahrens, B., Tian, Y., Heinzle, J., Wanek, W., Schindlbacher, A., and Borken, W.: Increase in carbon input by enhanced fine root turnover in a long-term warmed forest soil, Science of The Total Environment, 855, 158800, 2023.

Koarashi, J., Hockaday, W. C., Masiello, C. a., and Trumbore, S. E.: Dynamics of decadally cycling carbon in subsurface soils, Journal of Geophysical Research G: Biogeosciences, 117, G03033, https://doi.org/10.1029/2012JG002034, 2012.

Lehmann, J. and Kleber, M.: The contentious nature of soil organic matter, Nature, 528, 60–68, https://doi.org/10.1038/nature16069, 2015.

Leinemann, T., Preusser, S., Mikutta, R., Kalbitz, K., Cerli, C., Höschen, C., Mueller, C. W., Kandeler, E., and Guggenberger, G.: Multiple exchange processes on mineral surfaces control the transport of dissolved organic matter through soil profiles, Soil Biology and Biochemistry, 118, 79–90, https://doi.org/10.1016/j.soilbio.2017.12.006, 2018.

McKinnon, K. I.: Convergence of the Nelder–Mead simplex method to a nonstationary point, SIAM Journal on optimization, 9, 148–158, 1998.

Metzler, H., Müller, M., and Sierra, C. A.: Transit-time and age distributions for nonlinear time-dependent compartmental systems, Proceedings of the National Academy of Sciences, 201705296, https://doi.org/10.1073/pnas.1705296115, 2018.

O'Brien, L.: mpspline2: Mass-preserving spline functions for soil data, 2022.

Peixoto, L., Olesen, J. E., Elsgaard, L., Enggrob, K. L., Banfield, C. C., Dippold, M. A., Nicolaisen, M. H., Bak, F., Zang, H., Dresbøll, D. B., and others: Deep-rooted perennial crops differ in capacity to stabilize C inputs in deep soil layers, Scientific Reports, 12, 5952, 2022.

R Core Team: R: A language and environment for statistical computing, 2020.

Rasmussen, C.: Pedogenesis, Soil Mineralogy, and Soil Carbon Dynamics in Sierra Nevada Conifer Systems of California, 246, 2004.

Rasmussen, C., Southard, R. J., and Horwath, W. R.: Mineral control of organic carbon mineralization in a range of temperate conifer forest soils, Global Change Biology, 12, 834–847, https://doi.org/10.1111/j.1365-2486.2006.01132.x, 2006.

Rasmussen, C., Throckmorton, H., Liles, G., Heckman, K., Meding, S., and Horwath, W. R.: Controls on Soil Organic Carbon Partitioning and Stabilization in the California Sierra Nevada, Soil Systems, 2018.

Rasse, D. P., Rumpel, C., and Dignac, M. F.: Is soil carbon mostly root carbon? Mechanisms for a specific stabilisation, Plant and Soil, 269, 341–356, https://doi.org/10.1007/s11104-004-0907-y, 2005.

Reimer, P. J., Austin, W. E., Bard, E., Bayliss, A., Blackwell, P. G., Ramsey, C. B., Butzin, M., Cheng, H., Edwards, R. L., Friedrich, M., and others: The IntCal20 Northern Hemisphere radiocarbon age calibration curve (0–55 cal kBP), Radiocarbon, 62, 725–757, 2020.

Sah, S. P., Jungner, H., Oinonen, M., Kukkola, M., and Helmisaari, H.-S.: Does the age of fine root carbon indicate the age of fine roots in boreal forests?, Biogeochemistry, 104, 91–102, 2011.

Schimel, J. P.: Soil Organic Matter Does Not Break Itself Down : The Implications of Exoenzyme Activity on C Flow and Microbial Carbon and Nitrogen Limitation in Soil, 1–9, 2006.

Schmidt, M. W. I., Torn, M. S., Abiven, S., Dittmar, T., Guggenberger, G., Janssens, I. a., Kleber, M., Kögel-Knabner, I., Lehmann, J., Manning, D. a. C., Nannipieri, P., Rasse, D. P., Weiner, S., and Trumbore, S. E.: Persistence of soil organic matter as an ecosystem property, Nature, 478, 49–56, https://doi.org/10.1038/nature10386, 2011.

Sierra, C. A., Müller, M., and Trumbore, S. E.: Modeling radiocarbon dynamics in soils: SoilR version 1.1, Geoscientific Model Development, 7, 1919–1931, https://doi.org/10.5194/gmd-7-1919-2014, 2014.

Sierra, C. A., Malghani, S., and Müller, M.: Model structure and parameter identification of soil organic matter models, Soil Biology and Biochemistry, 90, 197–203, https://doi.org/10.1016/j.soilbio.2015.08.012, 2015.

Sierra, C. A., Müller, M., Metzler, H., Manzoni, S., and Trumbore, S. E.: The muddle of ages, turnover, transit, and residence times in the carbon cycle, Global Change Biology, 23, 1763–1773, https://doi.org/10.1111/gcb.13556, 2017.

Sierra, C. A., Hoyt, A. M., He, Y., and Trumbore, S. E.: Soil Organic Matter Persistence as a Stochastic Process: Age and Transit Time Distributions of Carbon in Soils, Global Biogeochemical Cycles, 32, 1574–1588, https://doi.org/10.1029/2018GB005950, 2018.

Sierra, C. A., E. Crow, S., Heimann, M., Metzler, H., and Schulze, E. D.: The climate benefit of carbon sequestration, Biogeosciences, 18, 1029–1048, https://doi.org/10.5194/bg-18-1029-2021, 2021.

Soetaert, K. and Petzoldt, T.: Inverse modelling, sensitivity and monte carlo analysis in R using package FME, Journal of Statistical Software, 33, 1–28, https://doi.org/10.18637/jss.v033.i03, 2010.

Sokol, N. W. and Bradford, M. A.: Microbial formation of stable soil carbon is more efficient from belowground than aboveground input, Nature Geoscience, 12, 46–53, https://doi.org/10.1038/s41561-018-0258-6, 2019.

Solly, E., Schöning, I., Boch, S., Müller, J., Socher, S. A., Trumbore, S. E., and Schrumpf, M.: Mean age of carbon in fine roots from temperate forests and grasslands with different management, Biogeosciences, 10, 4833–4843, https://doi.org/10.5194/bg-10-4833-2013, 2013.

Solly, E. F., Brunner, I., Helmisaari, H.-S., Herzog, C., Leppälammi-Kujansuu, J., Schöning, I., Schrumpf, M., Schweingruber, F. H., Trumbore, S. E., and Hagedorn, F.: Unravelling the age of fine roots of temperate and boreal forests, Nature Communications, 9, 3006, 2018.

Soong, J. L., Castanha, C., Hicks Pries, C. E., Ofiti, N., Porras, R. C., Riley, W. J., Schmidt, M. W. I., and Torn, M. S.: Five years of whole-soil warming led to loss of subsoil carbon stocks and increased CO2 efflux, Science Advances, 7, 1–9, https://doi.org/10.1126/sciadv.abd1343, 2021.

Stoner, S. W., Hoyt, A. M., Trumbore, S., Sierra, C. A., Schrumpf, M., Doetterl, S., Baisden, W. T., and Schipper, L. A.: Soil organic matter turnover rates increase to match increased inputs in grazed grasslands, Biogeochemistry, 156, 145–160, https://doi.org/10.1007/s10533-021-00838-z, 2021.

Stuiver, M. and Polach, H. A.: Reporting of 14C Data, Radiocarbon, 19, 355–363, https://doi.org/10.1017/S0033822200003672, 1977.

Tang, J., Misson, L., Gershenson, A., Cheng, W., and Goldstein, A. H.: Continuous measurements of soil respiration with and without roots in a ponderosa pine plantation in the Sierra Nevada Mountains, Agricultural and Forest Meteorology, 132, 212–227, https://doi.org/10.1016/j.agrformet.2005.07.011, 2005.

Todd-Brown, K., Zheng, B., and Crowther, T. W.: Field-warmed soil carbon changes imply high 21st-century modeling uncertainty, Biogeosciences, 15, 3659–3671, https://doi.org/10.5194/bg-15-3659-2018, 2018.

Trumbore, S.: Age of soil organic matter and soil respiration: Radiocarbon constraints on belowground C dynamics, Ecological Applications, 10, 399–411, https://doi.org/10.1890/1051-0761(2000)010[0399:AOSOMA]2.0.CO;2, 2000.

Trumbore, S.: Radiocarbon and Soil Carbon Dynamics, Annual Review of Earth and Planetary Sciences, 37, 47–66, https://doi.org/10.1146/annurev.earth.36.031207.124300, 2009.

Trumbore, S. E., Sierra, C. A., and Hicks Pries, C. E.: Radiocarbon nomenclature, theory, models, and interpretation: Measuring age, determining cycling rates, and tracing source pools, Radiocarbon and climate change: Mechanisms, applications and laboratory techniques, 45–82, 2016.

Wang, Y., Amundson, R., and Niu, X. F.: Seasonal and altitudinal variation in decomposition of soil organic matter inferred from radiocarbon measurements of soil CO2flux, Global Biogeochemical Cycles, 14, 199–211, https://doi.org/10.1002/(ISSN)1944-9224, 2000.

Wells, C. E., Glenn, D. M., and Eissenstat, D. M.: Changes in the risk of fine-root mortality with age: a case study in peach, Prunus persica (Rosaceae), American Journal of Botany, 89, 79–87, 2002.

Wickland, K. P. and Neff, J. C.: Decomposition of soil organic matter from boreal black spruce forest: environmental and chemical controls, Biogeochemistry, 87, 29–47, https://doi.org/10.1007/s10533-007-9166-3, 2008.

5. Synthesis

5.1.   Introduction

The central motivation for this dissertation was to quantify the effect of climatic and soil mineralogical variables on timescales of soil C cycling. In Chapter 2 (Study 1), I demonstrated the feasibility of a novel methodology for measuring the radiocarbon signature of heterotrophically respired CO_2 in incubations of archived soil samples. In Chapter 3 (Study 2), I implemented this method to construct radiocarbon time series for both bulk soil ($\Delta^{14}C_{bulk}$) and respired CO_2 ($\Delta^{14}C_{respired}$) at nine sites spanning a combined gradient of parent material and climate. Leveraging previous work at the study sites, I demonstrate how the change in $\Delta^{14}C_{bulk}$ and $\Delta^{14}C_{respired}$ between 2001 and 2019 varied in response to edaphic variables, including soil depth, mineral content, and climate. In Chapter 4 (Study 3), I developed compartmental models using the time series of $\Delta^{14}C_{bulk}$ and $\Delta^{14}C_{respired}$ as model constraints. I then applied these models to characterize the distribution of ages and transit times at the study sites, and furthermore, how the means and medians of these age and transit time distributions varied in response to mean annual soil temperature and reactive mineral content. In this chapter, I will assess the limitations of using $\Delta^{14}C$ from bulk and respired CO_2 to constrain soil C models (the approach taken in this dissertation), by comparing it to an alternative approach relying on $\Delta^{14}C$ of density fractions. To put the modeling results in context, I will discuss the implications of using reactive mineral content to predict how soil C stocks will respond to rising temperatures. Finally, I will demonstrate how climatic and mineralogical effects on age and transit time distributions affect the potential climate change mitigation benefits of soil C sequestration.

5.2.   Empirical approaches to partitioning soil organic matter

Soil contains a heterogeneous mixture of organic matter, some of which is readily decomposed and some of which persists for hundreds to thousands of years. The results of this dissertation add to a growing body of literature confirming this heterogeneity, and the need to account for it in models of soil C dynamics. Soil C cycling at annual to decadal timescales is of particular interest, as it is on these timescales that accelerated soil C losses or mitigation efforts are most relevant. Many methods have been developed to separate organic C into fractions believed to cycle at different rates on the basis of certain physical or chemical characteristics. However, defining meaningful pools empirically remains a key challenge in soil organic matter research.

Density fractionation is a common technique for separating particulate organic matter (POM), which is assumed to be readily decomposable, from mineral associated organic matter (MAOM), which is assumed to be protected from decomposition via bonding or complexation with minerals (Golchin, 1996). Mineral associated soil organic matter will tend to sink in a dense solution, in contrast to POM which floats freely on top of a solution that is denser than water. The density of the fractionating solution (commonly sodium polytungstate) can be varied in order to account for the density of known minerals, or to distinguish multiple MAOM fractions sequentially (Sollins et al., 2009). Particulate organic matter can also be found within soil aggregates, and aggregate disruption can be performed to separate this occluded POM (oPOM) fraction from the free-floating POM (fPOM) (Cerli et al., 2012).

Mineral associated soil organic matter is the largest pool of soil C on a global scale, and is the largest pool in most soils as well (Heckman et al., 2022). Historically, MAOM has been considered to be a highly persistent pool of soil C, in part because ^{14}C contents indicated mean ages on the scale of hundreds to thousands of years, and in part because of the "microbial signature" of MAOM indicated recycling of the organic matter via microbial processing. However, in a recent synthesis assessing abundance and persistence of soil C on a global scale, MAOM in near-surface soils (< 0.3 m) had Δ^{14}C values greater than zero, suggesting that a substantial component of this pool is likely cycling on decadal time scales (Heckman et al., 2022).

One interpretation of this finding is that MAOM is simply not as old as previously thought. Recent work in which thermal fractionation was used to further separate density fractionated MAOM demonstrated that soils rich in amorphous mineral phases, 2:1 clays, and short-range order metal oxides exhibited a large range of radiocarbon ages within the heavy fraction (Stoner, 2023). This provides support to the theory that organic matter associated with different minerals turns over at different rates (Wagai et al., 2018; Kaiser and Guggenberger, 2007; Kleber et al., 2007; Sollins et al., 2009). Given that the soil mineral assemblage in most soils consists of a mixture of mineral phases, this heterogeneity suggests that some of the C in MAOM cycles on faster timescales and has incorporated 'bomb' ^{14}C, while C that is tightly bound to other mineral phases may lack this bomb-C signal.

Recent empirical studies show that while the amount of C in MAOM may not change, a substantial proportion of MAOM may be exchangeable with DOC in the soil solution. In the laboratory, exchange rates between DOC and organic matter sorbed to goethite have been shown to range from one sixth

to one third of the total sorbed pool (Leinemann et al., 2018). Following desorption, DOC can cycle downward in the soil, contributing to a perceived pre-aging of soil C inputs in deeper soil layers (Kaiser and Kalbitz, 2012). This exchange mechanism is congruent with the bomb-C signal observed in surface MAOM pools and the delayed arrival of this signal deeper in the soil seen in this study (Ch. 4) and others (Koarashi et al., 2012). A key point about such exchange processes is that they can only be detectable through the use of tracers, given that in the laboratory experiment the total pool of sorbed C remained relatively constant (Leinemann et al., 2018).

Methodological considerations are also important for interpreting the radiocarbon signature of density fractions and their associated turnover rates. High loading rates of organic matter on mineral surfaces (or a high proportion of organic matter in mineral-organo complexes) decreases the density of MAOM, which can lead to misclassification of MAOM as POM (Kaiser and Guggenberger, 2007; Wagai et al., 2018). Another challenge for interpreting $\Delta^{14}C$ values of POM is the presence of charcoal, which may have strongly depleted $\Delta^{14}C$ values, but have low enough density to be captured in the POM fractions (Koarashi et al., 2012; Heckman et al., 2014). Soils replete with charcoal are common in ecosystems characterized by fire disturbance regimes with moderate to frequent burn intervals, such as the mixed conifer forest ecosystems studied in this dissertation (Beaty and Taylor, 2008; Koarashi et al., 2012; Castanha et al., 2008). Despite these challenges, density fractionation remains a useful tool for gaining mechanistic insight into the importance of parent material and mineral assemblages for soil C persistence, as well as the importance of temperature for persistence of POM.

Previous efforts employing density fractionation on the soils studied in this dissertation demonstrated clear patterns in the partitioning of total soil C stocks among POM and MAOM fractions as a function of climate zone and parent material (Rasmussen et al., 2018). The proportion of total soil C stock in the fPOM fraction declined with increasing elevation across all parent materials, which the authors attributed primarily to the increased abundance of clay sized particles in the well-weathered soils of the low elevation, warm climate sites (Rasmussen et al., 2018). In contrast, parent material was more important for determining the allocation of total C stocks to the MAOM fraction. Rasmussen et al. (2018) observed proportionally more MAOM in the andesitic soils than in the basaltic or granitic soils across all three climate zones, despite similar particle size distributions, highlighting the importance of reactive secondary minerals in determining the size of the MAOM pool.

The previous density fractionation work focused on soils collected during the 2009 sampling campaign. Building on this effort, I performed additional density fractionations and radiocarbon analysis of the 2001 and 2019 samples. Initially I sought to use the radiocarbon time series from the density fraction data to constrain three pool models using the SoilR package. However, this effort was not successful, as I was unable to achieve good model fits with the pool sizes and $\Delta^{14}C$ content constrained by the empirical data. This finding suggests that the density fractions, at least from these sites, do not comprise homogenous pools. Given current understanding of different bonding strengths and exchangeability of organic matter associated with different soil minerals, and the presence of recalcitrant charcoal in the POM fractions, the inability to model the density fractions directly is not surprising, and indeed has been demonstrated previously (Schrumpf and Kaiser, 2015).

A common assumption regarding the turnover of density fractions is that the fPOM fraction is easily decomposed, and the MAOM fraction is highly persistent. If this is true, the fPOM fraction should contribute more to heterotrophic respiration than MAOM. This hypothesis can be simply tested by regressing $\Delta^{14}C$ of fPOM and MAOM fractions against $\Delta^{14}C_{respired}$ and comparing the regression coefficients. Slopes close to unity indicate that changes in fraction $\Delta^{14}C$ and $\Delta^{14}C_{respired}$ are correlated, which in turn suggests that a substantial component of the fraction pool has a similar $\Delta^{14}C$ value as the CO_2 in the respiration flux. Deviations from unity indicate that different mechanisms control the change in fraction C $\Delta^{14}C$ with depth, parent material, or climate than in the respired CO_2 flux. With fraction $\Delta^{14}C$ on the y-axis, intercept values diverging from zero indicate the presence of more enriched or more depleted C in the fraction pool relative to respired CO_2.

I performed this test with fPOM and MAOM data from both the 2001 and 2019 samples collected at the Sierra Nevada sites. For both the fPOM and MAOM regressions the majority of the points fall below the 1:1 line, indicating the presence of older C in both fractions that is not actively utilized by the microbial community, e.g., charcoal in the fPOM fraction or organic material bound directly to the mineral surfaces in the MAOM fraction (**Figure 5-1**). The slopes and intercepts in both regressions varied by depth, climate zone, and parent material, suggesting that the contribution of the fractions to respiration varies with these factors.

I observed a nearly 1:1 relationship between fPOM $\Delta^{14}C$ and $\Delta^{14}C_{respired}$, with the slope of the relationship consistent across all parent materials and climate zones (**Figure 5-1**, panels **A-B**). The closest relationship between $\Delta^{14}C$ of the fPOM fraction and $\Delta^{14}C_{respired}$ was for the warm climate soils,

which had a slope of 1 and an intercept value of zero, indicating almost complete overlap in $\Delta^{14}C$ values. This correlation between fPOM $\Delta^{14}C$ and $\Delta^{14}C_{respired}$ indicates that the organic matter respired by the microbial community is the same age, on average as the organic matter in the fPOM fraction.

I observed more differences in intercept values when the data were grouped by parent materials, with values near 0‰ for the granite soils, -20‰ for the basalt soils, and -60‰ for the andesite soils. These differences suggest the presence of an older, more depleted pool of C within the fPOM fraction, which is not actively metabolized by the microbial community. The presence of more depleted C in the fPOM fractions of the andesitic and basaltic soils relative to the granitic soils could be explained by different fire histories among the three parent material transects. This would be particularly relevant during the fire suppression period (1850-present), as historical fire regimes were likely to have been consistent among sites with a similar vegetation and topographic setting, and therefore would not explain the consistent differences among parent materials (Kilgore and Taylor, 1979; Beaty and Taylor, 2008). An alternative explanation is that the more depleted $\Delta^{14}C$ values in the fPOM fraction of the andesitic and basaltic soils indicate the presence of organo-mineral complexes with a high enough proportion of organic matter to be less dense than the MAOM cut-off used in this study, i.e., <1.8 g cm^{-3} (Baisden et al., 2002; Sollins et al., 2006; Kaiser and Guggenberger, 2007; Cerli et al., 2012).

In contrast to the fPOM regressions, the slope for the relationship between MAOM $\Delta^{14}C$ and $\Delta^{14}C_{respired}$ were consistently less than one, with intercept values all less than zero (**Figure 5-1**, panels **C-D**). This indicates that the composition of the respired CO_2 flux is only likely to be similar to that of the MAOM fraction when it is highly depleted, a trend observed for the deeper soil layers in these samples. When grouped by climate zone, the slope for the warm climate MAOM fractions vs. $\Delta^{14}C_{respired}$ was notably closer to one (0.68±0.22‰) than the slopes for the cool and cold climate MAOM fractions (**Figure 5-1**, panel **D**). This suggests that the MAOM fraction could be contributing more to respiration in the warm climate soils than in the soils of the cooler climate zones.

The challenge of the regression approach is that it does not account for potential heterogeneity within the fractions. Although the strong correlations between $\Delta^{14}C$ of fPOM and $\Delta^{14}C_{respired}$ provides evidence that fPOM could make up a substantial proportion of the respiration flux, the weaker correlation of MAOM and $\Delta^{14}C_{respired}$ does not preclude the contribution to respiration from younger C in the MAOM fraction. In order to demonstrate this, I compared the C-weighted distribution of ^{14}C from the fractions to the distribution returned from the two-pool parallel models presented in Ch. 4

(**Figure 5-2**). From this comparison it is clear that the distribution of fraction $\Delta^{14}C$ tends to be biased towards the center of the modeled $\Delta^{14}C$ distribution. The fraction $\Delta^{14}C$ distribution excludes the enriched $\Delta^{14}C$ captured by the fast-cycling pool of the model in both soils, while also excluding the depleted tail of the ^{14}C distribution seen in the slow pool of the granitic soil (**Figure 5-2**, **b**). A major advantage of the modeling approach is that these histograms of $\Delta^{14}C$ can be more finely resolved by taking advantage of the probability distribution function for C ages returned by the model (Chanca et al., 2022). Converting the probability distribution of C ages from the model pools to $\Delta^{14}C$ reveals how misleading the mean values (as seen in **Figure 5-2**) can be when compared to the full distribution (**Figure 5-3**). However, since I could not successfully model the fraction data as pools, the C age distribution within the fractions remains hidden.

The distribution of $\Delta^{14}C$ within these density fractions can be obtained in an alternative way, however: through further fractionation. Techniques such as applying more finely resolved density steps, or applying chemical or thermal means can be used to reveal glimpses of the distribution of C ages hidden within density fractions. Such methods are time-consuming and are costly when combined with radiocarbon analysis, thus further fractionation of all of the soils in the study was beyond the scope of this dissertation. However, I was able to further fractionate the heavy fractions from a few selected soils using ramped combustion, which enabled testing of the hypothesis that this fraction contains a heterogeneous mixture of organic matter turning over at different rates (**Figure 5-4**).

The C-weighted distributions of $\Delta^{14}C$ in the heavy fractions of the basalt and granitic soils are characterized by long tails containing a small amount of C that is substantially depleted in comparison to the central tendency of the distribution. The bias created by this tail is evident when comparing the distribution of MAOM $\Delta^{14}C$ in the granite soil in **Figure 5-4**, which shows clearly that the majority of C in the fraction contains the bomb-C signal and is thus cycling on decadal timescales, to the histogram bar with a mean value of -25‰ in **Figure 5-2**, which suggests rather that the C in this fraction cycles on centennial timescales. Perhaps most interesting is the bimodal distribution of $\Delta^{14}C$ in the heavy fraction of the andesitic soil. Using mass spectrometry to analyze the source of C in the thermal fractions indicates that the thermal method successfully distinguishes between C bound to different types of minerals. For the andesitic soil, the more depleted peak around -180‰ is likely from organic matter bound to 2:1 clays, while the more enriched peak around -70‰ likely derives mainly from organic matter associated with pedogenic oxides. Both the andesitic and basaltic soils have overlapping peaks at -70‰, which aligns with the sequential extraction data that confirms the

presence of pedogenic oxides in both soils. See Stoner (2023) for more information about assigning functional groups to specific thermogram peaks.

5.3.   Transit time distributions and soil C sequestration

Human efforts to slow the accumulation of greenhouse gases in the atmosphere will require the use of negative emissions technologies (Amundson and Biardeau, 2018). Soil C sequestration is a promising option as it is low-tech, relatively low cost, and is thought to have high potential (Minasny et al., 2017; Paustian et al., 2019; Canadell et al., 2021; Matthews et al., 2022). The potential for C sequestration in a given soil depends on the total amount of C entering the soil, but also on how long C inputs remain in the soil before being respired back to the atmosphere—i.e., the distribution of organic matter among relatively faster or slower cycling soil C pools. Accordingly, in order to determine the amount of C that can be stored, and for how long, we must go beyond calculating the mean age or transit time of soil C and characterize their full distributions (Sierra et al., 2021).

Determining the efficacy of soil C sequestration as a climate change mitigation approach requires quantifying the amount of radiative forcing avoided by storing C in the soil that would otherwise be emitted to the atmosphere as CO_2. This can be quantified over specified time horizons using the climate benefit of sequestration metric developed by Sierra et al. (2021). The soil C transit time distribution is the key for calculating this metric as it gives the age distribution of CO_2 in the release flux—i.e., the distribution of time elapsed between C fixation and its return to the atmosphere. In this context, mean transit time can be interpreted as the average duration of storage for a given unit of soil C input, and median transit time as the amount of time taken to return half of that input to the atmosphere (Crow and Sierra, 2022). These different metrics provide a lens for understanding how potential changes in inputs or decomposition rates may affect soil C sequestration.

A major source of uncertainty in predicting future soil C stock changes in response to climate change is the relative impact of potential increases in ecosystem productivity versus increases in soil organic matter decomposition rates (Friedlingstein et al., 2014; Bradford et al., 2016). Increased ecosystem productivity is predicted for many ecosystems due to the CO_2 fertilization effect or alleviation of temperature constraints in colder ecosystems. At the same time, increases in decomposition rates have been predicted in response to increased temperature, largely based on laboratory estimates of Q10 values (Todd-Brown et al., 2018). Another important consideration is the potential interaction

between productivity and decomposition rates, i.e., if increasing soil C inputs stimulated increased microbial activity, decomposition rates would likely increase as well (Melillo et al., 2017).

The estimated inputs for the warm climate granitic and andesitic soils in this dissertation (Ch. 4) were much higher than the corresponding cool or cold climate sites on the same parent material, which in turn lead to much higher estimates of soil C storage at these sites (**Figure 5-5**). In Ch. 4, I proposed that the dramatic differences in these input estimates were likely related to the dense understory shrub layer present at the warm sites and absent at the cool and cold sites. These changes in the composition of the vegetative community in the lower elevation forests of the Sierra Nevada mountains where the warm climate study sites are located have already been documented as a consequence of climate change. The term "zombie forests" has been used to describe such transitions, in which the climate has shifted beyond the suitable climate envelope for the current vegetation (Hill et al., 2023). Coupled climate vegetation models predict similar transitions for the higher elevation forests in the coming decades as well (Lenihan et al., 2003; Shafer et al., 2001). Applying the results of this dissertation, we can begin to answer the important question of how the impact of these changes in vegetation might affect soil C dynamics and soil C storage in the coming decades.

The difference in mean annual soil temperature between the warm and cool climate sites described in Chs. 3 & 4 is approximately 4 °C, which is at the upper end of the range of the increase in global mean air temperature predicted for the end of the 21st century (+1.4 to +4.4 °C, relative to a 1850-1900 baseline) (Masson-Delmotte et al., 2021). Under the assumption that increases in inputs will follow increases in mean annual air temperature, a change in inputs from the current levels observed at the cool climate sites to those observed at the warm climate sites may well be within the scope of potential increases by 2100. The soils with high inputs in **Figure 5-5** (warm climate andesitic and granitic sites) lose a relatively higher proportion of the pulse of inputs on a 25 y time frame than the lower input soils do, e.g., from the cool and cold climate sites. This result suggests differences in input quantity may be positively correlated with input quality, with important implications for how changes in inputs will affect ages and transit times of soil C. This is best illustrated with the surface soils from the granite parent material elevation transect, for which we saw the strongest response of ages and transit times to temperature.

Along the granitic soil elevation transect mean annual soil temperature increases by approximately 2 °C between the warm and cool sites, and by an additional 2°C between the cool and cold sites. Using a space-for-time approach, we can simulate the effect of a 2 °C increase on soil C stock changes with

the CBS method by comparing the pulse response functions along the MAST gradient. These scenarios can be run with and without changes in inputs to assess the relative impact of potential changes in inputs versus changes in decomposition rates and input partitioning (given by the optimized model parameters) (**Figure 5-6**). In the first scenario (**a**) I adjusted the model parameters to match those of the next warmest climate zone, but maintained the same inputs. In the second scenario (**b**) I adjusted both the model parameters and inputs. These scenarios demonstrate that increasing decomposition rates had a smaller impact on soil C sequestration than changing inputs, which can likely be attributed to the high inputs currently estimated for the warm climate sites. These models predict a net increase in total C storage between the cool and cold climate sites under a 2 °C temperature increase, with small losses in the scenario with increased decomposition rates and current inputs, but large soil C gains in the scenario where we increased both decomposition rates and inputs.

Conspicuously absent from these predictions about future soil C sequestration are the effects of temperature changes beyond the limits of the temperature gradient in this study. Evidence from global scale studies report threshold changes in the sensitivity of soil C transit times to temperature, with temperature sensitivity increasing at temperatures < 4 °C and decreasing above ~18 °C (Koven et al., 2017), just outside the range of MAST at the study sites in this dissertation. The authors posit that these thresholds in temperature sensitivity are likely a product of environmental constraints on decomposition, for example climatic and hydrological thresholds beyond which microbial activity is sharply limited, such as in extremely dry or frozen soils. However, increasing temperatures could also lead to declining productivity (and therefore soil C inputs) if coupled with decreasing soil moisture. Accordingly, we could expect a corresponding reduction in C storage at the warm climate granite site if a 2 °C increase in temperature pushed the vegetation past such a threshold, in contrast to the net gains in C storage predicted for the cool and cold climate sites.

The lack of overlap in the range of soil wetness for the different parent materials in this study precluded analysis of the effect of soil moisture on soil C ages and transit times. However, the effect of soil moisture is likely to be highly relevant for both turnover of soil C and belowground inputs, as outlined in the scenario above. Changes in soil moisture are certain to occur under future climate change, thus future efforts aimed at quantifying age and transit time distributions across a soil moisture gradient would deepen our understanding of how these changes may affect changes in soil C stocks in the future.

Quantifying ages and transit times of soil C in response to temperature, and across soils with different soil mineral assemblages is an important step towards understanding soil C sequestration potential. However, improving predictions of changes to soil C stocks under future climate change will require a deeper understanding of how soil C is allocated among different pools of soil C, as well as quantifying the turnover rates of these pools. The results of this dissertation suggest that progress towards this goal could be made by applying density and thermal fraction Δ^{14}C data as additional constraints for the inner pool dynamics of a model also constrained by a time series of Δ^{14}C$_{bulk}$ and Δ^{14}C$_{respired}$.

5.4. Soil archives and the potential of ^{14}C$_{respired}$ time series

The primary challenge of interpreting soil Δ^{14}C is that soil is an open system, continuously exchanging C with the atmosphere. Heterogeneity of soil organic matter further complicates interpretation, as organic matter entering the soil has many possible fates, including immediately being respired, sorption to minerals, transformation into particulate organic matter, or further transformation into dissolved organic matter, microbial biomass, necromass, etc., before eventually leaving the soil as dissolved organic matter or a product of respiration. In such a system, Δ^{14}C represents the balance of decomposition in each pool as well as the process of radioactive decay.

Measuring Δ^{14}C$_{respired}$ provides a unique window into these dynamics as it integrates the flux-weighted contribution of each pool to the respiration flux without requiring quantification of the size or Δ^{14}C content of each pool. However, fluctuations in the Δ^{14}C concentration of the atmosphere also complicate interpretation, especially during the modern period when the Δ^{14}C of CO_2 fixed from the atmosphere is not unique to a single year. Time series offer a solution to this problem, as they capture the rate of incorporation of newly fixed C into soil organic matter over time, an insight that cannot be quantified from a single observation (Baisden et al., 2013). The contribution of the annual signal is diluted by the Δ^{14}C signature of the existing pool of soil C, a dynamic which can be seen clearly in the time series of Δ^{14}C$_{respired}$ in **Figure 3-3**.

Soil archives are uniquely positioned to provide time series data. Archived soils from the period immediately following the bomb-C pulse are especially valuable, as the high concentration of atmospheric ^{14}C during these years provides correspondingly high resolution for tracing annual to decadal soil C dynamics (Trumbore, 2009). The prohibitive cost and sample requirements of ^{14}C

analysis during this period also precluded many measurements of soil ^{14}C during this time period, thus soil archives represent a chance to make up for this lost opportunity.

The first study of this dissertation demonstrates the feasibility of measuring $\Delta^{14}C_{respired}$ in incubations of archived soils by quantifying the bias due to air-drying, rewetting, and storage duration, while the second and third studies (Chs. 3 & 4) demonstrate the application of this technique. The results from Chs. 3 & 4 underscore the power of $\Delta^{14}C_{respired}$ for constraining soil C models, as well as the advantages gained from the use of archived soils. The biases in $\Delta^{14}C_{respired}$ observed due to air-drying and rewetting were small in the proof-of-concept study (Ch. 2), corresponding to the changes observed in atmospheric $\Delta^{14}C$ over two to ten years. However, the specific mechanism behind this effect warrants additional study. For example, the difference in the magnitude of the bias introduced by air-drying and rewetting between forest and grassland soils, along with the changes in $\delta^{13}CO_2$, suggests that air-drying and rewetting increases availability of microbially derived C. The source of this microbial C could be microbial biomass, necromass, or highly processed soil organic matter sorbed to mineral surfaces. The strongly depleted $\Delta^{14}C_{respired}$ signature observed in Chs. 3 & 4 from the cold climate granitic soils, but not the soils from the other sites, may also provide another clue to the source of the C released following air-drying and rewetting, but without further study the mechanisms driving this release are only speculative. The results in this dissertation clearly illustrate the advantages of the archived incubation technique, and wider adoption of the method in the future may further elucidate the mechanisms driving the observed shift in substrate use following air-drying and rewetting.

5.5. Figures

Figure 5-1. Relationship of $\Delta^{14}C_{respired}$ to $\Delta^{14}C$ of free light and heavy fractions. Points show data from 2001 and 2019 sampling; size of points increases with increasing depth.
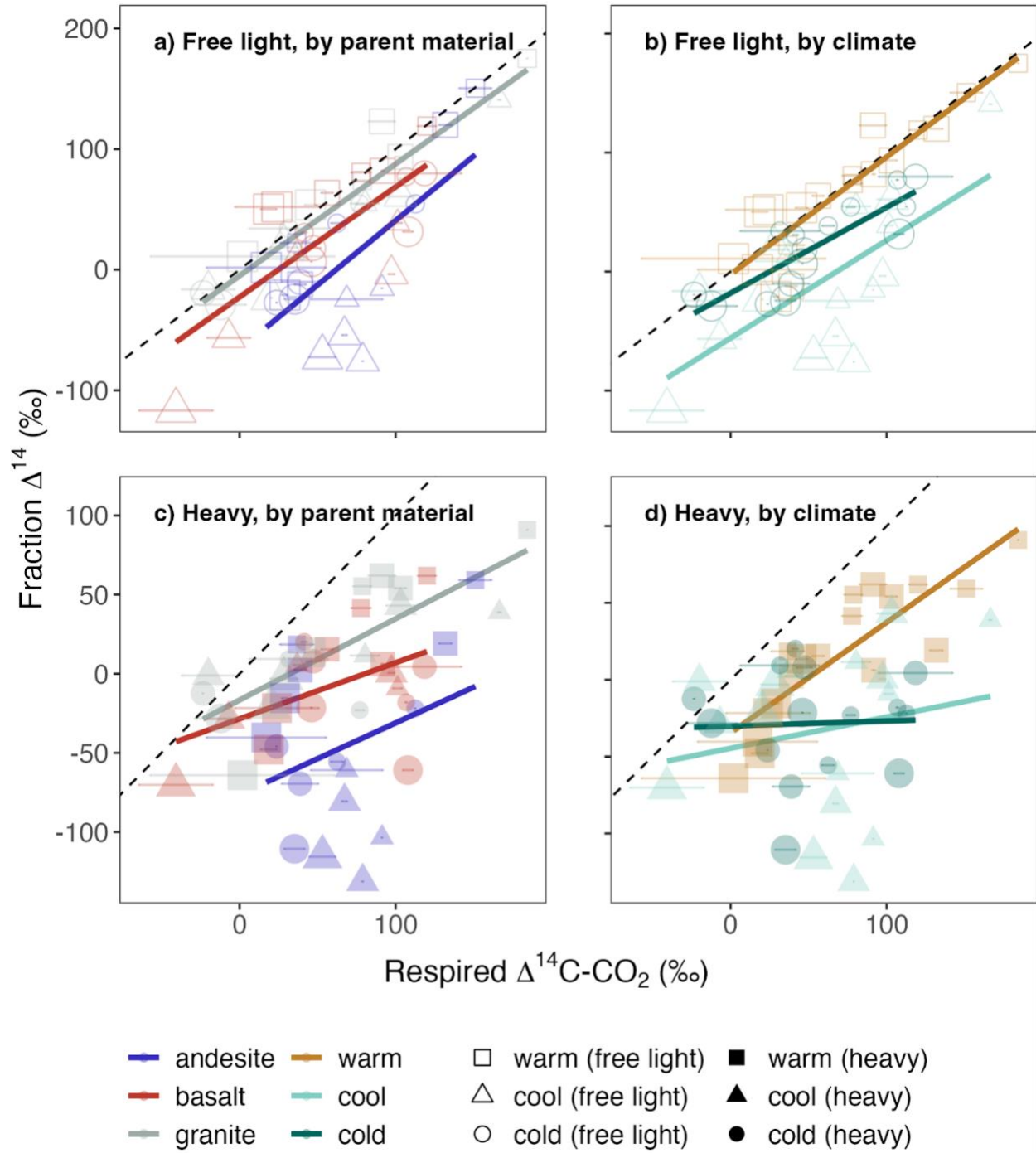
Figure 5-2. Distribution of C stocks and Δ^{14}C among modeled pools and density fractions. Data from cool climate andesite and granite soils collected in 2019 (0.2-0.3 m).
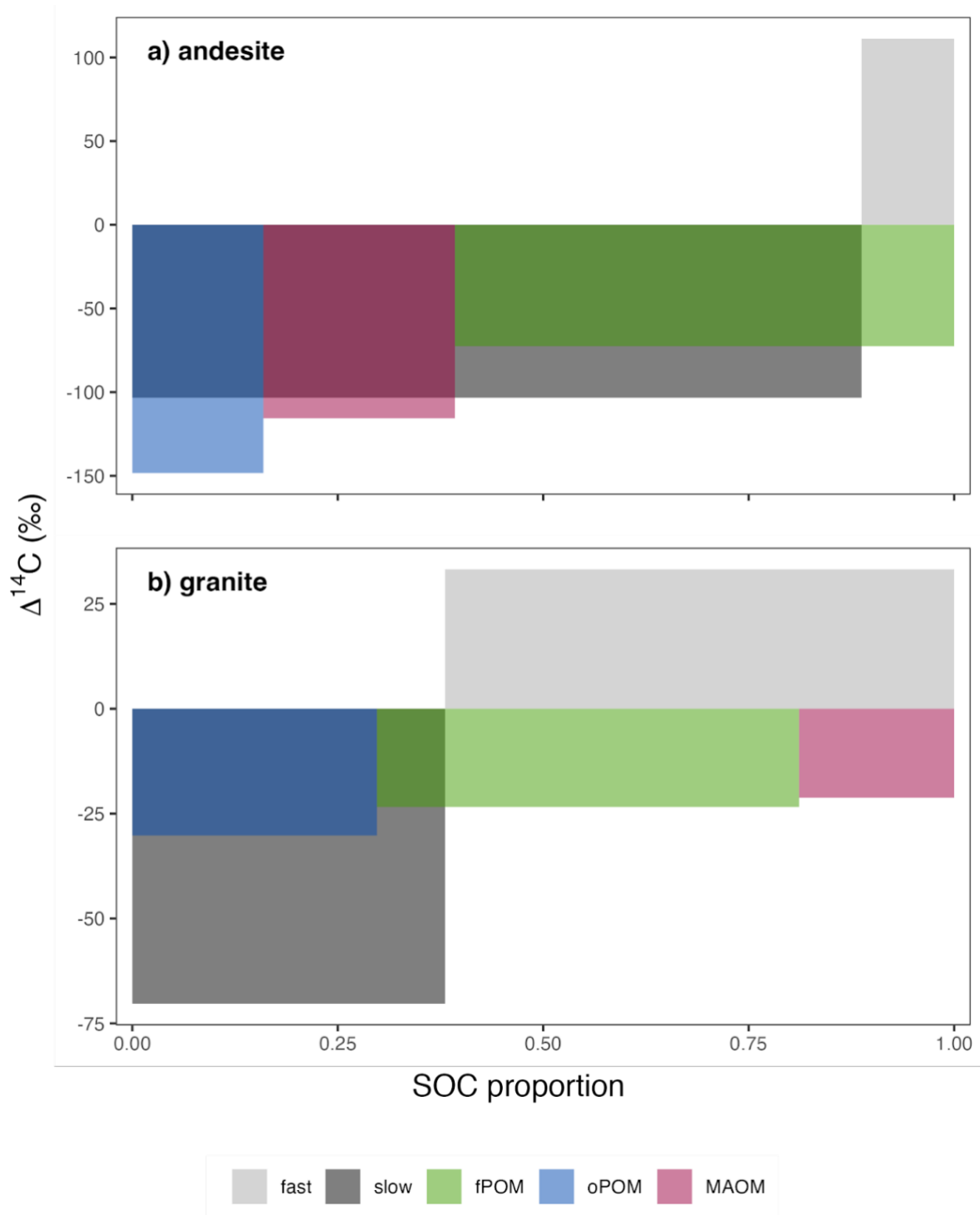
Figure 5-3. Probability density distribution of Δ^{14}C in model pools (two-pool parallel model)[1]

a) andesite

b) granite

C-weighted Δ^{14}C (‰)

fast   slow
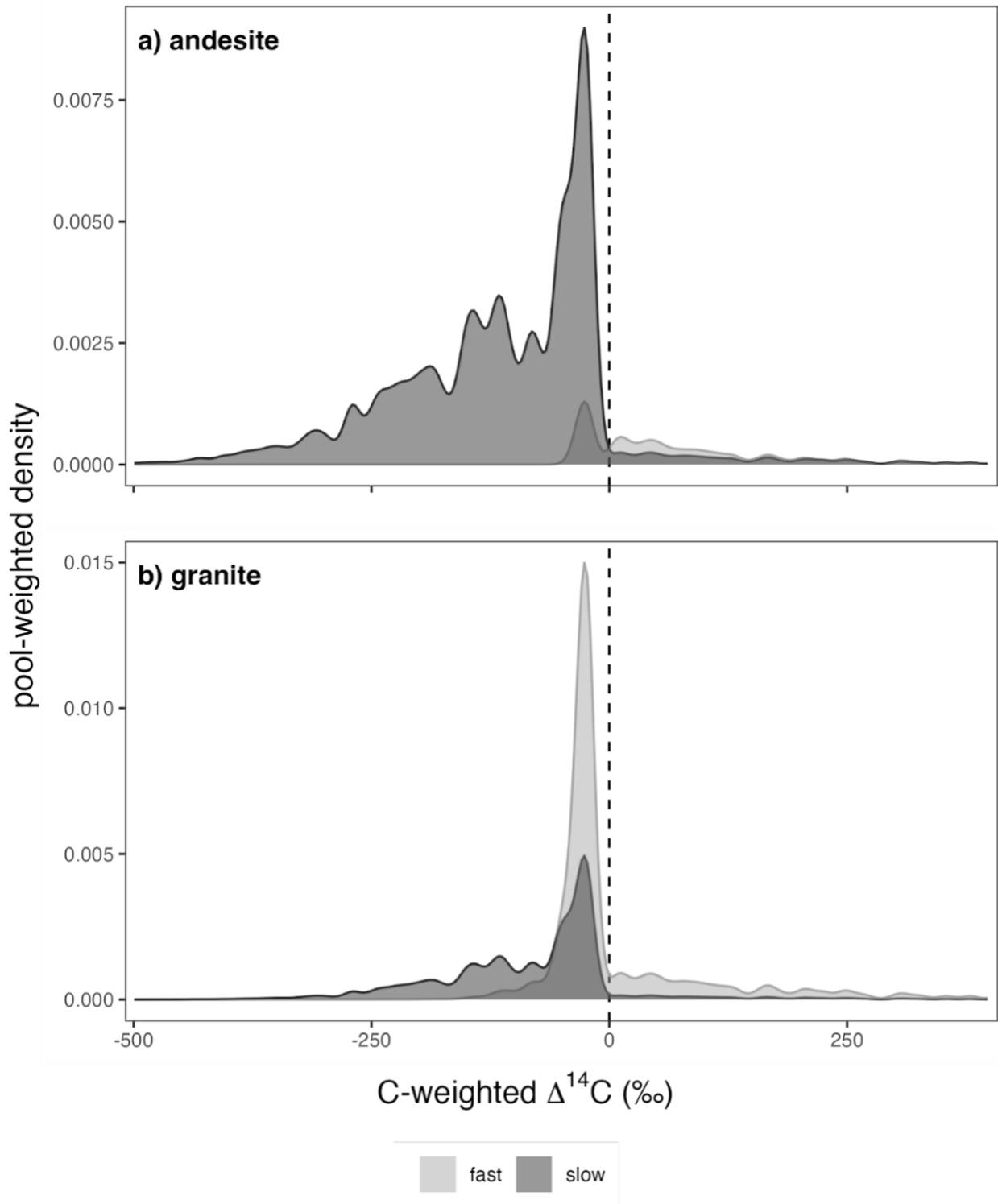
[1]Data from cool climate andesite and granite soils collected in 2019 (0.2-0.3 m). Note: tails of distribution truncated for display purposes.

227

Figure 5-4. Distribution of carbon-weighted Δ^{14}C in heavy fractions (thermal fractionation)[1]
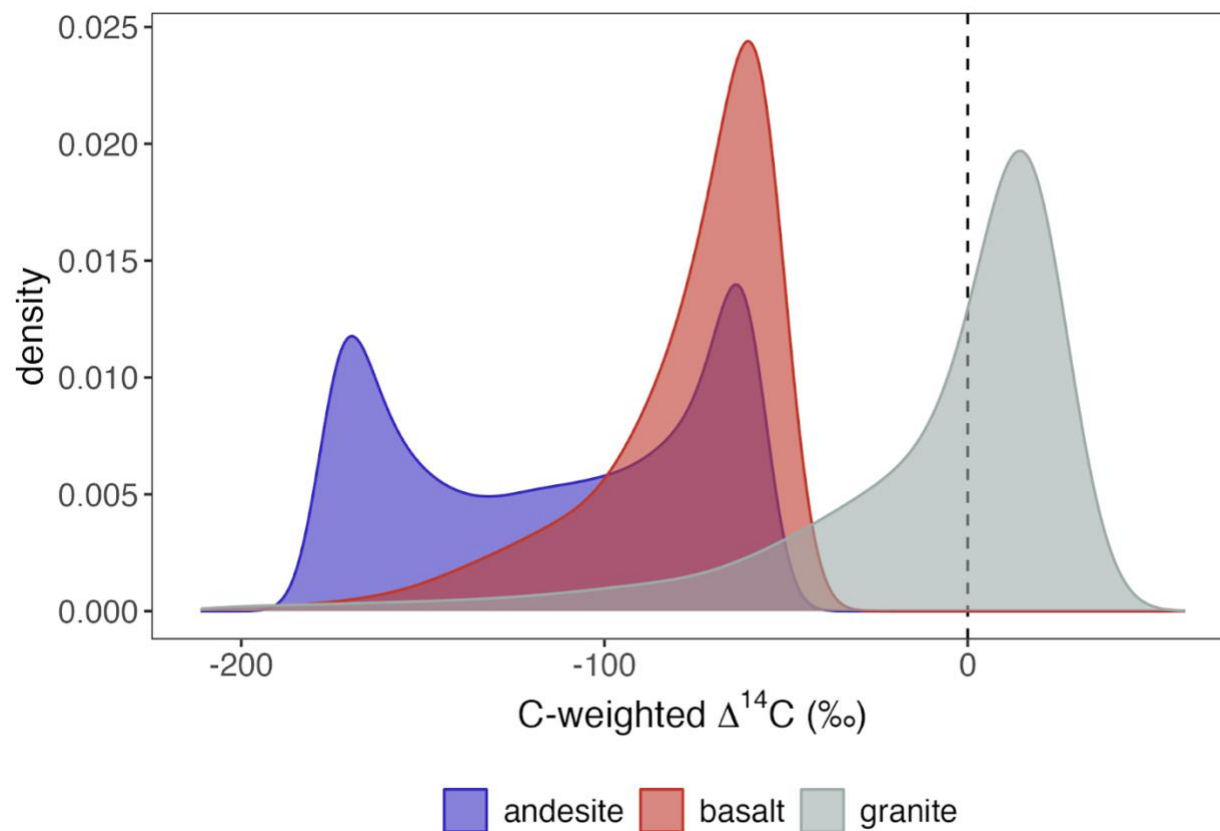
[1]Cool climate sites, 0.2-0.3 m, collected in 2019. Curves fit with Gaussian kernel smoothing function (as with modeled data in **Figure 5-3,** cf. Chanca et al., 2021).

Figure 5-5. Pulse response function for current inputs and decomposition rates, 0-0.1 m
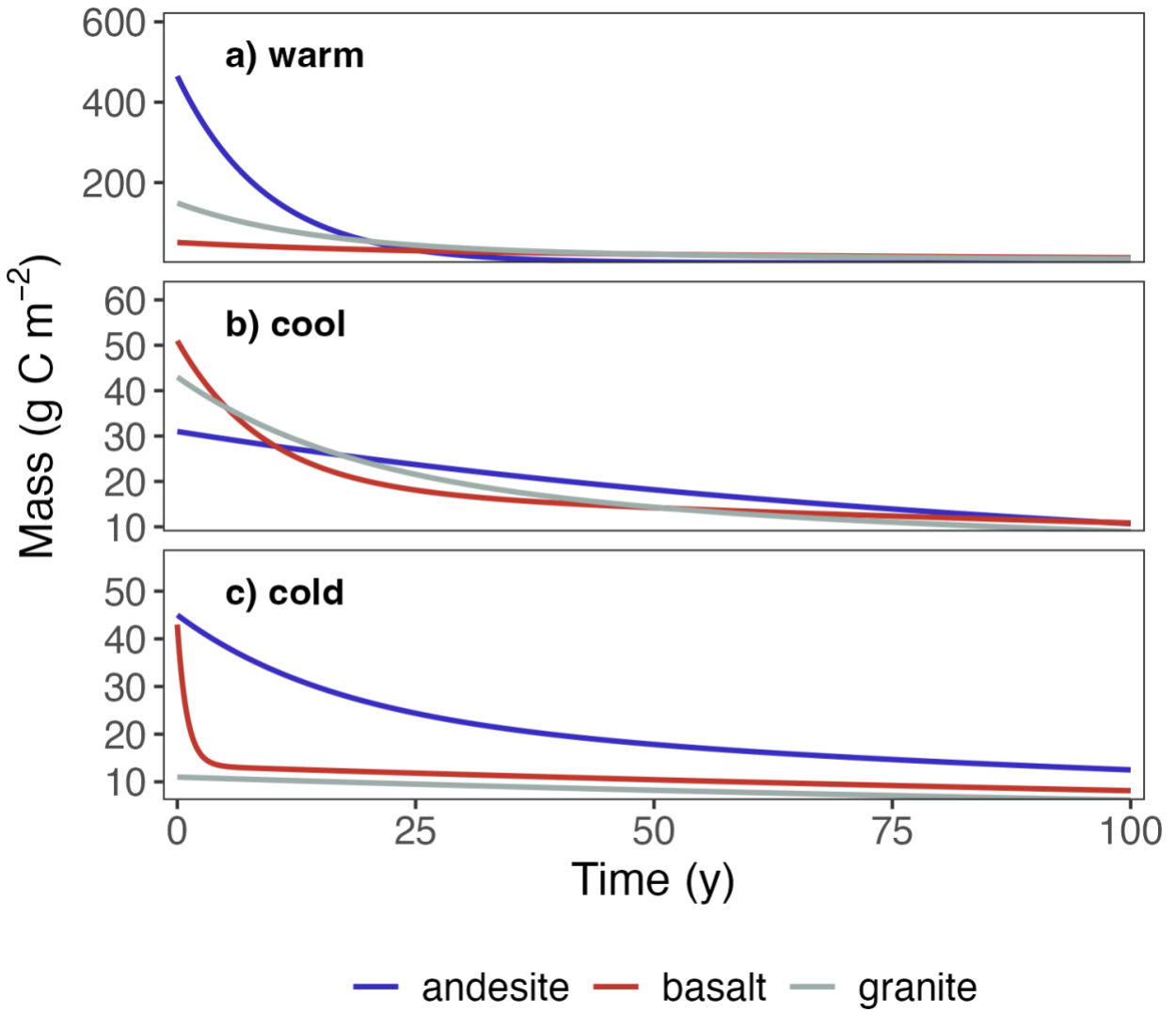
Figure 5-6. Change in carbon sequestration of a pulse of annual inputs with increased decomposition rates under two scenarios: **a)** unchanged inputs, and **b)** inputs shifted to match the those of the next warmest climate zone (cool to warm, cold to cool).
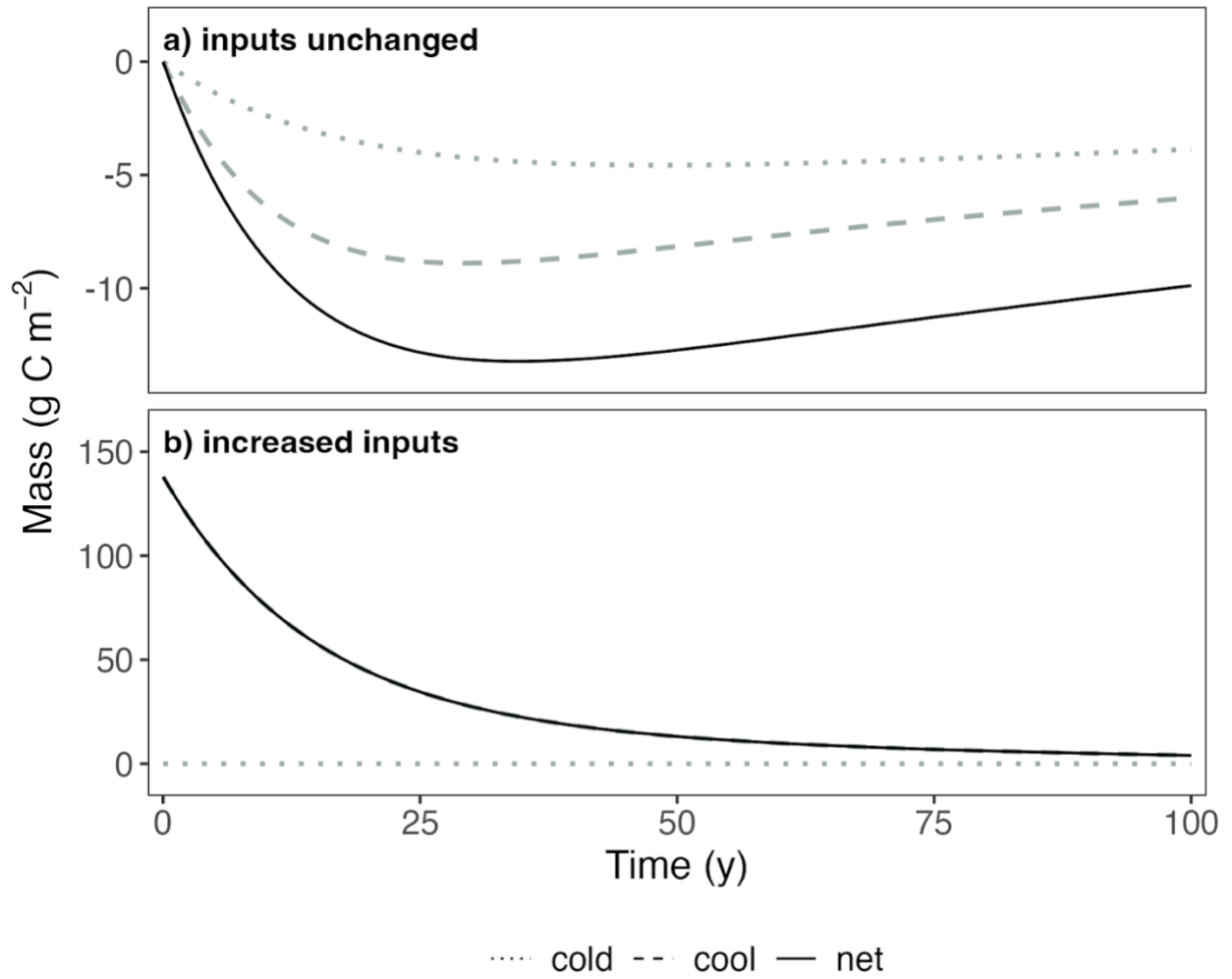
6. Conclusion

The key advances of this dissertation include developing a novel approach for determining timescales of soil C cycling and demonstrating the combined effect of climate and mineral assemblages on the distribution of ages and transit times in soils. The results of Chs. 3 & 4 provide evidence for the robust estimates of system age and transit time distributions that can be achieved when soil C models are constrained with a radiocarbon time series of both bulk soil and heterotrophically respired CO_2, and the advantages of the archived soil incubation technique introduced in Ch. 2. These models indicate that it takes decades for bomb-C to move downward and affect radiocarbon-depth relationships, which also suggests that fast-cycling C in deeper soil layers is likely to be pre-aged from its downward transit. In this final chapter, I suggest that modeling density fraction data may not be feasible or practical in soils where these fractions are likely to contain a mixture of organic matter with different turnover rates, and demonstrate this through a comparison with model pool age distributions and thermal fractionation for a subset of the soils studied in this dissertation.

A fundamental issue with the model approach taken in Ch. 4 is that while system age and transit time output is robust and independent of model structure, the size and turnover of model pools are relatively uncertain when using only bulk and respired $\Delta^{14}C$ data as model constraints. This issue of equifinality is particularly problematic when predicting future changes in soil C stocks in response to changes in the environment, given that different soil C pools are expected to differ in sensitivity to these changes. Further partitioning of density fractions, particularly the heavy fraction which makes up the majority of the soil C pool in most mineral soils (Heckman et al., 2022), may improve constraints on the internal dynamics of soil C models. For example, applying tools such as the thermal fractionation approach shown in **Figure 5-4** can be used to provide higher resolution information about the size and age of subfractions of the MAOM pool. Such data could enable the testing of hypotheses about model structure, e.g., via comparisons of $\Delta^{14}C$ distributions from models with measured $\Delta^{14}C$ distributions, that were not tractable with the exclusive use of bulk and respired CO_2 constraints used in this dissertation.

Understanding how soil C stocks will shift in response to environmental change over the coming decades will be invaluable for both predicting future climate changes as well as developing management strategies to mitigate the planet warming effects of greenhouse gas emissions. The abundance of soil in archives worldwide represents an invaluable resource for understanding how

soils change over time. This knowledge will be essential for predicting changes in soil C stocks, the distribution of soil C among pools with different turnover rates, and characterizing the mineral assemblages that play such a fundamental role in determining soil C persistence—on timescales ranging from annual to centennial and beyond. Soil organic matter research is at a critical threshold with unprecedented levels of interest from the public sphere, including both governmental and non-governmental institutions, as well as private companies seeking to monetize soil C sequestration. Radiocarbon measurements that once were rare due to high costs and a paucity of measurement facilities are now more readily available, yielding key indicators for the time scales of C sequestration in soils. The central tenet of this dissertation is that the soil organic matter research community must go beyond calculating simple radiocarbon ages or relying on mean C ages from bulk soils and soil organic matter fractions when quantifying soil C turnover. Instead, we must turn our attention to characterizing soil C age and transit time distributions if we are to provide a critical check against unrealistic promises of rapid drawdown of atmospheric CO_2 in soils and realize the full potential of soil C sequestration.

7. References for Chapters 5 & 6

Amundson, R. and Biardeau, L.: Opinion: Soil carbon sequestration is an elusive climate mitigation tool, Proceedings of the National Academy of Sciences, 115, 11652–11656, https://doi.org/10.1073/pnas.1815901115, 2018.

Baisden, W. T., Amundson, R., Cook, A. C., and Brenner, D. L.: Turnover and storage of C and N in five density fractions from California annual grassland surface soils, Global Biogeochemical Cycles, 16, 64-1-64–16, https://doi.org/10.1029/2001gb001822, 2002.

Baisden, W. T., Parfitt, R. L., Ross, C., Schipper, L. A., and Canessa, S.: Evaluating 50 years of time-series soil radiocarbon data : towards routine calculation of robust C residence times, Biogeochemistry, 112, 129–137, https://doi.org/10.1007/s10533-011-9675-y, 2013.

Beaty, R. M. and Taylor, A. H.: Fire history and the structure and dynamics of a mixed conifer forest landscape in the northern Sierra Nevada, Lake Tahoe Basin, California, USA, Forest Ecology and Management, 255, 707–719, https://doi.org/10.1016/j.foreco.2007.09.044, 2008.

Bradford, M. A., Wieder, W. R., Bonan, G. B., Fierer, N., Raymond, P. A., and Crowther, T. W.: Managing uncertainty in soil carbon feedbacks to climate change, Nature Climate Change, 6, 751–758, https://doi.org/10.1038/nclimate3071, 2016.

Canadell, J. G., Monteiro, P. M. S., Costa, M. H., Cotrim da Cunha, L., Cox, P. M., Eliseev, A. V., Henson, S., Ishii, M., Jaccard, S., Koven, C., Lohila, A., Patra, P. K., Piao, S., Rogelj, J., Syampungani, S., Zaehle, S., and Zickfeld, K.: Global carbon and other biogeochemical cycles and feedbacks, edited by: Masson-Delmotte, V., Zhai, P., Pirani, A., Connors, S. L., Péan, C., Berger, S., Caud, N., Chen, Y., Goldfarb, L., Gomis, M. I., Huang, M., Leitzell, K., Lonnoy, E., Matthews, J. B. R., Maycock, T. K., Waterfield, T., Yelekçi, O., Yu, R., and Zhou, B., Climate change 2021: The physical science basis. Contribution of working group I to the sixth assessment report of the intergovernmental panel on climate change, 673–816, https://doi.org/10.1017/9781009157896.007, 2021.

Castanha, C., Trumbore, S., and Amundson, R.: Methods of separating soil carbon pools affect the chemistry and turnover time of isolated fractions, Radiocarbon, 50, 83–97, https://doi.org/10.1017/S0033822200043381, 2008.

Cerli, C., Celi, L., Kalbitz, K., Guggenberger, G., and Kaiser, K.: Separation of light and heavy organic matter fractions in soil - Testing for proper density cut-off and dispersion level, Geoderma, 170, 403–416, https://doi.org/10.1016/j.geoderma.2011.10.009, 2012.

Chanca, I., Trumbore, S., Macario, K., & Sierra, C. A.: Probability Distributions of Radiocarbon in Open Linear Compartmental Systems at Steady-State, Journal of Geophysical Research: Biogeosciences, 127, 3, e2021JG006673, 2021.

Crow, S. E. and Sierra, C. A.: The climate benefit of sequestration in soils for warming mitigation, Biogeochemistry, https://doi.org/10.1007/s10533-022-00981-1, 2022.

Friedlingstein, P., Meinshausen, M., Arora, V. K., Jones, C. D., Anav, A., Liddicoat, S. K., and Knutti, R.: Uncertainties in CMIP5 climate projections due to carbon cycle feedbacks, Journal of Climate, 27, 511–526, https://doi.org/10.1175/JCLI-D-12-00579.1, 2014.

Golchin, A.: Spatial Distribution, Chemistry and Turnover of Organic Matter in Soils, PhD dissertation, 1996.

Heckman, K., Throckmorton, H., Clingensmith, C., Vila, F. J. G., Horwath, W. R., Knicker, H., and Rasmussen, C.: Factors affecting the molecular structure and mean residence time of occluded organics in a lithosequence of soils under ponderosa pine, Soil Biology and Biochemistry, 77, 1–11, 2014.

Heckman, K., Hicks Pries, C. E., Lawrence, C. R., Rasmussen, C., Crow, S. E., Hoyt, A. M., von Fromm, S. F., Shi, Z., Stoner, S., McGrath, C., Beem-Miller, J., Berhe, A. A., Blankinship, J. C., Keiluweit, M., Marín-Spiotta, E., Monroe, J. G., Plante, A. F., Schimel, J., Sierra, C. A., Thompson, A., and Wagai, R.: Beyond bulk: Density fractions explain heterogeneity in global soil carbon abundance and persistence, Global Change Biology, 28, 1178–1196, https://doi.org/10.1111/gcb.16023, 2022.

Hill, A. P., Nolan, C. J., Hemes, K. S., Cambron, T. W., and Field, C. B.: Low-elevation conifers in California's Sierra Nevada are out of equilibrium with climate, PNAS Nexus, 2, pgad004, https://doi.org/10.1093/pnasnexus/pgad004, 2023.

Kaiser, K. and Guggenberger, G.: Distribution of hydrous aluminium and Fe over density fractions depends on organic matter load and ultrasonic dispersion, Geoderma, 140, 140–146, https://doi.org/10.1016/j.geoderma.2007.03.018, 2007.

Kaiser, K. and Kalbitz, K.: Cycling downwards - dissolved organic matter in soils, Soil Biology and Biochemistry, 52, 29–32, https://doi.org/10.1016/j.soilbio.2012.04.002, 2012.

Kilgore, B. M. and Taylor, D.: Fire history of a sequoia-mixed conifer forest, Ecology, 60, 129–142, 1979.

Kleber, M., Sollins, P., and Sutton, R.: A conceptual model of organo-mineral interactions in soils: Self-assembly of organic molecular fragments into zonal structures on mineral surfaces, Biogeochemistry, 85, 9–24, https://doi.org/10.1007/s10533-007-9103-5, 2007.

Koarashi, J., Hockaday, W. C., Masiello, C. a., and Trumbore, S. E.: Dynamics of decadally cycling carbon in subsurface soils, Journal of Geophysical Research G: Biogeosciences, 117, G03033, https://doi.org/10.1029/2012JG002034, 2012.

Koven, C. D., Hugelius, G., Lawrence, D. M., and Wieder, W. R.: Higher climatological temperature sensitivity of soil carbon in cold than warm climates, Nature Climate Change, 7, 817–822, https://doi.org/10.1038/nclimate3421, 2017.

Leinemann, T., Preusser, S., Mikutta, R., Kalbitz, K., Cerli, C., Höschen, C., Mueller, C. W., Kandeler, E., and Guggenberger, G.: Multiple exchange processes on mineral surfaces control the transport of dissolved organic matter through soil profiles, Soil Biology and Biochemistry, 118, 79–90, https://doi.org/10.1016/j.soilbio.2017.12.006, 2018.

Lenihan J. M., Drapek R., Bachelet D., Neilson R. P.: Climate change effects on vegetation distribution, carbon, and fire in California. Ecological Applications, 13, 1667–1681, 2003.

Masson-Delmotte, V., Zhai, P., Pirani, A., Connors, S. L., Péan, C., Berger, S., Caud, N., Chen, Y., Goldfarb, L., Gomis, M., and others: Climate change 2021: the physical science basis, Contribution of working group I to the sixth assessment report of the intergovernmental panel on climate change, 2, 2021.

Matthews, H. D., Zickfeld, K., Dickau, M., MacIsaac, A. J., Mathesius, S., Nzotungicimpaye, C.-M., and Luers, A.: Temporary nature-based carbon removal can lower peak warming in a well-below 2 °C scenario, Communications Earth & Environment, 3, 65, https://doi.org/10.1038/s43247-022-00391-z, 2022.

Melillo, J. M., Frey, S. D., DeAngelis, K. M., Werner, W. J., Bernard, M. J., Bowles, F. P., Pold, G., Knorr, M. A., and Grandy, A. S.: Long-term pattern and magnitude of soil carbon feedback to the climate system in a warming world, Science, 358, 101–105, https://doi.org/10.1126/science.aan2874, 2017.

Minasny, B., Malone, B. P., McBratney, A. B., Angers, D. A., Arrouays, D., Chambers, A., Chaplot, V., Chen, Z. S., Cheng, K., Das, B. S., Field, D. J., Gimona, A., Hedley, C. B., Hong, S. Y., Mandal, B., Marchant, B. P., Martin, M., McConkey, B. G., Mulder, V. L., O'Rourke, S., Richer-de-Forges, A. C., Odeh, I., Padarian, J., Paustian, K., Pan, G., Poggio, L., Savin, I., Stolbovoy, V., Stockmann, U., Sulaeman, Y., Tsui, C. C., V??gen, T. G., van Wesemael, B., and Winowiecki, L.: Soil carbon 4 ‰le, Geoderma, 292, 59–86, https://doi.org/10.1016/j.geoderma.2017.01.002, 2017.

Paustian, K., Larson, E., Kent, J., Marx, E., and Swan, A.: Soil C sequestration as a biological negative emission strategy, Frontiers in Climate, 8, 2019.

Rasmussen, C., Throckmorton, H., Liles, G., Heckman, K., Meding, S., and Horwath, W. R.: Controls on Soil Organic Carbon Partitioning and Stabilization in the California Sierra Nevada, Soil Systems, 2018.

Schrumpf, M. and Kaiser, K.: Large differences in estimates of soil organic carbon turnover in density fractions by using single and repeated radiocarbon inventories, Geoderma, 239–240, 168–178, https://doi.org/10.1016/j.geoderma.2014.09.025, 2015.

Shafer S.L., Bartlein P.J., Thompson R.S.: Potential changes in the distributions of western North America tree and shrub taxa under future climate scenarios. Ecosystems, 4, 200–215, 2001.

Sierra, C. A., E. Crow, S., Heimann, M., Metzler, H., and Schulze, E. D.: The climate benefit of carbon sequestration, Biogeosciences, 18, 1029–1048, https://doi.org/10.5194/bg-18-1029-2021, 2021.

Sollins, P., Swanston, C., Kleber, M., Filley, T., Kramer, M., Crow, S., Caldwell, B. A., Lajtha, K., and Bowden, R.: Organic C and N stabilization in a forest soil: Evidence from sequential density fractionation, Soil Biology and Biochemistry, 38, 3313–3324, https://doi.org/10.1016/j.soilbio.2006.04.014, 2006.

Sollins, P., Kramer, M. G., Swanston, C., Lajtha, K., Filley, T., Aufdenkampe, A. K., Wagai, R., and Bowden, R. D.: Sequential density fractionation across soils of contrasting mineralogy: Evidence for both

microbial- and mineral-controlled soil organic matter stabilization, Biogeochemistry, 96, 209–231, https://doi.org/10.1007/s10533-009-9359-z, 2009.

Stoner, S.: Quantifying relevant timescales of soil carbon cycling through long-term modeling and novel fractionation techniques, phd, ETH Zurich, 2023.

Todd-Brown, K., Zheng, B., and Crowther, T. W.: Field-warmed soil carbon changes imply high 21st-century modeling uncertainty, Biogeosciences, 15, 3659–3671, https://doi.org/10.5194/bg-15-3659-2018, 2018.

Trumbore, S.: Radiocarbon and Soil Carbon Dynamics, Annual Review of Earth and Planetary Sciences, 37, 47–66, https://doi.org/10.1146/annurev.earth.36.031207.124300, 2009.

Wagai, R., Kajiura, M., Uchida, M., and Asano, M.: Distinctive Roles of Two Aggregate Binding Agents in Allophanic Andisols: Young Carbon and Poorly-Crystalline Metal Phases with Old Carbon, Soil Systems, 2018.

Acknowledgements

Curriculum Vitae

Personal Information
Citizenship: United States of America
Date of Birth: 06 August 1986, Ithaca, NY (USA)

Academic Training

Dr. rer. nat. (since 09/2017)	Leibniz University Hannover (in cooperation with the Max Planck Institute for Biogeochemistry) Thesis: *Radiocarbon constraints reveal time scales of soil carbon persistence*
Master of Science (08/2017)	Cornell University Thesis: *Soil carbon assessment: Confronting climate change on the farm*
Bachelor of Arts (05/2008)	Oberlin College, Biology & Environmental Studies majors
Certificate (2007)	School for International Training (Panama), Development and Conservation Program

Professional Experience

06/ 2011 – 12/2014	Laboratory manager Wolfe Lab, Cornell Univ. School for Integrative Plant Science
02/2011 – 07/2011; 10/2008 – 06/2009	Laboratory manager/technician Fahey/Yavitt Lab, Cornell Univ. Dept. of Natural Resources
01/ 2007 – 02/2007; 06/2007 – 08/2007	Laboratory technician Goodale Lab, Cornell Univ. Dept. of Ecology and Evolutionary Biol.

Internships

05/2012 – 12/2012	Botanist United States Bureau of Land Management, Carson City, NV
01/2011 – 06/2011	Carpenter Dave Burke Carpentry, Ithaca, NY
06/2008 – 08/2008	Naturalist Aspen Center for Environmental Studies, Aspen, CO
01/2005	Forest ecology intern Hamburg Lab, Brown University

Teaching

Cornell Univ. School of Integrative Plant Sci.

01/ 2017 – 05/2017	Teaching assistant, Viticulture and Vineyard Mgmt. (PLHRT 3440)
08/2016 – 12/2016	Teaching assistant, Climate Change and Food Security (PLHRT 3600)
01/2016 – 05/2016	Teaching assistant, Intro to Viticulture and Enology (PLHRT 1104)
08/2015 – 12/2015	Teaching assistant, Climate Change and Food Security (PLHRT 3600)

Publications

REFEREED JOURNAL ARTICLES

Beem-Miller, J., Rasmussen, C., Hoyt, A. M., Schrumpf, M., Guggenberger, G., and Trumbore, S.: Soil minerals mediate climatic control of soil C cycling on annual to centennial timescales, In review at: EGUsphere [preprint]. DOI: 10.5194/egusphere-2022-1083, 2022.

Todd-Brown, K.E., Abramoff, R.Z., **Beem-Miller, J.**, Blair, H.K., Earl, S., Frederick, K.J., Fuka, D.R., Guevara Santamaria, M., Harden, J.W., Heckman, K. and Heran, L.J. 2022. Reviews and syntheses: The promise of big diverse soil data, moving current practices towards future potential. Biogeosciences, 19:14:3505-3522. DOI: 10.5194/bg-19-3505-2022

Heckman, K., C.E. Hicks-Pries, C. Lawrence, C. Rasmussen, S.E. Crow, A.M. Hoyt, S.F. von Fromm, Z. Shi, S. Stoner, C. McGrath, **J. Beem-Miller**, A.A. Berhe, J.C. Blankinship, M. Keiluweit, E. Marín-Spiotta, J.G Monroe, A.F. Plante, J. Schimel, C.A. Sierra, A. Thompson, R. Wagai. 2021. Beyond bulk: Density fractions explain heterogeneity in global soil C abundance and persistence. Global Change Biol. 28:1178–1196. DOI: 10.1111/gcb.16023

Beem-Miller, J., M. Schrumpf, A.M. Hoyt, G. Guggenberger, S. Trumbore. 2021. Impacts of drying and rewetting on the radiocarbon signature of respired CO_2 and implications for incubating archived soils. Journal of Geophysical Research: Biogeosciences, 126, e2020JG006119. DOI: 10.1029/2020JG006119

Shi, Z., S.D. Allison, Y. He, P.A. Levine, A.M. Hoyt, **J. Beem-Miller**, Q. Zhu, W.R. Wieder, S. Trumbore, J.T. Randerson. 2020. The age distribution of global soil carbon inferred from radiocarbon measurements. Nat. Geosci. 13:555–559. DOI: 10.1038/s41561-020-0596-z

Schädel, C., **J. Beem-Miller,** M. Aziz Rad, S.E. Crow, C.E. Hicks Pries, J. Ernakovich, A.M. Hoyt, A. Plante, S. Stoner, C.C. Treat, C.A. Sierra. 2020. Decomposability of soil organic matter over time: The Soil Incubation Database (SIDb, version 1.0) and guidance for incubation procedures. Earth Sys. Sci. Data. DOI: 10.5194/essd-12-1511-2020

Lawrence, C.R., **J. Beem-Miller**, A.M. Hoyt, G. Monroe, C.A. Sierra, S. Stoner, K. Heckman, J.C. Blankinship, S.E. Crow, G. McNicol, S.E. Trumbore, P.A. Levine, O. Vindušková, K. Todd-Brown, Craig Rasmussen, C.E. Hicks Pries, C. Schädel, K. McFarlane, S. Doetterl, C. Hatté, Y. He, C. Treat, J.W. Harden, M.S. Torn, C. Estop-Aragonés, A.A. Berhe, M. Keiluweit, E. Marin-Spiotta, A.F. Plante, A. Thomson, J.P. Schimel, L.J. S. Vaughn, and R. Wagai. 2020. An open source database for the synthesis of soil radiocarbon data: ISRaD version 1.0. Earth Sys. Sci. Data. http://dx.doi.org/10.5194/essd-12-61-2020

Comstock J, S Sherpa, Feng, Richard Ferguson, S Bailey, **J. Beem-Miller**, F. Lin, J Lehmann, D Wolfe. 2019. Carbonate determination in soils by mid-IR spectroscopy with regional and continental scale models. PLOS One. http://dx.doi.org/10.1371/journal.pone.0210235

Beem-Miller J, A Kong, S Ogle, D Wolfe. 2016. Sampling for soil carbon stock assessment in rocky agricultural soils. Soil Sci. Soc. Amer. J. 80: 1411-1423. http://dx.doi.org/10.2136/sssaj2015.11.0405

OTHER SCIENTIFIC PUBLICATIONS

Beem Miller, J., M. Schrumpf, S. Stoner, A.M. Hoyt, C. Rasmussen, G. Guggenberger, S. Trumbore. 2022. Interactions Between Climate and Mineralogy Determine Soil Carbon Model Complexity and Temperature Sensitivity. Abstract B12C-07 presented at 2022 Fall Meeting, AGU, Chicago, IL, 12-16 Dec.

Beem Miller, J., A.M. Hoyt, M. Schrumpf, G. Guggenberger, C. Rasmussen, S. Trumbore. 2021. Parent material and climate interact to control soil carbon dynamics on timescales from years to centuries. Abstract B32D-07 presented at 2021 Fall Meeting, AGU, New Orleans, LA, 13-17 Dec.

Beem Miller, J., Schrumpf, M., Guggenberger, G., and Trumbore, S. 2020. Radiocarbon incubations of archived soils: insights into drying/rewetting effects and constraining soil C models, EGU General Assembly 2020, Online, 4–8 May 2020, EGU2020-10075.

Beem-Miller, J, C. Lawrence, J. Blankinship, A. Hoyt, S. Stoner, C. Sierra, G. Monroe, G. McNicol, Y. He, C. Hatté, S. Crow, K. Heckman, M. Keiluweit, S. Trumbore. 2018. From Fractions to Fluxes: The International Soil Radiocarbon Database. 2018. Presented at 23rd International Radiocarbon Conference, Trondheim, Norway.

Beem-Miller J, G. Guggenberger, C. Rasmussen, M. Schrumpf, S. Trumbore. 2019. Decadal cycling of mineral-associated soil carbon. Abstract BH21H-2249 presented at 2019 Fall Meeting, AGU, San Francisco, CA 9-13 Dec.

Beem-Miller J, M. Schrumpf, G. Guggenberger, C. Sierra, S. Trumbore. 2018. Beyond the first date: Soil incubations and the radiocarbon constraint. Abstract B23G-1956 presented at 2018 Fall Meeting, AGU, Washington DC, 10-14 Dec.

Beem-Miller J, J Lehmann, D Wolfe. 2017. Subsoil carbon accumulation on an arable Mollisol is retention-dominated, in contrast to input-driven carbon dynamics in topsoil. European Geosciences Union General Assembly, April 23-28, 2017.

Beem-Miller J and D Wolfe. 2016. Sampling for soil carbon stock assessment in rocky agricultural soils. Proceedings: Soil Science Society of America Annual Meetings Nov 6-9, Phoenix, AZ. ASA/CSSA/SSSA Madison, WI

Wolfe, D., **J. Beem-Miller**, L. Chambliss, A. Chatrchyan, and H. Menninger. 2011. Farming Success in an Uncertain Climate. Cornell Cooperative Extension Factsheet.

Wolfe, D., **J. Beem-Miller**, A. Chatrchyan, and L. Chambliss. 2011. Farm Energy, Carbon, and Greenhouse Gases. Cornell Cooperative Extension Factsheet.

DeGaetano, A., A. Chatrchyan, D. Wolfe, **J. Beem-Miller**, L. Chambliss, and H. Menninger. 2011. Earth's Changing Climate. Cornell Cooperative Extension Factsheet.

DeGaetano, A., A. Chatrchyan, D. Wolfe, **J. Beem-Miller**, L. Chambliss, and H. Menninger. 2011. New York's Changing Climate. Cornell Cooperative Extension Factsheet.